Answers Research Journal 17 (2024): 63–192.
https://assets.answersresearchjournal.org/doc/v17/whitmore_helipad_fold.pdf

ARJ

The Whitmore Helipad Fold, Western Grand Canyon, Arizona

Andrew A. Snelling, Answers in Genesis, PO Box 510, Hebron, Kentucky 41048

Abstract

Bright Angel Formation beds are bent in the Whitmore Helipad fold exposed along the Colorado River in western Grand Canyon. Conventional geologists accept that this folding occurred during the Laramide orogeny at ~40–70 Ma when the Colorado Plateau was uplifted. However, the Bright Angel Formation had been deposited at 502–507 Ma, so after ~450 million years it should have been fully cemented and lithified. Yet the sandstone, siltstone, and shale beds look as though they were bent smoothly while they were still unlithified and soft. Such a conclusion would be preposterous if there were ~450 million years between deposition of the Bright Angel Formation and its deformation in the Whitmore Helipad fold. To investigate this further, Bright Angel Formation samples were collected from the hinge and limb zones of the Whitmore Helipad fold, as well as samples many miles away from the fold. Macroscopic features that should be present if the Bright Angel Formation beds in the fold had been bent via ductile deformation over millions of years are indications of bedding plane slip, slickensides on bedding plane surfaces, thickening of hinge zones and thinning of limb zones, as well as more fracturing in the hinge zones compared to the limbs. At the microscopic scale there should be evidence of grain-boundary sliding, rotation and fracturing of grains, and within many quartz grains there should be sub-grains, undulose extinction, deformation lamellae and deformation kink bands. Field observations are inconsistent with ductile deformation under low pressure-low temperature metamorphic conditions. While bedding plane slip may have occurred, instead of slickensides being found on any bedding plane surfaces, trace fossils are preserved. There is little thickening of beds in the hinge zones, except for lateral bulging of beds above the lower hinge zone. Also, fracturing is minimal throughout the fold and confined to within each bed, but there are faults with trivial displacements in the hinge zones and one limb zone. All these observed features have been replicated using water-saturated soft sediment layers in experiments simulating compressional folding, which equates to soft-sediment deformation. None of the microscopic features expected from ductile deformation are present in any of the samples. There are no deformation lamellae or deformation kink bands in the quartz grains which rarely display even trivial undulose extinction, and there is no obvious evidence of any rotation of grains or grain boundary sliding. The few quartz grains containing sub-grains are likely derived from metamorphic source rocks rather than being a product of ductile deformation, and the few occasional fractures in some quartz grains and broken quartz grains are consistent with fracturing due to compaction of the sand and silt grains under the confining overburden pressures. Instead, the well-sorted, angular to sub-rounded quartz and K-feldspar grains, oval glauconite pellets, muscovite flakes, and brachiopod shell fragments comprising the sandstones and shales, and the finer-grained shales, are still in their detrital condition, except for illite alteration of tiny K-feldspar grains in the shales. There are no indications of the silica cement having been disturbed since lithification of these sediment beds or of any metamorphic changes to these constituent minerals or the rock fabric. Furthermore, SEM images clearly demonstrate that the quartz cement has not been disrupted since lithification, with many cement crystals still being pristine with terminal faces intact. And muscovite flakes are bent but not internally sheared between sheets. Both the macroscopic and microscopic evidence are conclusively consistent only with soft-sediment deformation before cementation and lithification. Therefore, it is concluded that the Bright Angel Formation had to be folded while still relatively water-saturated, unlithified and soft soon after deposition and before cementation and lithification. Problems with the radioisotope dating methods and the U-Pb dates obtained for the underlying Tapeats Sandstone rule out the vast claimed ages. This can all be easily reconciled with rapid deposition of the Bright Angel Formation early in the biblical global Flood cataclysm only ~4,350 years ago, and rapid deposition of maybe up to ~3,300–4,500 m (~10,800–14,750 ft) of overlying sedimentary layers caused by the catastrophic plate activity during the Flood year. Late in the Flood year, as the Farallon plate underplated the western North American plate, it caused isostatic reequilibration which likely resulted in the Late Cretaceous-Early Cenozoic Laramide uplift of the Colorado Plateau and the monocline folding in the Grand Canyon region. Because the Bright Angel Formation beds were still relatively unlithified and soft less than a year after rapid burial, they easily responded to soft-sediment deformation to form the smooth bending in the Whitmore Helipad fold before the beds hardened, and were cemented and lithified. Thus, nearly 500 million years of claimed geologic history are eliminated. And since the Flood, isolated earthquake-induced movements on the Hurricane Fault have caused minor faulting in the Whitmore Helipad fold.

Keywords: Bright Angel Formation, Whitmore Helipad fold, Laramide orogeny, Hurricane Fault, soft-sediment deformation (SSD), ductile deformation, bedding plane slip, grain-boundary sliding, microstructures, quartz, K-feldspar, muscovite, detrital grains, silica cement, global Flood cataclysm

Summary of Findings

(1) Microscopic features in the Bright Angel Formation samples within the Whitmore Helipad fold, whether from the hinge zones or the limbs, are no different to the distal samples in their mineral constituents, and textures, and though their porosities are less, they are still essentially in their original detrital sedimentary condition.

(2) Detrital muscovite flakes are still bent around quartz, K-feldspar, glauconite pellets and grains, and fossilized brachiopod shell fragments, and sometimes having frayed ends, confirming that all the sandstone, siltstone, and shale samples are still in their original sedimentary condition.

(3) There is no evidence of any grain-boundary sliding between the quartz and the other sand and silt grains, nor are there any deformation lamellae, but only isolated trivial undulose extinction within quartz grains, none of which are consistent with ductile (plastic) deformation having occurred in the sandstone and siltstone layers in the Whitmore Helipad fold, nor is there any evidence of any metamorphism due to deep burial and the deformation.

(4) The quartz cement is pristine with only evidence of trivial disruption in some the samples due to compactional loading, and instead the quartz cement crystals have overgrown the original detrital grains and meet at triple points, often with good crystal terminations, thus infilling pore spaces, all indicating the cement formed after the folding.

(5) Thus, conditions in the history of the sandstone, siltstone, and shale have not been different during the deformation in this fold compared to the same sandstone, siltstone, and shale beds distant from this fold.

(6) All the macroscopic features in the Whitmore Helipad fold, including a lack of evidence showing bedding plane or flexural slippage between beds, the minor fracturing, as well as some minor faulting in the hinge and limb zones with trivial to minor displacements (that are possibly due to more recent earthquakes), and the bulging or flow of some beds in one hinge zone, have all been readily replicated in soft-sediment deformation experiments at laboratory scale.

(7) There is no macroscopic or microscopic evidence consistent with the conventional explanation that the Whitmore Helipad fold was produced by ductile (plastic) deformation under low pressure-low temperature metamorphic conditions over millions of years some 450 million years after deposition and cementation of the Bright Angel Formation.

(8) Instead, all the macroscopic and microscopic evidence combined is only consistent with the Whitmore Helipad fold having been produced by soft-sediment deformation of the Bright Angel Formation soon after deposition and before dewatering caused joint development and cementation.

Introduction

Many structures in sedimentary rock layers result from the primary depositional processes, such as graded bedding and cross-bedding (Boggs 1995). On the other hand, soft-sediment deformation or penecontemporaneous structures are so called because they develop at the time of deposition or shortly thereafter, during the early stages of the sediment's consolidation and before full lithification. This is because the sediments need to be unsolidified or "liquid-like" for such deformation to occur (Boggs 1995).

However, other structures in sedimentary rocks are caused by deformation long after lithification and diagenesis have occurred. Rocks buried deep in the earth may be under sufficient confining pressures or stress and temperatures to cause them to undergo metamorphism and deform plastically. Prolonged, incremental strain over a long period can also cause plastic deformation. These processes are believed to be able to fold rock layers. These types of behaviors are called ductile deformation, defined as the ability of a rock to accumulate strain (folding) on a mesoscopic scale. Under high enough confining pressures and accompanying elevated temperatures, rock grains may recrystallize and/or the minerals undergo metamorphism, causing new minerals such as micas to grow perpendicular to the maximum principal stress direction. Hand and thin section analyses should be able to determine if rocks experienced ductile deformation. Paleozoic rocks, including the Tonto Group of Grand Canyon, most likely were not buried deep enough to experience ductile (plastic) deformation as they were well above the brittle-ductile transition zone, which occurs at a depth of 15–20 km (~49,000–65,600 ft) at temperatures of 250–400°C (Condie 2005; Zhamaletdinov 2019). This is well below the estimated depth of ~3,300–4,500 m (~10,285–14,750 ft) to which the Tapeats Sandstone and Bright Angel Formation were likely buried (Dumitru, Duddy, and Green 1994; Peak et al. 2021; Thurston et al. 2022). Incremental strain over sustained periods of time is harder to differentiate. As noted above, it can also result in ductile deformation.

On the other hand, under some near surface conditions, rock layers may remain coherent because the grains and/or layers within them can facilitate the folding. This type of deformation is most

common in near surface rocks and is a type of brittle deformation. Most near surface rock layers undergo brittle fracturing and faulting, leaving the rock's grains fractured. Some coherent units may slide past one another along bedding planes as the rocks are folded. This helps accommodate folding through flexural slip. Telltale signs of this should be clearly evident in outcrops and from microscope examination of the rock fabric and the sediment grains.

There are several prominent locations in Grand Canyon where the Paleozoic sedimentary rock layers are folded, sometimes in conjunction with faulting in the underlying Precambrian basement rocks, where there are unresolved questions as to whether the folding represents soft-sediment deformation folding or later tectonic folding (ductile or brittle) well after the whole strata sequence was deposited. In most instances the folding is usually claimed to be the result of ductile (plastic) behavior of the lithified sedimentary rocks under prolonged stress due to Late Mesozoic-Early Cenozoic deformation during the Laramide orogeny, hundreds of millions of years after the whole Paleozoic strata sequence was deposited (Huntoon 2003; Karlstrom and Timmons 2012). However, the macroscopic fabric of the Tapeats Sandstone, Bright Angel Formation, and Muav Formation of the Cambrian Tonto Group sedimentary rock layers involved in these folds might suggest, and seems to be more consistent with, the folding being due to soft-sediment deformation (Snelling 2023a, b). Any soft-sediment deformation should have occurred after deposition and before lithification of these sedimentary units in the Cambrian (499–508Ma) (Karlstrom et al. 2020), well before the tectonic activity associated with the Laramide orogeny that began in the terminal Mesozoic and earliest Cenozoic (~40–70Ma). This poses an apparent paradox that obviously needs resolving, and thus a focused study was designed to determine the timing and nature of this folding, beginning with a thorough investigation of the petrology of each of these rock units generally, and subsequent detailed examination of these rock units in each fold.

It has been extensively documented that lithified rocks which have suffered ductile deformation will exhibit outcrop evidence of bedding plane slip and attenuation, such as flexural slippage (Ramsay 1967). However, field examination of these folds is insufficient to determine whether they were due to such ductile behavior of the lithified rocks under much later prolonged stress or due to soft-sediment deformation soon after deposition. Detailed microscopic examination is absolutely necessary to document the character of the various lithologies, specifically, the textural relationships between the constituent grains and the timing of the formation of the cement (lithification). Telltale microscopic textures should be evident, such as grain boundary sliding, a preferred orientation and recrystallization of the original detrital grains, as well as deformation lamellae and undulose extinction in those grains, and the original sedimentary cement between them should be broken or fractured, or metamorphosed. Such textural features should be absent if the folding were due to soft-sediment deformation, as the original detrital grains and the cement binding them together in the various lithologies in the folds should be essentially identical to those in the same lithologic units some distance from the folds.

Yet it appears that no previous investigators have done any thin section investigations of the Tapeats Sandstone, Bright Angel Formation and Muav Formation to substantiate the claims of ductile deformation of these rock units in these folds other than Snelling (2021a, b, 2022a). Obviously, more detailed field and laboratory studies (especially intensive microscope examination) are needed to resolve the questions of what condition the sandstone, siltstone, shale and limestone were in when they were deformed into these folds, and how soon after deposition the deformation occurred, before or after lithification of the sandstone, siltstone, shale, and limestone. Any field and laboratory study of the Tapeats Sandstone, Bright Angel Formation, and Muav Formation in the folds should also include a field and laboratory study of these rock units in other locations distant from these folds. This would enable observations and conclusions at the one location to be confirmed in the studies at the other locations, because the evidence seen in thin section examination of these rock units in these folds should be different from that in the distant sandstone, siltstone, shale, and limestone samples if the folding was due to ductile behavior during deformation of the lithified sandstone, siltstone, shale, and limestone in the folds. On the other hand, the microscope evidence should be essentially identical in all samples if the folding was due to soft-sediment deformation.

Therefore, on a research and sampling trip through Grand Canyon to investigate these folds with National Park Service approval, ten samples of the Bright Angel Formation within the Whitmore Helipad fold with the approval of the Hualapai Nation and two samples from the Bright Angel Formation at similar stratigraphic positions within the formation at sufficient distances away from that fold were collected so as to provide comparative control samples for the subsequent detailed thin section examination (fig. 1). Snelling (2021b) reviewed extensively what is already known about the petrology of the Bright Angel Formation and reported detailed microscope observations made on the collected samples. From the

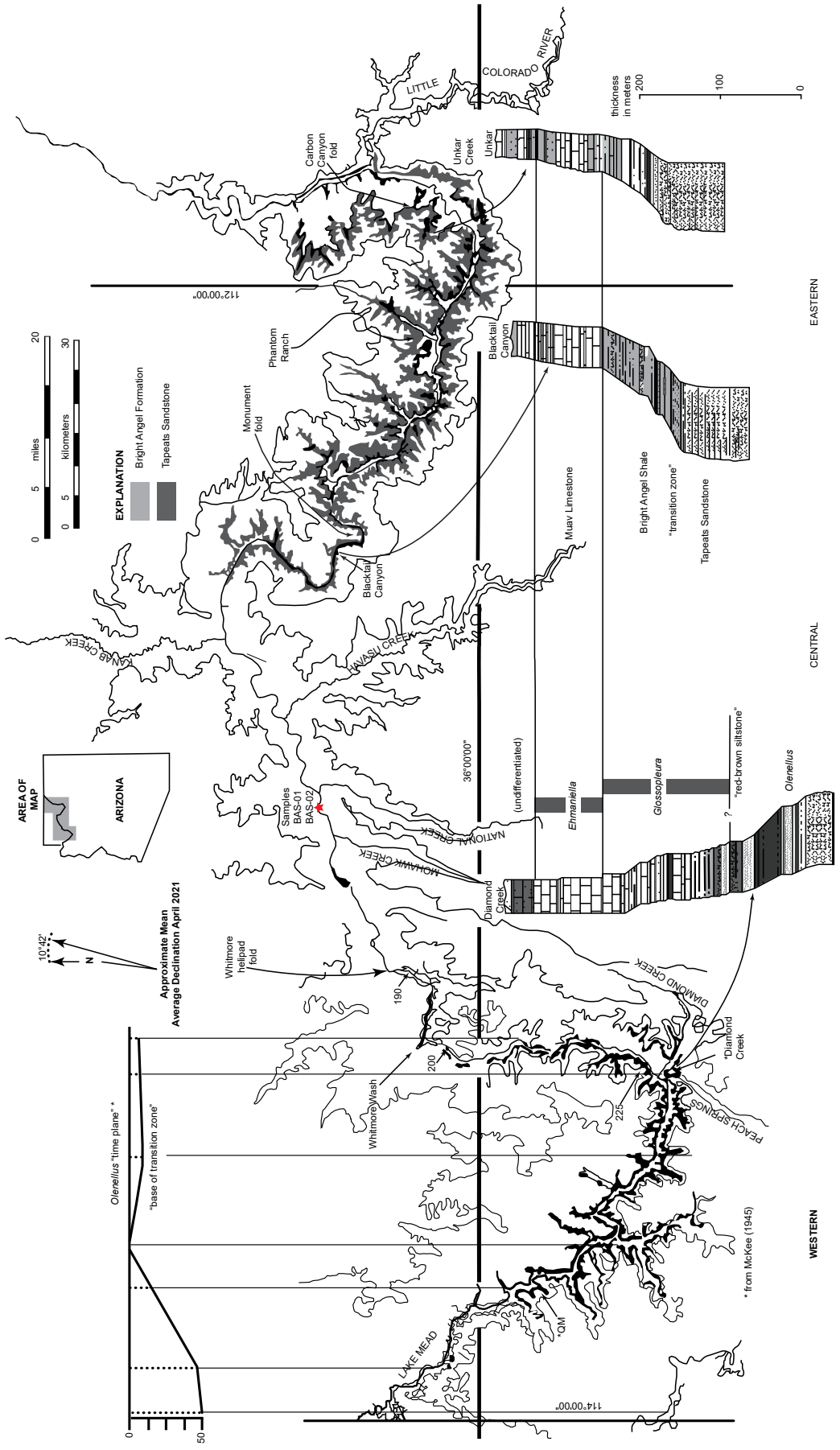

Fig. 1. Map of Grand Canyon showing the extent of exposure of the siliciclastic components of the Tonto Group, the Tapeats Sandstone, and the overlying Bright Angel Formation (after Rose, 2006, 225, fig. 1). Below the map are three representative stratigraphic sections shown in stylized profile of geomorphic expression. The inset in the upper left is the basis for the time-transgressive model proposed by McKee (1945). The datum was compiled from the reported height (in meters) at which McKee reported collecting *Olenellus* fossils from seven sites above the base of the "base of the transition zone" in the western Grand Canyon.

mineralogy and textures of these samples, inferences were drawn about the sediment source, its transport and deposition, and the subsequent history of the formation's strata. This same procedure provided the documentation of the underlying Tapeats Sandstone (Snelling 2021a) that was referred to and built on in the subsequent papers on the Carbon Canyon and Monument folds which focused on the timing of lithification (cementation) of the Tapeats Sandstone in those folds before or after the folding occurred, that is, soft-sediment deformation or ductile deformation, respectively (Snelling 2023a, b). In those papers it was demonstrated that folding was due to soft-sediment deformation. Now in this paper, the same issues will be similarly investigated for the overlying Bright Angel Formation in the Whitmore Helipad fold to ascertain whether it is due to either ductile deformation or soft-sediment deformation.

The Laramide Orogeny

The Laramide orogeny occurred in western North America during the latest Cretaceous through the Eocene (~40–70 Ma) (Huntoon 2003; Karlstrom and Timmons 2012). It is named after the Laramie Mountains of eastern Wyoming and should not be confused with the Siever orogeny with which it overlaps in space and time. Conventional geologists place the Grand Canyon region near sea level from 100 to 70 Ma, during which time the Sierra Nevada magmatic arc was building a series of volcanic peaks near the margin of the North American plate. The later Laramide orogeny also included widespread uplift of the Colorado Plateau, by an average of ~2 km (~6,500 ft) (Karlstrom and Timmons 2012) and a significant eastward expansion of Cordilleran deformation beyond previous limits of accretion, subduction, and magmatism. Laramide deformation was characterized by crustal shortening and northeast to eastward basement transport in a zone extending from the subduction trenches along the West Coast to the eastern limits of the Rocky Mountains (in the Black Hills). Types of deformation included east-verging thrust faulting and reverse displacements along many new and reactivated Precambrian basement faults. Faulting was accompanied by the development of monoclines and anticlines in the covering sedimentary rocks, especially in the Grand Canyon region (Huntoon 2003).

The position of the high Rocky Mountains, and the associated and intimately-related high-elevation Colorado Plateau adjacent to them, ~1,000 km (~620 mi) from the edge of the North American plate remains poorly understood. Epeirogeny (plateau building) is the uplift of regions without major tilting, folding, or thrusting of strata to build high elevation but relatively flat plateaus, which requires buoyancy of the crust on a regional scale. The plate tectonic explanation generally favored for Laramide orogenesis was a flattening of the angle of subduction of the oceanic plate known as the Farallon plate under western North America. Several hypotheses have been proposed as the cause of the flat-slab subduction—a more rapid rate of subduction, and/or the oceanic Farallon plate was thickened, and may have consisted of an oceanic plateau (Liu et al. 2010). In addition, Clarey (2020, 330–334) suggested the subducted plate under western North America contained a divergent boundary which caused flattening of the subduction angle due to its high heat and buoyancy. As a consequence of the shallow subduction angle, it has been suggested that no magmatism occurred (a magmatic gap) in part of the central west of the North American continental plate during the Paleogene (Dickinson and Snyder 1978), and the underlying oceanic lithosphere actually caused drag on the root of the overlying continental lithosphere (Jones et al. 2011). This so-called magmatic gap occurred because the subducted slab was in contact with relatively cool continental lithosphere, rather than hot asthenosphere (Dumitru et al. 1991). And another result of the shallow subduction angle and drag on the continental root was that it caused a broad belt of basement-cored mountains, some of which became the Rocky Mountains.

Dickinson (1981, 125) summarized how this concept of flat-slab subduction of the Farallon plate under western North America would have "played out" (fig. 2):

(1) The belt of magmatism moved inland as the locus of melting near the top of the subducted slab shifted away from the subduction zone;
(2) Magma generation waned as slab descent became sub-horizontal because the slab no longer penetrated as deeply into the asthenosphere; and
(3) Shallower descent of the slab increased the degree of shear and the area of interaction between the descending slab and the overriding cratonic crust (fig. 2c).

As rapid subduction took place, the subducted hot, buoyant, oceanic Farallon plate would have underplated North America as far east as the Great Plains, thereby contributing to the uplift of the West. The area that was to become the Colorado Plateau was apparently caught in the eastward compressing Laramide cordillera, but its exact cause in unclear.

According to conventional geologists, numerous prior major tectonic episodes during and since the Proterozoic had deformed the relatively stable Colorado Plateau region, producing a network of faults (Karlstrom and Timmons 2012). In each case, the stresses were different, and the resulting

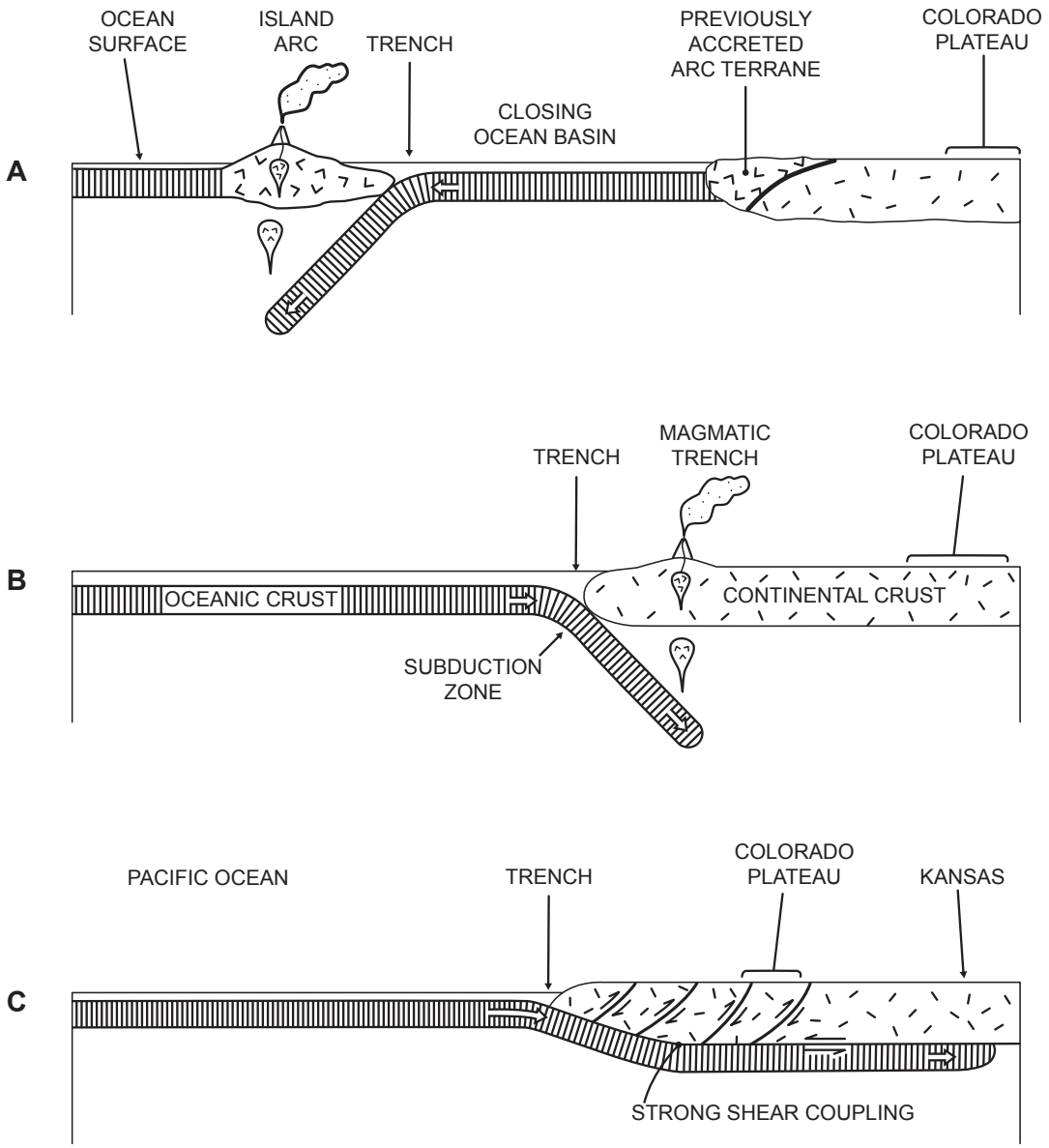

Fig. 2. Convergent margin orogens along western North America (after Dickinson 1981). Vertical scales are exaggerated. (a) Intra-oceanic arc-trench orogen active periodically in post-Precambrian through Late Triassic time. Note that the ocean basin progressively closed, causing the island arc to be accreted to the continent. Then another subduction zone and its island arc apparently formed offshore and likewise was eventually accreted to the continent. (b) Subsequent landward subduction caused development of a magmatic arc inboard on the continent above the steeply descending slab active from the Late Triassic to Late Cretaceous. (c) Then the subduction became rapid, even in the conventional timescale, resulting in shallow slab descent and slab underplating of the continent to produce buoyant uplift and strong shear-coupling with eastward telescoping of the continental crust during the Laramide orogeny.

fault networks had different orientations and styles. Walcott (1890) was the first to recognize that reactivation of earlier-formed Proterozoic faults occurred during the Laramide orogeny. Due to the compressional stress regime of the Laramide orogeny, what had been normal faults in the Proterozoic became high-angle (steeply-dipping) contractional reverse faults, such that older Paleozoic rocks on the west sides of fault lines were pushed up over younger Paleozoic strata on the east sides. Hence Laramide shortening structures have been called basement-cored "thick-skinned" structures, referring to the fact that Proterozoic crystalline basement rocks were pushed upward along faults.

The Laramide orogeny thus profoundly impacted the Grand Canyon region (Huntoon 2003; Karlstrom and Timmons 2012). It caused widespread uplift, east-northeast crustal shortening, compartmentalization of the Colorado Plateau into subsidiary uplifts and basins, and widespread erosion. This resulted in the development of generally north-striking, east-dipping monoclines as the underlying basement

failed along the major Proterozoic faults in response to east-northeast contraction (fig. 3). These monoclines were essentially "forced folds" of the Paleozoic strata due to the upward movement of the underlying basement blocks on high-angle normal faults forcing the overlying Paleozoic strata to bend passively into steeply dipping limbs (the monoclines) separating flat-lying beds of the upthrown blocks from the flat-lying beds of the downthrown sides. Laramide monoclinal folding in the Grand Canyon region was accompanied by mild regional warping of the intervening structural blocks, resulting in uplifts such as the Kaibab Plateau and downwarps such as the Cataract Basin (fig. 3).

Massive erosion followed the uplift of the Laramide orogeny. It progressively uncovered older rocks to the south and west, including the Precambrian basement along the southwestern edge of the Colorado Plateau region. The enormous volume of detritus from Mesozoic strata eroded off of the Grand Canyon region and areas to the south was apparently transported northeastward into the intracontinental basins of Utah and beyond (Huntoon 2003).

In the Early Eocene, there was a northeastward reorientation of Laramide stresses within the Colorado Plateau region (Chapin and Cather 1983). This caused 100 km (~60 mi) of north-northeast translation of the Colorado Plateau along right-lateral, strike-slip faults that partially decoupled the Colorado Plateau from the North American continent along the future Rio Grande Rift. This Early Eocene reorganization of stresses appears to have resulted in minor development, or reactivation, of northwest-trending monoclines in the Grand Canyon region.

Grand Canyon Monoclines

Most Laramide monoclines in the Grand Canyon region formed in the Paleozoic sedimentary cover strata in response to reverse movements along favorably oriented faults in the Precambrian basement (Huntoon 2003) (fig. 4). Three lines of evidence demonstrate that most faults under the monoclines were inherited from Precambrian time:

(1) juxtaposition of Precambrian basement crystalline rocks having different lithologies and fracture-foliation fabrics (Karlstrom et al. 2003) that cannot be restored by removal of Laramide offsets,
(2) juxtaposition of the overlying Precambrian Supergroup strata that cannot be restored to pre-fault conditions by removal of Laramide offsets, and
(3) presence of the Early Cambrian, potentially synorogenic, Sixtymile Formation (Karlstrom et al. 2018, 2020) along the west side of the Butte fault in eastern Grand Canyon.

Total crustal shortening resulting from the deformation within the monoclines was less than one percent across the Grand Canyon region (Davis 1978). There are two reasons for this low percentage, namely, the spacings between the monoclines are large in comparison to the local shortening across them, and the dips of the underlying Precambrian faults are steep.

The maximum offset across a Grand Canyon monocline is at least 750 m (~2,500 ft) along the East Kaibab Monocline (Huntoon 2003). The longest monocline, the East Kaibab Monocline, is ~300 km (~190 mi) long. The regional trends of the monoclines in the Grand Canyon region are generally north-south, and the east-west spacings between them vary from 11 to 50 km (7 to 30 mi). They are characterized by great sinuosity but they also tend to branch in en echelon patterns (fig. 3). For example, branching is well-developed along the East Kaibab Monocline. This includes the prominent northwest-trending Phantom-Grandview branch which splays from the main fold, and the Fossil-Monument-Eremita branch which is a weakly-developed detached western extension that is segmented with intervening gaps exhibiting no discernible deformation. Such changes in the trend and the complicated branching are linked directly in outcrops on the floor of Grand Canyon to Precambrian fault patterns which have been reactivated (Huntoon 1993).

Most segments of Grand Canyon monoclines are developed in the Paleozoic section over a single, high-angle reverse fault in the Precambrian basement (Huntoon 2003) (fig. 4). Laramide displacements are along the faults, and generally produced abrupt offsets at the top of the Precambrian basement. The dips of the faults are typically between 60° and 70°, dipping to the west. In profile, the anticlinal and synclinal axial surfaces in the monoclines converge downward on, and terminate against, the underlying faults at or below the Precambrian-Cambrian contact. Consequently, the dips of the strata increase and the widths of the folds decrease with depth in the monoclines. The heights to which the faults propagated into the overlying Paleozoic strata are proportional to the offsets at the Precambrian-Cambrian contact. The displacements on the faults gradually attenuated with elevation largely through apparent ductile deformation of the Paleozoic rocks so that they rarely extend above the top of the Supai Group. Deformation in close proximity to the faults at the cores of the monoclines includes (fig. 4):

(1) minor horizontal shortening folds and kink bands in the footwall block,
(2) highly localized drag-folding adjacent to the fault surface, and
(3) numerous conjugate sets of minor thrust faults.

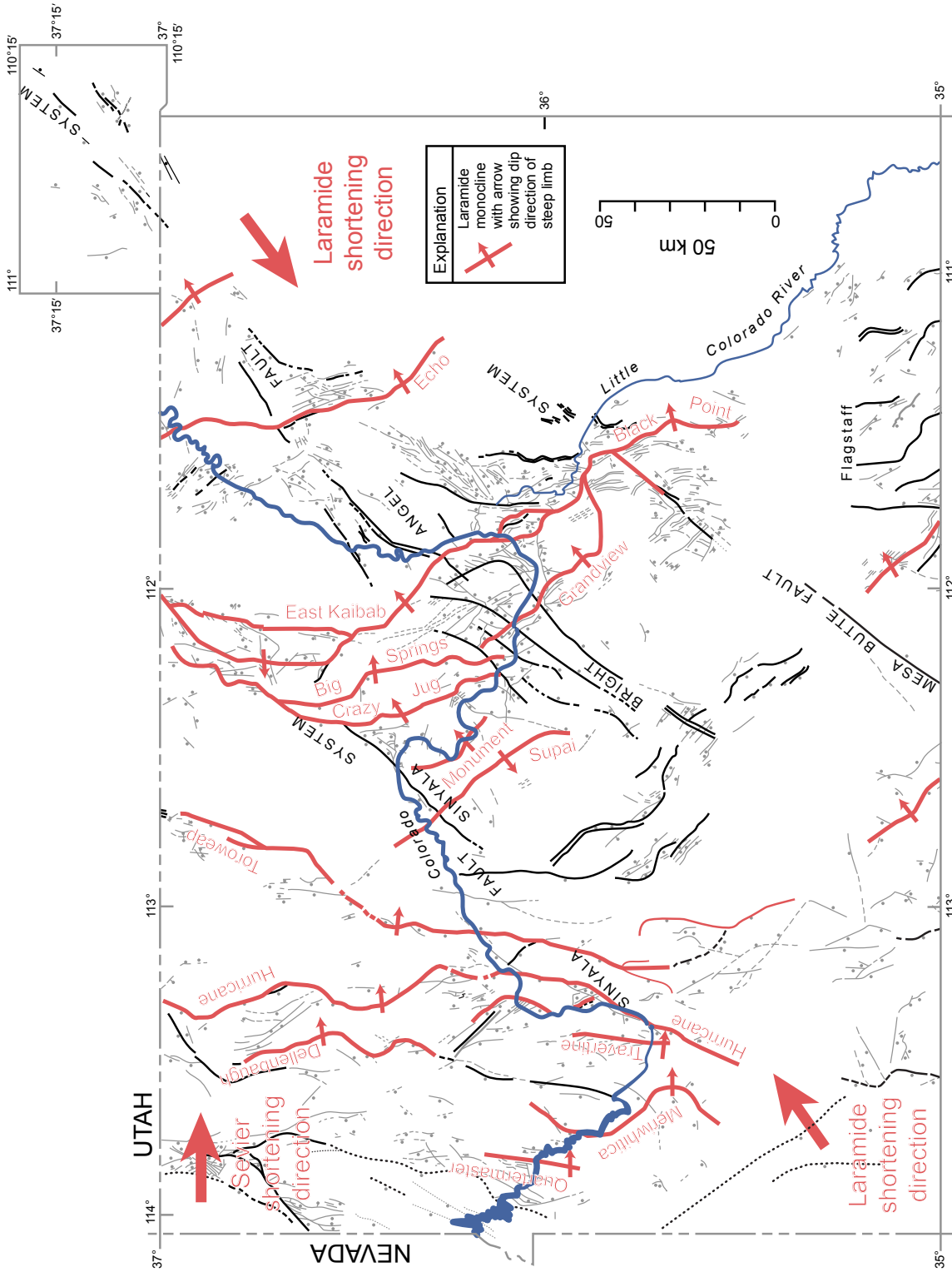

Fig. 3. Laramide compressional deformation of the Grand Canyon region that caused earlier normal faults in the Precambrian basement rocks to be inverted as a result of that reactivation into reverse faults and to be linked together into complex, segmented and bifurcating monoclinal uplifts of the Paleozoic sedimentary strata draped over them (after Karlstrom and Timmons 2012).

Shortening across a monocline at all levels is equal to the heave of the Precambrian-Cambrian contact across the underlying reverse fault (Huntoon 2003).

Where the Paleozoic rocks were deposited directly on the crystalline basement rocks, the strength of the unfaulted crystalline rocks tends to be isotropic, being the same regardless of direction prior to failure. In contrast, the Grand Canyon Supergroup sedimentary strata are highly anisotropic as a result of their bedding, especially in the Chuar Group. However, the Paleozoic beds in the monoclinal limbs can be strongly thinned owing to slip on bedding planes and braided networks of minor faults, and, with continued slip, can even be overturned and mimic the dips of the master faults (Karlstrom and Timmons 2012).

Monocline profile variations are most easily observed by the degree of folding of the Precambrian-Cambrian contact in the hanging wall block, as well as by the level within the fold where the anticlinal axial surface converges on the reactivated fault. An ideal monocline is one developed over a single reactivated fault that dips at 60° and is contained wholly within isotropic, rigid, crystalline rocks. Reactivation of the fault under the monocline produced a step-like offset at the Precambrian-Cambrian contact (fig. 4a). Both the anticlinal and synclinal axial surfaces in the overlying fold converge downward on the intersection between the Precambrian-Cambrian contact and the fault surface on the respective sides of the structure. Thus, the Precambrian-Cambrian contact remains planar, and the fold does not extend down into the Precambrian crystalline basement.

In contrast, the Precambrian-Cambrian contact in the hanging wall is folded downward toward the reactivated fault in locations where Grand Canyon Supergroup strata are preserved in the hanging wall block (fig. 4b). Dips of the contact in the hanging wall block adjacent to the fault range up to 20°. The degree of flexing and setback of the anticlinal hinge from the fault increase in proportion to the thickness of the underlying Supergroup section. This variant is a function of the considerably greater ductility of the Grand Canyon Supergroup sedimentary strata in contrast to the rigidity of the crystalline rocks. The Precambrian-Cambrian contact in the footwall block remains essentially planar until it very closely abuts the reactivated fault regardless of whether sections of the Supergroup strata are present in the footwall block. Consequently, the synclinal axial surface always converges on the intersection between the contact and the fault surface in the footwall block in the monoclines.

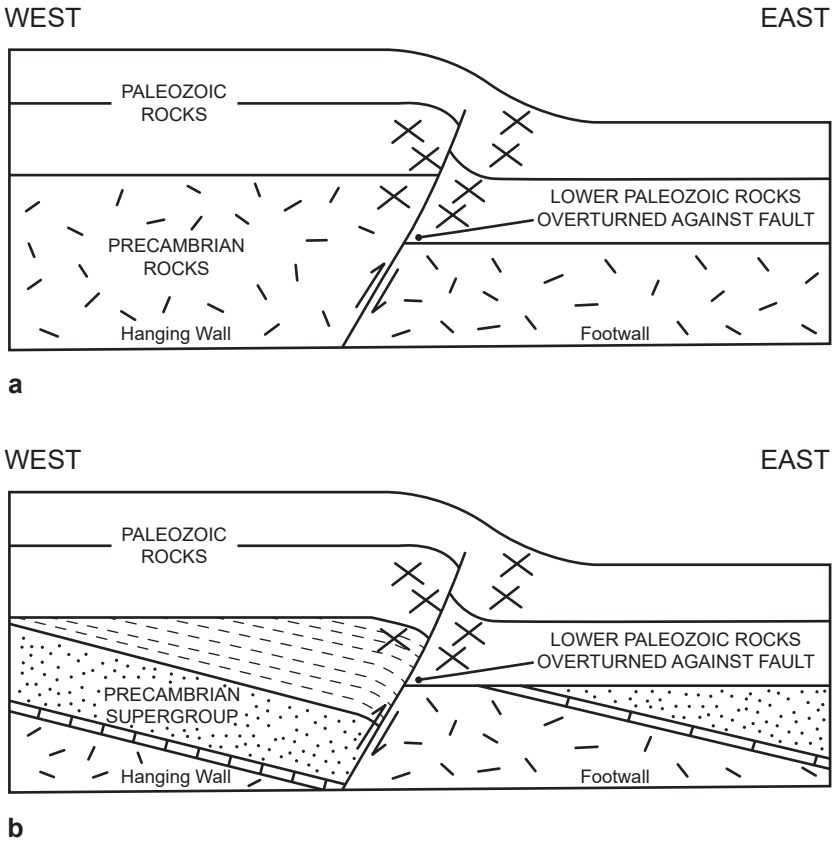

Fig. 4. Idealized composite profiles of Grand Canyon monoclines contrasting with and without the ductile Precambrian Grand Canyon Supergroup in the hanging wall of the underlying reactivated fault (after Huntoon 2003). Small crosses represent small-scale conjugate thrust faults. (a) Precambrian crystalline rocks in the hanging wall. (b) Precambrian sedimentary strata in the hanging wall.

The stress regime responsible for the development of the monoclines involved east-northeast-oriented maximum principal stresses and vertical minimum principal stresses, typical of the Laramide orogeny (Huntoon 2003). Orientations of the maximum principal stresses have been deduced from conjugate shear fractures in both Precambrian and lower Paleozoic rocks at numerous locations along the monoclines (Huntoon 1993). According to Huntoon (2003) conjugate shears occur at all scales from microscopic (for which he provided no photomicrographs as evidence) to mesoscopic, and they appear as intersecting second-order thrust faults. In contrast to the second-order thrusts, the basement failed along steeply dipping first-order Precambrian normal faults that were already in place. These preexisting faults accommodated Laramide strain by inverting their throw direction, becoming reverse faults. The presence of these weaknesses rendered the rocks anisotropic, which destroys the ideal relationship between the principal stress and fracture orientations predicated by Hubbert (1951). Consequently, the dips of the reactivated faults in the basement rocks do not reveal exclusive information about the Laramide stress regime.

It is difficult to establish the timing for the inception of monoclinal folding in the Grand Canyon using stratigraphic evidence because the Late Cretaceous section has been eroded from the region. However, Late Cretaceous rocks containing unconformities are present in the southern high plateaus of Utah and elsewhere in the Rocky Mountains region, and these establish a Maastrichtian initiation for Laramide deformation (Anderson et al. 1975; Dickinson et al. 1987). It is assumed that the Grand Canyon region was undergoing concurrent uplift. The beveling of some Grand Canyon monoclines indicates they were developing concurrently with the regional upwarping that produced similar unconformities in Utah.

An analysis of apatite fission-track thermochronology data collected from Grand Canyon rocks led Naeser et al. (1989) to conclude Laramide uplift and monoclinal folding commenced about 60 million years ago followed by a second pulse of uplift beginning in Late Eocene time between 40 and 35 million years ago, younger than most of the Laramide deformation. Dumitru, Duddy, and Green (1994) also interpreted their apatite fission-track thermochronology data as recording two phases of cooling of Grand Canyon rocks, one during the Laramide deformation at 70Ma, and another at 50–30Ma. Flowers, Wernicke, and Farley (2008) used apatite (U-Th)/He thermochronology data to constrain the <70°C cooling history of eastern Grand Canyon as denudation occurred during and after the Late Cretaceous-Cenozoic Laramide orogeny with a more recent cooling event occurring after ~25Ma. Kelley and Karlstrom (2012) added further apatite fission-track thermochronology data for Paleozoic strata of eastern Grand Canyon and likewise concluded exhumation occurred during the Late Cretaceous (90–70Ma) part of the Laramide deformation event, followed by further exhumation at ~25–17Ma. These findings are consistent with the timing of tectonism deduced from the incomplete stratigraphic record at Grand Canyon.

The East Kaibab and Hurricane Monoclines

One of the largest monoclines in the Colorado Plateau is the East Kaibab Monocline, named by Powell after the Native American word "Kaibab," which means "mountain buried below" (Reches 1978a). The East Kaibab Monocline structure is ~300km (~190mi) long, and is composed of flexures, folds and faults (figs. 3, and 5–7). Its exposure changes laterally from a smooth flexure to a fault to a combination of fault and flexure. It trends generally north-south from the Bryce Canyon area, Utah, to San Francisco Peaks, Arizona, but locally trends east. The maximum offset along the East Kaibab Monocline is at least 750m (~2,500ft), the most of any Grand Canyon monocline (Huntoon 2003), while its vertical displacement ranges up to 1,200m (~3,935ft) (Reches 1978a).

The East Kaibab Monocline is conspicuously sinuous like so many of the Grand Canyon monoclines, being systematically curvilinear as a composite of north-northwest- and north-northeast-trending segments (Davis 1978). Branching is also well-developed along the East Kaibab Monocline, with the prominent Phantom-Grandview branch and the weakly-developed detached Fossil-Monument-Eremita branch that is segmented with intervening gaps exhibiting no discernible deformation (fig. 3) (Huntoon 2003).

The Colorado River, Grand Canyon and their tributaries or side canyons cut through the East Kaibab Monocline and provide three-dimensional exposures for about 30km (~19mi) along the structure (Reches 1978a). The Butte Fault is intermittently exposed beneath the flexure for about 18km (~11mi), providing opportunities to study the fault-fold relations also. Fig. 7 depicts the geologic history of the Butte Fault that underlies the East Kaibab Monocline. West of Lava Chuar Hill, the East Kaibab Monocline splits into two branches, one of which continues southward, and the second of which trends southeastward into Palisades Creek (fig. 3). About 4km (~2.5mi) of the first branch appears as the Butte Fault in Precambrian units. Some remnants of the overlying Paleozoic strata indicate that this segment of the Butte Fault was not active

Fig. 5. The East Kaibab Monocline: (a) As seen overhead from an aircraft. In the middle and to the left in the photo can be seen where a tributary in a side canyon of the Colorado River has cut through the monocline. In the left foreground can be seen the dipping Kaibab Formation limestone layers that form the rim rock of the Grand Canyon. (b) As seen from ground level, looking north from highway 89A. Again, the dipping Kaibab Formation limestone layers can be seen.

Fig. 6. The Carbon Canyon fold in which beds of the Tapeats Sandstone have been folded (bent) through ~90° adjacent to the Butte Fault. Carbon Canyon is a side canyon to the Colorado River corridor at river mile 65 and the fold is exposed best in the southern wall of the side-canyon about 2 km (about 1.2 mi) from the river. The man who is ~1.8 m (6 ft) tall standing on the fold provides the scale.

after Precambrian time (Walcott 1890, 56). The second branch is now known as the Palisades Fault because it lies along Palisades Creek, where one can observe the transition from fault to continuous flexure in the Paleozoic strata. The two branches of the East Kaibab Monocline rejoin southeast of Desert View (fig. 3).

The thicknesses of the Cambrian through Pennsylvanian strata (Tapeats Sandstone through the Supai Group) between the anticlinal and synclinal axial surfaces in the East Kaibab Monocline are attenuated between 30 and 60% (Huntoon 2003), that is, the strata thin in the limbs. This contrasts with comparatively gentle dips of less than 15° with virtually no attenuation at the level of the Permian strata (Hermit through Kaibab Formations). Those Permian strata occupying the anticlinal hinge are rarely thinned by brittle failure in the form of downward propagating grabens because of space-compensating horizontal shortening across the monocline. The Precambrian-Paleozoic contact in the footwall block to the east of the East Kaibab Monocline is broadly flexed for the ~5–8 km (~3–5 mi) in the area immediately north of Grand Canyon. The flexing adds ~300 m (~1,000 ft) of structural relief to the fold where it is best developed (fig. 7). Furthermore, the Precambrian-Paleozoic contact in the hanging wall is folded down toward the reactivated, west-dipping Precambrian Butte Fault, with dips up to 20 degrees adjacent to the fault, in locations where the Grand Canyon Supergroup strata are preserved in the hanging wall block.

Reches (1978a) used a variety of stress indicators to determine that the average orientation of the maximum principal stress was N76°E along the Palisades segment of the East Kaibab Monocline. His analysis used stress orientations deduced from the Paleozoic strata from calcite twinning, minor faults, kink bands, and minor folds.

Davis and Tindall (1996) deduced that there had been a component of right-lateral strike-slip motion along the Precambrian basement fault underlying the northern part of the East Kaibab Monocline. Their findings were based on the orientations and motions along minor faults in the Cretaceous strata within the fold. They estimated that lateral slip was as much as three times the vertical offset at that location, consistent with the motion expected along

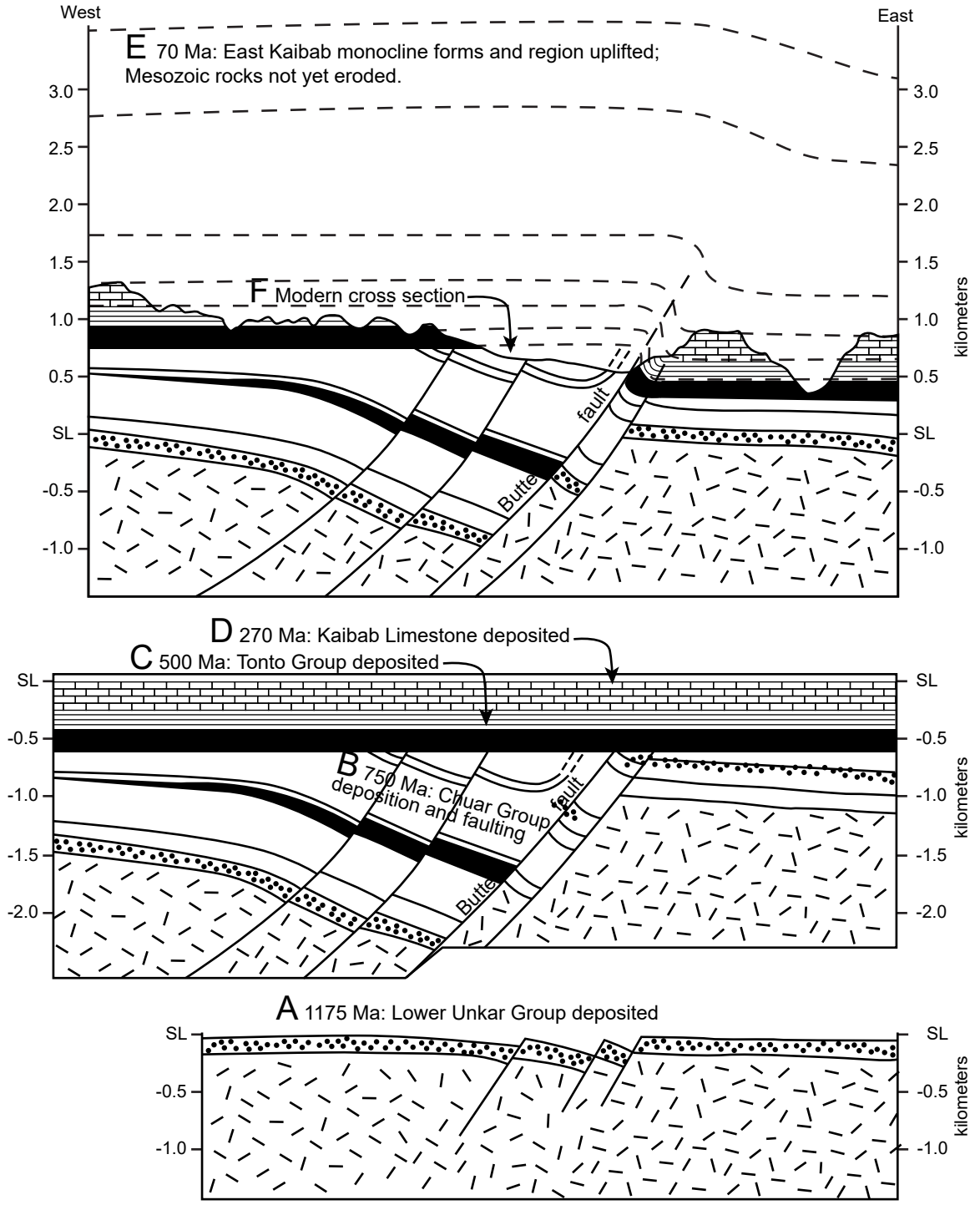

Fig. 7. The history of the Butte Fault, eastern Grand Canyon, illustrating the fault reactivation that produced the Carbon Canyon and other related folds along its length. (a) Between 1200 and 1100 Ma, lower Unkar Group sedimentary strata (dot pattern) were deposited and tilted owing to normal faulting of them and the underlying Paleoproterozoic crystalline basement rocks on northwest-striking faults like the Palisades Fault, a branch of the Butte Fault. (b) By 742 Ma, Chuar Group sedimentary strata had been deposited, folded, and faulted owing to west-side-down movement on the Butte Fault. (c) Deposition of the Cambrian Tonto Group sedimentary strata (black band) took place by 500 Ma on top of the Great Unconformity over the tilted Grand Canyon Supergroup strata. (d) The region remained near sea level throughout the deposition of the Paleozoic strata, ending c.270 Ma with deposition of the Kaibab Limestone (brick pattern). (e) By 70 Ma, the region was compressed and uplifted, and the Butte Fault was reactivated with west-side-up slip to create the East Kaibab Monocline, with the ~2 km (~6,560 ft) of Mesozoic strata that once covered the region (dashed lines). (f) Present topographic profile shows the west-side-down net displacement of the Proterozoic rocks of the Butte Fault, but west-side-up displacement of the Paleozoic strata.

a reactivated basement fault that was not oriented perpendicular to the minimum principal stress.

The history of tectonic activity along the East Kaibab Monocline was outlined by Walcott (1890) in a study on the eastern Grand Canyon. According to Walcott, movement along the trend of the East Kaibab Monocline began in the Grand Canyon region as a Precambrian fault, downthrowing older, "Algonkian" strata on the west from 15 to 1,500 m (~49 to ~4,920 ft). During the late Paleozoic, the sense of displacement on the Precambrian basement fault reversed and an eastward-facing monoclinal fold was formed, displacing strata a few tens of meters. The same sense of movement resumed during the Cenozoic, producing the East Kaibab Monocline and the accompanying faults. The net displacement aggregated more than 900 m (~2,950 ft) in the vicinity of Grand Canyon.

In contrast, there have been no published investigations of the Hurricane Monocline in western Grand Canyon, except for the mapping of it (Billingsley and Wellmeyer 2003) (fig. 8). It is a totally separate north-south-trending monocline associated with, and developed above, the adjacent Hurricane Fault, and it bifurcates southward into two parallel branches (Huntoon 2003) (fig. 3). Changes in the trends of the monoclines and the complicated branching are linked directly in outcrops on the floor of Grand Canyon to Precambrian fault patterns demonstrating they were reactivated during the Laramide orogeny (Huntoon

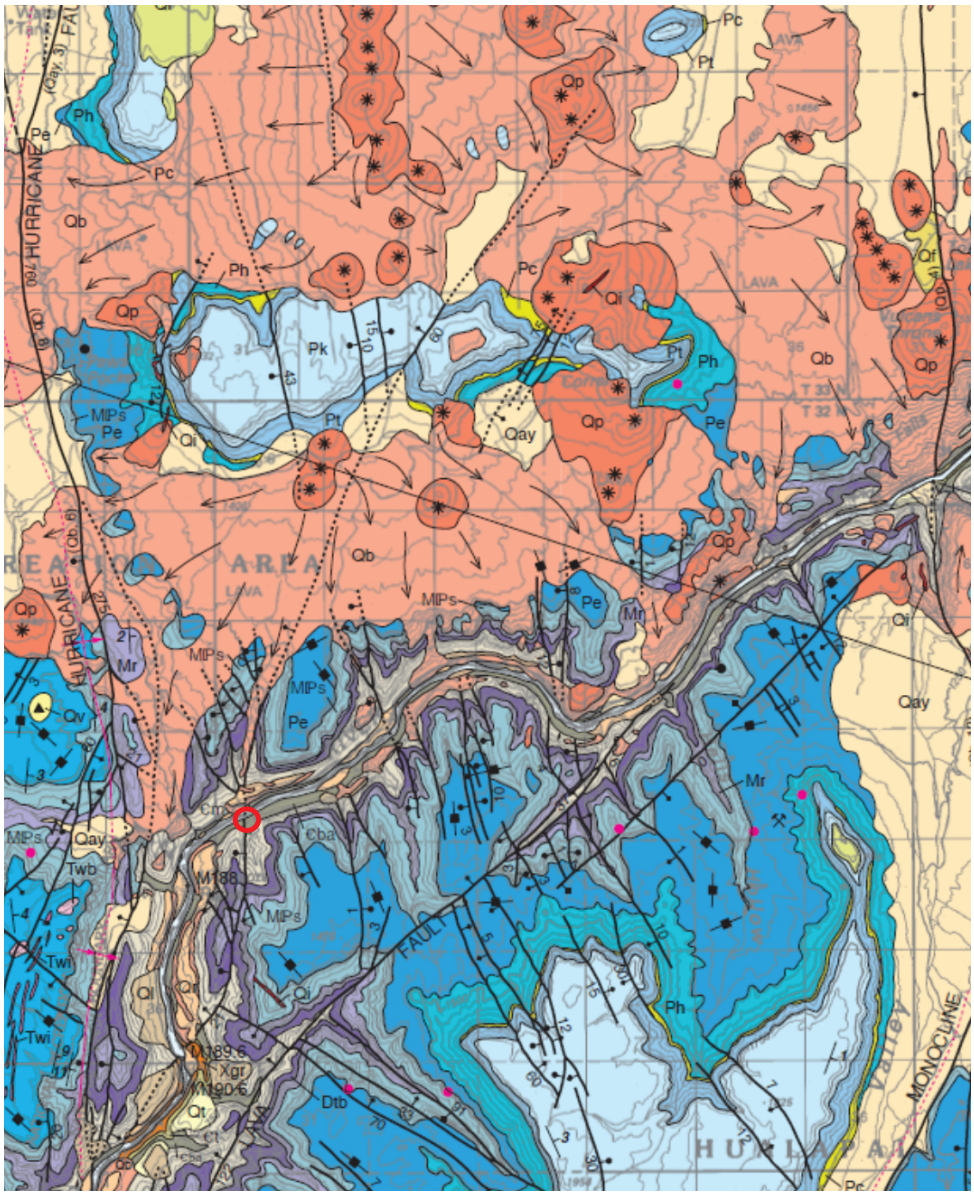

Fig. 8. Geologic map of the Whitmore Helipad fold area in the western Grand Canyon (from Billingsley and Wellmeyer 2003). The location of the Whitmore Helipad fold in the Bright Angel Formation at river mile 187.4 is marked. The north-south-trending Hurricane Fault is accompanied in parallel by the Hurricane Monocline. Both cross the Colorado River to the west of the Whitmore Helipad fold which sits on a branch fault to the Hurricane Fault.

1993). Just east of the Hurricane Fault and monocline and paralleling it where they cut across the Colorado River corridor is the Toroweap Fault and monocline (figs. 3 and 8).

The East Kaibab Monocline marks the eastern boundary of the Kaibab Plateau in eastern Grand Canyon, whereas the Hurricane Monocline is within the Kaibab Plateau in western Grand Canyon, about 120 km (~75 mi) to the west and close to the western edge of the plateau (fig. 3). The Hurricane Monocline, like most other segments of Grand Canyon monoclines, is developed in the Phanerozoic strata over a single, high angle reverse fault in the Precambrian basement which is not exposed within the Canyon where it crosses it (Huntoon 2003; Karlstrom et al. 2003) (figs. 4a and 8). However, unlike the Butte Fault underlying the East Kaibab Monocline, the Hurricane Fault underlying the Hurricane Monocline is contained mostly within the rigid, isotropic Precambrian granitic rocks that directly underlie the Great Unconformity (Billingsley and Wellmeyer 2003; Ilg et al. 1996; Karlstrom et al. 2003). And unlike the adjacent Toroweap Fault, which significantly displaces the overlying Tonto Group and other Phanerozoic strata, the Hurricane Fault minimally penetrates them (Billingsley and Wellmeyer 2003) (fig. 4a). This could be due to the position of this fault within Kaibab Plateau. The Hurricane Fault is at least 170 km (105 mi) long in the Canyon area (Karlstrom and Timmons 2012) (fig. 3), but it extends northwards at least another 100 km (60 mi) to St. George, Utah (Stewart et al. 1997). The vertical displacement on the Hurricane Fault in the Canyon area varies along this length from 195 m (~640 ft) in the north to 550 m (~1,805 ft) to the south (Billingsley and Wellmeyer 2003), much less than up to 1,200 m [~3,935 ft] vertical displacement of the Butte Fault. Thus, the Phanerozoic strata in the Hurricane Monocline mostly just drape over the Hurricane Fault, as depicted in fig. 9.

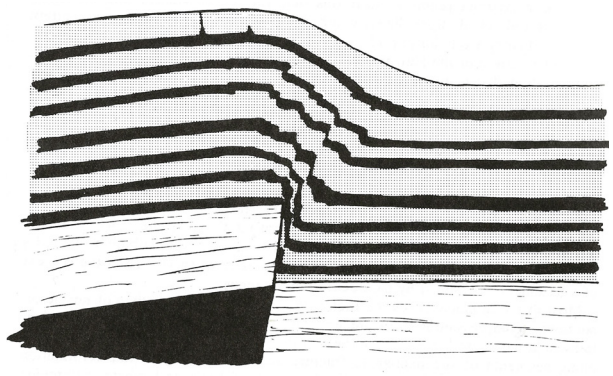

Fig. 9. Simulated development of a monoclinal flexural fold over a re-activated Precambrian basement fault, as happened along the Hurricane Fault to produce the Hurricane Monocline in the western Grand Canyon (after Davis 1978).

The Whitmore Helipad Fold

The prime example of the folds investigated is the folding of the Cambrian Tapeats Sandstone (Middleton and Elliott 2003; Snelling 2021a) where those sandstone beds were dragged upwards into, against and by the Butte Fault at the synclinal hinge of the East Kaibab Monocline in eastern Grand Canyon during the Laramide orogeny (Huntoon 2003; Karlstrom and Timmons 2012). The best exposed fold in this system is in Carbon Canyon (Snelling 2023a) (fig. 6), a side canyon to Grand Canyon through which flows Carbon Creek, a tributary of the Colorado River at river mile 65 from Lees Ferry (fig. 1). Another prominent fold in the Tapeats Sandstone is the Monument fold produced by the vertical displacement of the Monument Fault along and underneath the Monument Monocline (Snelling 2023b) (figs. 1 and 3).

The overlying Bright Angel Formation is likewise bent in both those folds, but exposures are poor and are not readily accessible. However, a small fold in the Bright Angel Formation is exposed and accessible in the cliff above the banks on southern side of the Colorado River (river left) in western Grand Canyon adjacent to the Whitmore Helipad at river mile 187.4 from Lees Ferry (figs. 1, 8, and 10). Although this Whitmore Helipad fold does not sit directly on either the Hurricane Fault or Monocline, it coincides with a branch fault that splays north-northeasterly from the Hurricane Fault where it crosses the Canyon and the Colorado River a few miles downstream (Fig. 8). Therefore, the generation of this fold would still appear to be related to the movements on the Hurricane Fault and thus the Hurricane Monocline that are claimed to have occurred during the Laramide orogeny and thereafter (Karlstrom and Timmins 2012). However, that occurred a very long time after the Cambrian deposition of the Bright Angel Formation, yet the character of the shale, siltstone, and sandstone beds all appear to be consistent with soft-sediment deformation soon after deposition hundreds of millions of years earlier.

The Whitmore Helipad fold is a very tight fold with very little mechanical crowding of the constituent relatively thin shale, siltstone, and sandstone beds in the Bright Angel Formation, but there is some small offsetting along two fault lines associated with the two hinge zones (fig. 10). Yet in spite of those two minor faults through the hinge zones, the shale, siltstone, and sandstone beds appear to have been bent smoothly when still soft, the faulting potentially having occurred subsequently after the folding and their lithification. This mixture of lithologies of variegated colors matches the heterolithic facies sequence described by Martin (1985). The Tapeats Sandstone is not mapped as exposed beneath the

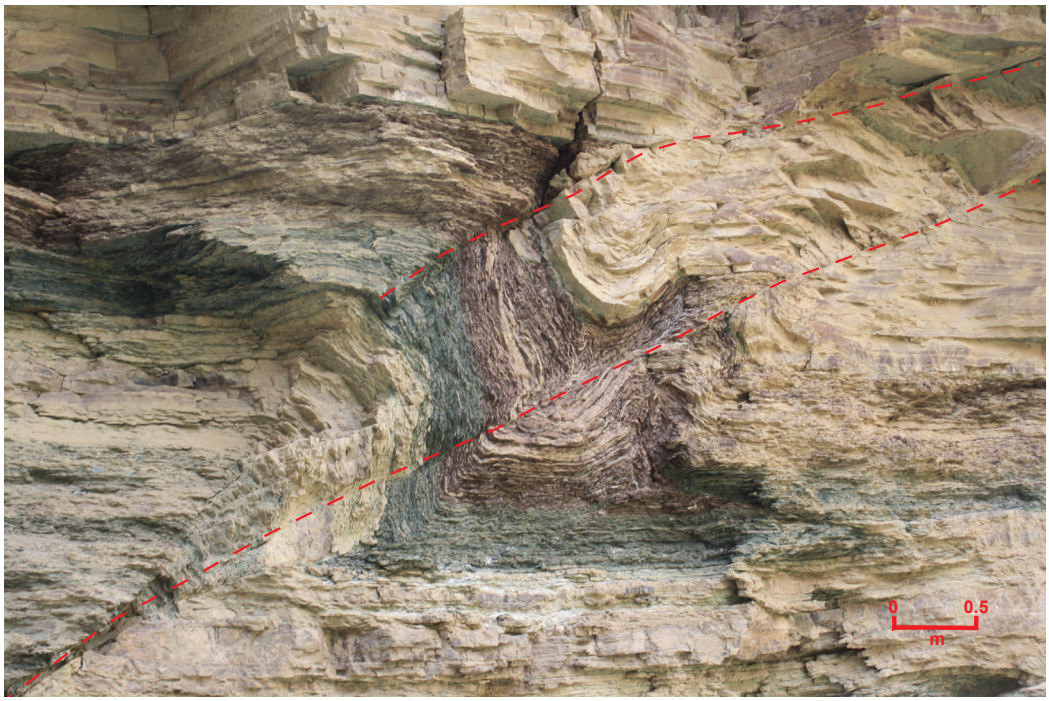

Fig. 10. The Whitmore Helipad fold at river mile 187.4, river left, in which sandstone, siltstone, and shale beds of the Bright Angel Formation are bent monoclinally with two hinge zones through which the beds were subsequently faulted with minimal offsets. The faults have been marked and scale is indicated.

Bright Angel Formation in the Whitmore Helipad fold or in its vicinity for miles upstream and downstream, so the stratigraphic level of the Bright Angel Formation in the Whitmore Helipad fold must be well above the transition zone with the Tapeats Sandstone.

In commenting on the Carbon Canyon fold, Hill and Moshier (2009) claim that evidence from field studies and rock deformation experiments demonstrate that these solid rocks behaved in a ductile manner as the Tapeats Sandstone beds in that fold were deformed slowly under great stress, and that the beds thus were "bent" by microscopic re-orientations of mineral grains and by changes in bedding thickness along the fold. They then reference Huntoon (2003) to state that these tight folds in beds of the Tapeats Sandstone in Carbon Canyon can be explained by mechanical crowding at the synclinal hinge of the East Kaibab Monocline during slow deformation under stress of the solid sandstone in a ductile manner. Because the Bright Angel Formation sandstone, siltstone, and shale beds directly overlie the Tapeats Sandstone, Hill and Moshier (2009) would undoubtedly explain their bending in the Whitmore Helipad fold as due to the same processes and mechanisms.

However, Hill and Moshier (2009) offer no supporting evidence of these claims about the bending of the Tapeats Sandstone beds in the Carbon Canyon fold. They provide no documentation of the quoted rock deformation studies, nor any evidence from any thin section examination of the Tapeats Sandstone from the Carbon Canyon fold of the claimed microscopic reorientations of mineral grains. And the only documentation they provide of any field studies is a single photograph of the vertical beds of the Tapeats Sandstone at the Carbon Canyon location, but not of the folded beds showing the mechanical crowding. For that they refer to Huntoon (2003), but his field photograph, while showing the bent Tapeats Sandstone beds at the Carbon Canyon location, is incorrectly labeled as the south wall of Chuar Canyon, when it is in fact the south wall of Carbon Canyon. Furthermore, Huntoon (2003) also did not provide any thin section evidence for any reorientation of mineral grains.

Subsequently, Tapp and Wolgemuth (2016) similarly focused on the Carbon Canyon fold. They showed a photo of the fold (their fig. 12-13), describing it as compressional folding in the Tapeats Sandstone (reproduced here in fig. 11). On an overlay they traced some of the sandstone beds through the fold, some of the fractures, and the apparent changing direction of the fold hinges, which they claimed to be due to flexural slippage. They claimed that the bending resulted in numerous fractures in each sandstone bed that did not heal (reseal). They then illustrated what flexural slippage would look like in two hypothetical folds (their fig. 12-14), describing how flexural slippage creates gaps in the fold hinges that may be filled in later with weathered material or weaker rock may deform into the spaces (fig. 12). Either way, the layering in the fold hinges should

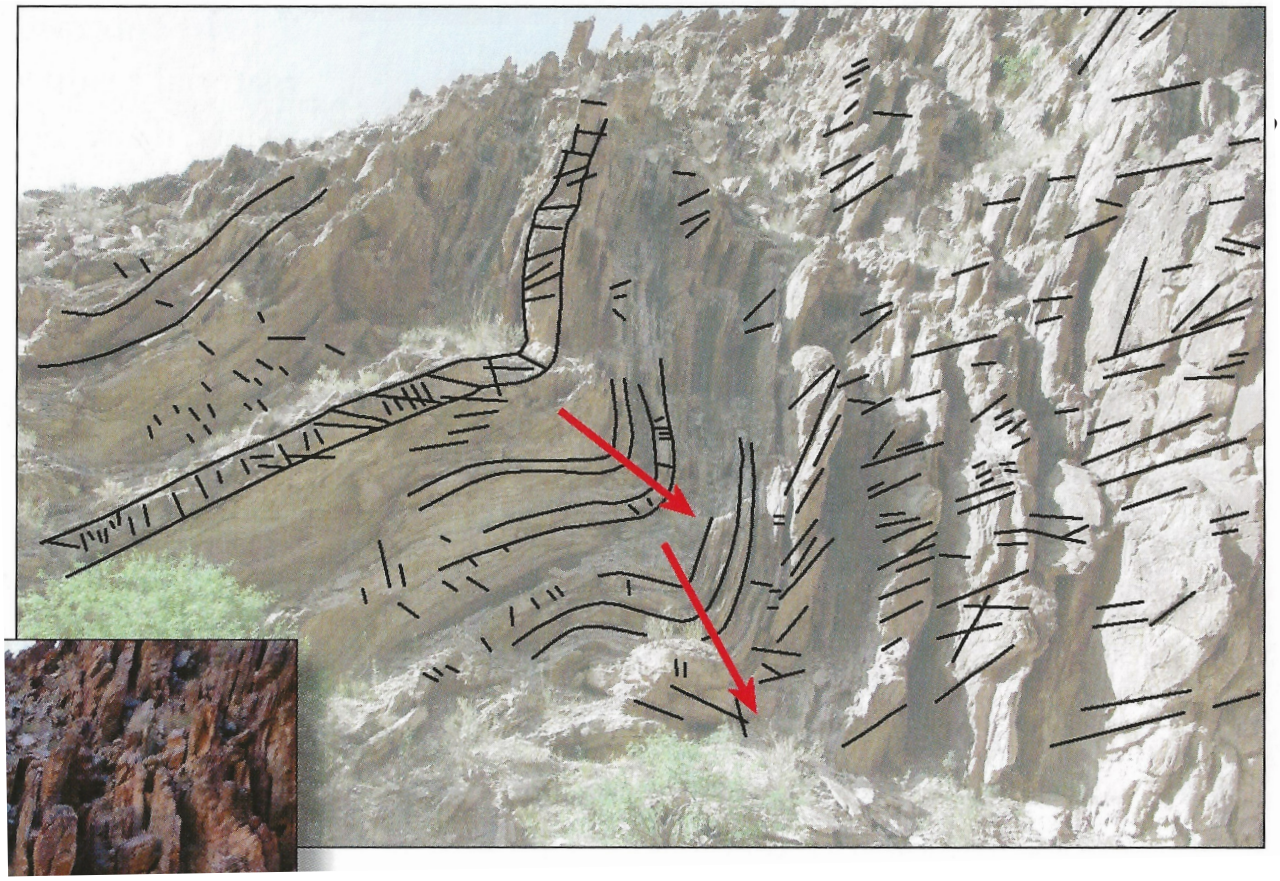

Fig. 11. The Carbon Canyon fold in the eastern Grand Canyon with overlaid annotations (after Tapp and Wolgemuth 2016, fig.12-13). Their annotations show traces of some of the sandstone beds, some of the fractures, and their interpretation of the changing direction of the folds apparently resulting from bedding plane or flexural slippage.

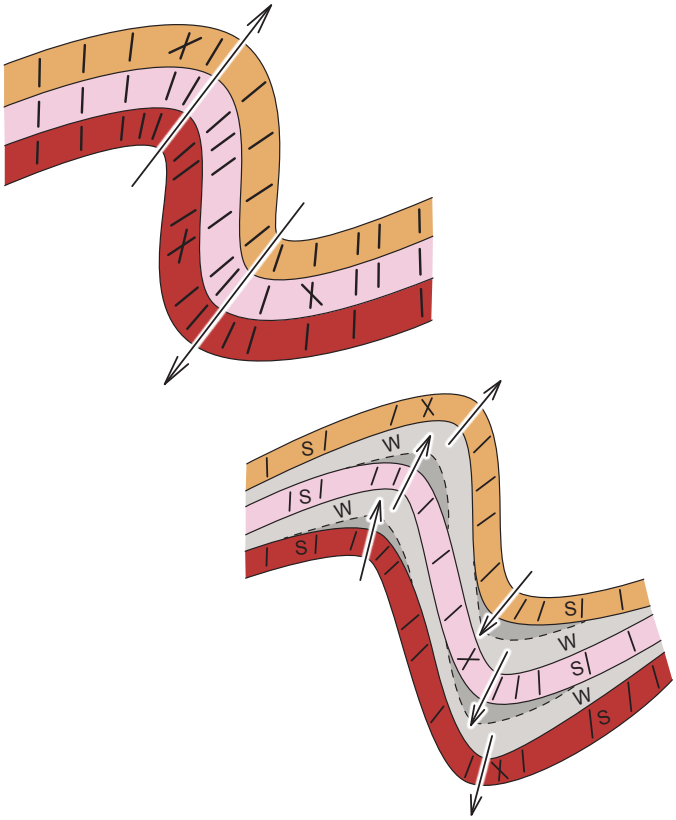

Fig. 12. Folding from two scenarios as presented by Tapp and Wolgemuth (2016, fig.12-14). (a) Rock layers all of equal strength. They maintain that compacted sediments will look similar, but without the fractures. (b) Rock layers of different strength (w=weak, s=strong). The dashed lines show bedding plane or flexural slippage filled with weaker rock.

be thicker relative to the widths of the sandstone beds along the fold limbs. They claimed that neither of these features would be present if this fold had occurred due to soft-sediment deformation. However, their photo of the fold shows no such thickening of the sandstone beds in the fold hinges, and they fail to discuss alternate explanations for the fractures, such as joints due to horizontal contraction within the beds during dewatering and lithification, and especially due to unloading caused by erosion of Grand Canyon and its side canyons. Similarly, there is no such thickening of the Bright Angel Formation sandstone, siltstone, and shale beds in the hinge zones of the Whitmore Helipad fold (fig. 10). There are the two faults through the two hinge zones in the Whitmore Helipad fold, with only trivial offsets, while the alternating thin brown shale and buff-colored sandstone beds in the lower hinge zone appear to have "flowed" upwards in that hinge zone in response to soft-sediment deformation. Thus, those two faults can be explained as due to horizontal contraction within Bright Angel Formation subsequent to the folding and after dewatering and lithification of these beds.

The Bright Angel Formation

Snelling (2021b) provided a detailed review of past investigations of the Bright Angel Formation, including its stratigraphy, trace fossils, sedimentary structures, U-Pb detrital zircon ages, provenance, and depositional environment. Additionally, based on the detailed petrographic study of his 12 samples collected from a fold and a location distal to it, Snelling (2021b) documented and described in detail the mineral grains and textures within the sandstone, siltstone and shale beds then discussed his findings to draw conclusions as to the petrology of the Bright Angel Formation.

The Cambrian Bright Angel Formation is the 82–137 m (325–450 ft) thick slope-forming formation that recessively outcrops in the middle of the Tonto Group across ~500 km in the walls of Grand Canyon, Arizona, and beyond (Elston 1989; Martin 1985; McKee 1945; Middleton and Elliott 2003; Noble 1914, 1922; Rose 2003, 2006, 2011). It is usually an integral component of the fining upwards lithologies of the Cambrian Tonto Group, which has been touted conventionally as the classic example of the time-transgressive "deepening seas" sedimentation model. Originally described as the Bright Angel Shale, it has been recently designated to formation status due to it consisting of only ~40% green fissile and strongly laminated shales, with the majority made up of ~30% crumbly and laminated siltstones, and ~30% sandstone beds which are often hard and ledge-forming. The Bright Angel Formation immediately overlies a transitional boundary to the Tapeats Sandstone, which mostly sits directly on a pronounced erosion surface known as the Great Unconformity (Karlstrom et al. 2018, 2020; Peters and Gaines 2012). The underlying rocks eroded at the Great Unconformity include granitic plutons intruded into the Granite Gorge Metamorphic Suite schists unconformably overlain by the tilted sedimentary strata and basalt layers of the Grand Canyon Supergroup, all dated as Precambrian (Ilg et al. 1996; Karlstrom et al. 2003). Both the correlated equivalents of the Bright Angel Formation and the Great Unconformity have been traced across several continents and around the globe, respectively (Clarey 2020; Clarey and Werner 2023; Peters and Gaines 2012).

Within the Bright Angel Formation well-preserved trilobites and some brachiopods are found in certain of the green fissile shales in some locations, and also a "hash" of unidentifiable fossil fragments is found concentrated locally elsewhere (Foster 2011; Martin 1985; McKee 1945; Resser 1945). In contrast, abundant trace fossils occur throughout the formation, primarily burrows and trails likely left by various worms and other invertebrates, and trails left by trilobites (Baldwin et al. 2004; Martin 1985; McKee 1932; Resser 1945). These are often found on megaripples and the tops of sandstone beds but are ubiquitous within the silty and muddy inter-laminae areas at the interfaces between sandstone beds and laminated silty shales. Abundant cryptospores of land plants and algae are present in the shales in the basal section of the formation, but surprisingly no spores of marine algae or pollen (Baldwin et al. 2004; Strother and Beck 2000, Strother et al. 2004; Taylor and Strother 2008). Some ledge-forming sandstone beds are conglomeratic, while most are variously cross-laminated (Martin 1985). The formation itself is well-bedded and the siltstones and shales strongly laminated. Detrital zircon grains extracted from the underlying Tapeats Sandstone have been U-Pb dated to determine the maximum depositional age of that formation and coupled with biostratigraphic trilobite faunal zones correlated globally have constrained the conventional age of the Bright Angel Formation to 502–507 Ma (early Middle Cambrian) (Karlstrom et al. 2018, 2020; Matthews, Guest, and Madronich 2018). Additionally, U-Pb dates obtained from detrital zircon grains extracted from the Bright Angel Formation potentially identify the provenance of its sediment grains (Gehrels et al. 2011). U-Pb age peaks among the detrital zircons matched the nearby Paleoproterozoic Yavapai and Mazatzal provinces, indicating the primary source of the sediment grains was the locally underlying granitic plutons and schists, plus a very small portion from the underlying

Grand Canyon Supergroup strata (though a long-distance transport of some grains cannot be entirely ruled out). The consensus conventionally-interpreted depositional environments for accumulation of the Bright Angel Formation are intertidal to subtidal shallow-marine environments (Martin 1985; McKee 1945; Rose 2003, 2006; Wanless 1973), yet it has been described as part of "one of the most dramatic global marine transgressions in Earth history" (Karlstrom et al. 2018).

Snelling (2021b) reported that quartz grains are the dominant component of the Bright Angel Formation, but bulk rock XRD analyses of the 12 samples studied demonstrated that K-feldspar features prominently, ranging from 11.0% to 46.9%. Various carbonates are present up to 32.4% and illite is ubiquitous, indicative of glauconite and muscovite. In thin sections, the sandstones are fine-grained and generally massive and well-sorted, dominated by angular to sub-rounded, coarse silt to fine sand-sized quartz grains. Many variously small-sized K-feldspar grains are scattered through the rock fabric, with occasional thin edge-on detrital muscovite flakes wedged between quartz and K-feldspar grains. Most samples contain small glauconite pellets and grains, and a few brachiopod shell fragments. There are virtually no original pores remaining, the rock fabric being cemented by silica as quartz overgrowths. The siltstones are very similar, but their grains are silt-sized and occasional patches are carbonate cemented. The shales consist of alternating thin illite (after K-feldspar) dominated laminae with scattered tiny quartz and K-feldspar grains and muscovite flakes, interstratified with thin laminae and "augen" of siltstone. There is no evidence, macroscopic or microscopic, of any metamorphic changes to the detrital mineral grains or textures.

Snelling (2021b) concluded that these mineral constituents of the Bright Angel Formation are consistent with the underlying local basement rocks being the sediment provenance, as indicated by the detrital zircon U-Pb ages. The rare presence of siltstone and shale fragments within the sandstones underscores the conclusion that transport was over a short distance and likely rapid. Indeed, due to the very short-distance rapid transport of the sediment and rapid deposition of the sandstones, siltstones and shales, K-feldspar grains and former laths are scattered randomly through the entire formation and are often angular or sub-angular, while the extremely soft detrital muscovite flakes have survived, sometimes bent with frayed ends. The strongly cross-laminated sandstone beds, including occasional hummocky cross-stratification, and the laminated siltstones and shales are consistent with rapid deposition by high-energy storm-like surges, which is consistent with observational evidence of spontaneous stratification during rapid deposition of heterogranular sediment mixtures and of mud floccules.

Oddly, numerous detrital zircon grains in the underlying Tapeats Sandstone yield U-Pb ages that are considerably younger than its designated depositional age (Karlstrom et al. 2018, 2020; Snelling 2021a). These coupled with the well-documented problems with the many assumptions undergirding the U-Pb dating method (Snelling 2000, 2009, 2022b), and the evidence of past grossly accelerated nuclear decay rates (Vardiman, Snelling, and Chaffin 2005), totally undermine the validity of the conventional age for the Bright Angel Formation. Instead, Snelling (2021b) found that when combined, the mineralogical content, textural features, sedimentary structures, the continental-scale deposition, the invertebrate fossils and fragments, and even the tracks and traces of transitory invertebrates that had to be buried and fossilized rapidly, are all consistent with the catastrophic erosion of the Great Unconformity near the onset of the global Genesis Flood cataclysm about 4,350 years ago and the hurricane- and tsunami-driven rapid short-distance transport and deposition of the Bright Angel Formation within the fining upwards Sauk megasequence in the first few days or weeks of that year-long event.

Folding Mechanisms in Folds

It has been claimed that the Tapeats Sandstone was bent in the Carbon Canyon fold by ductile deformation (Hill and Moshier 2009; Huntoon 2003; Tapp and Wolgemuth 2016). By ductile deformation they presumably mean continuous deformation at the scale of observation in which the rock flowed under the influence of stress without macroscopic fracturing (Fossen 2016). They make no mention of any possible accompanying metamorphism due to elevated temperatures at the depth of burial. As summarized by Paterson (2001), ductile flow of rocks can occur by the following three mechanisms:

(1) change of shape of grains by crystal plasticity, which is referred to as dislocation creep,
(2) change of grain shape by diffusion through or around grains, called diffusion creep, and
(3) relative movement of grains, referred to as granular flow or grain-boundary sliding.

In (3), in order to minimize the formation of voids (dilatancy), the grains must change their shapes by mechanism (1) or (2). Except for these local accommodations, very large strains may be achieved without change of overall grain shape, as in "superplastic flow" in very fine-grained aggregates.

Thus, where folding of sedimentary rock units has occurred subsequent to their diagenesis and

deep burial, ductile deformation during folding of the otherwise brittle rock can be facilitated by grain-boundary sliding and bedding-plane slip and attenuation. The role of grain-boundary sliding has been thoroughly investigated theoretically, experimentally and in field situations, and the resulting macroscale and microscopic features of rock textures and mineral grain characteristics are well documented (Bestmann and Prior 2003; Billia et al. 2013; Etheridge and Wilkie 1979; Gratier et al. 2011; Hansen, Zimmerman, and Kohlstedt 2011; Hippertt 1994; Hiraga et al. 2013; Jackson, Faul, and Skelton 2014; Langdon 1970; Lee and Morris 2010; Lee, Morris, and Wilkening 2011; Massey, Prior, and Moecher 2011; Menegon et al. 2015; Morris and Jackson 2009; Ree 1994; Sundberg and Cooper 2010; Vernon 2018, Watanabe et al. 2013; Wojtal, Blenkinsop, and Tikoff 2022). Similarly, bedding-plane slip and attenuation have been demonstrated to facilitate folding without brittle fracturing, being simulated with numerical modeling and well-studied in laboratory and field settings (Becker 1994; Behzadi and Dubey 1980; Borja, Sama, and Sanz 2003; Chapple and Spang 1974; Cooke and Pollard 1997; Cooke et al. 2000; Cooke and Underwood 2001; Couples and Lewis 1999; Crook et al. 2006; Epard and Groshong 1995; Horne and Culshaw 2001; Hughes and Shaw 2015; Kuenen and de Sitter 1938; Nino, Philip, and Chéry 1998; Ramsay 1974; Roth, Sweet, and Goodman 1982; Sanz et al. 2008; Suppe 1983; Suppe and Medwedeff 1990; Tanner 1989).

Furthermore, the pressures inherent in the folding process have also been shown to cause elastoplasticity and visco-elastic compression of the particle matrices within sedimentary rocks which facilitates accommodation of the volume changes in the hinges and limbs of the resultant folds (Benesh et al. 2007; Borja 2006; Cundall and Strack 1979; Erickson and Jamison 1995; Guiton, Leroy, and Sassi 2003; Matsuoka and Nakai 1974; Mühlhaus et al. 2002; Sanz, Borja, and Pollard 2007; Simo and Taylor 1985). The effects of all of these processes on the rock fabric and texture, and on the rock matrix and its mineral grains, can be observed and documented in the outcropping folds and under the microscope in rock sections.

Rock deformation laboratory studies have demonstrated that solid rock can deform in a ductile manner slowly under stress (Davis and Reynolds 1996; Friedman et al. 1976; Friedman, Hugman, and Handin 1980; Gangi, Min, and Logan 1977; Ghosh 1968; Griggs 1936, 1939; Handin et al. 1976; Weinberg 1979), but mechanical crowding and thinning of sandstone, siltstone, or shale beds at the macroscopic scale is not definitive proof that folding occurred slowly under stress as if those lithified beds were deformed in a ductile manner. It is also readily demonstrated in such laboratory studies that beds of soft sand, silt, and mud will similarly be crowded and thinned mechanically when deformed while still soft due to the confining pressures in the hinges of the folds (Borg and Maxwell 1956). Only if thin section examination of the sandstone, siltstone and shale reveals *deformation lamellae* and *undulose extinction* in the quartz grains under cross-polarized light due to deformation stress (Bailey, Bell, and Peng 1958; Carter 1971; Carter, Christie, and Griggs 1964; Christie and Ardell 1974; Christie, Griggs, and Carter 1964; Davis and Reynolds 1996; Fairbairn 1939; Groshong 1988; Hansen and Borg 1962; Hansen, Borg, and Maxwell 1959; Mitra and Tullis 1979; Tullis, Christie, and Griggs 1973; Twiss 1974, 1976; Whisonant 1970; White 1973a, b) can it be demonstrated that any mechanical crowding of the sandstone, siltstone, and shale beds in this fold was caused by slow deformation of these lithified alternating beds.

Detailed field and laboratory studies are always needed to resolve the questions of what condition the various sandstone, siltstone, and shale beds were in when they were deformed into folds, and thus how the deformation occurred. Such field studies should involve careful documentation and analysis of the folding and faulting (Aydin and Johnson 1983; Davis and Reynolds 1996; Groshong 1988; Hafner 1951; Jessell 1988a, b; Reches 1978b; Reches 1983; Reches and Dieterich 1983; Reches and Johnson 1978) and would require sampling of those lithologies so that thin sections could then be prepared for detailed microscope examination. For control purposes the same sandstone, siltstone, and shale beds need to be sampled from areas distant from the fold under investigation to compare under the microscope the grains and rock fabric/texture in those distal sandstone, siltstone, and shale samples with those in the samples obtained from the fold.

Expected Macroscopic Features Due to Ductile Deformation

Though somewhat similar, two classification schemes of folds have been proposed. Donath and Parker (1964) classified folds according to a generic-mechanical scheme based on mean ductility and ductility contrast within the folded sequence of layers (Hatcher and Bailey 2020) (fig. 13a). Accordingly, there are two broad groups of folds—flexural folds in which the fold shape is determined by the layering in the rocks, and passive folds in which the layering only serves as a displacement marker during folding (fig. 13b). A second, broad twofold subdivision is fundamentally a separation of brittle from ductile behavior. Slip along bedding, cleavage or foliation

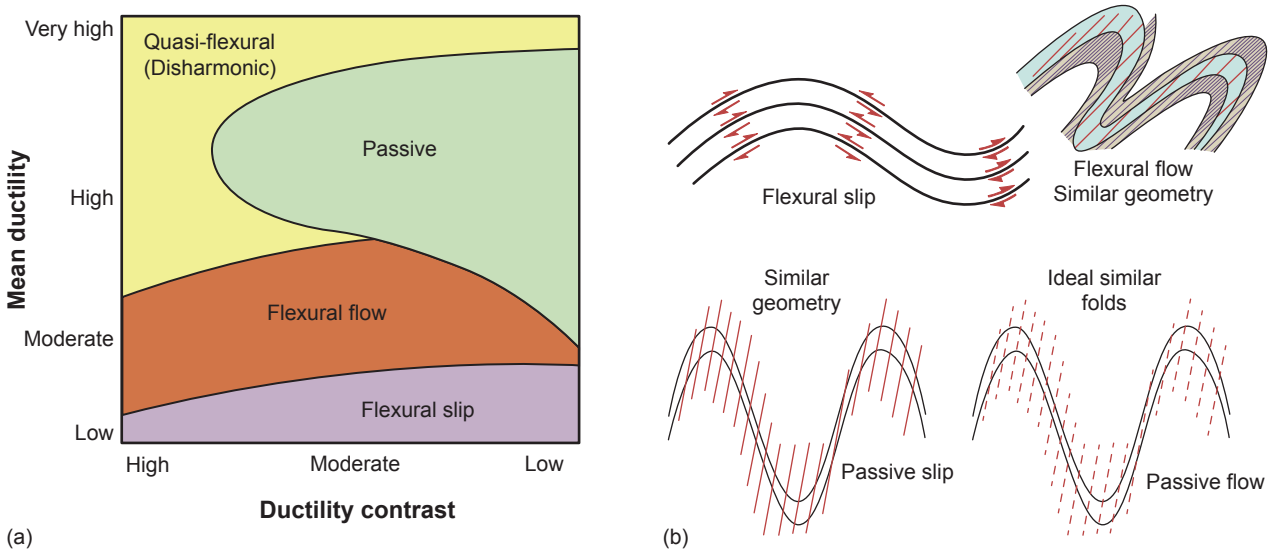

Fig. 13. The Donath and Parker (1964) classification of folds. (a) The basis for the classification with respect to the ductility contrast versus the mean ductility. (b) The types and mechanisms on fold types. Red lines represent cleavage. In flexural-slip folds, layer thicknesses remain constant and folding is accomplished by slip along layers. In flexural-flow folds, strong layers change thickness little or not at all, weak layers undergo appreciable thickening, and cleavage is strong in weak layers but poorly developed in strong layers. Passive-slip folds are ideally developed by movement parallel to a strong cleavage. Passive-flow folds develop by ductile flow with limbs thinned (or relatively thickened) equally in all rock types (similar folds).

planes is important in forming brittle folds. The process of ductile flow dominates in passive folds. Thus, in flexural-slip folds, layer thicknesses remain constant, and folding is accomplished by slip along and between layers. They are easily recognized by slickensides, fibers, or other movement indicators such as slip lines or lineations on layer surfaces, and by constant layer thickness (Hatcher and Bailey 2020). In flexural-flow folds, the stronger beds change thickness little or not at all, while the weaker beds undergo appreciable thickness changes, and cleavage is strong in the weak layers, but poorly developed in the strong layers. Thus, some beds were thickened in the hinge (axial) zones and thinned into limbs as folding proceeded, indicating a higher contrast in internal ductility. In contrast, passive-slip folds are ideally developed by movement parallel to a strong cleavage or shearing along planes, both of which are inclined to the layering. And finally, passive-flow folds develop by ductile flow due to plastic deformation so that the fold limbs are thinned, and the hinges are relatively thickened equally in all rock types, thus producing similar folds.

However, Ramsay (1967) subsequently classified folds into several classes based instead on their descriptive geometric shapes as determined on their profiles perpendicular to their hinge zones (Fossen 2016; Hatcher and Bailey 2020) (fig. 14). His classification involves an indirect relationship between layer thickness, both perpendicular to the layering and parallel to the fold axial surface, and the angle of dip at different points on successive folded surfaces. Lines connecting points of equal dip across a layer are called dip isogons. The relative convergence, divergence or parallelism of dip isogons is the classification key, with the degree of convergence of isogons directly related to fold tightening. Thus, folds where the isogons converge towards the concave part of the fold are classified as Class 1 folds, folds with parallel isogons belong to Class 2, and folds with isogons that diverge toward the concave part of the fold are in Class 3 (fig. 14). Class 1 folds are further subdivided into three groups. Class 1A folds have strongly convergent isogons which change direction through distance along the bedding more than the dip of the bedding surfaces they connect (fig. 14a). Class 1B folds correspond to parallel-concentric folds with convergent isogons which change direction the same as the bedding surfaces they connect (fig. 14b). And Class 1C folds are modified similar or parallel folds that have weakly convergent isogons which change direction less that the bedding surfaces they connect (fig. 14c). Then, Class 2 folds are ideal similar folds in which the isogons are parallel (fig. 14d), while Class 3 folds have extremely thickened hinges or extremely thinned limbs in which the isogons change direction in the opposite sense to the bedding surfaces they connect (fig. 14e).

Fossen (2016) noted that Class 1B folds are due to active folding, buckling, or bending that was initiated when the layers were shortened parallel to the layering. A contrast in competence or viscosity between the folding layers and their host rock is required for the folding to have occurred, with the

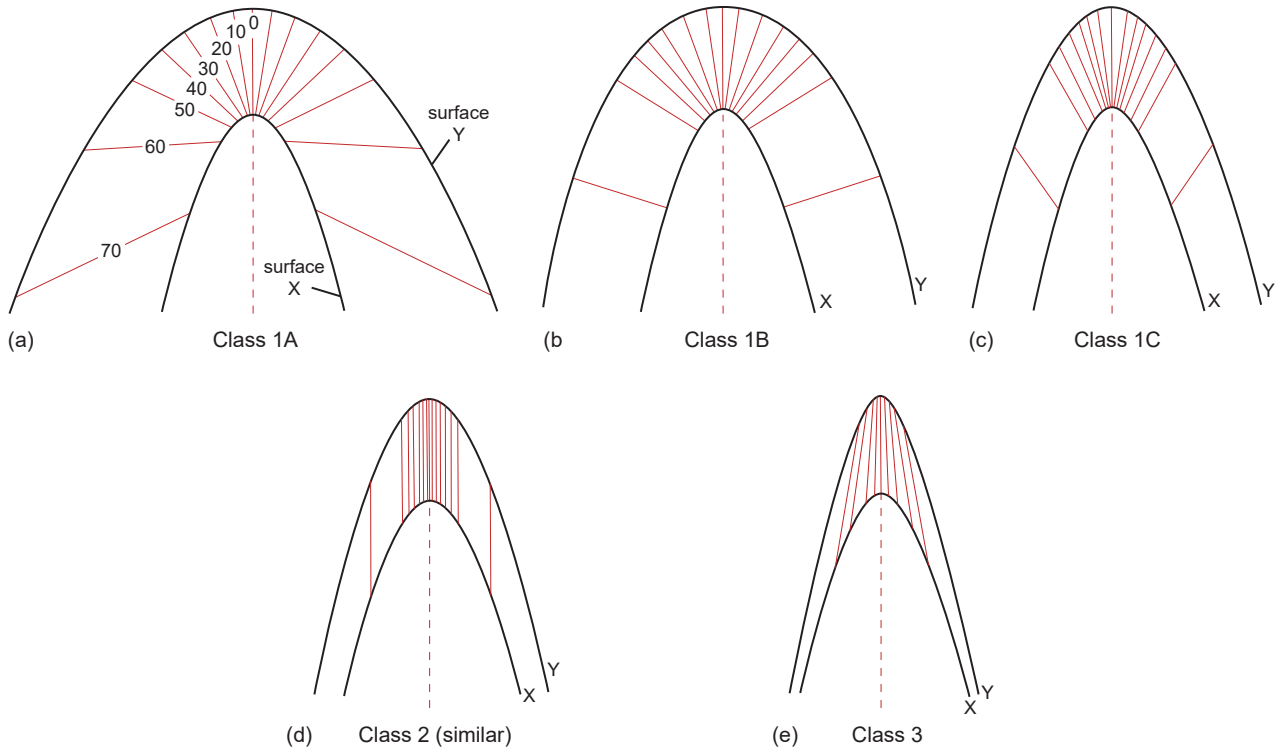

Fig. 14. The Ramsay (1967) fold classes. (a) In a class 1A fold, isogons change direction through distance along the bedding more than the dip of the bedding surfaces they connect. (b) Isogons change direction the same in a class 1B fold as the bedding surfaces they connect. (c) Isogons change direction less in a class 1C fold than the bedding surfaces they connect. (d) Isogons are parallel in class 2 folds. (e) Isogons in a class 3 fold change direction in the opposite sense to the surfaces they connect.

folding layers evidently more competent than the host rock or matrix. Fossen (2016) also equated Ramsay's (1967) Class 1B folds with Donath and Parker's (1964) flexural folding. Furthermore, Fossen (2016) distinguished bending, where the forces act across layers at a high angle, from buckling, where the main forces act parallel to the layers. He then cited the classic geologic results of bending as the forced folds created in sedimentary layers blanketing faulted rigid basement blocks. Displacement is forced on the sedimentary layers by movements along preexisting faults, and the sedimentary layers are soft enough to respond to monoclinal folding until at some critical point they rupture and the faults start propagating up-section, for example, the Laramide-uplift created monoclines of the Colorado Plateau (fig. 9). In contrast, Fossen (2016) equated Donath and Parker's (1964) passive folding with Ramsay's (1967) Class 2 folds in which the layering exerts no mechanical influence on the folding due instead to passive flow occurring. Thus, passive folds form in response to any kind of ductile strain, whether shearing, transpression, or even coaxial strain.

Bedding plane or flexural slip implies slippage along interfaces between layers or along thin layers during folding with bed thickness maintained and is the dominant mode of folding at the low temperatures and pressures at shallow depths in the upper crustal brittle regime (Fossen 2016; Hatcher and Bailey 2020). As already noted, bedding plane or flexural slip has been demonstrated to facilitate folding without brittle fracturing, being simulated with numerical modeling and well-studied in laboratory and field settings, including along the East Kaibab Monocline (Becker 1994; Behzadi and Dubey 1980; Borja, Sama, and Sanz 2003; Chapple and Spang 1974; Cooke et al. 2000; Cooke and Pollard 1997; Cooke and Underwood 2001; Crook et al. 2006; Couples and Lewis 2000; Epard and Groshong 1995; Horne and Culshaw 2001; Hughes and Shaw 2015; Kuenen and de Sitter 1938; Nino, Philip, and Chéry 1998; Ramsay 1974; Roth, Sweet, and Goodman 1982; Sanz et al. 2008; Suppe 1983; Suppe and Medwedeff 1990; Tanner 1989).

Furthermore, it is a prerequisite for flexural slip that the deforming medium is layered or has a strong mechanical anisotropy (Fossen 2016; Hatcher and Bailey 2020). Thus, for a layered sequence of beds to maintain constant thickness during folding, it must be uniformly strong rock such as bedded sandstone (for example, the Tapeats Sandstone) or carbonates so the beds can slip past one another. On the other hand, where the mechanical properties of successive layers differ (mechanical anisotropy), as with interlayered sandstone, siltstone, and shale, flexural slippage still occurs, but the shale may become thickened or even

crumpled into the hinge zone of the folds without any ductile flow. In both cases, the bedding surfaces act like fault planes and thus flexural slippage is easily recognized by slickensides or fibers on the slipped bedding surfaces. Maximum slip occurs at the inflection points and dies out towards the hinge line, where it is zero. The sense of slip is opposite on each limb, and slip is constant relative to the hinge where the sense of the slip changes. Relative slip on the convex side of a flexural-slip fold is always towards the fold hinge, whereas the concave side slip is opposite. The net result is that layering plays a pivotal role in parallel folding, the bending of massive sandstone or carbonate beds being an ideal example.

In contrast, a layered sequence of beds is said to deform by flexural flow if some beds flow ductilely, while others remain brittle and buckle or bend (Hatcher and Bailey 2020). Flexural flow requires moderate- to high-ductility contrast between layers. The whole rock mass may be in a state of ductile flow, but some rocks have higher viscosities under moderate temperatures (300–500°C) and higher pressures than interlayered weaker rocks. Such conditions do not apply to unmetamorphosed sedimentary rocks. The products of flexural flow are also mostly similar-type folds (Classes 1C and 3), and rarely ideal similar folds (Class 2). Similarly, passive flow involves uniform ductile flow of an entire rock mass, but there is no mechanical contribution from the rock material being deformed. Furthermore, there must be little or no ductility contrast between beds or layers, even if their compositions differ markedly, and there must be flow across the layering. Again, the necessary conditions for passive flow to occur do not apply to unmetamorphosed sedimentary rocks, and the products are again similar and similar-type folds (Classes 2 and 3 and 1C respectively). And finally, passive slip as described by Donath and Parker (1964) and Ramsay (1967) as slip at an angle to the layering that produces new cleavage and schistosity does not apply to unmetamorphosed sedimentary rocks. In any case, it is now often considered as a problematical fold mechanism (Hatcher and Bailey 2020).

Therefore, the focus needs to be on what details might apply to the sandstone, siltstone, and shale beds of the Bright Angel Formation within the Whitmore Helipad fold that should be observed at the macroscopic field scale. Field observations that would classify the type of fold are also critical in determining the mechanism and the conditions under which the folding occurred. If flexural slip occurred after lithification during ductile deformation, then slickensides should be observed on the surfaces of the beds that moved relative to one another. Was there bed attenuation observed in the limbs or bed thickening in the hinges, and any mechanical crowding? Yet even after such field observations are made, it is the microstructures that are the best clues as to the conditions under which the folding occurred.

Expected Microstructures Due to Ductile Deformation

Vernon (2018) and Wojtal, Blenkinsop, and Tikoff (2022) reviewed the various mechanisms by which minerals and rocks undergo deformation, that is, change of shape and strain, at the scale of grains or small aggregates, with particular reference to the optical microstructures produced by each mechanism. To relate microstructures to deformation mechanisms, Vernon (2018) concluded:

(1) the microstructures produced by different deformation mechanisms must be known from natural and especially experimental observations, and
(2) the microstructures must be stable enough to survive subsequent deformation and/or heating events.

Furthermore, deformation mechanisms can be classified in various ways, but brittle and ductile deformation can be distinguished at the microscope scale.

In brittle deformation, fractures occur across and/or between grains, and the resulting fragments move relative to one another. Fig. 15 depicts the textures that would be observed under the microscope as a result of brittle deformation either by granular flow

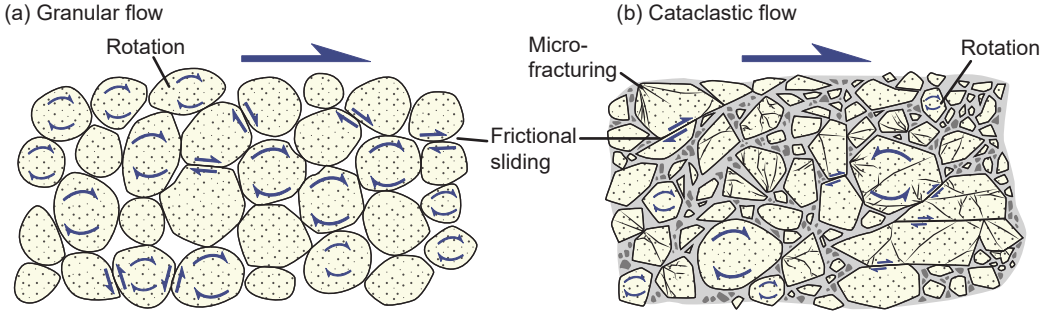

Fig. 15. Brittle deformation mechanisms (after Fossen 2016). (a) Granular flow is common during shallow deformation of porous rocks. (b) Cataclastic flow occurs during deformation of well-consolidated and brittle sedimentary and non-porous rocks.

grain rotation and frictional sliding, which is common during deformation at shallow depths of porous sediments, or by cataclastic flow, which also produces micro-fracturing of grains during deformation of well-consolidated sedimentary and non-porous rocks (Fossen 2016). In ductile deformation, the grains change their shapes or move relative to one another without fracturing (loss of cohesion) at the grain scale (Passchier and Trouw 1996). In both situations, but especially during brittle deformation, a change of shape of an aggregate may be accomplished or assisted by dissolution of minerals at some sites, transfer of dissolved chemical components in solution, and deposition at other sites in the deforming aggregate, known as stress-induced solution transfer.

There is much documentation of the grain shapes and rock fabrics/textures in undeformed and deformed sandstones and siltstones in both field, laboratory, and theoretical studies (Adams, MacKenzie, and Guildford 1984; Borg et al. 1960; Davis and Reynolds 1996; Etchecopar and Vasseur 1987; Friedman 1963; Gallagher et al. 1974; Hobbs 1968; Ingerson and Ramisch 1942; Jessell 1988a, b; Kamb 1959; Lister and Hobbs 1980; Lister, Paterson, and Hobbs 1978; Means 1990; Rowland 1946). There are also ample published studies on the effects on sand grains of their deformation under stress—*deformation lamellae* in the quartz grains and *undulose extinction* in quartz grains under cross-polarized light (Bailey, Bell, and Peng 1958; Carter 1971; Carter, Christie, and Griggs 1964; Christie and Ardell 1974; Christie, Griggs, and Carter 1964; Davis and Reynolds 1996; Fairbairn 1939; Groshong 1988; Hansen and Borg 1962; Hansen, Borg, and Maxwell 1959; Mitra and Tullis 1979; Tullis, Christie, and Griggs 1973; Twiss 1974, 1976; Whisonant 1970; White 1973a, b). Attention also needs to be paid during thin section examination of the samples from the folds for any evidence of thermal effects on the quartz grains, such as recrystallization, and on the matrix, such as conversion to metamorphic minerals (Carter, Christie, and Griggs 1964; Groshong 1988; Hobbs 1968; Lister and Hobbs 1980; Lister, Paterson, and Hobbs 1978; Mitra and Tullis 1979; Tullis, Christie, and Griggs 1973; White 1973a; Yardley, MacKenzie, and Guildford 1990).

Vernon (2018) and Wojtal, Blenkinsop, and Tikoff (2022) have provided details of the specific microstructures each of these mechanisms produces and which should be visible in petrographic examination of thin sections (fig. 16). Even though many of the illustrated examples they provide are from metamorphic rocks, the same observations are applicable to sandstones and siltstones, and in particular, potentially to the Bright Angel Formation within the Whitmore Helipad fold.

Crystal Plasticity or Dislocation Creep

Crystal plastic flow is permanent deformation by non-cataclastic (ductile) flow, which involves slip (translation gliding) and/or deformation twinning, without loss of cohesion on the grain scale. These processes enable a grain to change its shape by allowing one part of the crystal to undergo shear with respect to a neighboring part (Hobbs, Means, and Williams 1976). Microstructural evidence of such crystal plastic deformation includes *kink bands*, *deformation lamellae*, and *deformation twins* (fig. 16).

These microstructures have been duplicated experimentally—for example, Carter, Christie, and Griggs (1964); Drury and Urai (1990); Etheridge and Hobbs (1974); Etheridge, Hobbs, and Paterson (1973); Griggs et al. (1960); Hirth and Tullis (1992); Hobbs (1968); Hobbs, McLaren, and Patterson (1972); Mares and Kroenenberg (1993); Tullis (1983); Tullis, Christie, and Griggs (1973); Wilson and Bell (1979). Individual grains may become very elongated or may become converted to stretched out aggregates of much smaller grains formed by recrystallization during deformation. The mechanisms of crystal plastic flow in mineral deformation are summarized by Barber (1985); Barber and Meredith (1990); Gottstein and Mecking (1985); Green (1992); Hobbs, Means, and Williams (1976); and Knipe (1989).

Slip (Translation Gliding)

Slip is the primary mechanism of deformation of rocks (Vernon 2018). It causes layers of a grain to slide past each other without fracturing and without changing the orientation of the slipped portion of the grain. Therefore, it cannot be detected in thin section, in contrast to deformation twinning in which a change of orientation is produced (fig. 17). However, the shape of the grain is changed in the slip process. Slip occurs on specific planes (commonly planes of dense atomic packing) and in specific directions in the crystal. A slip system is the combination of a slip plane and a slip direction in that plane. Slip systems have been determined for many minerals at various temperatures. Because of the crystallographic control of slip planes, ductile deformation of grain aggregates typically results in a strong *crystallographic preferred orientation*.

The ease with which a slip system operates depends on the strain rate and temperature (Vernon 2018). Some minerals with relatively high crystallographic symmetry, such as quartz and calcite, have several slip systems and can deform relatively easily over a range of conditions, especially at elevated temperatures of 400–600°C in the presence of water and above 700°C if dry. In contrast, many other minerals, such as mica and plagioclase, are of lower

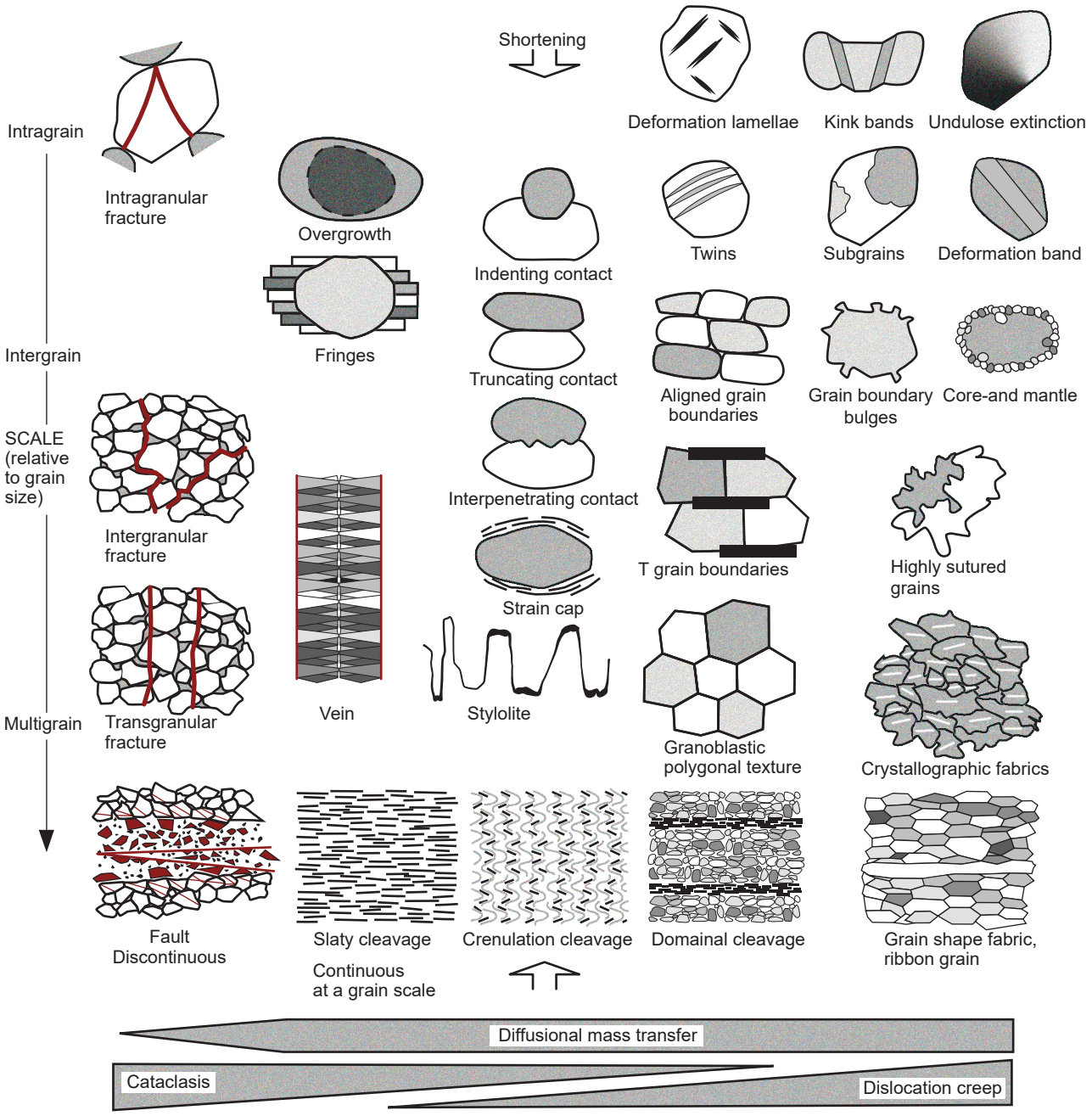

Fig. 16. A framework for analyzing secondary microstructures (after Wojtal, Blenkinsop, and Tikoff, 2022). Microstructures within a grain (intragrain) are at the top, microstructures between adjacent grains (intergrain) are in the center, and microstructures involving many grains (multigrain) are at the bottom. Red lines indicate fractures. Microstructures are drawn in an orientation that shows vertical shortening. This diagram excludes asymmetric microstructures used for shear sense indicators.

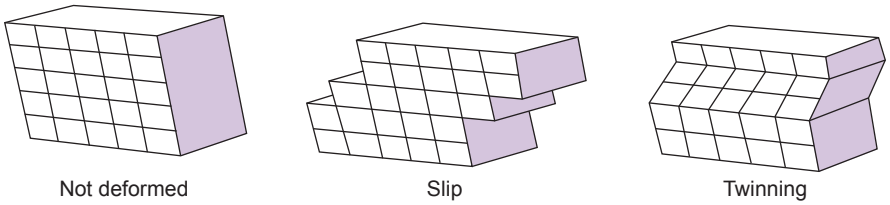

Fig. 17. Diagrams showing the general processes of slip and deformation twinning (after Vernon 2018). Note that twinning produces a change in orientation, which shows up as a change of color and/or birefringence under the microscope, but slip does not.

symmetry and may have only one dominant slip system, so they deform with greater difficulty. The more slip systems a mineral has, the more readily a grain of that mineral can change its shape in response to local differential stress. Minerals with at least five active independent slip systems can deform homogeneously by slip (Kelly and Groves 1970), quartz and calcite being common examples.

In grains of minerals with few slip systems, slip is commonly assisted by *deformation twinning* and *kinking* (fig. 16). In effect, a set of kink bands or of deformation twins acts as an additional independent slip system if repeated on a fine enough scale. Grains that are unfavorably oriented for slip may deform by fracturing and displacement along cleavages. Moreover, because of the common contrast between deformability of different minerals, local transient voids at grain boundaries may be relatively common, especially during deformation at lower temperatures. Those spaces may assist movement of fluid through the otherwise coherent rocks.

Slip takes place by movements of *dislocations*, as explained by Hobbs, Means, and Williams (1976) and Vernon (1976, 2000). Dislocations are line defects in which one row of atoms is decoupled from the rest of the lattice, effectively moving the dislocation through the solid crystal. The movement of dislocations through crystals enables solid crystalline materials to change their shapes without breaking. The stress on the mineral causes one row of atoms at a time to break. Then the next row breaks and the one behind it joins together again. So, successive rows break, one at a time, until the break (dislocation) moves right through the mineral grain, causing a displacement of one row of atoms. If many thousands of these minute displacements occur, they cause the mineral grain to change its visible shape. Each dislocation needs only a very small amount of energy, and the process does not require the mineral to change the overall arrangement of its atoms, so the mineral retains its identity during the deformation.

Kinking

Kinking occurs when slip on a single slip plane is inadequate to maintain homogeneous deformation (Vernon 2018). The grain sharply bends (kinks), and the deformation localizes into *kink bands*, which enable shortening of the grain to continue (fig. 16). The whole grain may divide into kink bands, or the kink bands may be separate and commonly lenticular, or wedge shaped. A kink band may be defined as part of a grain that undergoes rotation with respect to the unkinked part of the grain, the axis of rotation coinciding with the line of intersection of the kink band and the slip plane, perpendicular to the slip direction (Nicolas and Poirier 1976; Spry 1969).

Kink bands in a mineral grain are usually revealed by differences in absorption color, owing to their orientation differences. The widths and degrees of misorientation of the kink bands are variable, which distinguishes them from *deformation twins*, between which the misorientation is constant. By contrast, *deformation lamellae* are regularly-spaced "lines" across a mineral grain, while *deformation twins* are also regularly-spaced bands that can be lenticular (fig. 16). Broadly similar microstructures, reflecting heterogeneous deformation from one layer to another in a deforming grain but which cannot be described as kink bands according to their definition, are best referred to as *deformation bands* (Hobbs, Means, and Williams 1976; Spry 1969) (fig. 16).

Elongate sub-grains (extinction bands) formed by recovery in quartz are often referred to as "kink bands," but should not be confused with kink bands formed by slip alone (Nicolas and Poirier 1976). Elongate sub-grains and true kink bands may be present in the same grain of quartz. Kinking is common in minerals with strongly anisotropic crystal structures and consequently only one slip plane, such as biotite, but also occurs in minerals with several slip systems, such as quartz (Christie, Griggs, and Carter 1964).

Deformation Lamellae

Deformation lamellae are narrow (0.5–10 μm), planar, crystallographically oriented zones with slightly different refractive index from that of the adjacent grain (Blenkinsop and Drury 1988; Carter 1971; Carter, Christie, and Griggs 1964; Christie, Griggs, and Carter 1964; Drury 1993; Green and Radcliffe 1972; Hobbs, Means, and Williams 1976; Turner 1948; White 1973b) (fig. 16). Deformation lamellae parallel to slip planes have been produced experimentally, but some natural deformation lamellae have complicated and variable structures and may not reflect slip alone.

Deformation lamellae generally are aligned perpendicular to extinction bands (elongate sub-grains). They are most common in quartz, but have also been observed in plagioclase (Borg and Heard 1970) and calcite (Turner 1948). They tend to be formed most commonly during lower-temperature deformation. Deformation lamellae typically occur in one plane in quartz and may be slightly curved. They are generally visible due to their slightly different extinction and/or relief (refractive index) compared to the host grain and are often very closely spaced (on the order of their width) (Wojtal, Blenkinsop, and Tikoff 2022). They may be pervasive across a whole grain or localized into smaller domains. They form parallel to crystallographic planes (for example, parallel to the rhomb planes in quartz), and they may occur in more than one set in a grain.

Deformation Twinning (Twin Gliding)

Some minerals, such as calcite and plagioclase, undergo *deformation twinning* (mechanical twinning, secondary twinning, or twin gliding) in response to deformation (Vernon 2018) (figs. 16 and 17). The distribution of these twins within grains is typically heterogeneous. Deformation twinning operates by a limited amount of simple shear (at the microscopic scale, though it may be more complicated at the atomic scale) parallel to a glide plane (the twin plane) and in a particular direction (the glide direction), both of which depend on the crystal structure of the mineral, and which together constitute the twinning system. Thus, deformation twinning occurs in some minerals but not in others. In contrast to slip, the amount of deformation that can be achieved by twinning is limited by these requirements, especially because twins have only one sense of shear. Each atomic layer is sheared (not translated) by an amount sufficient to produce a mirror image of the original crystal (fig. 17). This restores the original structure, each half of the twin being misoriented symmetrically with respect to the other.

Twinning tends to be favored over slipping at lower temperatures and faster strain rates (Vernon 2018). Deformation (secondary) twins are distinguished from growth (primary) twins on the basis of their typically lenticular shapes. Deformation twins are always multiple, never simple, and have been produced experimentally in calcite and plagioclase (fig. 16). Deformation twinning is common in plagioclase, where it occurs according to two "twin laws," namely, albite-law twinning and periclase-law twinning, Both of these twin laws are favored by the same local stress system, and so they tend to operate simultaneously (Vernon 1965). Another example is calcite (Paterson and Turner 1970). Burkhard (1993) reviewed deformation twinning in calcite, inferring that micro-twins and straight, narrow twins (<1 μm thick) are characteristic of very low temperature deformation, whereas above about 100°C wider (>1–5 μm), fewer twins occur. Above ~200°C, curved twins, twins that are themselves twinned and completely twinned grains occur, and above ~250°C, older twins commonly show evidence of boundary migration. Deformation twinning also occurs in dolomite, and oxide minerals, such as rutile and hematite (Hennig-Michae 1977).

Hardening and Softening During Deformation

Broadly speaking, crystal plasticity may be divided into low- and high-temperature types (Vernon 2018). Low-temperature plasticity occurs at roughly less than half the melting temperature at laboratory strain rates and is dominated by glide of dislocations in slip planes. This leads to interference, tangling and hence immobilization of dislocations, causing the mineral to resist strain. Thus, the process is called strain hardening (strengthening). High-temperature plasticity is dominated by thermally activated recovery and recrystallization processes, which cause softening (weakening). The process involves untangling of dislocations, and consequently the mineral is able to continue to deform (creep) at relatively small differential stresses. The amount of strain accumulation depends on competition between strain hardening and recovery/dynamic recrystallization.

Plastic deformation at high temperatures (dislocation creep) is probably the main deformation process in the deeper parts of the earth's crust (Yund and Tullis 1991). The resulting grains may show undulose (undulatory) extinction and sub-grains, sutured grain boundaries, and a pronounced shape and/or crystallographic preferred orientation. At very high temperatures, ductile grain-boundary sliding may occur. However, water-assisted cataclastic deformation may be responsible for some sub-grains and recrystallized grains in quartz that are optically identical to those commonly inferred to be due to dislocation creep (den Brok 1998).

Undulose Extinction and Sub-Grains

Undulose extinction is a smooth variation in the extinction position of a single grain when examined in cross-polarized light (Wojtal, Blenkinsop, and Tikoff 2022) (fig. 16). It is a very common feature of deformed rocks, especially in quartz and feldspar grains. The variation in extinction position indicates a variation in the orientation of the crystal lattice of the grain, affecting the polarizing direction of transmitted light and thus the extinction position of different parts of the grain. In moderately deformed grains, these undulose variations in the extinction position and thus lattice orientation are commonly localized into sub-grains, which are intracrystalline domains where the lattice orientation may vary by up to 10° from the rest of the grain (White 1977). This upper limit to the lattice mis-orientation for sub-grains distinguishes a sub-grain that forms within grains from two separate grains.

Sub-grains may have relatively planar walls in crystallographically controlled directions (fig. 16). In quartz, the basal (perpendicular to the sides of the hexagonal shape seen in large quartz crystals) and prism (parallel to the sides of the hexagonal crystal shape) planes are common sub-grain boundaries. If both directions have developed, the resulting effect is a pattern of square or rectangular domains of contrasting extinction, which is called a chessboard pattern of sub-grains (Wojtal, Blenkinsop, and Tikoff 2022). Some sub-grains have distinctly tabular shapes that define deformation bands (fig. 16). If

the sub-grain boundaries are sharply defined and straight, they can be referred to as kink bands. Deformation lamellae are also tabular features but restricted to very small widths.

Diffusion Creep

Diffusion creep (diffusive mass transfer) involves change of grain shape by diffusion of chemical components, either in aqueous solution (stress-induced solution transfer or dissolution-precipitation creep) or by solid-state diffusion along grain boundaries (grain-boundary diffusion or Coble creep) or through crystals (volume diffusion or Nabarro-Herring creep), which requires high temperatures (Fossen 2016; Vernon 2018; Wojtal, Blenkinsop, and Tikoff 2022) (fig. 18). In both cases, vacancies in the atomic lattice of the minerals move toward high-stress sites so that the minerals accumulate strain over time. Stress-induced solution transfer (also called pressure solution) is equivalent to Coble creep in dry rocks (Wheeler 1992). Typically, material is removed from sites of high normal compressive stress and deposited at low-stress sites, with the result that a volume of rock changes its shape (Rutter 1976).

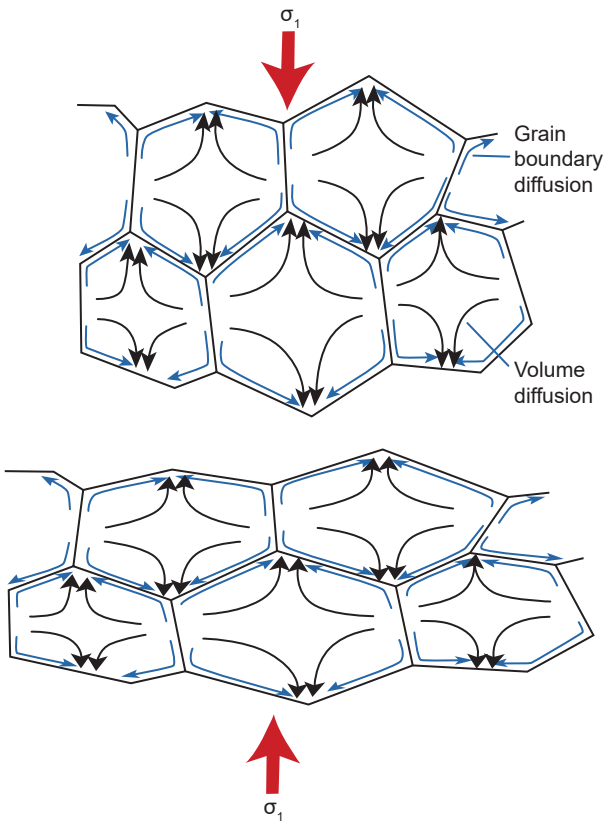

Fig. 18. Diffusion in a mineral can occur within grains by means of volume diffusion, or along grain boundaries by means of grain-boundary diffusion (after Fossen 2016). In both cases crystal lattice vacancies move toward high-stress sites so that the minerals accumulate strain over time. Note that the atoms involved move in the opposite way.

The term "pressure solution" strictly refers to the actual dissolving of minerals, and so the term "solution-transfer" has been proposed for the overall process of solution, transfer and redeposition of chemical components (Durney 1972). A preferable term is "stress-induced solution transfer" (Passchier and Trouw 1996), which emphasizes the necessity of deformation in the process. The term "dissolution-precipitation creep" or simply "solution-precipitation creep" (den Brok and Spiers 1991) also implies a deformation-controlled process.

Stress-induced solution transfer (dissolution-precipitation creep) is especially effective at low metamorphic grades and produces microstructures such as truncated detrital grains, truncated ooliths, truncated fossils, truncated pebbles, stylolitic surfaces, tectonic overgrowths, and "beard" structures (Cox and Etheridge 1982; McClay 1977; Powell 1982 [fig. 16]). However, the process can also occur in

(1) the deformation of high- and medium-grade metamorphic rocks, producing veins and beard structures (Wintsch and Yi 2002),
(2) during fluid-assisted "superplastic" deformation (ductile grain-boundary sliding), and
(3) especially in ductile shear zones.

McClay (1977) estimated that stress-induced solution transfer in fine-grained quartz and calcite rocks can produce geologically reasonable strain rates at 200–300°C and that Coble creep in calcite rocks can produce geologically reasonable strain rates at around 300°C.

Microstructures generally taken to indicate diffusion creep in deformed rocks include equant grain shapes, indented grains, overgrowths, and a lack of crystallographic preferred orientation (Bons and den Brok 2000) (fig. 16). However, crystallographic preferred orientations resulting from crystallographic orientation-dependent dissolution and growth have been described for naturally deformed quartz-rich rocks (Becker 1995), and for experimentally deformed quartz rocks (den Brok 1996). Additionally, modeling by Bons and den Brok (2000) has indicated that dissolution-precipitation creep may be important in the development of crystallographic preferred orientations in rocks, and thus, the presence of a crystallographic preferred orientation alone cannot be used as evidence for dislocation creep.

Diffusion creep can grade into ductile grain-boundary sliding, and frictional grain-boundary sliding (during brittle deformation) (Vernon 2018). An example is provided by deformation experiments on fine-grained (2–10 μm) albite (plagioclase) with a small amount of water (<1%) in which the deformation changed directly from cataclastic flow to grain-boundary diffusion creep with increasing temperature and decreasing strain rate, without

any intermediate dislocation creep (Tullis and Yund 1987, 1991). The resulting microstructures include rectangular grain shapes, overgrowths of different composition from the original grains and low concentrations of dislocations (Tullis and Yund 1991).

Den Brok (1998) has shown that rates of stress-induced solution transfer depend on micro-cracking, which may increase greatly with sudden increase in stress or fluid pressure. This can enhance grain-boundary diffusion rates and cause rock weakening. Stress-induced solution transfer tends to predominate at lower temperatures, at which diffusion occurs more readily than dislocation creep. But dislocation creep tends to swamp stress-induced solution transfer at higher temperatures (Wheeler 1992). However, because diffusion occurs along grain boundaries, stress-induced solution transfer is accentuated by finer grain sizes and so can dominate dislocation creep, even at the higher temperatures of the lower crust, where dislocation creep would otherwise predominate. Calculations made by Wheeler (1992) also suggest that stress-induced solution transfer is more effective in polymineralic rocks than in single-mineral aggregates, owing to chemical interactions during the deformation.

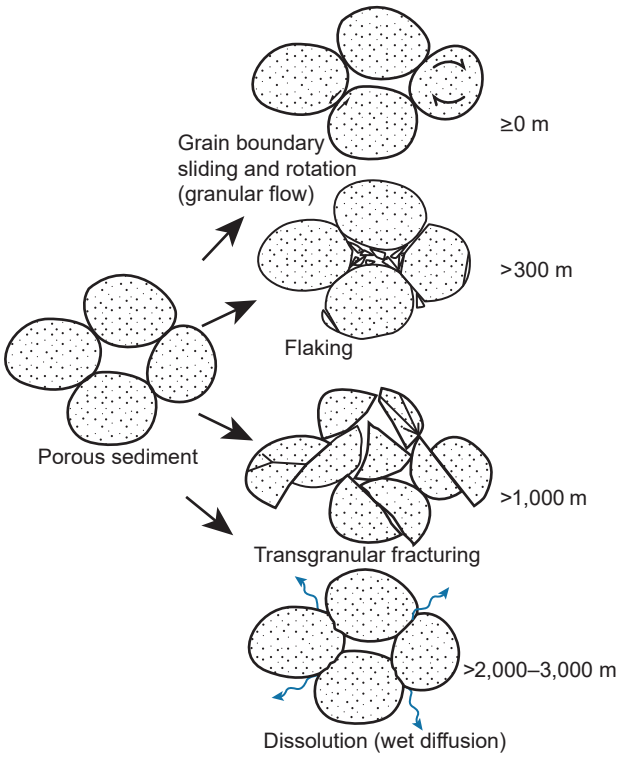

Fig. 19. Deformation mechanisms operative at shallow depths (after Fossen 2016). Very approximate depths are indicated.

Ductile Grain-Boundary Sliding

Grain-boundary or frictional sliding and fracturing during granular flow are characteristic features of brittle deformation (Fossen 2016) (fig. 15). However, a distinction is drawn between intergranular fracturing, intragranular fracturing, frictional sliding on fractures and grain boundaries, and grain rotation, which in combination are due to cataclastic flow (figs. 15 and 16). In contrast, granular flow, which is characterized by grain rotation (or rolling) and frictional grain-boundary sliding, is only intergranular deformation in that there is no permanent internal deformation of the grains. It occurs at very shallow depths on porous sediments such as weakly consolidated sandstone or siltstone buried at less than ~1,000 m (~3,300 ft) depth. It involves deformation in a shearing mode or in response to vertical loading (compaction). In these processes, if the stresses across grain contacts become high enough it may cause the sedimentary rock's grains to fracture. Those fractures are confined to individual grains and are therefore intragranular microfractures. Under low pressure conditions and with small grain contact areas microfractures may form close to the grain surfaces, commonly chipping small flakes off of the surfaces of the grains (fig. 19). This microfracturing is referred to as spalling or flaking. At higher confining pressures, corresponding to depths in excess of ~1,000 m (~3,300 ft), fractures can split the grains into more evenly sized parts, and the mechanism is known as transgranular fracturing. Once fractured, the grains reorganize themselves by frictional sliding and rotation, leading to porosity reduction.

However, *grain-boundary sliding* also occurs during ductile deformation (Wojtal, Blenkinsop, and Tikoff 2022). Some very fine-grained polyphase metal alloys, at certain conditions of temperature (at least half the melting temperature) and strain rate, can be deformed experimentally in tension up to strains of more than 1,000% without fracturing (Vernon 2018). This is referred to as superplastic deformation (grain size-sensitive flow). The mechanism involved is *grain-boundary sliding*, which involves relative grain movement without loss of cohesion and normally in the absence of fluid. Resulting potential gaps between grains are filled by diffusive mass transfer (Ashby and Verall 1973; Edington, Melton, and Cutler 1976; Nicolas and Poirier 1976; Poirier 1985; Schmid, Boland, and Paterson 1977), dislocation motion (Tullis 1983), or both these processes (Kenkmann and Dresen 2002), and so the aggregate remains coherent.

Superplasticity is a state in which solid crystalline material is deformed well beyond its usual breaking point, usually over about 600% of its breaking point during tensile deformation, which is usually achieved at high temperature. The mechanisms of superplasticity are still debated, but the consensus

is that it relies on atomic diffusion and the sliding of grains past each other (grain-boundary sliding). Superplasticity has been proposed for quartz (Behrmann 1985; Behrmann and Mainprice 1987; Boullier and Guegen 1975), calcite (Behrmann 1983), and feldspar (Allison, Barnett, and Kerrich 1979). Some have suggested that normal crystal plasticity can change rapidly to superplasticity below a critical grain size (Behrmann 1983; Schmid, Boland, and Paterson 1977), possibly in millimeter-scale domains (Behrmann and Mainprice 1987).

However, it is not easy to determine the extent to which superplasticity occurs in natural rock deformation (Gilotti and Hull 1990). The following microstructural features have been suggested as indicators of superplastic behavior in rocks (Boullier and Guegen 1975; Schmid 1982):

(1) grains remaining equant, even after large accumulate strains,
(2) very small grain size around 1–10 μm, and
(3) moderate concentrations of dislocations without dislocation cells (that is, no sub-grains).

However, small grain sizes and equant grains are also compatible with dynamic recrystallization during dislocation-induced flow (Schmid 1982; White 1977) so that superplasticity generally cannot be inferred with confidence from microstructure alone. Another characteristic feature of superplasticity may be the absence of strong preferred orientation, since diffusion-accommodated grain-boundary sliding tends to weaken existing preferred orientations, in contrast to aggregates recrystallized dynamically, which typically have crystallographic preferred orientations. However, the lack of strong preferred orientation cannot be always taken to imply superplasticity, because static recrystallization may or may not reduce the strength of preferred orientations produced during dynamic recrystallization (Law 1990). Thus, more general terms such as "non-cataclastic grain size-sensitive flow" or "non-cataclastic granular flow" would better describe natural deformation.

In some rocks, non-cataclastic grain size-sensitive flow may be promoted by the formation of transient, fine-grained reaction products in metamorphic reactions, or by fluid, which assists diffusion and results in a kind of high-temperature pressure solution (Mukai et al. 2014; Tullis and Yund 1991; Tullis, Yund, and Farver 1996). This can be called fluid-assisted diffusion creep. Experiments deforming fine-grained feldspar aggregates have shown that fluid occurring in pores at hydrostatic conditions spreads along grain boundaries during deformation, causing a change from dislocation creep to diffusion creep with consequent reduction in strength (Tullis, Yund, and Farver 1996). Because minerals continuously dissolve in and precipitate from the fluid as deformation proceeds, microstructural evidence of fluid-assisted diffusion creep may be difficult or impossible to distinguish from other forms of grain-sensitive flow. However, rectangular grain shapes and compositionally different grain overgrowths have been observed in high-temperature diffusion creep experiments on fine-grained sodic plagioclase (Tullis and Yund 1991). Fluid-assisted ductile grain-boundary sliding should be conceptually distinguished from frictional grain-boundary sliding, which involves not only intergranular fluid, but also rotation of discrete fragments, rather than maintaining a coherent aggregate during deformation.

Conditions Favoring Various Deformation Mechanisms

Different deformation mechanisms dominate at different conditions of temperature, pressure, strain rate, differential stress, grain size, fluid content, and fluid composition, though several deformation mechanisms may operate simultaneously, even if one dominates (Vernon 2018) (fig. 16). For example, higher confining pressure and lower fluid pressure tend to promote dislocation creep over cataclastic behavior, and larger grain sizes tend to favor dislocation creep and deformation twinning, owing to greater ease of accommodation of strain produced by these processes at grain boundaries, compared with the situation in finer-grained aggregates.

The different deformation mechanisms that are operative in a deforming mineral under various physical conditions can be expressed by means of a deformation mechanism map of stress versus temperature contoured for a range of strain rates (Rutter 1976) (fig. 20). Deformation mechanism maps

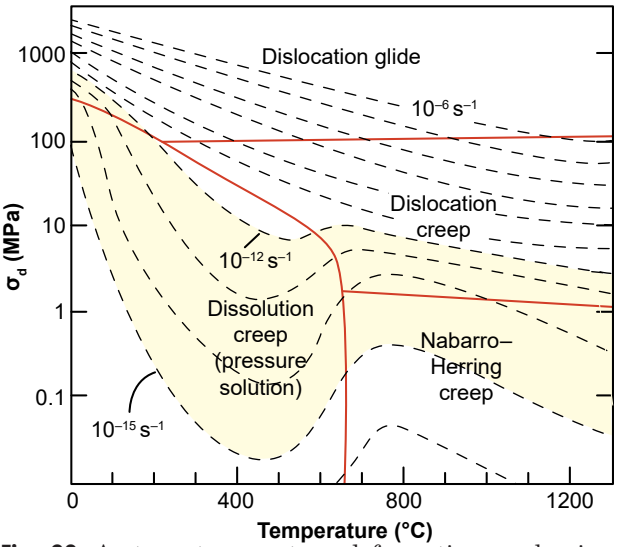

Fig. 20. A stress-temperature deformation mechanism map for quartz (after Rutter 1976). Realistic natural strain rates are indicated in yellow (10^{-12}–10^{-15}s^{-1}).

show the range for which a particular deformation mechanism dominates. They are partly based on experimental data that have been extrapolated into geologically realistic strain rates and temperatures, and partly on theoretical considerations (Fossen 2016). The example in fig. 20 is for quartz. Realistic natural strain rates are indicated in yellow. It should be noted that such maps are hampered by many uncertainties and limited data availability.

Experiments have shown that the main factors favoring ductile flow of solid dry rocks are (Vernon 2018):

(1) high confining pressure, which makes it difficult for the rock to expand and hence break during deformation,
(2) high temperature, which allows dislocations to move freely through minerals, and
(3) slow application of the deforming force, which gives the dislocations enough time to move.

Therefore, in dry rocks, flow tends to dominate in the deeper parts of the earth's crust, where rocks are hot and under high-confining pressures. Generally, fractures dominate at depths of less than ~15 km (~9 mi) and flow dominates at greater depths, though many exceptions occur, and the conditions vary with the minerals concerned. For example, quartz tends to be ductile at lower temperatures than feldspars.

Microstructural evidence of dynamic recrystallization is generally taken to indicate relatively high temperature, but the temperature varies greatly with the mineral. For example, though calcite typically undergoes ductile deformation and dynamic recrystallization at greenschist facies or higher temperatures (Busch and van der Pluijm 1995; Rutter 1976; Vernon 1981), these processes can also occur in calcite in temperatures as low as 150–250°C (Kennedy and White 2001).

Fluids are also important. For example, small amounts of water in the crystal structure increase the ductility of quartz. However, water films on grain boundaries may block atomic bonding between grains and so reduce the "effective pressure," leading to fracturing and brittle deformation. Nevertheless, water may assist diffusive flow in fine-grained calcite aggregates deformed at low differential stress (Rutter 1974), and greatly assists grain-boundary migration crystallization (Mancktelow and Pennacchioni 2004).

The overall situation, summarized by Wintsch and Yi (2002), is that at geological strain rates in quartz-rich rocks, brittle deformation dominated by fracture mechanisms changes to deformation by dislocation creep at ~200°C. In plagioclase, brittle-to-ductile transition occurs at ~450°C. If water is present, a field of stress-induced solution transfer displaces dislocation creep by 200–300°C. Wintsch and Yi (2002) inferred that, though biotite and quartz deformed by dislocation creep, most of the deformation was accommodated by deformation-enhanced dissolution of minerals at grain boundaries perpendicular to the shortening direction (evidenced by truncated zoning patterns in plagioclase and orthoclase) and precipitation in the form of beards (or fringes in fig. 16) on the ends of grains that face the extension direction. Thus, solution-precipitation creep can accompany and even dominate over dislocation creep at high temperatures in the presence of water. However, quartz microstructure and crystallographic preferred orientation are also sensitive to other variables, such as strain rate and water weakening, as pointed out by Law (2014).

Recovery and Recrystallization

During deformation, dislocations in different slip planes can interfere with each other and form "tangles," which inhibit their movement and hence further deformation of the mineral (strain strengthening or strain hardening). *Recovery* and *recrystallization* are processes that tend to reduce the concentration and/or tangling of dislocations, and so produce volumes of material capable of continued deformation (Vernon 2018; Wojtal, Blenkinsop, and Tikoff 2022). Thus, ductile deformation is a competition between strain strengthening (hardening) and recovery processes.

Recovery includes all processes that attempt to return a crystal to the undeformed state without the formation of high-angle (high-energy) boundaries (Hobbs, Means, and Williams 1976). In other words, no new grains are formed. Recovery may be dynamic or static, depending on whether or not it occurs during or after deformation, respectively.

During recovery, dislocations free themselves from tangles by dislocation "climb" (the movement of edge dislocations out of their slip planes by the addition or loss of point defects, which is a heat-activated process), and by dislocation "cross-slip" (the movement of screw dislocations from one slip plane to another) (Vernon 2018). Both these processes untangle dislocations and so reduce the amount of strain strengthening. The freed dislocations migrate to form sub-grain boundaries, which become "walls" of organized dislocations (Hobbs, Means, and Williams 1976; Spry 1969). This leaves relatively strain-free volumes (sub-grains) between the sub-grain boundaries so that further deformation can proceed.

Optically, sub-grain boundaries tend to be relatively evenly spaced and show small mis-orientation angles (Vernon 2018). Bending of grains, presumably involving dispersed dislocations, produces *undulose (undulatory) extinction*, which grades into slightly misoriented sub-grain boundaries. A maximum misorientation of 10° is often taken as a rough

guide for sub-grains in quartz (White 1977). Larger mis-orientations produce grain boundaries. Precise distinction between sub-grain and grain boundaries on the basis of dislocation arrangements requires transmission and scanning electron microscopy (TEM and SEM).

However, slightly mis-aligned fragments that optically resemble sub-grains can be formed by microfracturing (Lloyd and Freeman 1994; Urai, Means, and Lister 1986). Yet normally such microfractures are formed in the presence of fluid, and thus sub-grains of this type potentially may be recognized by the presence of healed lines of fluid inclusions along the sub-grain boundaries, provided it can be ascertained that the inclusions were not formed along microfractures that developed along existing sub-grain boundaries.

The optical relief of sub-grain (low-angle) boundaries generally is not as marked as with grain (high-angle) boundaries, and together with the small mis-orientations, makes it clear that the sub-grains occur within grains (hence the name). Sub-grains may be equant or elongate. Elongate sub-grains form perpendicular to slip planes and appear optically as "extinction bands" at high angles to the slip planes. Sub-grains have been observed in a variety of minerals, including quartz (Hobbs, Means, and Williams 1976), calcite (Vernon 1981) and plagioclase (Fitz Gerald, Etheridge, and Vernon 1983; Vernon 1975).

Recrystallization involves the formation of strain-free volumes inside deformed grains by the creation and/or movement of grain boundaries in response to deformation (Vernon 2018; Wojtal, Blenkinsop and Tikoff 2022). During recrystallization, strain energy is reduced by:

(1) migration of existing high-angle (high-energy, random, irrational) grain boundaries, kink-band boundaries, or twin boundaries,
(2) development and migration of new high-angle grain boundaries (excluding kink-band boundaries and fractures), and
(3) development of new low-energy crystal faces, *all in the same mineral*.

A generally applicable definition of recrystallization is the development and/or migration of high-angle (random) grain boundaries or crystal faces in solid state in response to deformation and in the same mineral.

Recrystallization typically produces aggregates of new (recrystallized) grains that are strain free and therefore capable of continued deformation (Vernon 2018). The new grains may be:

(1) polygonal in minerals with relatively uniform three-dimensional lattice structures, such as quartz, feldspar, and calcite (fig. 16),
(2) crystals with low-energy faces in minerals with strongly anisotropic lattice structures, such as mica (Bell 1978; Etheridge and Hobbs 1974; Vernon 1977b), or
(3) irregularly shaped where grain-boundary migration recrystallization is the dominant process.

However, recrystallization does not involve the production of new minerals, although small compositional changes between new and old grains commonly occur in minerals with complex compositions (for example, Etheridge and Hobbs 1974; Vernon 1975, 1977a). Stünitz (1998) has shown that differences in composition between old and recrystallized plagioclase grains can contribute to the driving force for recrystallization.

Nucleation of new grains during recrystallization generally does not involve the formation of completely new grains (that is, from new nuclei developed randomly within old grains), but typically involves either sub-grain rotation or strain-induced grain-boundary migration ("bulge nucleation"). However, both processes can produce similar microstructures (Lloyd and Freeman 1994), and microfracturing can produce slightly misaligned fragments that optically resemble sub-grains (den Brok and Spiers 1991; Lloyd and Freeman 1994; Urai, Means, and Lister 1986). The following three processes are involved in recrystallization.

Sub-grain rotational recrystallization (Hobbs 1968; Poirier and Guillopé 1979) occurs when dislocations accumulate in sub-grain boundaries, causing the boundaries to progressively increase their complexity and misorientation. When a dislocation is added to a sub-grain boundary it changes the angle mismatch between the two sub-grains. By this process, sub-grain boundaries become grain (high-energy, high-angle) boundaries. It involves progressive crystallographic misorientation with limited grain-boundary migration, so that orientation relationships between the old and new (recrystallized) grains may be recognized (Hobbs 1968; Vernon 1975). Sub-grains leading to recrystallization have been observed in quartz (Hobbs 1968; Tullis, Christie, and Griggs 1973), calcite (Vernon 1981), K-feldspar (Altenberger and Wilhelm 2000; Bell and Johnson 1989), and plagioclase (Bell and Johnson 1989; Dornbusch, Weber, and Skrotzki 1994; Vernon 1975). Photographic evidence under the microscope of progressive rotation of sub-grains to produce new (recrystallized) grains during deformation of transparent minerals has been presented by Means and Xia (1981) and Means (1989).

Recrystallization by *strain-induced grain-boundary migration* involves differential migration of parts of a high-angle boundary, such as a grain

boundary, kink-band/deformation-band boundary, or a deformation-twin boundary (Vernon 2018). The migration occurs by diffusion of atoms across the boundary, which consequently moves in the opposite direction to the diffusion direction and forms a "bulge." Strain-induced grain-boundary migration is driven by strain energy differences (differences in the dislocation concentration) on either side of the grain, kink-band, or twin boundary. The process tends to relax gradients in strain (recrystallization) and/or composition. So, as the boundary moves into a deformed grain it leaves undeformed mineral behind it. The microstructural result is a *sutured* (bulged) grain boundary, kink-band boundary, or deformation-twin boundary, with markedly smaller new grains along the boundary (fig. 16). The process occurs at low temperatures in quartz and calcite (Drury, Humphreys, and White 1985; Schmid, Panozzo, and Bauer 1987; Schmid, Paterson, and Boland 1980).

Sutured grain boundaries, kink-band boundaries and twin boundaries have been observed in a wide variety of minerals including quartz, plagioclase and calcite (Vernon 1981), and K-feldspar (Altenberger and Wilhelm 2000) (fig. 16). In minerals with relatively isotropic crystal structures (quartz, feldspar, calcite), strain-induced grain-boundary migration produces equant new grains, whereas in minerals with strongly anisotropic crystal structures (sheet silicates such as micas), it produces aggregates of elongate new grains.

Poirier and Guillopé (1979) have pointed out that trace amounts of water increase the rate of grain-boundary migration, even in anhydrous minerals such as quartz (Green, Griggs, and Christie 1970). They suggested that water may enhance grain-boundary mobility by increasing the glide and/or climb mobility of grain-boundary dislocations, in the same way as it appears to induce easier glide or climb of lattice dislocations (Griggs 1974; McLaren and Retchford 1969).

Though bulges in grain boundaries commonly appear rounded (except for minerals such as sheet silicates), long-lasting strain-induced grain-boundary migration at relatively high temperature can lead to a stepped rather than smooth sutured interface (Kruhl 2001; Kruhl and Peternell 2002). The steps or sharp deflections appear to be due to crystallographic control, such as the formation of rhombohedral planes in quartz (Masberg, Hoffer, and Hoernes 1992).

Grain-boundary migration recrystallization (fast grain-boundary migration) is a more pronounced form of grain-boundary bulging that occurs during recrystallization (Vernon 2018). It has been observed in materials progressively deformed under the microscope (Means 1989; Urai 1983). The process produces bulges with long wavelengths of the order of the grain size, which migrate through the aggregate, continuously converting parts of it from one lattice orientation to another. These changing "orientation domains" move through the aggregate in a complex way, leading to irregular grain shapes, though locally interfaces may have marked steps, suggesting crystallographic control, especially if fluid occurs along the grain boundaries. Though no new grains are produced, some can be removed or dissected, and others can coalesce or amalgamate by progressive reduction of misorientation. The process affects large areas, so that original grains may be completely consumed (Urai, Means, and Lister 1986). Fast grain-boundary migration can change rapidly to slow grain-boundary migration and vice versa, owing to sudden changes in the grain-boundary structure or the absorption of impurities (Urai 1983).

Grain-boundary migration recrystallization occurs at relatively high temperatures (amphibolite facies) in quartz and calcite (Schmid and Casey 1986; Schmid, Panozzo, and Bauer 1987; Schmid, Patterson, and Boland 1980; Stünitz and Fitz Gerald 1993). However, the process is also promoted by water on the migrating boundaries (Mancktelow and Pennacchioni 2004). This interpretation is supported by experiments in which fluid-assisted grain-boundary migration recrystallization can produce new grains with crystal faces (Urai 1983; Urai, Means, and Lister 1986). In wet samples, a continuous fluid film occurs along the migrating boundary, incorporating fluid inclusions as it moves. The boundary migration occurs by dissolution of the grain with the higher dislocation concentration, diffusion through the fluid film, and precipitation on the other grain.

In principle, recrystallization may occur either during deformation (*dynamic recrystallization* or *syndeformational recrystallization*) or after deformation (*static recrystallization*), which is equivalent to static grain growth (Vernon 2018). Static recrystallization has been inferred to occur if temperatures remain high enough for grain-boundary migration after strain rates decrease (in which case it could modify microstructures formed by dynamic recrystallization).

Dynamic recrystallization of low-melting-temperature minerals has been observed directly in in situ experiments under the microscope (Vernon 2018). Such studies have enabled detailed observation of grain-boundary movements and changes in grain shapes with progressive deformation and recrystallization. For example, Urai (1983) found that:

(1) dynamically recrystallized grains do not necessarily have undulose extinction,

(2) recrystallization may occur by grain and twin-boundary migration (bulge nucleation) and progressive misorientation of sub-grains,
(3) recrystallization may occur along fractures,
(4) grain boundaries may progress and regress cyclically,
(5) one grain may be cut up into two grains by grain-boundary movement,
(6) two grains may coalesce in to one,
(7) incomplete elimination of serrations may lead to the preservation of "leftover grains,"
(8) bimodal grain-size distributions may form, and
(9) "orientation families" of grains with similar orientations may develop, owing to different rates of boundary migration in different directions.

White (1977) suggested that dynamically recrystallized grains can be recognized by the presence of sub-grains, deformation bands and deformation lamellae, in contrast to optically strain-free new grains expected from static recrystallization. Even though Urai (1983) and Urai, Means, and Lister (1986) found that dynamically recrystallized grains do not necessarily have undulose extinction, new (recrystallized) grains with undulose extinction are at least consistent with dynamic recrystallization. In fact, any evidence of deformation in new (recrystallized) grains is diagnostic of dynamic recrystallization, such as optically-observable sub-grains. Similarly, orientation families, that is, groups of several apparently independent grains with identical crystallographic orientations, may also be reliable indicators of dynamic recrystallization. Furthermore, while aggregates of relatively coarse-grained, optically strain-free polygonal grains have been interpreted as indicating static recrystallization, strain-free grains have also been produced by dynamic recrystallization in experiments (Urai, Means, and Lister 1986). And one potentially useful microstructural feature is the observation that boundaries of grains developing during strain-induced grain-boundary migration (dynamic recrystallization involving bulge nucleation) grow away from their centers of curvature, whereas the reverse applies to static grain growth.

In both sub-grain rotation and strain-induced grain-boundary migration, new grains are smaller than the original deformed grains, so that *grain size reduction* is typical of dynamic recrystallization (Vernon 2018; Wojtal, Blenkinsop, and Tikoff 2022). New grains tend to be much smaller at lower temperatures (250–300°C for quartz and 400–450°C for feldspar) and/or fast strain rates. Indeed, at relatively low temperatures (200–300°C for quartz and 400–500°C for feldspar) and/or fast strain rates, recrystallization mainly involves grain-boundary migration, which involves bulging of grain boundaries in response to variable dislocation concentrations, forming small strain-free grains. However, grain-boundary migration recrystallization is restricted to the relatively high temperatures of amphibolite facies conditions for quartz and calcite (Schmid and Casey 1986; Schmid, Panozzo, and Bauer 1987; Schmid, Patterson, and Boland 1980; Stünitz and Fitz Gerald 1993) and granulite facies conditions for feldspar (Lafrance, John, and Scoates 1996).

Experimental studies on quartz aggregates have identified three regimes of dislocation creep, defined by different mechanisms of dynamic recrystallization (Hirth and Tullis 1992; Tullis et al. 2000). These regimes operate at different temperature-strain rate conditions and produce different microstructures, which have also been recognized in naturally-deformed quartzites. However, they form at much lower temperatures, owing to presumed slower natural strain rates.

Regime 1 occurs at the lowest temperatures of deformation and is characterized by difficult dislocation climb, low grain-boundary mobility and high dislocation-density contrasts between different grains. Dislocation glide is accommodated by recovery and strain-induced grain-boundary migration (bulging recrystallization) at slow rates, producing very small bulges. The bulging occurs mainly at triple junctions and along fractures, if present. Regime 2 is characterized by recrystallization involving progressive sub-grain rotation, and occurs at intermediate temperatures. Regime 3 is characterized by grain-boundary migration recrystallization at fast rates, and occurs at high temperatures. During this recrystallization whole grains may be swept clear of dislocations, and sub-grain rotation is only important for the initial formation of new grains.

Deformation of Polymineral Aggregates

Ductile behavior of minerals and rocks is generally defined as the capacity to deform without fracturing on the grain scale (Passchier and Trouw 1996; Vernon 2018). However, ductility has also been defined as "the capacity for substantial change of shape without gross fracturing" (Paterson 1978). The latter definition refers to megascopic or macroscopic flow and is independent of the microscopic mechanisms of deformation, which can include not only crystal plasticity and diffusional flow (which maintain cohesion at the microscopic scale) but also cataclastic (microscopically brittle) mechanisms. In other words, based on that definition, a rock can be ductile on the scale of a hand specimen or outcrop but partly brittle on the microscopic scale.

A major factor governing ductility is the number of slip systems available for deformation to occur without producing holes or cracks (Murrell 1990).

Five independent slip systems are necessary for plastic deformation without fracturing at grain boundaries (Groves and Kelly 1963). However, many minerals have strongly anisotropic structures (for example, micas) and so have fewer slip systems than those with more three-dimensional structures (for example, quartz). The result is that some minerals can change their shapes in response to general local stress fields more readily than others. This can lead to localization of deformation into high-strain zones or to the opening of pores or local cracks, which are important in localizing fluids.

Natural rocks typically have several minerals with different deformation properties that can vary with external conditions (for example, temperature, pressure, water activity) (Vernon 2018). This situation produces deformation contrasts between different minerals, which occur when stronger and weaker minerals coexist. For example, strong feldspar and weak quartz typically coexist, deforming at relatively low temperature (<500°C). The feldspar deforms plastically a little before it fractures (brittle deformation), whereas the quartz flows and recrystallizes in a ductile manner, commonly forming "ribbons" of fine-grained recrystallized aggregates. Those ribbons originate as kink bands or deformation bands that recrystallize with progressive deformation.

Evidence of both ductile and brittle behavior is seen in many felsic mylonites in which feldspar deforms cataclastically, whereas quartz and mica deform mainly by dislocation creep, commonly assisted by neocrystallization (Vernon, Williams, and D'Arcy 1983). On the other hand, sometimes biotite deforms by fracturing along the cleavage, forming "shreds" or cleavage platelets that become stretched out along a developing foliation (Johnson, Vernon, and Upton 2004; Vernon, Johnson, and Melis 2004), as indicated by experimental results (Shea and Kronenberg 1993).

Though fluid-enhanced microcracking is commonly an important deformation mechanism in such rocks, both brittle and ductile processes alternate, and cohesion is maintained during deformation (Gapais 1989; Stel 1986). This has been referred to as "semi-brittle" behavior. In some rocks, hydrous minerals that grow from fluids that enter the rock during brittle deformation undergo ductile deformation (Simpson 1986), which may be followed by more fracturing and mineral growth in a cyclic process (Stel 1986).

The effect of ductility contrasts in rocks can be so great that deformation is forced to partition preferentially into zones rich in weak minerals, such as mica (Goodwin and Tikoff 2002; Shea and Kronenberg 1993) and/or fine-grained aggregates (Stünitz and Fitz Gerald 1993), promoting the formation of local zones of high strain (shear zones).

As already noted, contrasts in the deformation of quartz and feldspar are strongly temperature dependent. Similarly, strain rate is important when considering deformation contrasts between minerals. Furthermore, large grains generally deform more readily by dislocation flow than smaller grains of the same mineral, probably because intracrystalline slip can occur with less interference from adjacent grains (Rutter 1976). However, in many rocks, large grains of quartz and K-feldspar are stronger than surrounding finer-grained aggregates of weaker minerals such as mica. This is because intergranular deformation is important in fine-grained aggregates (for example, by grain-boundary sliding, reaction-assisted diffusion), leading to increased strain rates (Etheridge and Vernon 1981; Stünitz and Fitz Gerald 1993). However, as pointed out by de Bresser, ter Heege, and Spiers (2001), dynamic recrystallization can lead to major zones of weakening and strain localization only if grain growth is inhibited.

In summary, the focus needs to be on what should be observed at the microscopic scale in the sandstone, siltstone, and shale beds of the Bright Angel Formation within the Whitmore Helipad fold. Ductile deformation features, especially in quartz grains, that should be evident if these lithologies were lithified before the folding occurred should include undulose extinction, kink bands, deformation bands, deformation lamellae, deformation twins, pressure effects at the contacts between grain boundaries, sub-grains, sutured grain boundaries, grain boundary bulges, intragranular fractures, intergranular fractures, crystallographic preferred orientations, any rotated grains or sub-grains, any grain size reduction, and/or recrystallized grains.

A Petrographic Study

So, was the folding of the sandstone, siltstone, and shale beds of the Bright Angel Formation within the Whitmore Helipad fold due to slow processes of ductile deformation over millions of years that occurred hundreds of millions of years after these lithologies lithified, or was the folding due to soft-sediment deformation soon after deposition before dewatering and lithification? It should be very evident that to resolve this debate requires a petrographic examination of sandstone, siltstone, and shale samples from the fold to determine what microstructural features are present. Ductile deformation should have resulted in definitive microstructural features which should be visible in the grains and cement of the sandstone, siltstone, and shale under the microscope, as described in detail above. On the other hand, the absence of such microstructural features, and instead the presence of preserved primary depositional features, would

indicate soft-sediment deformation had occurred, particularly if those preserved primary depositional features in sandstone, siltstone, and shale samples from the fold are identical to those in samples from the same Bright Angel Formation beds distant from the fold.

No such petrographic study has previously been published. So, during an investigation of four folds in the Grand Canyon, ten samples of the Bright Angel Formation were collected from the Whitmore Helipad fold, and two samples from outcrops along the Colorado River corridor distant from that fold (fig. 1 and table 1). The purpose was to compare under the microscope the samples from the fold (fig. 21) with the distal samples (fig. 1) to ascertain what effects the folding had on the sandstone, siltstone, and shale, and thus determine the conditions during, and the timing of, the folding relative to the conditions and timing of the deposition and subsequent lithification (cementation) of these lithologies. Details of the locations of those samples are provided in figs. 1 and 21, and in table 1, as well as in the appendix (in the Supplementary material). Within the Whitmore Helipad fold, the alternating

Table 1. Locations and stratigraphic details of all the Bright Angel Formation samples examined in this study.

Sample	Location	Location Coordinates	Stratigraphic Position	Notes
BAS-01	River Mile 167.9	N 36° 15.322' W 112° 54.439'	Sandstone relatively high in the Bright Angel Formation stratigraphic section	River right between National and Fern Glen Canyons (closer to latter)
BAS-02	River Mile 167.9	N 36° 15.322' W 112° 54.439'	Sandstone relatively high in the Bright Angel Formation stratigraphic section	River right between National and Fern Glen Canyons (closer to latter)
HF-01	Whitmore helipad fold River Mile 187.4	N 36° 9.250' W 113° 11.400'	Sandstone in heterolithic sequence horizon near the base of the stratigraphic section	River left, cliff behind the scrub-covered slope up from the river-bank
HF-02	Whitmore helipad fold River Mile 187.4	N 36° 9.250' W 113° 11.400'	Shale in heterolithic sequence horizon near the base of the stratigraphic section	River left, cliff behind the scrub-covered slope up from the river-bank
HF-03	Whitmore helipad fold River Mile 187.4	N 36° 9.250' W 113° 11.400'	Shale in heterolithic sequence horizon near the base of the stratigraphic section	River left, cliff behind the scrub-covered slope up from the river-bank
HF-04	Whitmore helipad fold River Mile 187.4	N 36° 9.250' W 113° 11.400'	Sandstone in heterolithic sequence horizon near the base of the stratigraphic section	River left, cliff behind the scrub-covered slope up from the river-bank
HF-05	Whitmore helipad fold River Mile 187.4	N 36° 9.250' W 113° 11.400'	Siltstone in heterolithic sequence horizon near the base of the stratigraphic section	River left, cliff behind the scrub-covered slope up from the river-bank
HF-06	Whitmore helipad fold River Mile 187.4	N 36° 9.250' W 113° 11.400'	Sandstone in heterolithic sequence horizon near the base of the stratigraphic section	River left, cliff behind the scrub-covered slope up from the river-bank
HF-07	Whitmore helipad fold River Mile 187.4	N 36° 9.250' W 113° 11.400'	Siltstone in heterolithic sequence horizon near the base of the stratigraphic section	River left, cliff behind the scrub-covered slope up from the river-bank
HF-08	Whitmore helipad fold River Mile 187.4	N 36° 9.250' W 113° 11.400'	Sandstone in heterolithic sequence horizon near the base of the stratigraphic section	River left, cliff behind the scrub-covered slope up from the river-bank
HF-09	Whitmore helipad fold River Mile 187.4	N 36° 9.250' W 113° 11.400'	Siltstone in heterolithic sequence horizon near the base of the stratigraphic section	River left, cliff behind the scrub-covered slope up from the river-bank
HF-10	Whitmore helipad fold River Mile 187.4	N 36° 9.250' W 113° 11.400'	Sandstone in heterolithic sequence horizon near the base of the stratigraphic section	River left, cliff behind the scrub-covered slope up from the river-bank

Fig. 21. The Whitmore Helipad fold at river mile 187.4, river left, with the location of the collected samples labeled. The ladder provides the scale, the ladder's steps being approximately 12 in (~30.5 cm) apart.

sandstone, siltstone, and shale beds were sampled laterally from the lower limb through the two hinges of the fold, and those sampling locations can be seen on fig. 21. All samples were sent to Calgary Rock and Materials Services, Inc. (Calgary, Canada) for thin sectioning and for scanning electron microscope (SEM) examination.

Thin Section Examination

Thin sections for this study were mounted on standard glass microscope slides. Before the slices were cut using a diamond saw, the rock samples were impregnated under confining pressure with epoxy resin that contained a blue dye. This ensured that grains did not get dislocated, or the rock fabrics did not get distorted during the sawing of the slices. However, this process left the thin sections with a blue dye stain as the surrounding background and in any holes or pores within the rock fabrics. Before cover slips were added, the thin sections were stained so as to make the K-feldspar and calcite in the rock fabrics more easily distinguished. Thus, the K-feldspar grains have a distinctive yellow color, and the calcite is pinkish in plane polarized light.

Detailed petrographic descriptions of all samples from extensive thin section examination are provided in the appendix (in the Supplementary material), along with photomicrographs of the whole thin sections from which the descriptions were derived. The locations and stratigraphic details of all samples is provided in table 1, as well as in the Appendix. All samples were collected from heterolithic facies sections of the Bright Angel Formation (Snelling 2021b). The results of the XRD analyses which provided a quantitative estimate of the mineral constituents of each sandstone, siltstone, and shale sample are compiled in table 2. These estimated mineral constituents could then be verified under the petrographic microscope. The porosities of each sample were also estimated from the thin sections and those data are included in the last column of table 2.

Thin sections of the complete set of samples are shown at normal scale in fig. 22, while the photomicrographs in fig. 23 show typical textures within the complete set of 12 samples of the Bright Angel Formation for this study. It should be noted that the blue dye staining caused by the impregnated epoxy between the grains sometimes encroaches on the grain edges or even across grain surfaces. Thus, some patches of blue dye mark the occasional pore spaces. The details of the mineral constituents in these samples and their textures that indicate rapid deposition of the Bright Angel Formation are reported by Snelling (2021b).

Table 2. Mineral compositions of the Bright Angel Formation samples in this study from X-ray diffraction (XRD) analyses, courtesy of Ray Strom, Calgary Rock and Materials Services, Inc., Canada, and the estimated average porosities.

Sample	Lithology	Quartz	K-Feldspar	Calcite	Dolomite	Ankerite	Siderite	Illite	Kaolinite	Pyrite	Total	Porosity
BAS-01	sandstone	74.3%	21.7%	1.8%	1.2%	–	–	0.5%	0.5%	–	100.0%	~1.3%
BAS-02	sandstone	33.7%	19.6%	32.4%	9.2%	–	–	2.3%	–	2.8%	100.0%	~1.0%
HF-01	sandstone	57.3%	28.7%	3.4%	3.2%	6.8%	–	0.6%	–	–	100.0%	~1.4%
HF-02	shale	33.8%	43.1%	–	–	2.9%	–	20.2%	–	–	100.0%	~0.3%
HF-03	shale	25.4%	36.7%	–	–	3.7%	–	34.2%	–	–	100.0%	~0.2%
HF-04	sandstone	46.5%	33.5%	–	–	17.6%	–	2.4%	–	–	100.0%	~0.15%
HF-05	siltstone	31.1%	46.9%	–	–	3.3%	–	18.7%	–	–	100.0%	~0.1%
HF-06	sandstone	86.8%	11.0 %	–	2.2%	–	–	–	–	–	100.0%	~0.1%
HF-07	siltstone	29.6 %	32.4 %	–	11.9%	–	8.6%	17.5%	–	–	100.0%	~0.05%
HF-08	sandstone	47.6%	42.2 %	–	7.9%	–	–	2.3%	–	–	100.0%	~0.5%
HF-09	siltstone	27.3%	45.1%	–	5.3%	–	–	22.3%	–	–	100.0%	~0.05%
HF-10	sandstone	42.6%	45.3%	–	9.1%	–	–	2.5%	–	0.5%	100.0%	~0.8%

In the thin sections, the fine-grained sandstones are generally massive and well-sorted, sometimes laminated parallel to the bedding or sometimes with a hint of being partially cross-laminated. They are usually dominated by angular, and even euhedral, to sub-rounded quartz grains ranging in size from medium to coarse silt to very fine and fine sand and very occasional medium sand, using the standard definitions and terminologies for sorting of Folk (1966, 1980) and Pettijohn, Potter, and Siever (1973), for shape of Powers (1953) and Folk (1955), and for size of Udden (1914) and Wentworth (1922). Usually, coarse silt to fine sand-size, sub-angular to sub-rounded K-feldspar grains, and sometimes even sub-euhedral laths, are subordinate to the quartz grains, but occasionally the K-feldspar grains predominate. Most of the sandstones contain small oval-shaped olive green-brown glauconite pellets or sub-angular to sub-rounded grains. Scattered muscovite flakes are usually sub-parallel to the bedding or occasional laminae, and there are occasional brachiopod shell fragments (distinguished by their thick internal structure and composition). Generally, there are virtually no original pore spaces remaining because they were filled with quartz (silica) cement, usually as overgrowths around the detrital quartz grains, which are occasionally outlined by the original iron oxide coatings, so that many grains now meet at triple points. In finer-grained rocks the grain radii are smaller than the microscope slide thickness and thus the grains stack up on each other, obscuring the porosity. So, there may be a few very small pore spaces that are difficult to see. Alteration is marked by carbonates (calcite, dolomite, and/or ankerite) or clay minerals (predominantly illite), often accompanied by iron oxides filling former pores, replacing K-feldspar grains, or filling fractures. Thus, these are glauconitic sub-arkosic quartz arenites according to the classifications of Dott (1964), Folk (1980), McBride (1963) Pettijohn (1954, 1957), Pettijohn, Potter, and Siever (1972), Scholle (1979), and Ulmer-Scholle et al. (2015), and some are even glauconitic arkoses where the K-feldspar contents are greater than 25%.

In the thin sections, the siltstones are very similar to the sandstones except that their grain sizes are smaller. In fact, it is difficult to distinguish the siltstones from the fine-grained sandstones because the latter also contain some silt-sized grains, and some of the shales have selvages or laminae of siltstone. The siltstones are interlocking mosaics of tiny to very small, angular to sub-rounded quartz and K-feldspar grains with subordinate sub-euhedral, angular, and sub-rounded to rounded greenish glauconite grains and fragments, numerous muscovite flakes at various angles but sometimes parallel to the bedding, and occasional brachiopod shell fragments. However, there are also brown patches in the rock fabric dominated by very small, sub-angular to sub-rounded, iron-oxide-stained carbonate grains and rhombs (dolomite, siderite, and calcite), some of which may be detrital, and there is illite alteration of some K-feldspar grains. Some of these may even be carbonate clasts. While there is some silica cement apparent, likely as overgrowths on the original detrital quartz grains, much of the mosaic is now cemented by a combination of illite and carbonates, some of which is iron-oxide-coated, so there are virtually no pore spaces remaining (although the tight stacking of many of the very small grains may obscure any trivial pore spaces). If the same sandstone classification criteria are applied, the siltstones would likewise have originally been glauconitic arkoses.

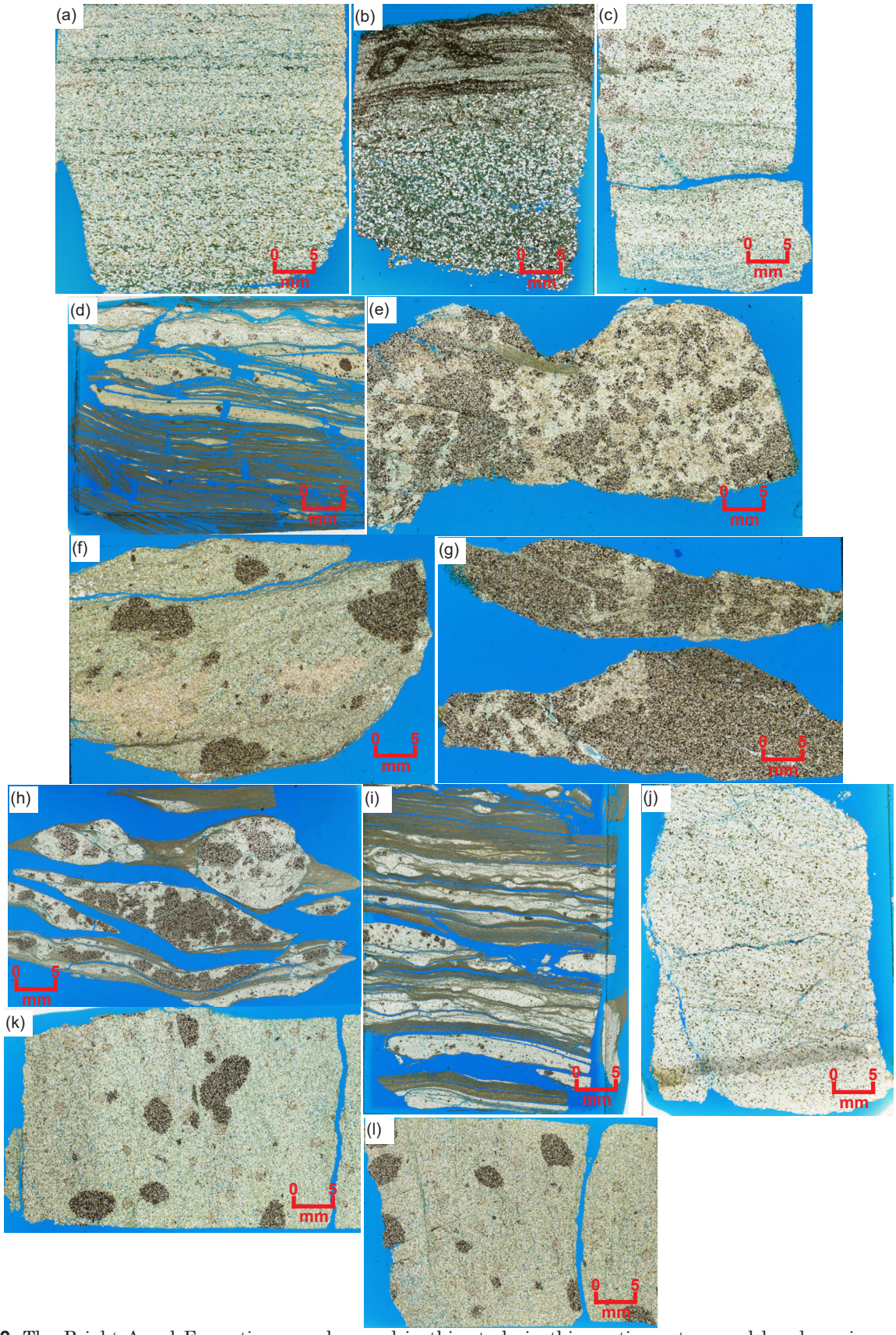

Fig. 22. The Bright Angel Formation samples used in this study in thin sections at normal hand specimen scale, showing the textures, the varying degrees of sorting, and the variations in grain sizes of quartz and K-feldspar that constitute the sandstone, siltstone, and shale bands/beds, as well as the friability of the samples. (a) BAS-01, (b) BAS-02, (c) HF-01, (d) HF-02, (e) HF-04, (f) HF-05, (g) HF-07, (h) HF-09, (i) HF-03, (j) HF-06, (k) HF-08, and (l) HF-10.

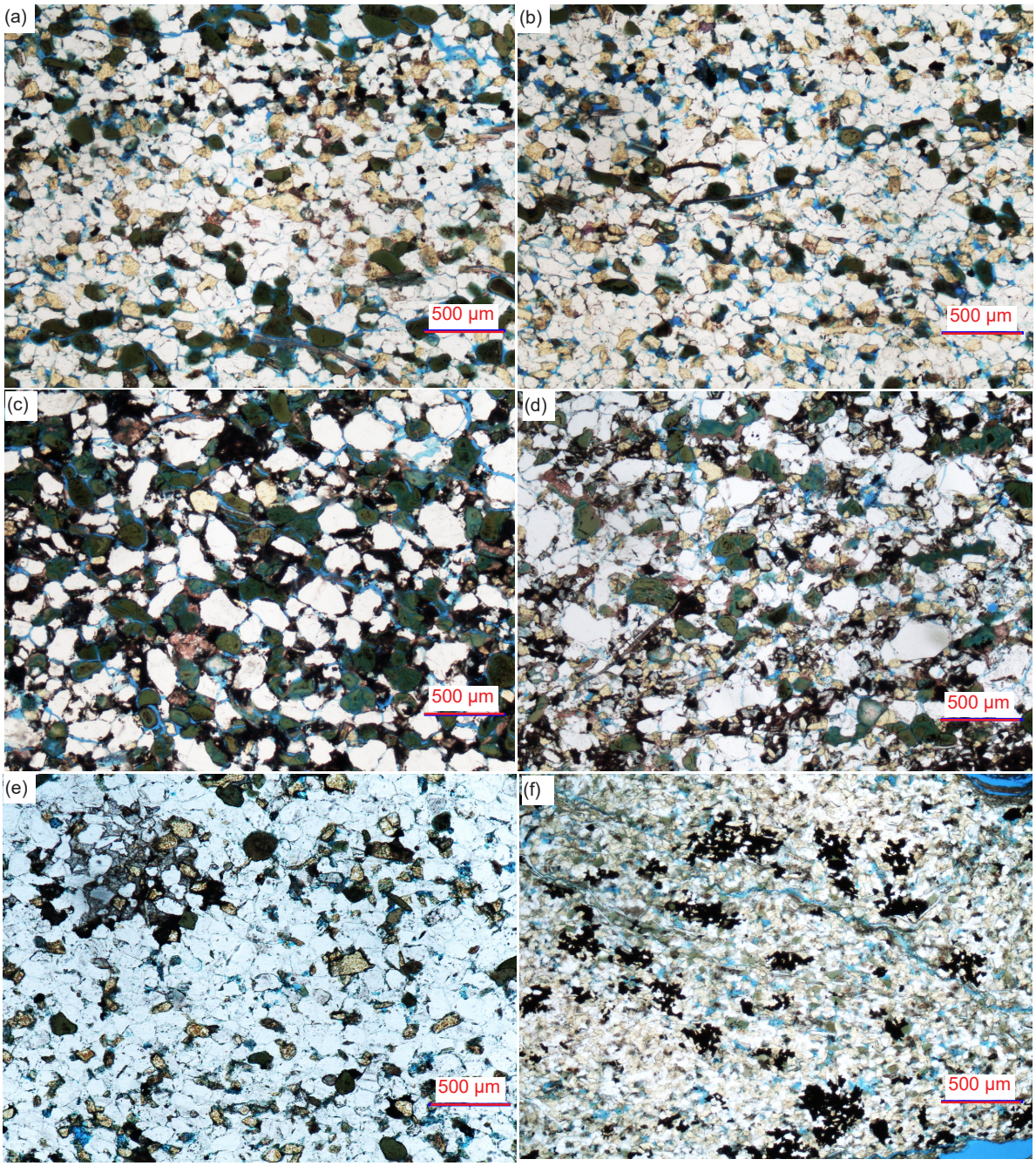
(a)
500 μm
(b)
500 μm
(c)
500 μm
(d)
500 μm
(e)
500 μm
(f)
500 μm

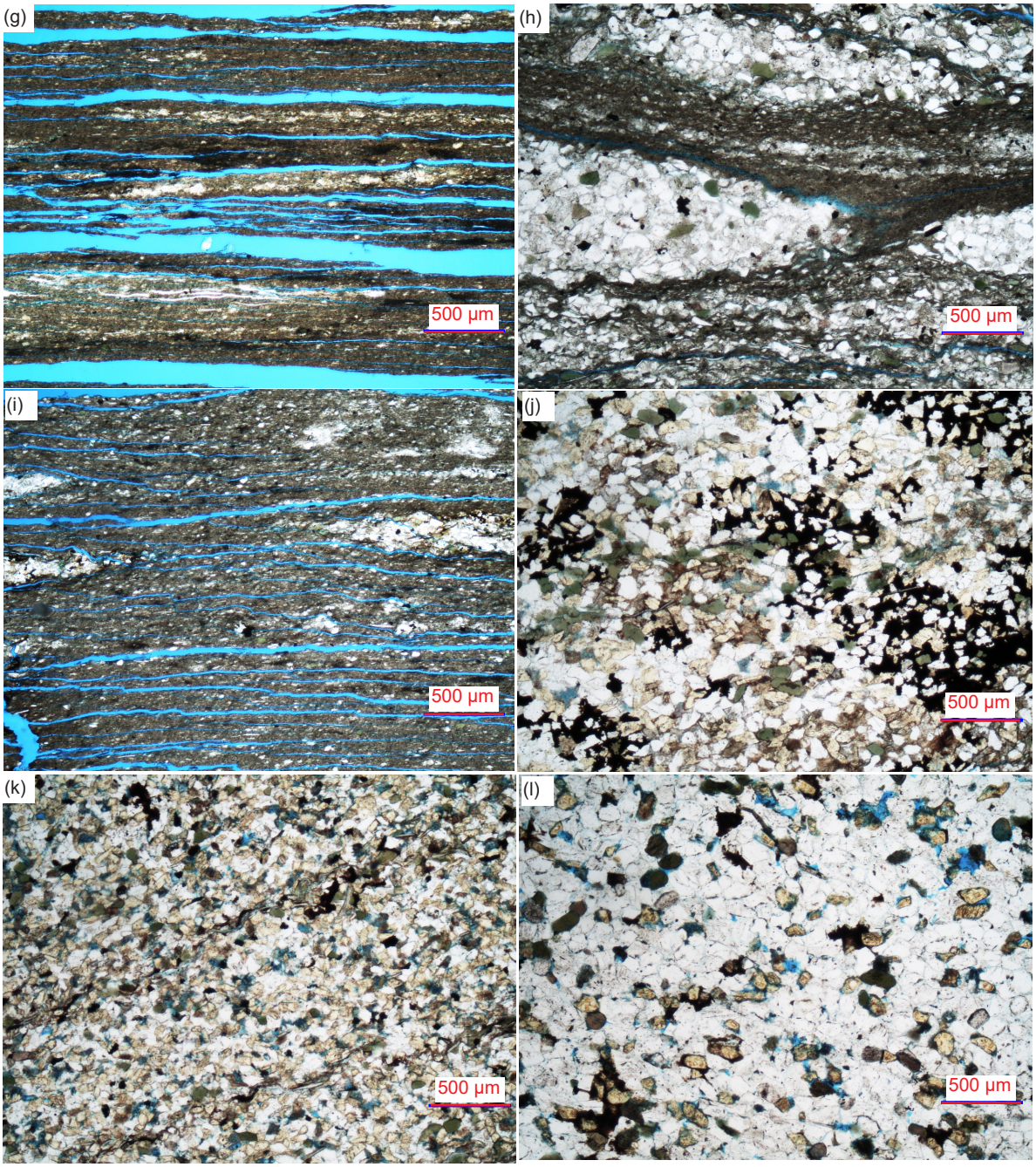
(g)
500 µm
(h)
500 µm
(i)
500 µm
(j)
500 µm
(k)
500 µm
(l)
500 µm

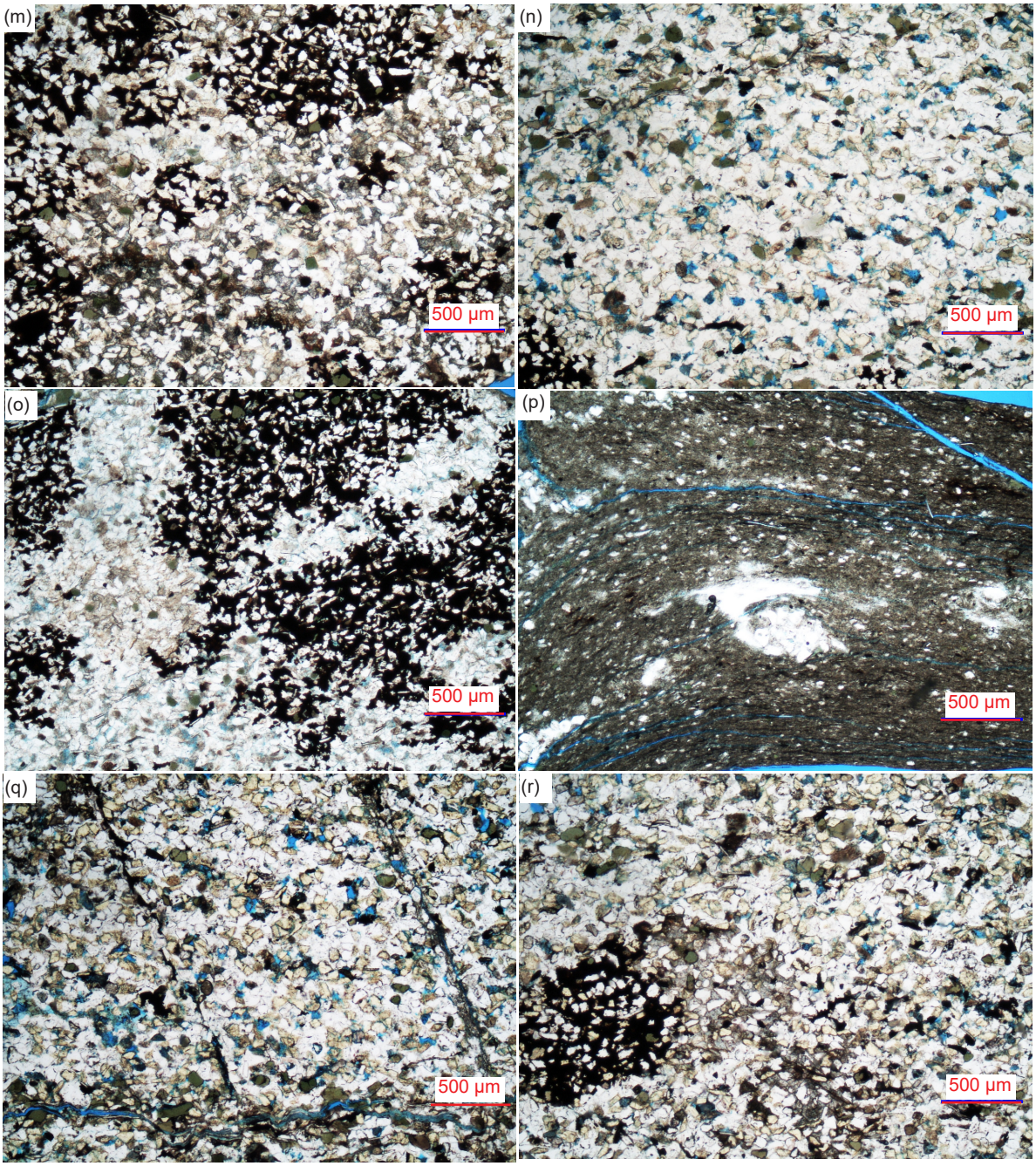

Fig. 23 (pages 102–104). Textures of all the Bright Angel Formation samples used in this study, showing the wide variations in grain sizes and thus rock types, as well as the abundances of K-feldspar and occasional glauconite. (a), (b) BAS-01, (c), (d) BAS-02 (e) HF-01, (f), (g) HF-02, (h), (i) HF-03, (j) HF-04, (k) HF-05, (l) HF-06, (m) HF-07, (n) HF-08, (o), (p) HF-09, and (q), (r) HF-10.

Shales or mudstones in the thin sections consist of alternating thin bands or laminae and selvages of "softer" predominantly iron-oxide-stained yellow-brown, very-fine-grained illite and "harder" laminae and "augen"-like bands or "eyes" of siltstone consisting of a "clean" fine-grained mosaic of quartz and K-feldspar grains. According to the classification scheme for shales of Ulmer-Scholle et al. (2015, page 183, fig. 8.1), given the large amounts of quartz and K-feldspar in these shales (table 2) they would be termed "siliceous mudstones." The illite-dominated laminae appear to be primarily due to the alteration of tiny K-feldspar grains because there are tiny remnant K-feldspar grains and residual tiny irregularly-shaped quartz grains scattered through the rock fabric. There are also numerous tiny muscovite flakes at various angles but mostly inclined parallel to the bedding, some tiny irregularly-shaped blotches of greenish glauconite, and many scattered very tiny-tiny specks, blotches, and streaks of heavy iron oxide, as well as the pervasive iron oxide staining. There are virtually no pores as the original mosaic was already tightly fitted and the pervasive illite alteration is now the predominating cement, perhaps along with the occasional patches of heavy iron oxide. The siltstone bands and "eyes" consist of the same mineral grains but they are slightly larger silt-sized and are often dominated by quartz, though K-feldspar is still present, as well as the greenish glauconite grains, and numerous muscovite flakes often parallel the borders of the bands, laminae and "eyes." Some tiny carbonate grains are sometimes present, often accompanied by iron oxides and clumped together in brown patches. Some trivial pores may also still be present. It is to be expected that the shales would have a similar mineral composition to that of the interbedded siltstones and sandstones, their segregation being due to sorting of grain sizes during deposition.

Scanning Electron Microscope (SEM) Examination

The scanning electron microscope (SEM) used in the laboratory at Calgary Rock and Materials Services, Inc. is an Amray 1820i instrument equipped with a 4pi digital control and image acquisition system and is used in its secondary mode. Energy Dispersive Spectrometry (EDS) spectra are acquired using a Gresham Titan near-windowless piezo-cooled detector.

Samples as supplied in vertical orientation were all fractured/broken vertically. This ensured that the horizontal bedding is not the major feature of the sample examination process. Samples were glued using five-minute adhesive to 10 mm aluminum stubs, maintaining the vertical fracture orientation. After curing, the samples were gently blown clear of debris using dry air. Following this, the samples were placed in a Polaron sputter coating unit for application of gold coating used to ensure good surface conductivity. This unit is equipped with a piezo-cooled stage to assist in preventing thermal damage to the samples. Additionally, coating was done in a burst mode—one minute on, one minute off, continued for a total coating time of five minutes for each sample.

Following coating, samples were individually and sequentially placed into the Amray 1820i for analysis. Image sequences from low magnification to high magnification were taken and reviewed for significant features. Bulk EDS is normally run on the low magnification scanned surface in order to get a composite elemental analysis. Beam accelerating voltage is normally held at 30 kV in order to provide best resolution and least beam distortion. This also assists in providing the best EDS response over the emission range of interest.

Results

The focus of this study was to investigate the microstructures in the sediment grains and the textures within the rock samples to ascertain whether the original sedimentary rock grains and textures had been changed by the deformation in the fold, particularly the hinge zones, compared to those samples collected from the fold limb and those distant from the fold. The detailed petrographic descriptions of all 12 samples (two regional samples distant from the fold and ten samples from the Whitmore Helipad fold) are available in the appendix in the Supplementary material.

Grains and Textures

Several observations are very evident, being uniformly and ubiquitously present in all samples, both those collected from the fold hinges and limbs, and those collected from the locations distant to the fold. However, there are also some features that are different in some of the samples from the fold compared to the distal samples.

The quartz grains are invariably in tightly-packed interlocking mosaics with the other mineral grains, principally K-feldspar grains, with virtually no pore spaces remaining. Many of the *original detrital quartz grains* or their outlines can still be observed, as well as the later quartz overgrowths that cement the grains together (fig. 24). Depending on whether the rock is a sandstone, siltstone, or shale, the quartz grains in each are in narrow size ranges corresponding to fine to coarse silt and very fine and fine sand, so each rock fabric appears well-sorted. The quartz grains are sometimes irregularly-shaped angular (sometimes elongated parallel to the bedding), but invariably are

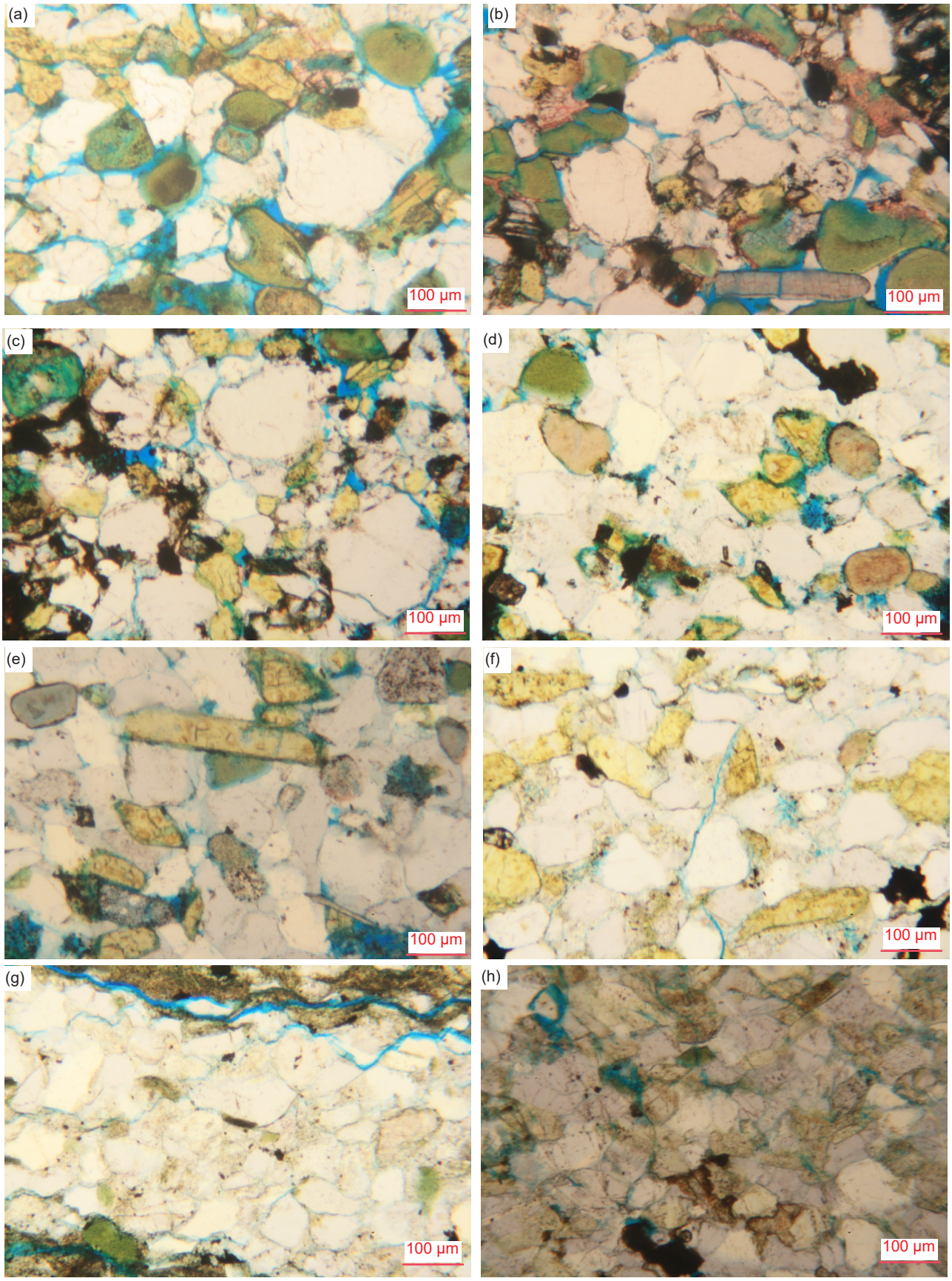
(a)
100 µm
(b)
100 µm
(c)
100 µm
(d)
100 µm
(e)
100 µm
(f)
100 µm
(g)
100 µm
(h)
100 µm

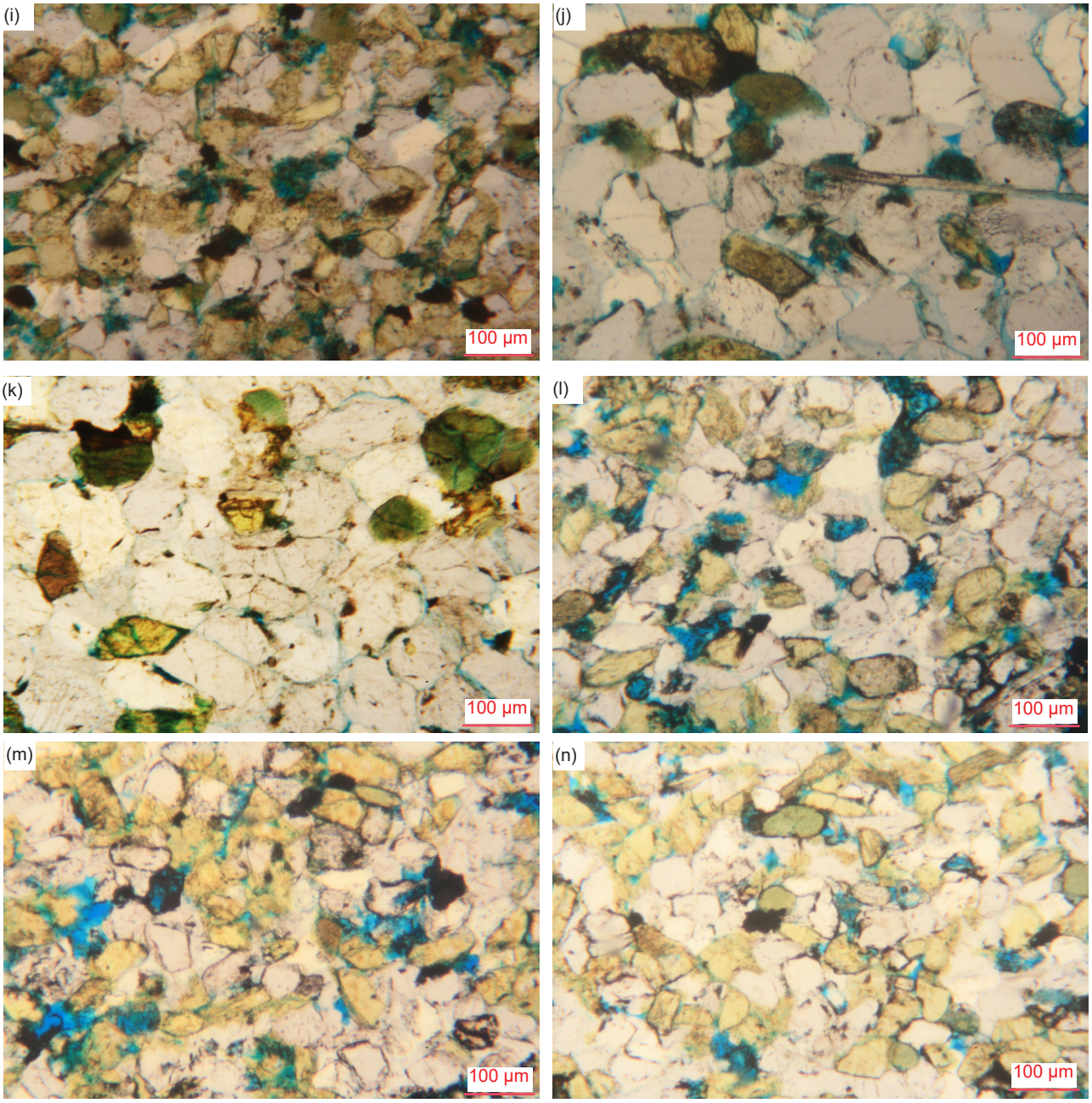

Fig. 24 (pages 106–107). Quartz grains with quartz overgrowths in the Bright Angel Formation samples, the original detrital shapes of some of the quartz grains being outlined with dust and iron oxides. (a) BAS-01, (b), (c) BAS-02, (d), (e) HF-01, (f) HF-02, (g) HF-03, (h) HF-04, (i) HF-05, (j), (k) HF-06, (l), (m) HF-08, and (n) HF-10.

euhedral and sub-angular to sub-rounded, some with internal iron oxide "ghost" outlines of the original sub-rounded detrital grains with the overgrowths in optical continuity (fig. 24a, b, e, j, k, m, n). While the overburden pressure has obviously compacted the originally-deposited sediment grains, their close packing still left a very few small pore spaces even in the samples from the fold (table 2). These pores would initially have been filled with connate water but were later mostly filled by quartz cement growing over the sand grains.

The quartz and K-feldspar *grains often meet at triple points* produced by the quartz (silica) cement growing as overgrowths on the original detrital grains (fig. 25). These quartz overgrowths would have resulted from dewatering of the pore spaces, the dissolved silica in the connate water precipitating to infill most of the pore spaces. Usually, the quartz overgrowths precipitated in optical continuity with the original detrital grains. Often the original detrital grain outlines have been obliterated during this silica cementation process so that the quartz grains have uniform optical appearances with few internal markings and simply interlock tightly with sub-euhedral outlines meeting at triple points. This suggests silica for the cement was probably derived mostly from the connate water in the original pore spaces dissolving silica in situ from the edges of the detrital grains, particularly at pressure points at grain-to-grain contacts due to the compacted close packing of the detrital grains. When the silica precipitated within the pore spaces, it overlaid the grain surfaces and grew inwards to eventually meet at triple points, the most ergonomic configuration.

Also, of significance are the porosity estimates listed for each sample in table 2 (in the last column). In all samples there are very few pore spaces left in the rock fabric, yet the blue dye that accompanied the resin used under pressure to impregnate the samples before the thin sections were cut has stained between the grains and encroached onto some of their surfaces, sometimes covering grains and thus distorting their colors, which can make some look like pore spaces. It should be noted that where the grains have smaller radii than the microscope slide thickness, the tight stacking of the grains may obscure some residual pores. However, the estimated porosities range from ~1.0% to ~1.3% in the two distal samples (average ~1.15%) and from ~0.05% to ~1.4% in the samples from the Whitmore Helipad fold (average ~0.37%). Furthermore, within the Whitmore Helipad fold, samples in the two hinge zones generally have lower porosities (~0.05%–~0.5%) compared to those along the limbs (~0.1%–~1.4%). This is not surprising, as it is expected that the porosities would be a bit less in the hinge zones because squeezing and shaking during soft-sediment deformation can dewater the sand and thus press the sand grains tighter together (Lonergan et al. 2007; Owen 1987; Scott, Vigorito, and Hurst 2009). Similarly, in the conventional view that this folding was due to ductile deformation, the porosity should be reduced in the hinge areas due to the higher compactional forces, pressure solution, and grain fracturing to fill the pore spaces there. So, the prevalence or absence of evidence of grain fracturing could be a key observation in distinguishing between these two views of the type of deformation that produced this fold (see below).

There are a few quartz grains in every sample that contain *sub-grains* (that is, grains that are or have become internally subdivided), regardless of whether the sample is from the limbs or hinges of the fold or from the distant location (fig. 26). Often the internal subdivisions are very subtle and difficult to see, sometimes being evident because of slight color differences that likely are due to trivial differences in optical orientations which result in slightly different extinction angles under crossed polars. In most instances the sub-grains in these quartz grains appear to have been features in the original clasts, because the outlines of these quartz grains preserve their detrital shapes. This likely indicates they were eroded and transported from metamorphic rocks. There are no uniform sizes or shapes of these sub-grains. Most are irregularly-shaped with sutured boundaries, and often they are of vastly different sizes within the same quartz grain. However, in a few quartz grains, the sub-grains are more uniform in size and smoother in shape. Also, the sharpness of the sub-grain boundaries varies between quartz grains. Overall, though, sub-grains within most of the quartz grains in which they occur are only trivial features, which suggests they are not related to the deformation, especially since they occur in all samples, whether in the fold or distant from it.

Almost all the quartz grains display uniform extinction under crossed polars (fig. 27). The quartz grains generally do not show signs of any *undulose extinction* under crossed polars, nor are any *deformation lamellae* or *deformation kink bands* present. A few quartz grains display some undulose extinction (particularly near fracture planes and zones). Where there is an appearance of slightly undulose extinction (fig. 27g, h, l), it could be an artifact in the original quartz grains of the source rocks, probably derived from the metamorphic schists below the Great Unconformity, that was then retained unchanged in those deposited clasts. On the other hand, there is no indication or even any hint of any deformation lamellae or deformation kink bands in any of the quartz grains in these samples, including the samples from the hinge zones of the fold.

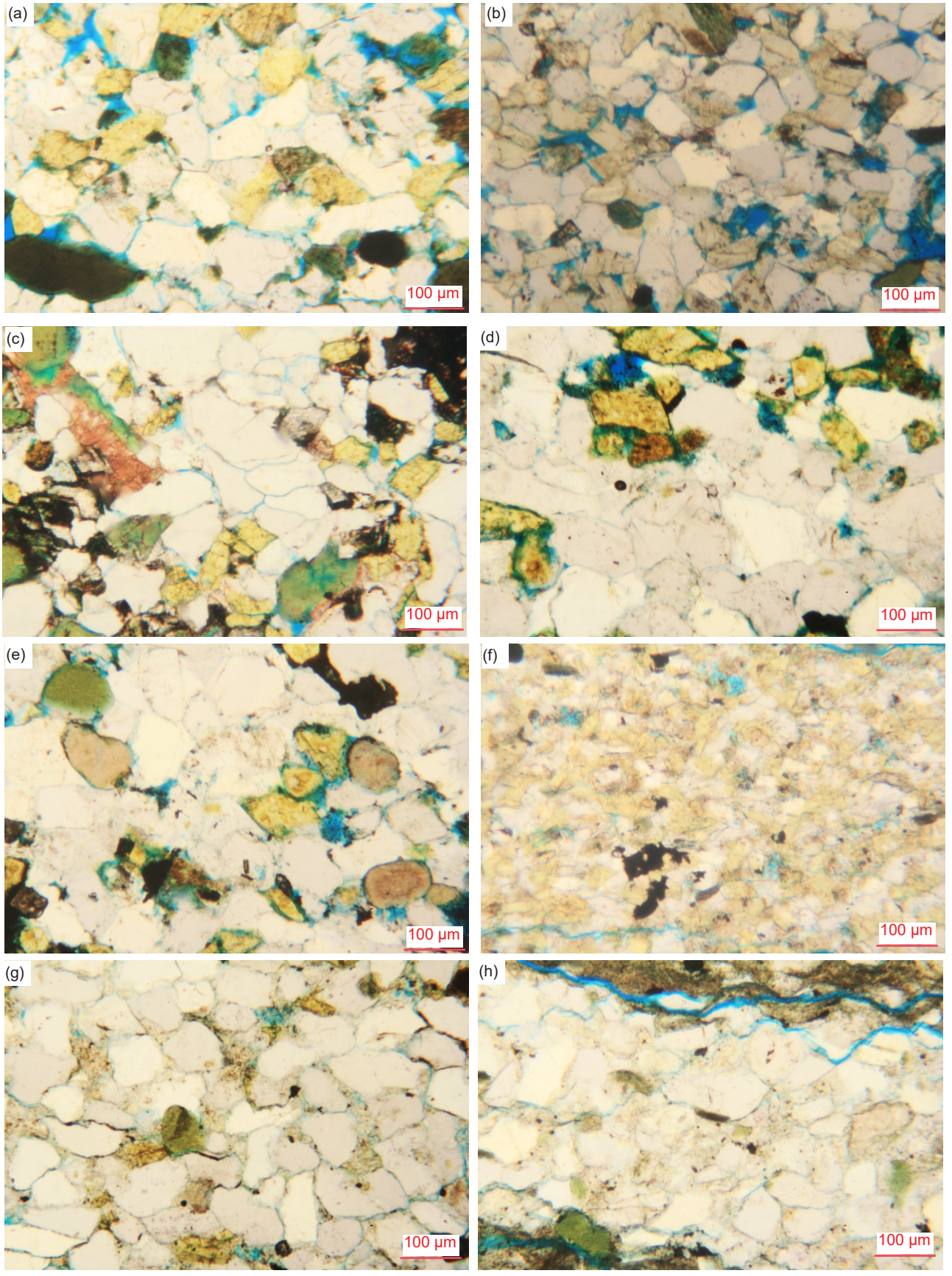
(a)
100 µm
(b)
100 µm
(c)
100 µm
(d)
100 µm
(e)
100 µm
(f)
100 µm
(g)
100 µm
(h)
100 µm

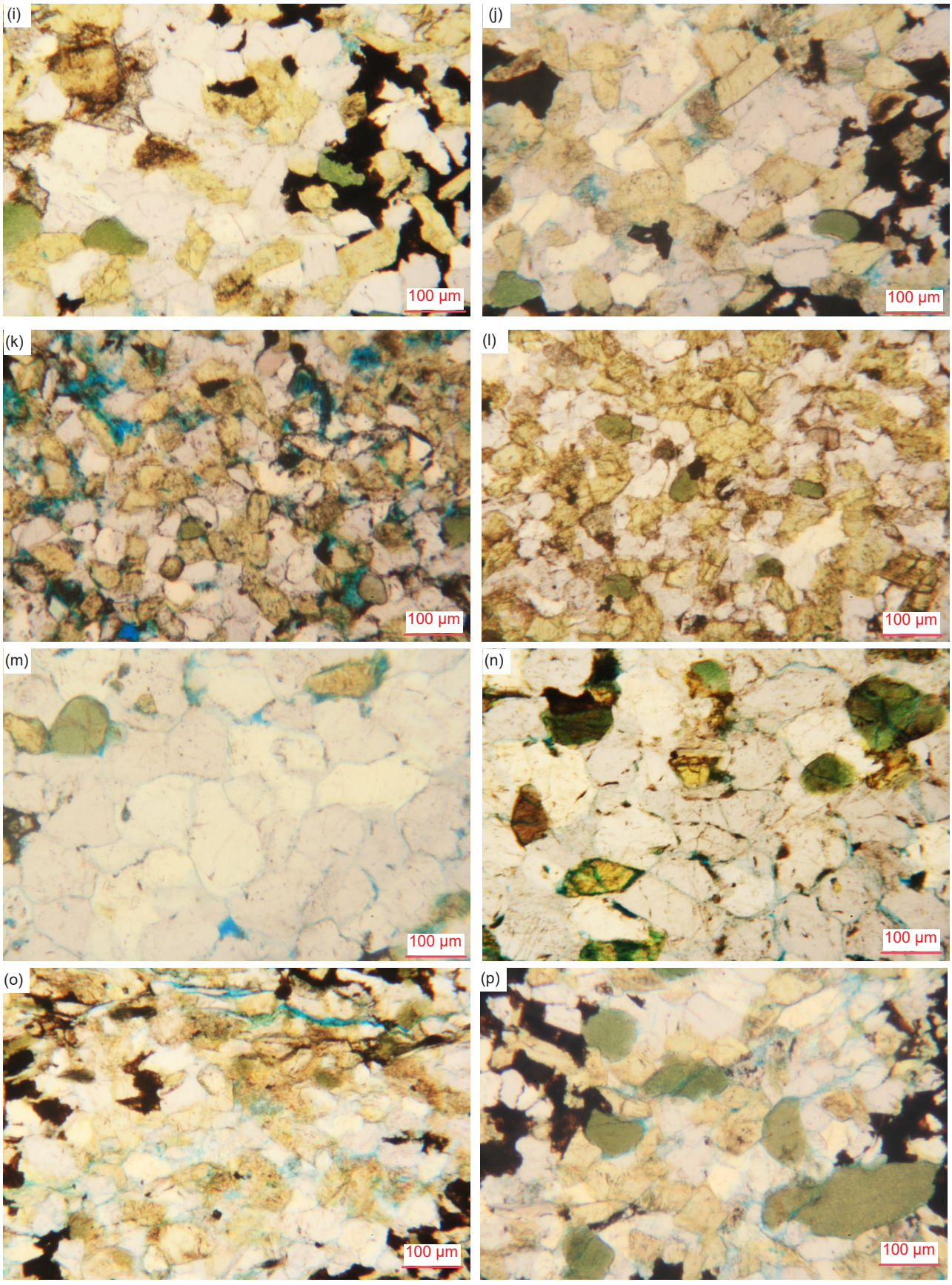
(i)
100 µm
(j)
100 µm
(k)
100 µm
(l)
100 µm
(m)
100 µm
(n)
100 µm
(o)
100 µm
(p)
100 µm

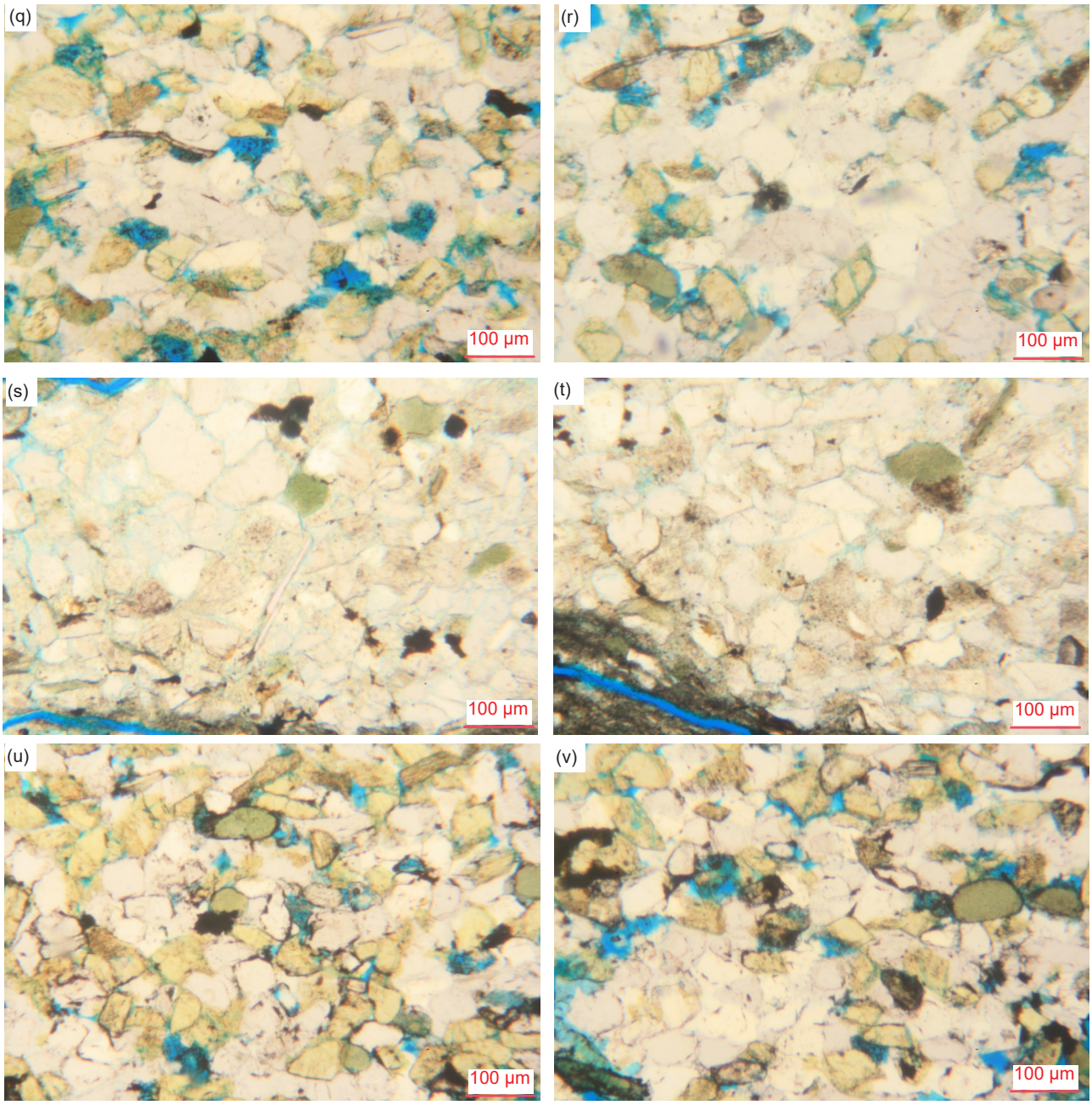

Fig. 25 (pages 109–111). Some quartz grains that meet at triple points within the Bright Angel Formation samples. (a), (b) BAS-01, (c) BAS-02, (d), (e) HF-01, (f), (g) HF-02, (h) HF-03, (i), (j) HF-04, (k), (l) HF-05, (m), (n) HF-06, (o), (p) HF-07, (q), (r) HF-08, (s), (t) HF-09, and (u), (v) HF-10.

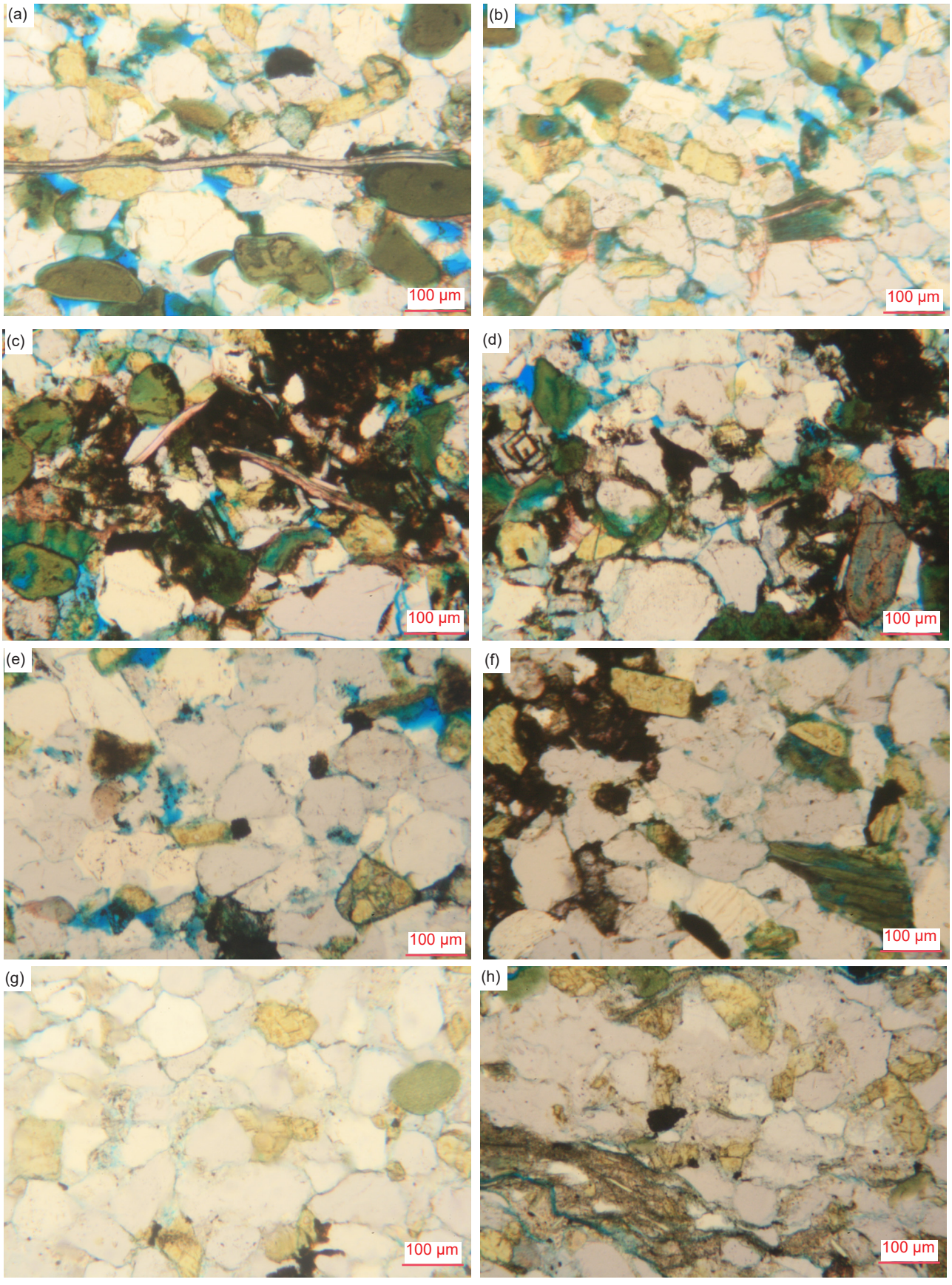
(a)
100 μm
(b)
100 μm
(c)
100 μm
(d)
100 μm
(e)
100 μm
(f)
100 μm
(g)
100 μm
(h)
100 μm

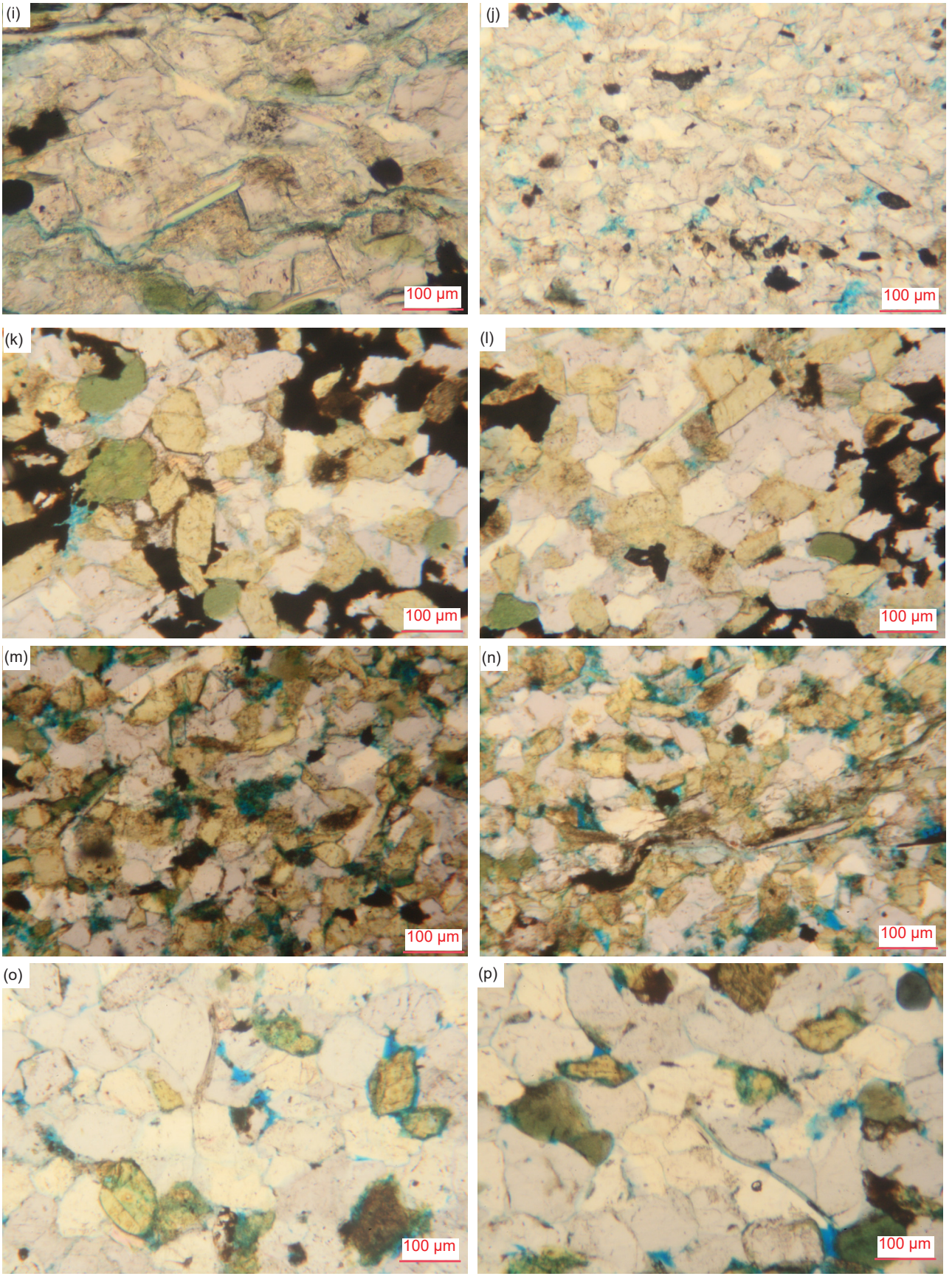
(i)
100 µm
(j)
100 µm
(k)
100 µm
(l)
100 µm
(m)
100 µm
(n)
100 µm
(o)
100 µm
(p)
100 µm

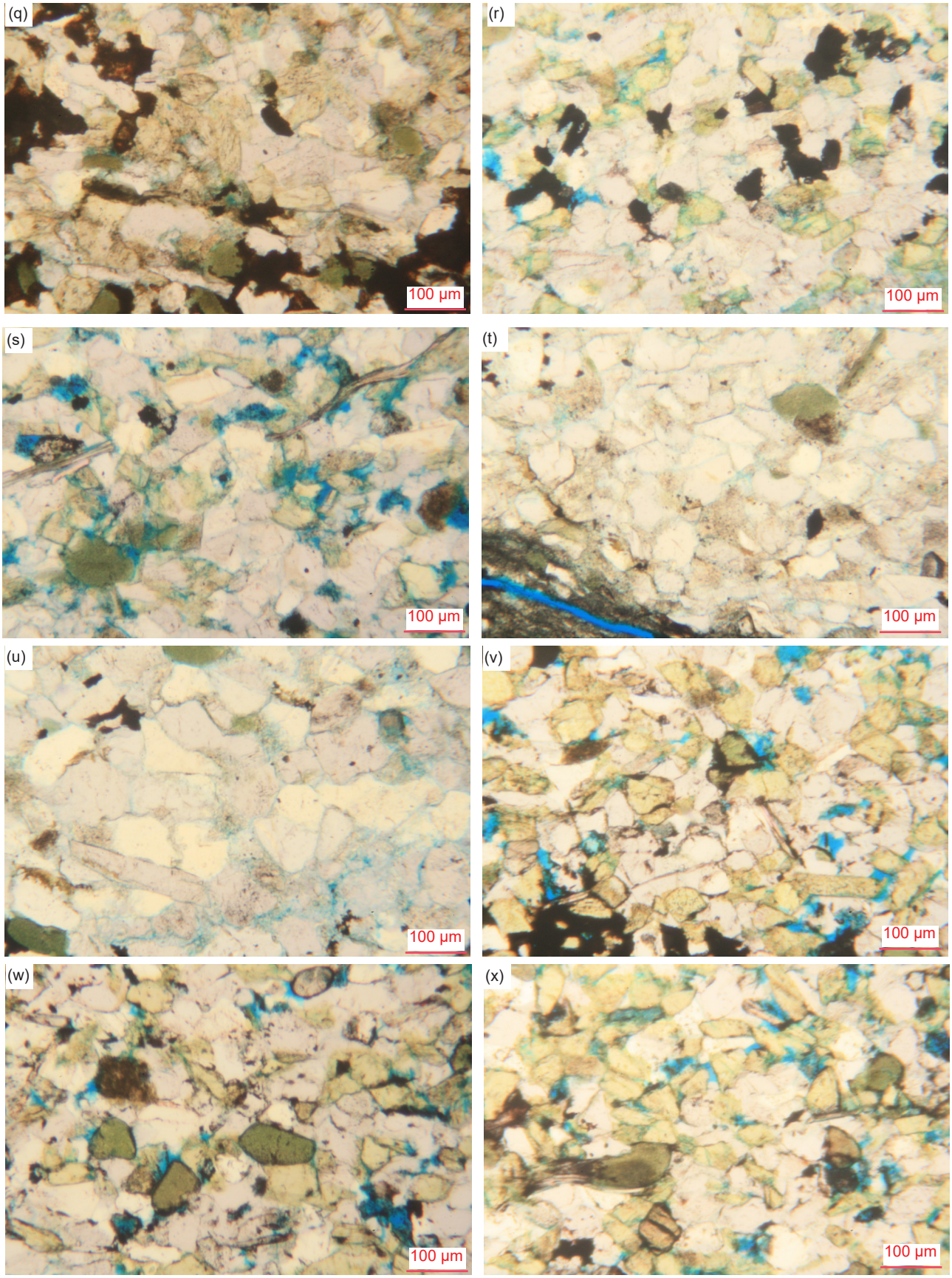

Fig. 26 (pages 112–114). Quartz sub-grains within some quartz grains of the Bright Angel Formation samples. (a), (b) BAS-01, (c), (d) BAS-02, (e), (f) HF-01, (g), (h) HF-02, (i), (j) HF-03, (k), (l) HF-04, (m), (n) HF-05, (o), (p) HF-06, (q) HF-07, (r), (s) HF-08, (t), (u) HF-09, and (v), (w), (x) HF-10.

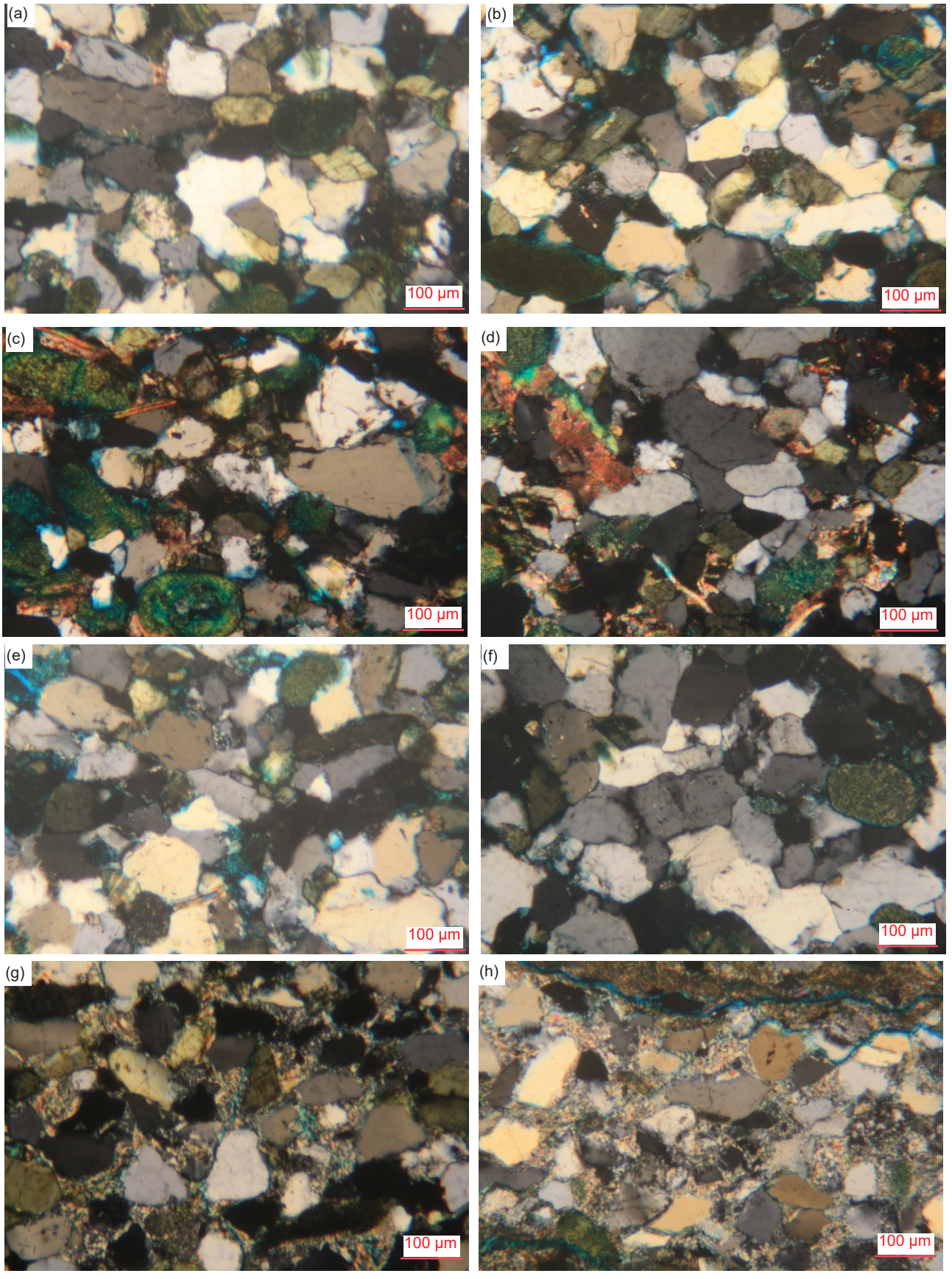
(a)
100 µm
(b)
100 µm
(c)
100 µm
(d)
100 µm
(e)
100 µm
(f)
100 µm
(g)
100 µm
(h)
100 µm

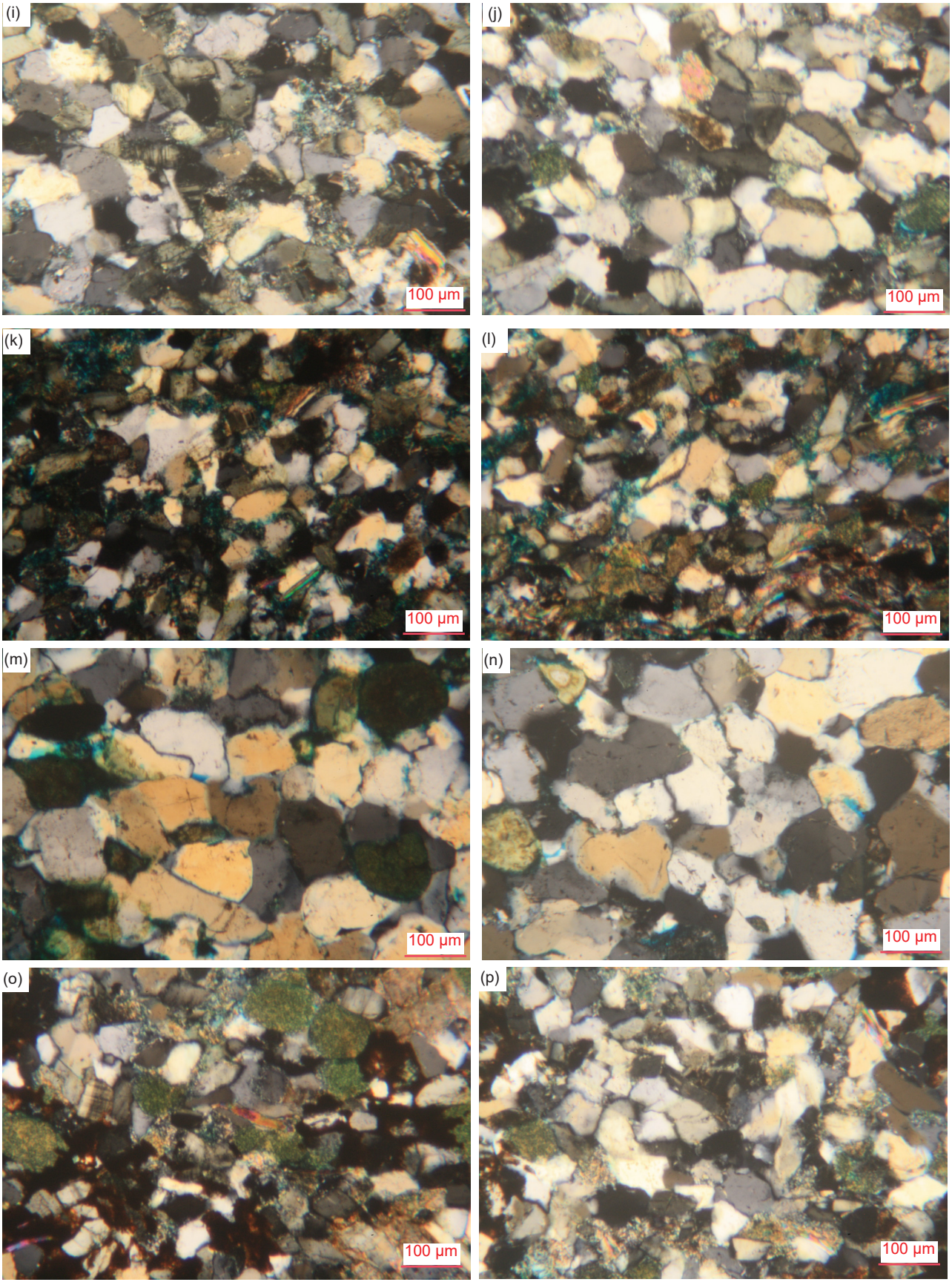
(i)
100 µm
(j)
100 µm
(k)
100 µm
(l)
100 µm
(m)
100 µm
(n)
100 µm
(o)
100 µm
(p)
100 µm

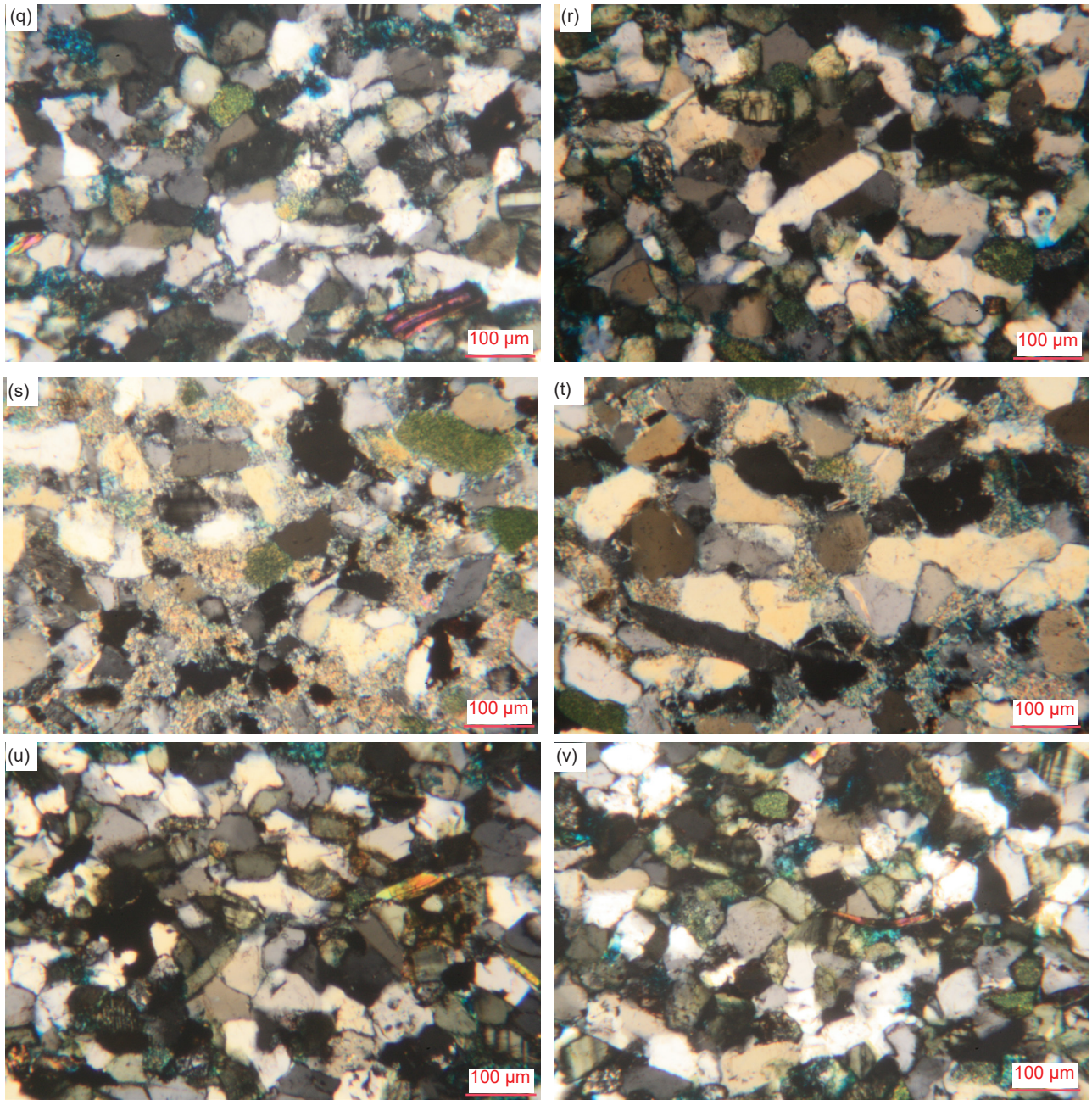

Fig. 27 (Pages 115–117). The extinction under crossed polars within quartz grains of the Bright Angel formation samples, showing how so few grains have even trivial undulose extinction. (a), (b) BAS-01, (c), (d) BAS-02, (e), (f) HF-01, (g) HF-02, (h) HF-03, (i), (j) HF-04, (k), (l) HF-05, (m), (n) HF-06, (o), (p) HF-07, (q), (r) HF-08, (s), (t) HF-09, and (u), (v) HF-10.

Fractures within quartz grains are observed more readily in some samples than in others, but they are present in every thin section, regardless of where in the fold the samples came from or whether they were distal samples (fig. 28). These internal fractures generally have no preferred orientation and there are no dislocations along them. Often these internal fractures are subtle in most samples, whereas in a few samples they are more pronounced (fig. 28a, b, c, k, n), although even then in some instances the internal fractures are hard to distinguish from sub-grain boundaries. Yet, those samples in which some of the quartz grains have pronounced internal fractures are from samples not only from within the hinge zones of the fold, but also from the limb zones and distant to the fold (only in one sample from each location), which is intuitively unexpected. Since the thin sections were oriented perpendicular to the bedding, this perhaps suggests that those pronounced fractures are most likely due to continued compactional overburden loading subsequent to deposition which would have been uniform throughout the interbedded sandstone, siltstone, and shale layers. In comparison, localized stresses in the hinge of the fold should have been more layer parallel. Furthermore, these fractures are unlikely to be an artifact of the sample collection procedure and/or the preparation of the thin sections. Similarly, the lack of pronounced or prominent fractures within many quartz grains in samples from both the hinge and limb zones of the fold would also reflect the prevalent conditions during deformation of the sandstone, siltstone, and shale beds in the fold, which was likely neither brittle or ductile deformation.

In all samples, there are occasional *broken quartz grains*, estimated at much less than 1% of the quartz grains (fig. 29). In many instances the breakage is not pronounced, nor is the displacement of the pieces. Once again, these occurrences are just as prevalent (that is, there is no statistically significant difference) in samples distal to the fold as in samples from the hinge and limb zones in the fold. Since the thin sections were oriented parallel to the bedding, this may again suggest these occurrences are likely due to continued compactional overburden loading subsequent to deposition which would have been uniform throughout the interbedded sandstone, siltstone, and shale layers, rather than being due to the localized stresses in the hinge of the fold, or being an artifact of the sample collection procedure and/or the preparation of the thin sections. However, in at least six samples, the two distal samples BAS-01 and BAS-02 (fig. 29a–d), the two limb zone samples HF-01 and HF-03 (fig. 29e and i), and two hinge zone samples HF-05 and HF-08 (fig. 29l, m, r, s), the presence of detrital muscovite flakes broken and/or bent around some of the broken quartz grain fragments suggests that both the broken muscovite flakes and the broken quartz grains may be a primary depositional feature due to breakage during deposition, rather than being due to the deformation of the sandstone, siltstone, and shale beds in the fold. Otherwise, in some instances the broken quartz grains are associated with localized fracture zones (discussed below), but these occur in both a limb zone sample HF-06 (fig. 29n, o) and three hinge zone samples HF-05, HF-07, and HF-08 (fig. 29m, p-s). However, these three samples are only from one of the two hinge zones in the fold (fig. 21), which suggests they are not necessarily due to the deformation during folding, or even the subsequent faulting.

Original *detrital K-feldspar grains* are still preserved in all samples (fig. 30). They are commonly preserved as altered fragments and sub-euhedral to sub-rounded grains and former laths of various sizes from very small to large, scattered randomly between the many quartz grains in all samples. In some samples there are more K-feldspar grains than there are quartz grains (table 2). The K-feldspar grains are sometimes fractured, usually along cleavage planes. Often all the K-feldspar grains are altered, especially within the shale samples HF-02 and HF-03 (figs. 22d, i, and 30e-g), and the siltstone samples HF-05 and HF-09 (figs. 22f. h, and 30j, q, r). This alteration occurs regardless of whether the samples are from the hinge or limb zones in the fold. Indeed, the detrital K-feldspar grains appear the same and similarly altered in both the distal samples and those samples from the hinges and limbs of the fold, which confirms the alteration occurred either prior to deposition or is due to post-depositional alteration uniformly through the interlayered sandstone, siltstone, and shale beds. However, there is no evidence of any modifications due to any metamorphism to the detrital appearance of these K-feldspar grains after their deposition, and/or especially due to the subsequent deformation of the sandstone, siltstone, and shale beds in the fold.

The original *detrital muscovite flakes* are likewise still preserved in all samples without any evidence of modification due to any metamorphism or any effects of deformation (fig. 31). They are observed in thin sections as mostly edge-on flakes wedged between quartz and K-feldspar grains, that is, cross-sections through thin stacked sheets ("books"), but sometimes they are altered and thus the "books" have expanded in thickness (for example, fig. 29c). Since the thin-sections were cut perpendicular to the bedding, the observation that most muscovite flakes are edge-on in cross-section indicates that the muscovite flakes are aligned parallel and sub-parallel to the bedding. This is consistent with these muscovite flakes being original detrital grains. Because of their flatness, they

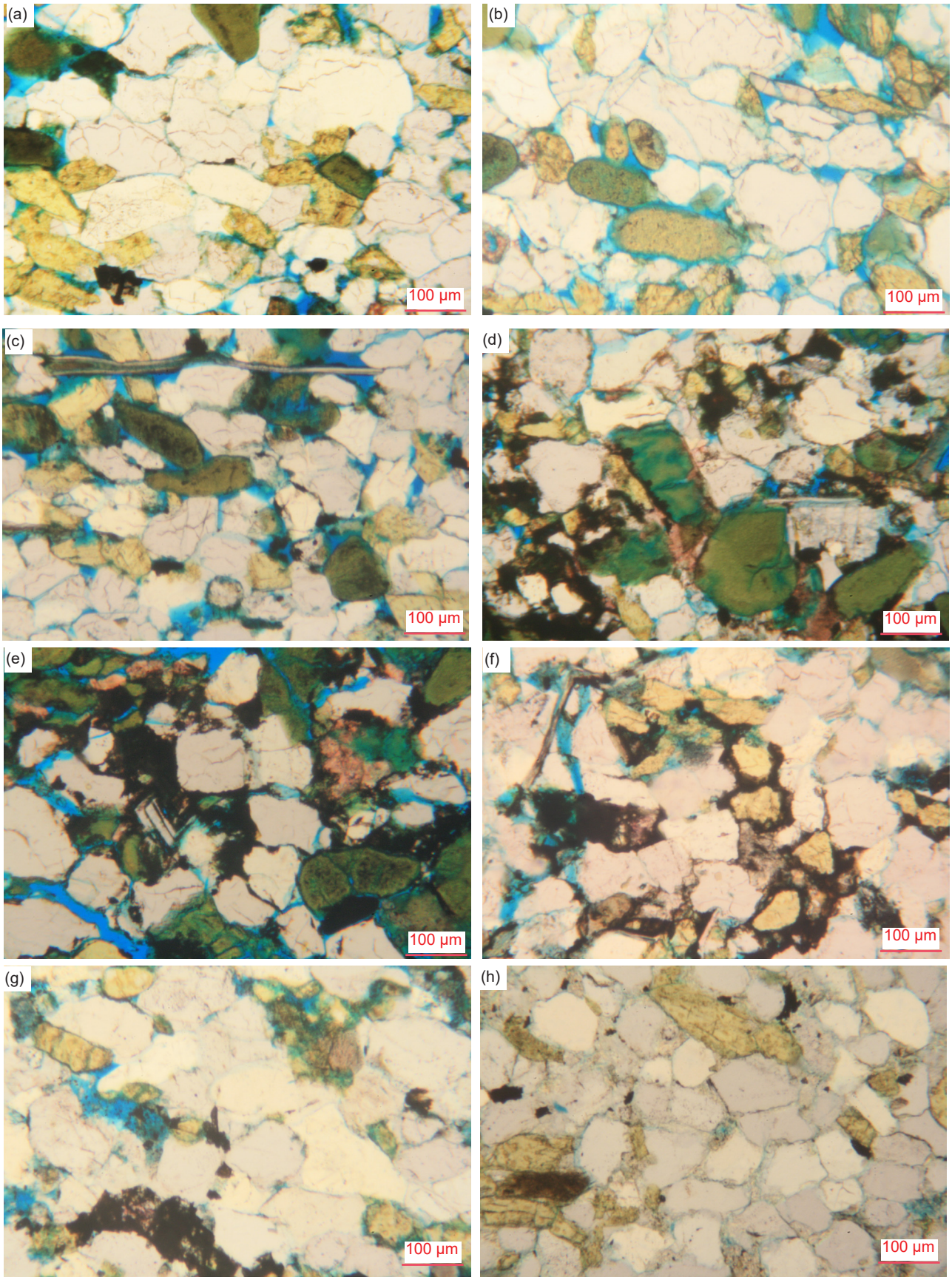
(a)
100 µm
(b)
100 µm
(c)
100 µm
(d)
100 µm
(e)
100 µm
(f)
100 µm
(g)
100 µm
(h)
100 µm

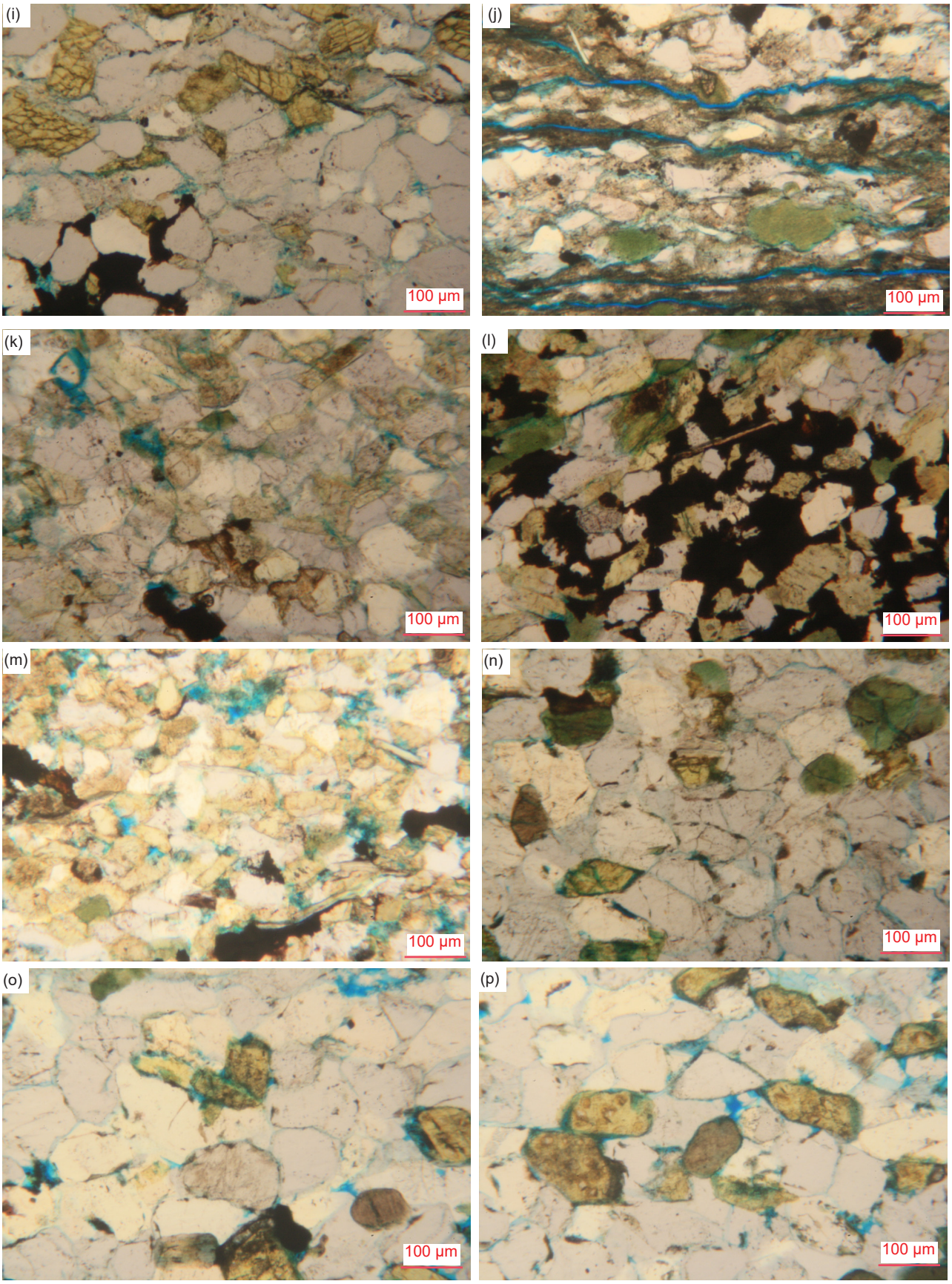
(i)
100 µm
(j)
100 µm
(k)
100 µm
(l)
100 µm
(m)
100 µm
(n)
100 µm
(o)
100 µm
(p)
100 µm

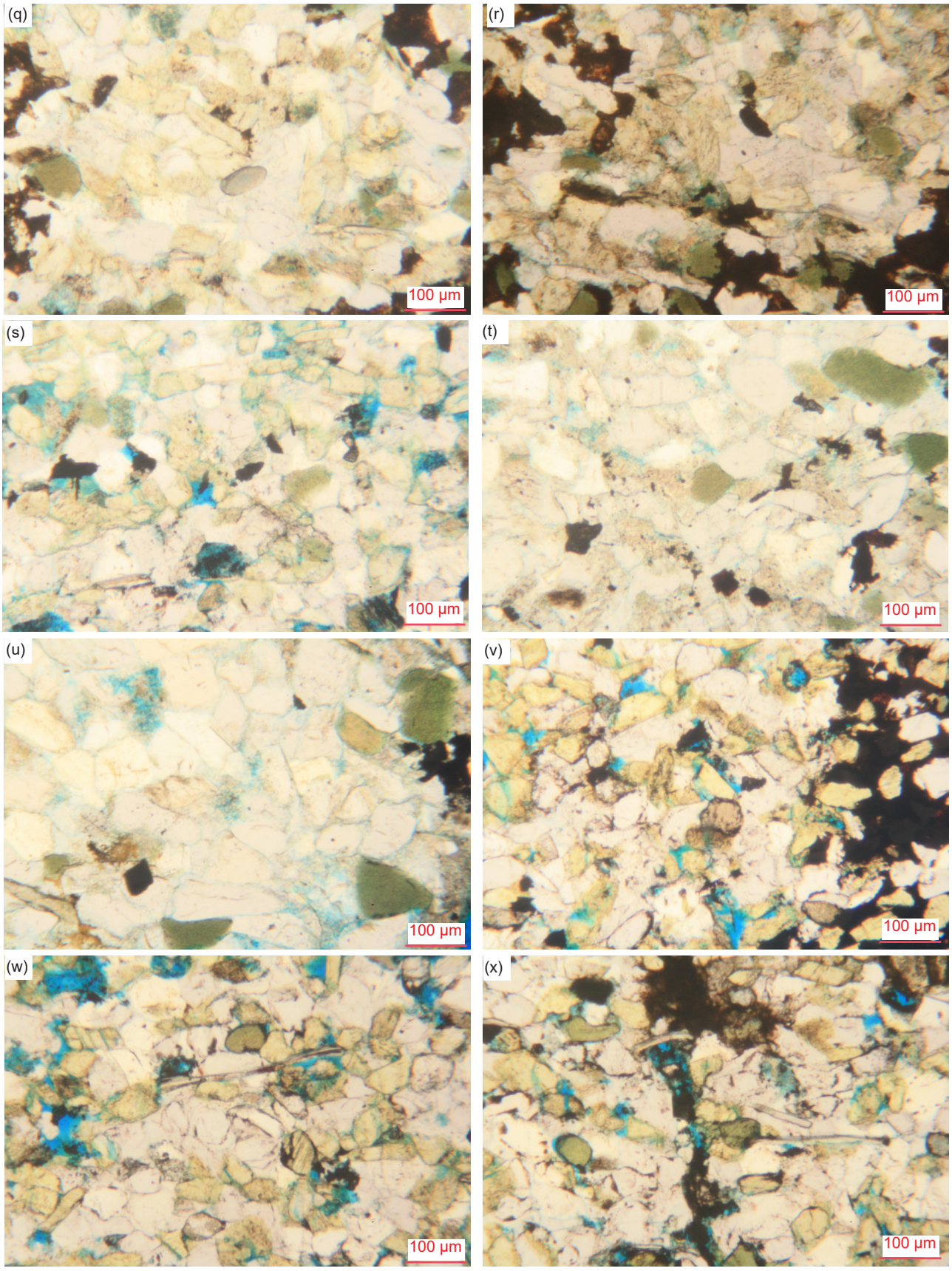

Fig. 28 (pages 119–121). Some quartz grains within the Bright Angel Formation samples that have internal fractures. (a), (b), (c) BAS-01, (d), (e) BAS-02, (f), (g) HF-01, (h), (i) HF-02, (j) HF-03, (k), (l) HF-04, (m) HF-05, (n), (o), (p) HF-06, (q), (r) HF-07, (s) MF-08, (t), (u) HF-09, and (v), (w), (x) HF-10.

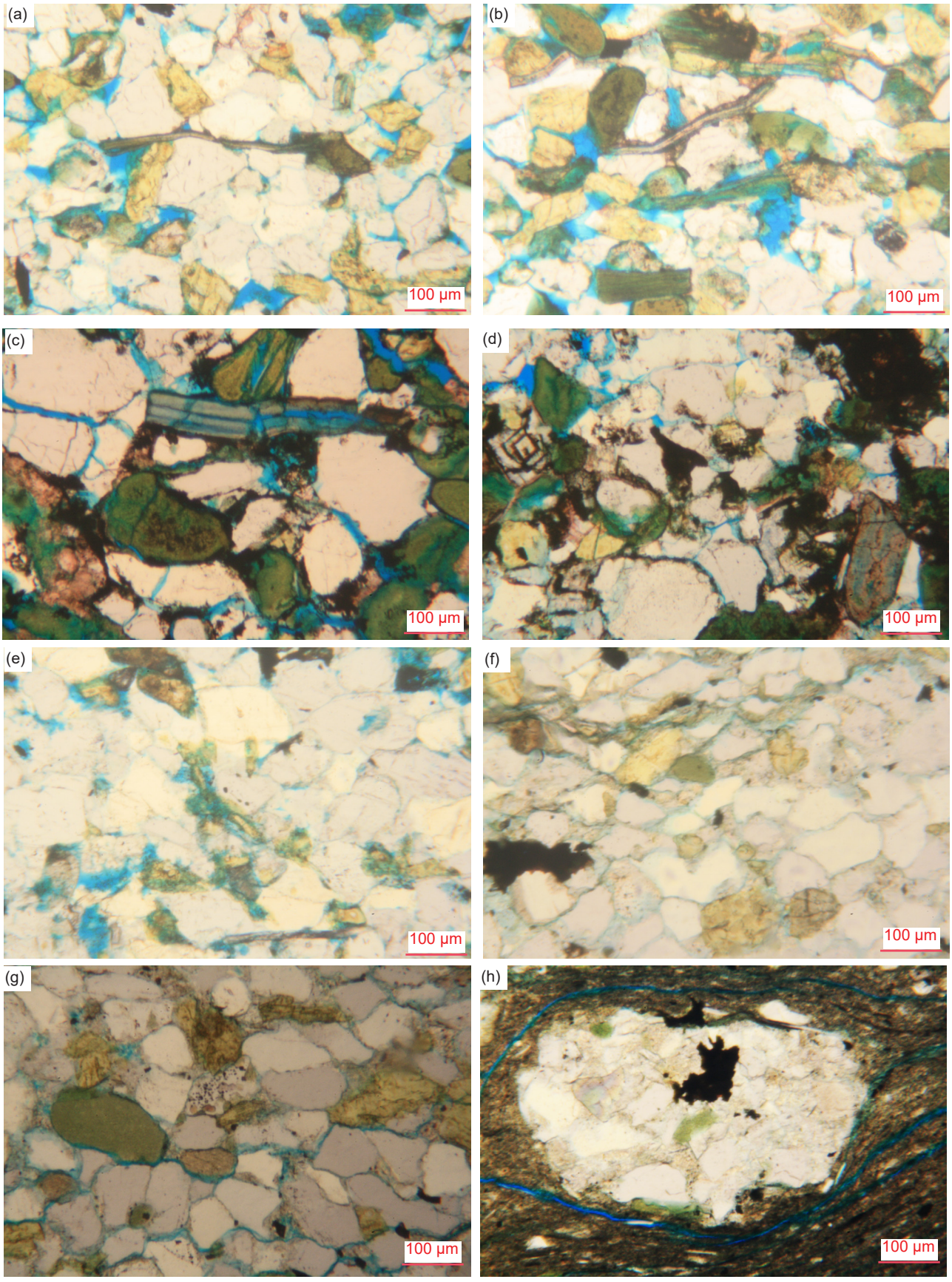
(a)
100 μm
(b)
100 μm
(c)
100 μm
(d)
100 μm
(e)
100 μm
(f)
100 μm
(g)
100 μm
(h)
100 μm

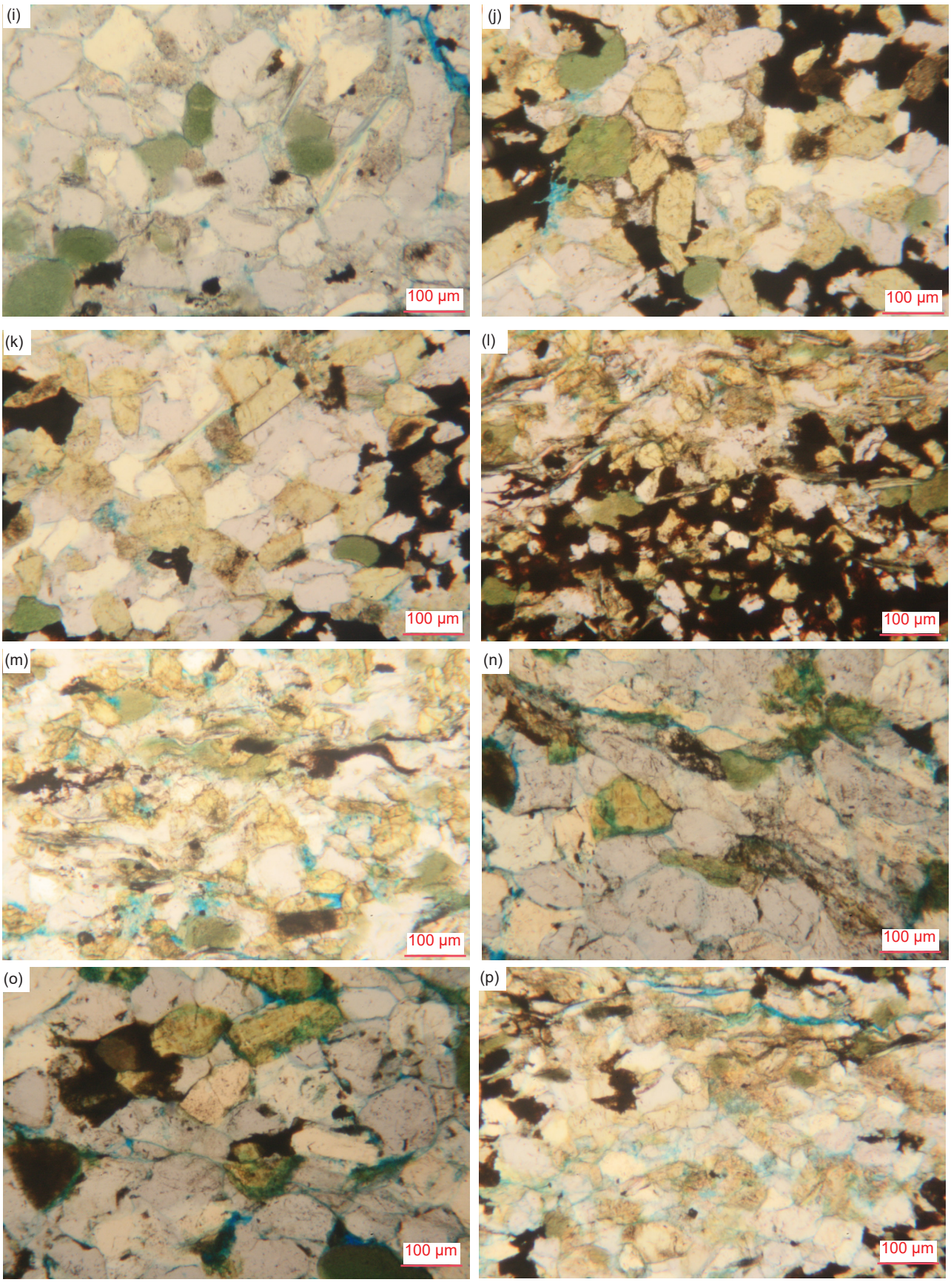
(i)
100 µm
(j)
100 µm
(k)
100 µm
(l)
100 µm
(m)
100 µm
(n)
100 µm
(o)
100 µm
(p)
100 µm

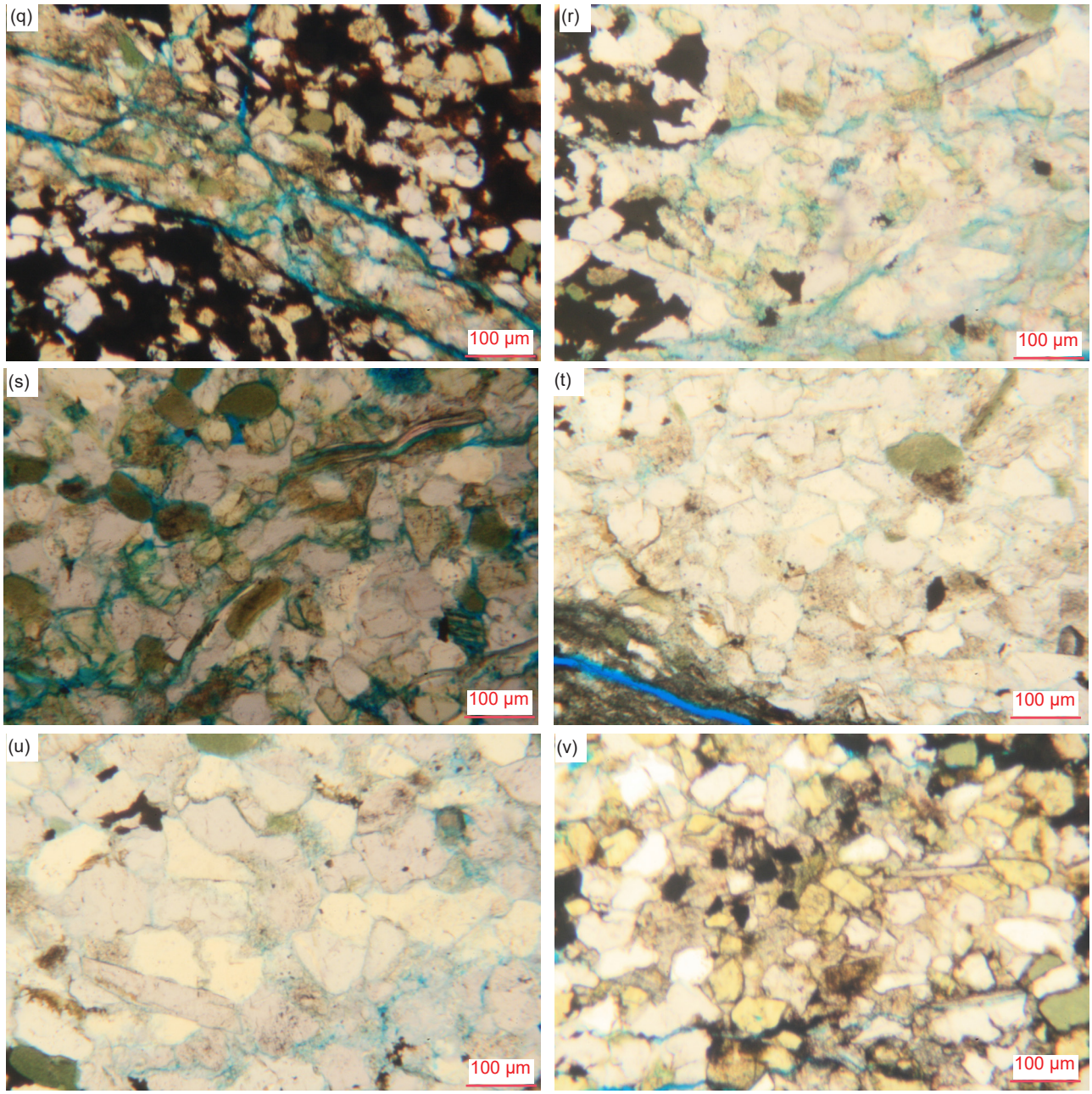

Fig. 29 (pages 122–124). Some broken quartz grains within the Bright Angel Formation samples. (a), (b) BAS-01, (c), (d) BAS-02, (e) HF-01, (f), (g) HF-02, (h), (i) HF-03, (j), (k) HF-04, (l), (m) HF-05, (n), (o) HF-06, (p), (q) HF-07, (r), (s) MF-08, (t), (u) MF-09, and (v) MF-10.

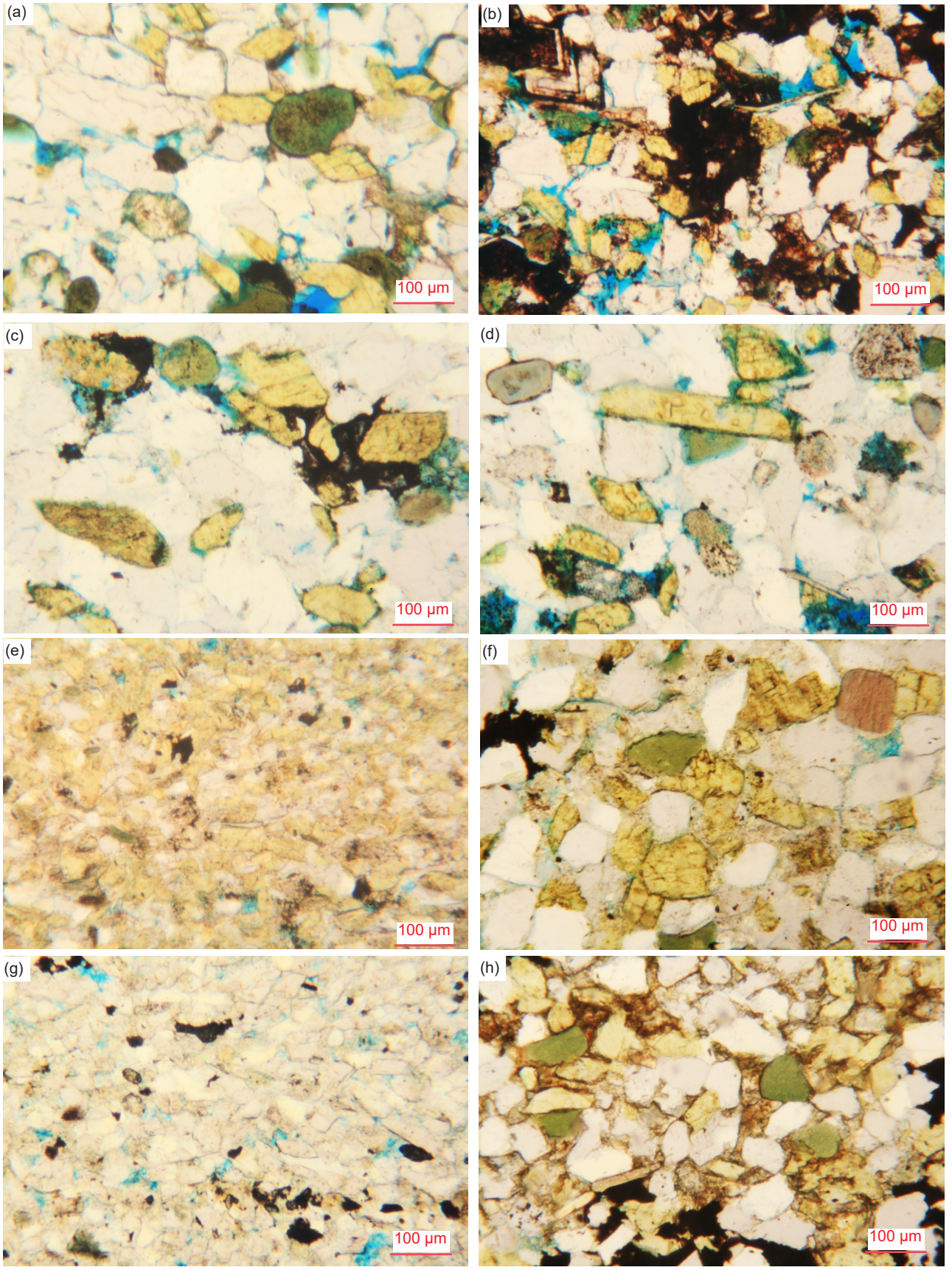
(a)
100 µm
(b)
100 µm
(c)
100 µm
(d)
100 µm
(e)
100 µm
(f)
100 µm
(g)
100 µm
(h)
100 µm

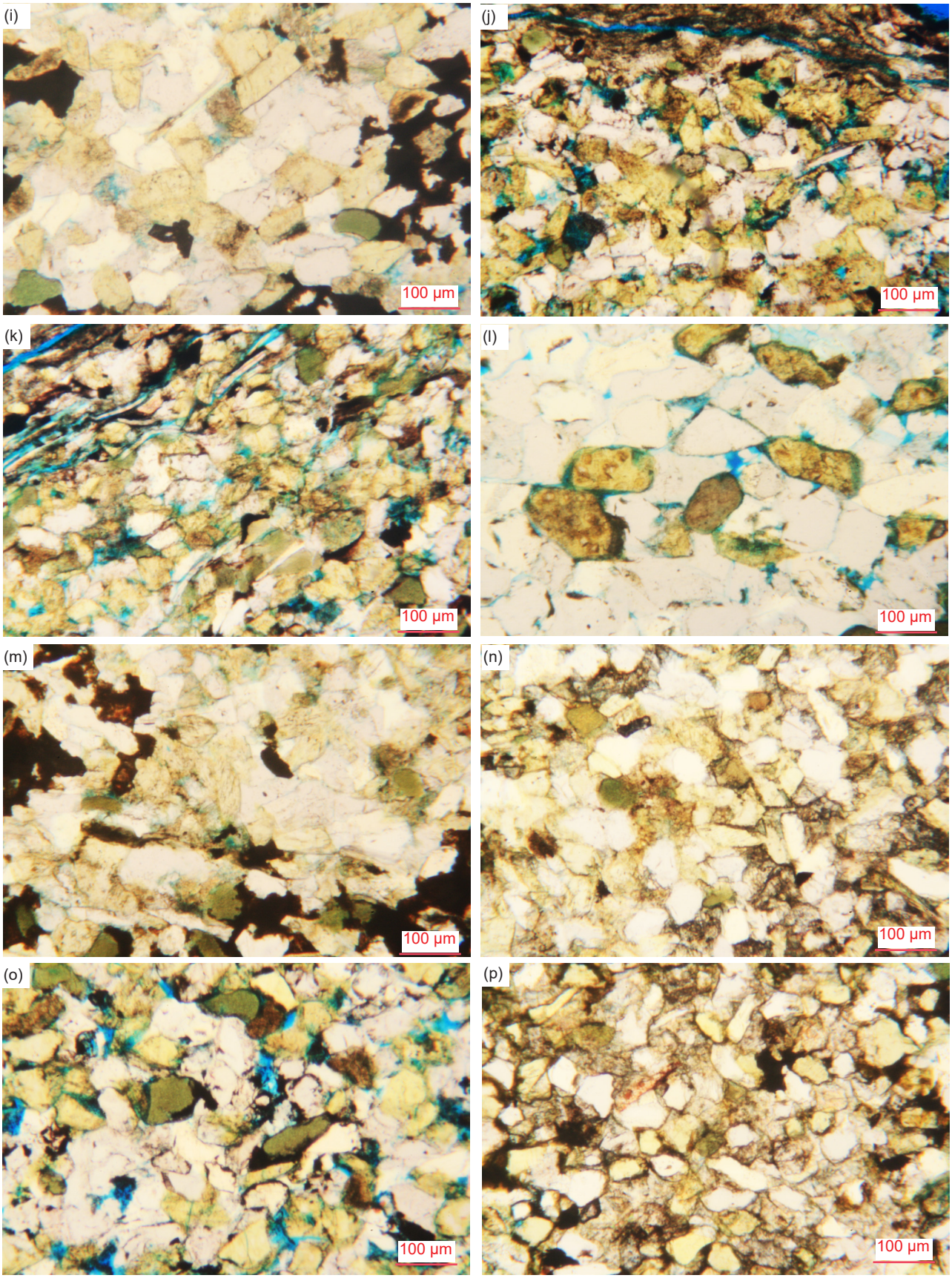
(i)
100 μm
(j)
100 μm
(k)
100 μm
(l)
100 μm
(m)
100 μm
(n)
100 μm
(o)
100 μm
(p)
100 μm

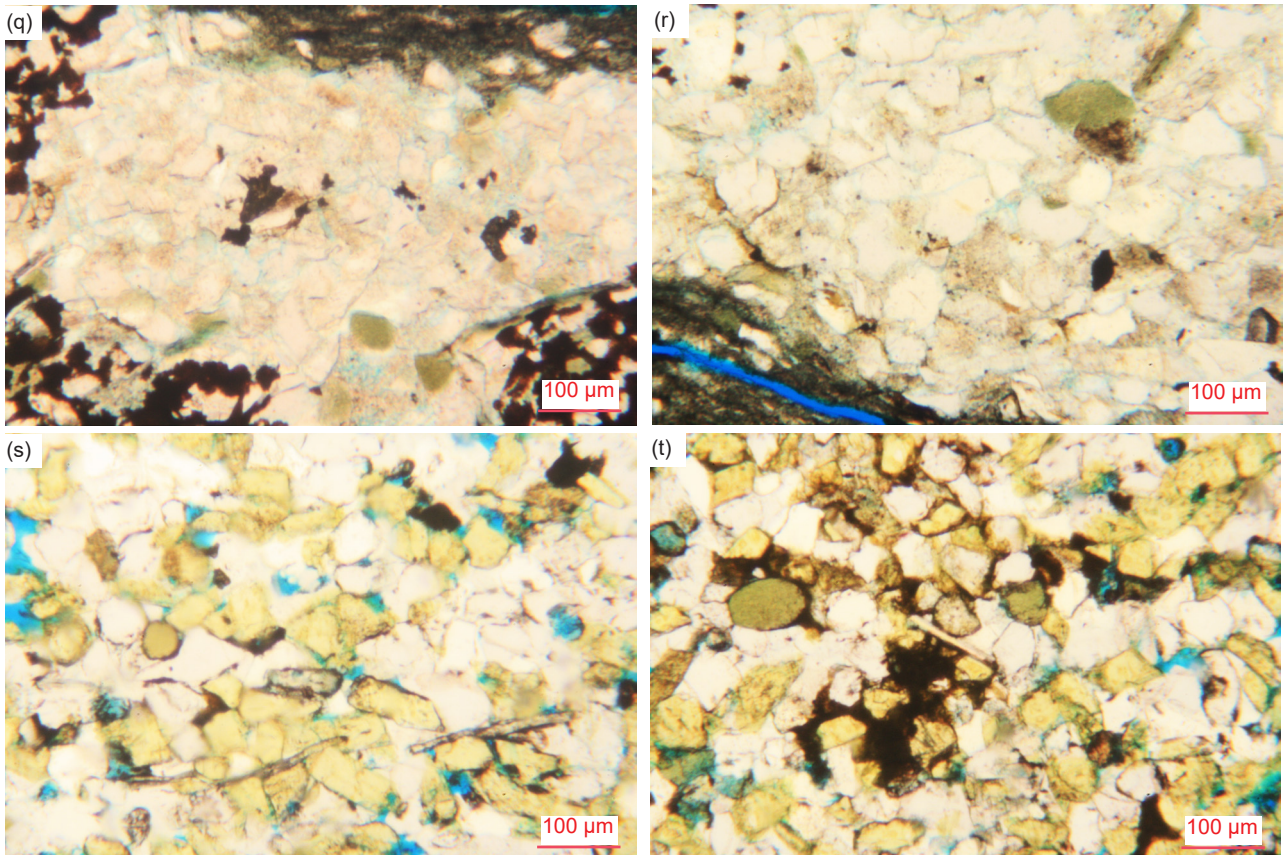

Fig. 30 (pages 125–127). Detrital K-feldspar grains within the Bright Angel Formation samples. (a) BAS-01, (b) BAS-02, (c), (d) HF-01, (e), (f) HF-02, (g) HF-03, (h), (i) HF-04, (j), (k) HF-05, (l) HF-06, (m), (n) HF-07, (o), (p) HF-08, (q), (r) HF-09, and (s), (t) HF-10.

were cushioned in the water column and deposited on the accumulating sediment surfaces parallel and sub-parallel to the bedding. Further evidence that these muscovite flakes are still preserved in their detrital condition is the observation that many of the edge-on flakes in the thin-sections are wedged not only between, but are often bent around, the quartz and K-feldspar grains (fig. 31). And sometimes the flakes are broken and/or their ends are frayed and split apart (figs. 29c and 31b, d). Much of the bending and breaking of flakes may, of course, have been due to compaction of the sediments subsequent to deposition. Furthermore, the bending and breaking of flakes does not appear to have been caused by the deformation of the sandstone, siltstone, and shale beds in the fold, because bent and broken flakes are found in the distal samples compared to just bent flakes in the samples from the fold. Nor are bent flakes more prevalent in the hinge zones compared to in the limbs of the fold. Similarly, the occasional altered state of some of the muscovite flakes in a few samples correlates with other late secondary alteration with clay minerals (illite) and calcite in the same samples. However, all muscovite flakes in all samples still display their original detrital character with no effects of any metamorphism or deformation that might have been associated with the folding if deformation had been brittle or ductile.

Also evident in most samples are *original detrital glauconite grains* (fig. 32). In the two distal samples it is clear they are detrital grains because they consist of rounded concentric coatings on central "seed" grains of mostly K-feldspar, but sometimes quartz (fig, 32a–c). This would likely reflect the original depositional environment, typically regarded as marine (Snelling 2021b). In the samples from the fold, the grains are more uniform in their internal texture and color, and appear to likely be totally altered K-feldspar grains (fig. 32d–n). Furthermore, there are no differences in their occurrence and appearance in samples from both hinge and limb zones. Such alteration would have occurred subsequent to deposition of the detrital K-feldspar grains. For both origins of these glauconite grains, any effects associated with deep burial of the sampled distal Bright Angel Formation layers or with ductile deformation of the same layers in the fold should have either metamorphosed the grains to change their mineral identity or physically distorted the grains. The observation that neither metamorphic nor physical dislocation effects are present is evidence that neither metamorphism nor ductile deformation has occurred, especially in the fold.

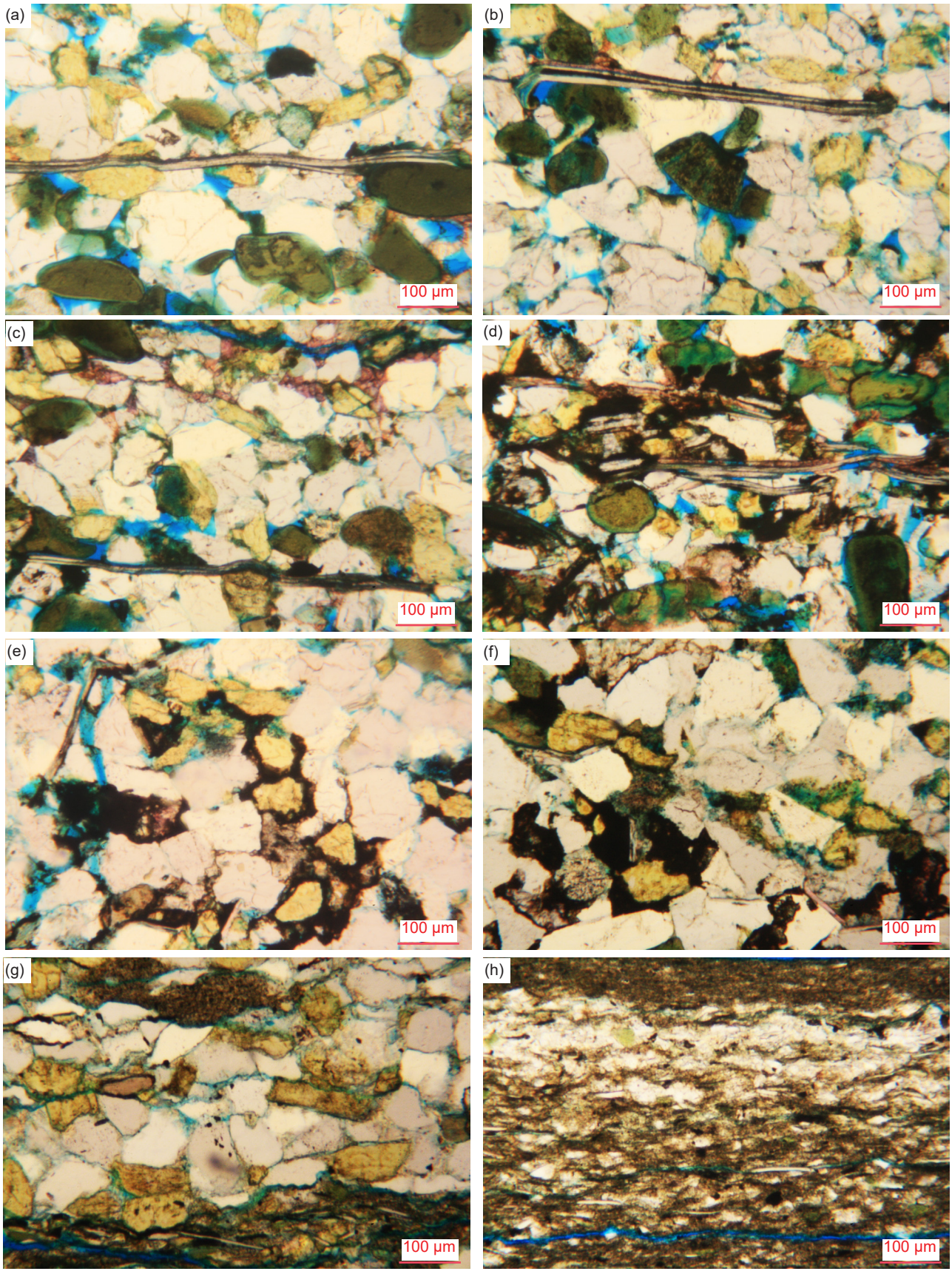
(a)
100 µm
(b)
100 µm
(c)
100 µm
(d)
100 µm
(e)
100 µm
(f)
100 µm
(g)
100 µm
(h)
100 µm

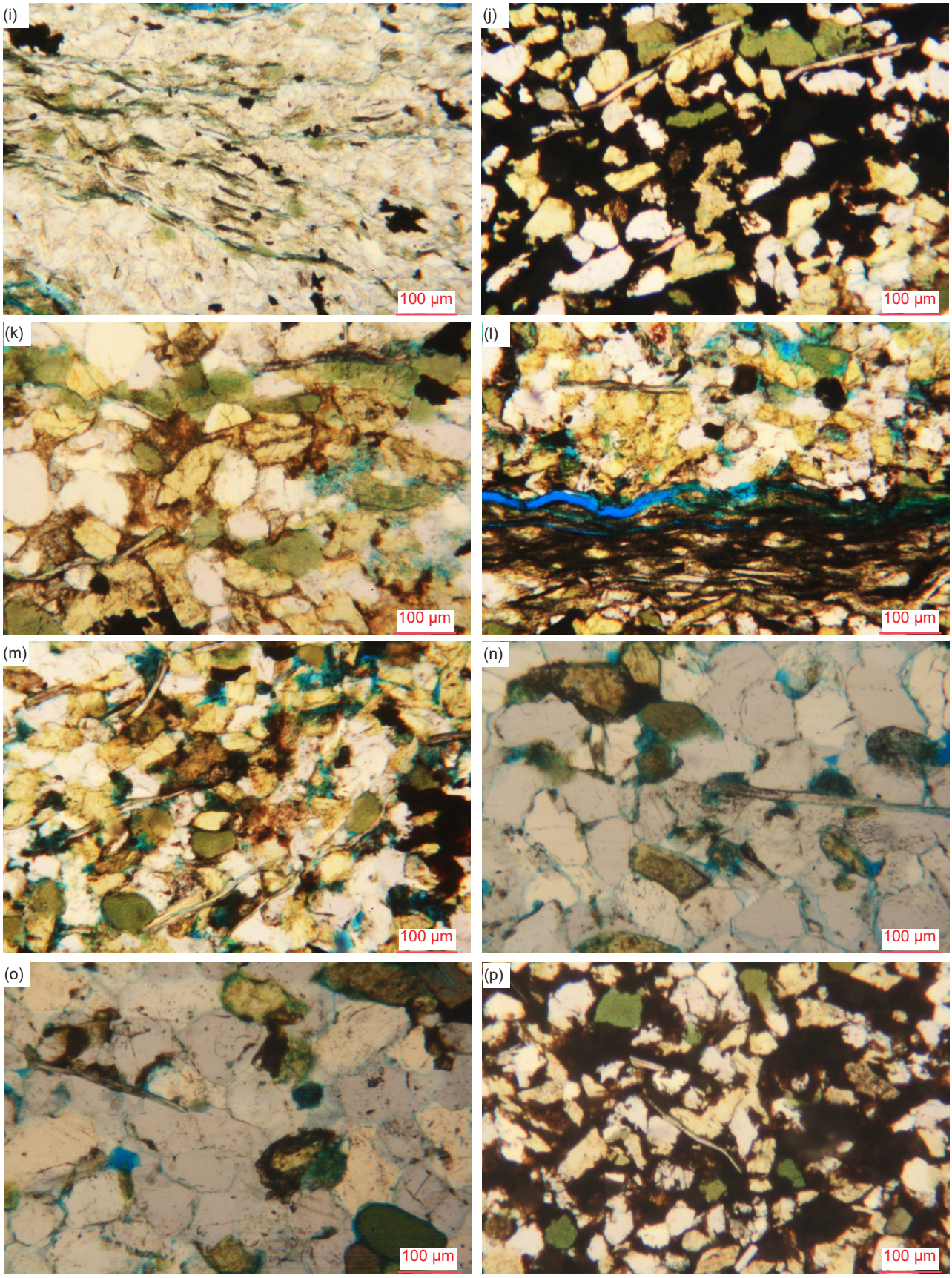
(i)
100 µm
(j)
100 µm
(k)
100 µm
(l)
100 µm
(m)
100 µm
(n)
100 µm
(o)
100 µm
(p)
100 µm

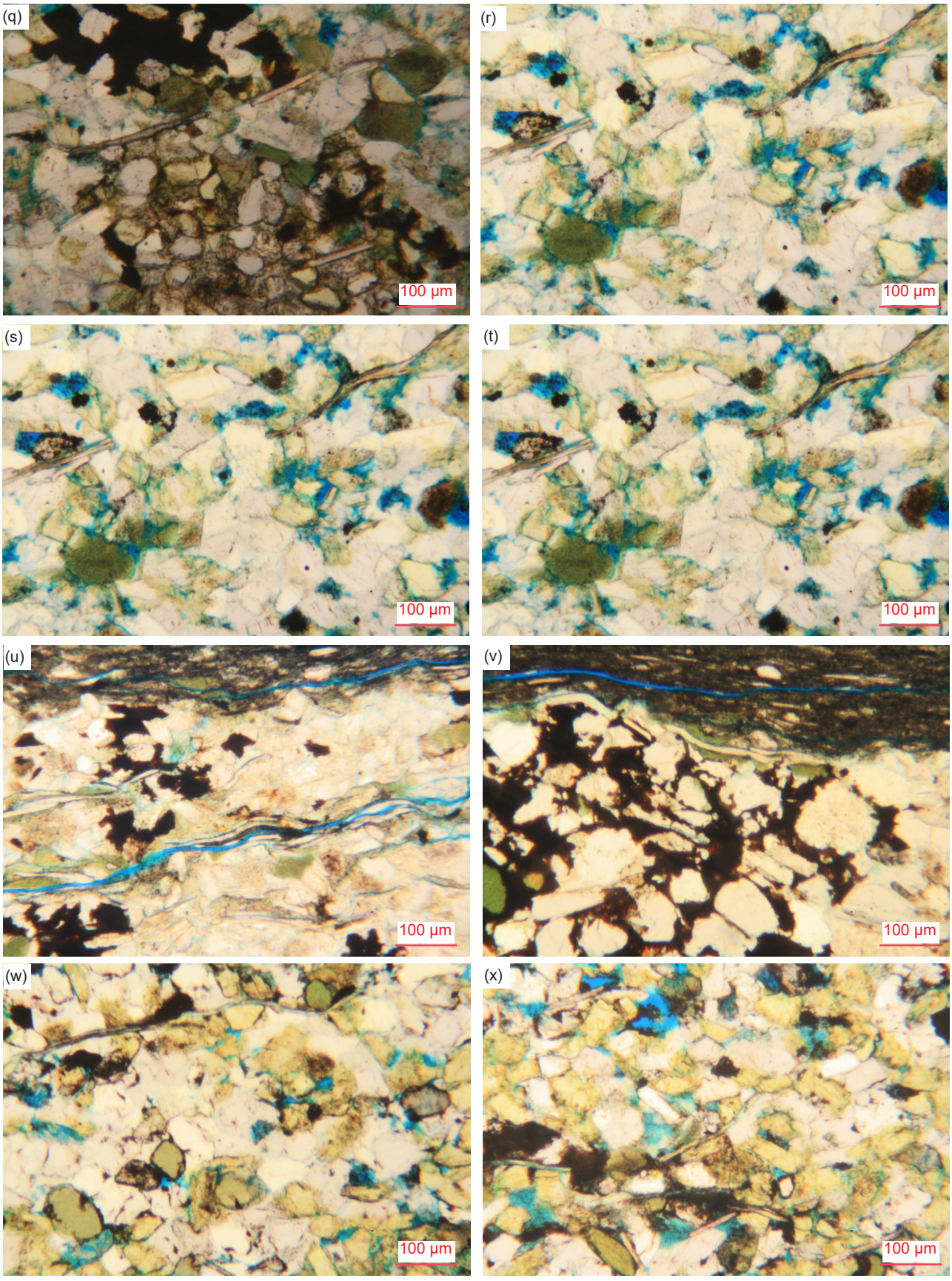
(q)
100 µm
(r)
100 µm
(s)
100 µm
(t)
100 µm
(u)
100 µm
(v)
100 µm
(w)
100 µm
(x)
100 µm

Fig. 31 (pages 128–130). Detrital muscovite flakes within the Bright Angel Formation samples showing some bent around quartz and K-feldspar grains, some broken, and some with frayed ends. (a), (b), (c) BAS-01, (d) BAS-02, (e), (f) HF-01, (g) HF-02, (h), (i) HF-03, (j), (k) HF-04, (l), (m) HF-05, (n) HF-06, (o), (p) HF-07, (q), (r) HF-08, (s), (t), (u), (v) HF-09, and (w), (x) HF-10.

Nine of the twelve samples contain at least one edge-on *fossilized brachiopod shell fragment*, while some samples contain several (fig. 33). They are easily confused with edge-on muscovite flakes but are distinctive because they are thicker and composed of collophane, a birefringent cryptocrystalline form of apatite. They also often exhibit a two-layered internal structure of the shell wall (fig. 33e, g, h). Some are very thick and appear altered (fig. 33a, b, d). They are often broken into shorter segments and are tightly wedged and/or bent between the various other grains in the mosaics, often parallel to the bedding. They all occur in both distal and fold samples equally without any evidence of the effects of metamorphism or ductile deformation, especially in the fold samples from both hinge and limb zones. Thus, in all these samples they are still in their detrital condition, and have not subsequently suffered from either metamorphism or ductile deformation.

Clay minerals occur in all samples (Snelling 2021b) and are dominated by *illite with subordinate illite/smectite* (fig. 34). The most obvious occurrence of illite and illite/smectite is that which constitutes the glauconite grains (McRae 1972; Thompson and Hower 1975) easily recognized in most samples (fig. 32). Otherwise, these clay minerals are not always so easily recognized, except under crossed polars when it is immediately evident that K-feldspar grains have been totally altered to illite. The shales exhibit laminae and bands that are predominantly illite alteration, mainly of tiny K-feldspar grains and laths (fig. 34d, e, h, i, o). These selvages or laminae of intense illite alteration are evident from the heavy dusting of iron oxides associated with it. Other areas of illite alteration are less dusted with iron oxides and the illite alteration can be seen to be after K-feldspar grains. In the sandstones and siltstones, the illite alteration has extended beyond the green glauconite grains (after K-feldspar) to infill between them and between some of the mosaic quartz grains so that the pervasive illite alteration is now the predominating cement, along with the occasional patches of heavy iron oxides and/or carbonates (for example, fig. 34f, g, l–q). This illite alteration is common to both distal and fold samples, and is no different in hinge and limb samples. Thus, it cannot be due to any metamorphism associated with the claimed ductile deformation in the fold, which would have transformed the illite to other minerals, even back to K-feldspar. Instead, the illite alteration must have simply occurred after deposition of these sediments, because it is still preserved with the shapes of the replaced detrital grains.

XRD analyses (Snelling 2021b) (table 2) indicate that there are *various carbonate minerals* present in all samples—calcite [$CaCO_3$], dolomite [$Ca,Mg(CO_3)_2$], ankerite [$Ca(Fe,Mg,Mn)(CO_3)_2$] or siderite [$FeCO_3$] (fig. 35). *Dolomite* is the most prevalent, whereas ankerite solely dominates in several samples. Typically, dolomite is easily recognized when it occurs as rhomboidal crystals, with concentric growth zones marked by iron-oxide staining (fig. 35c, d). Otherwise, dolomite often occurs as occasional small sub-angular to rounded "dirty" (iron-oxide-stained) grains, elongated clear fragments or irregularly-shaped patches, which usually are wedged within the mosaic of scattered quartz, K-feldspar and glauconite mosaic grains, and muscovite flakes, or in places, as cement, probably infilling former pores, but may replace some K-feldspar mosaic grains (fig. 35f, n–v). Some dolomite may be replacing calcite because of the visible calcite remnants within the dolomite rhombs, while some dolomite may instead have been partially replaced by calcite.

Calcite is usually recognizable as pink because of the stain applied to the thin sections during their preparation. However, it is harder to recognize when it too is iron-oxide-stained. Some calcite which infills spaces between mosaic grains acts as the cement (fig. 35a) (significantly in a few places), and partly replaces or veins K-feldspar, quartz, or muscovite grains/flakes (fig. 35b). Calcite also occurs as many small and medium, sometimes iron-oxide-coated, sub-angular to sub-rounded and rounded grains wedged in the mosaic as apparent detrital grains similar to the quartz and K-feldspar grains.

Ankerite is harder to recognize, though it is usually reddish-brown due to being iron-oxide-stained. It occurs as many very small to small-medium sub-angular to sub-rounded and rounded grains, while others are oval-shaped and elongated. Some ankerite rhombs with the characteristic cleavage are also evident. All these are scattered through and wedged in the mosaic similar to the other detrital grains, and thus some may be detrital (fig. 35e, g–m). There are also later pervasive scattered patches of very small sub-angular ankerite grains infilling as cement between scattered quartz and K-feldspar grains.

Siderite is also difficult to recognize from iron-oxide-coated dolomite. It is unclear in the one sample in which it occurs (HF-07, table 2) whether any of the small siderite grains might also be detrital since

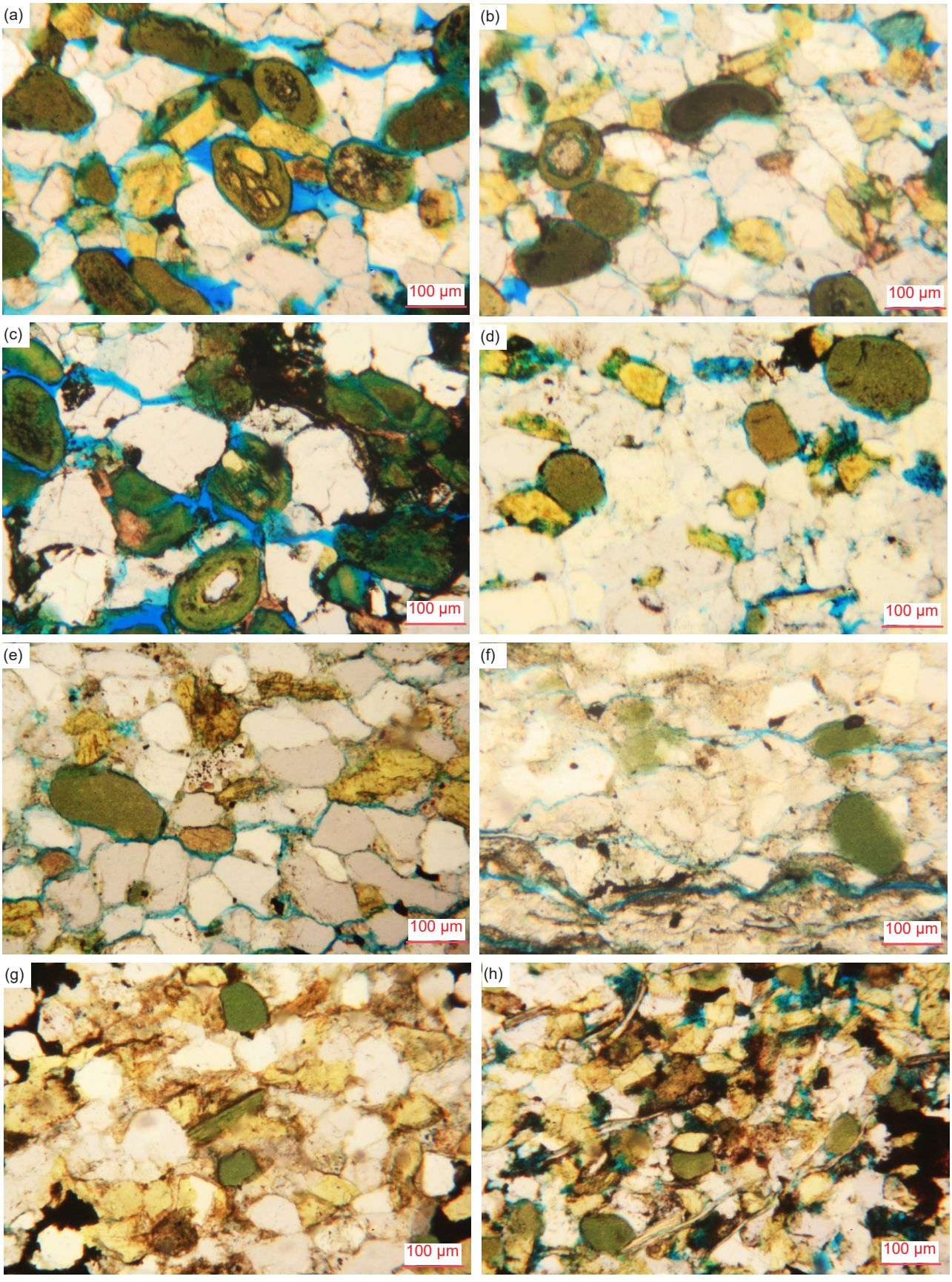
(a)
100 µm
(b)
100 µm
(c)
100 µm
(d)
100 µm
(e)
100 µm
(f)
100 µm
(g)
100 µm
(h)
100 µm

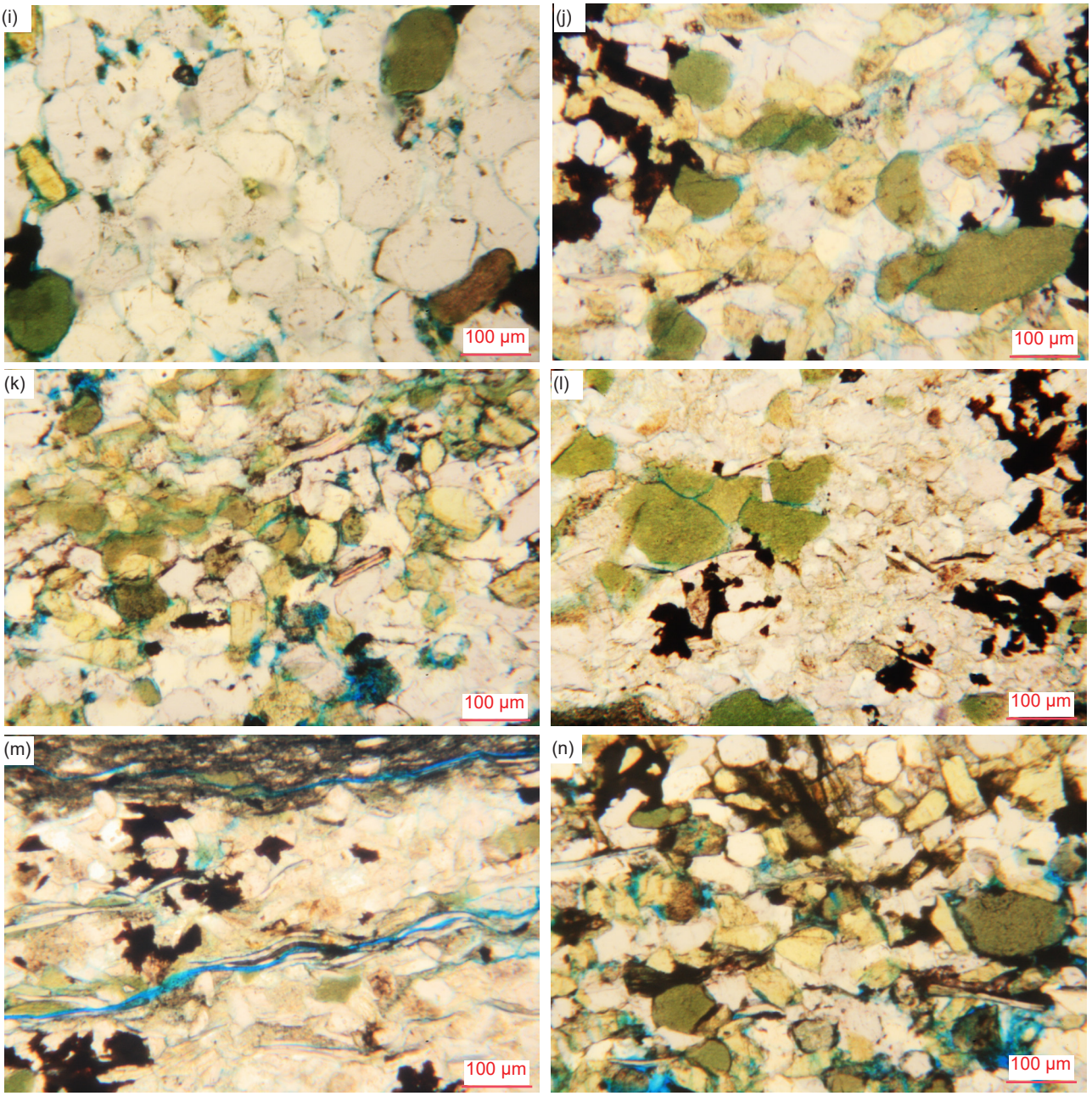

Fig. 32 (pages 132–133). Detrital, usually rounded glauconite grains in the Bright Angel Formation samples. (a) BAS-01, (b), (c) BAS-02, (d) HF-01, (e) HF-02, (f) HF-03, (g) HF-04, (h) HF-05, (i) HF-06, (j) HF-07, (k), (l) HF-08, (m) HF-09, and (n) HF-10.

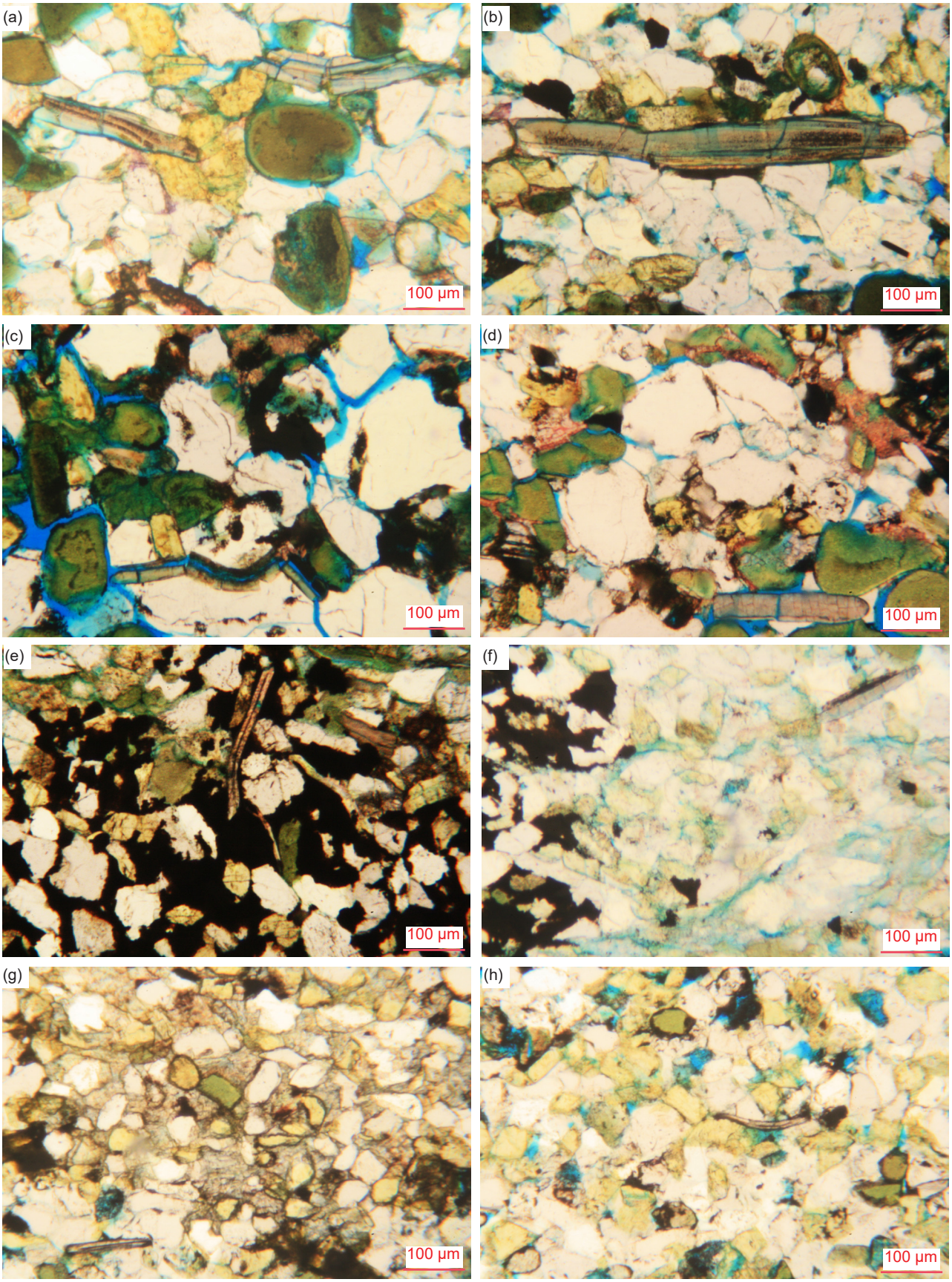

Fig. 33. Detrital fossil shell fragments in some of the Bright Angel Formation samples. (a), (b) BAS-01, (c), (d) BAS-02, (e) HF-04, (f) HF-08, and (g), (h) HF-10.

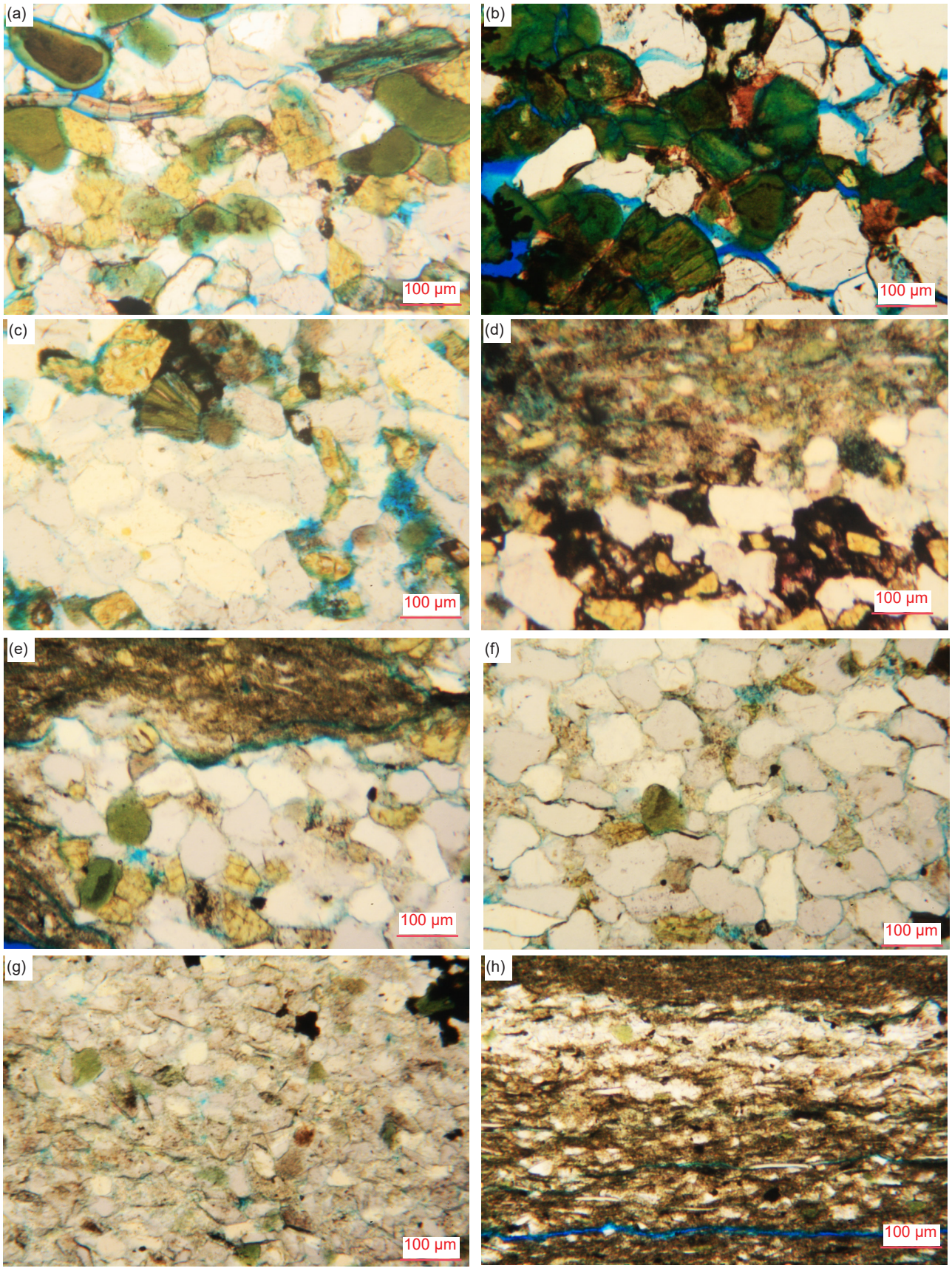
(a)
100 µm
(b)
100 µm
(c)
100 µm
(d)
100 µm
(e)
100 µm
(f)
100 µm
(g)
100 µm
(h)
100 µm

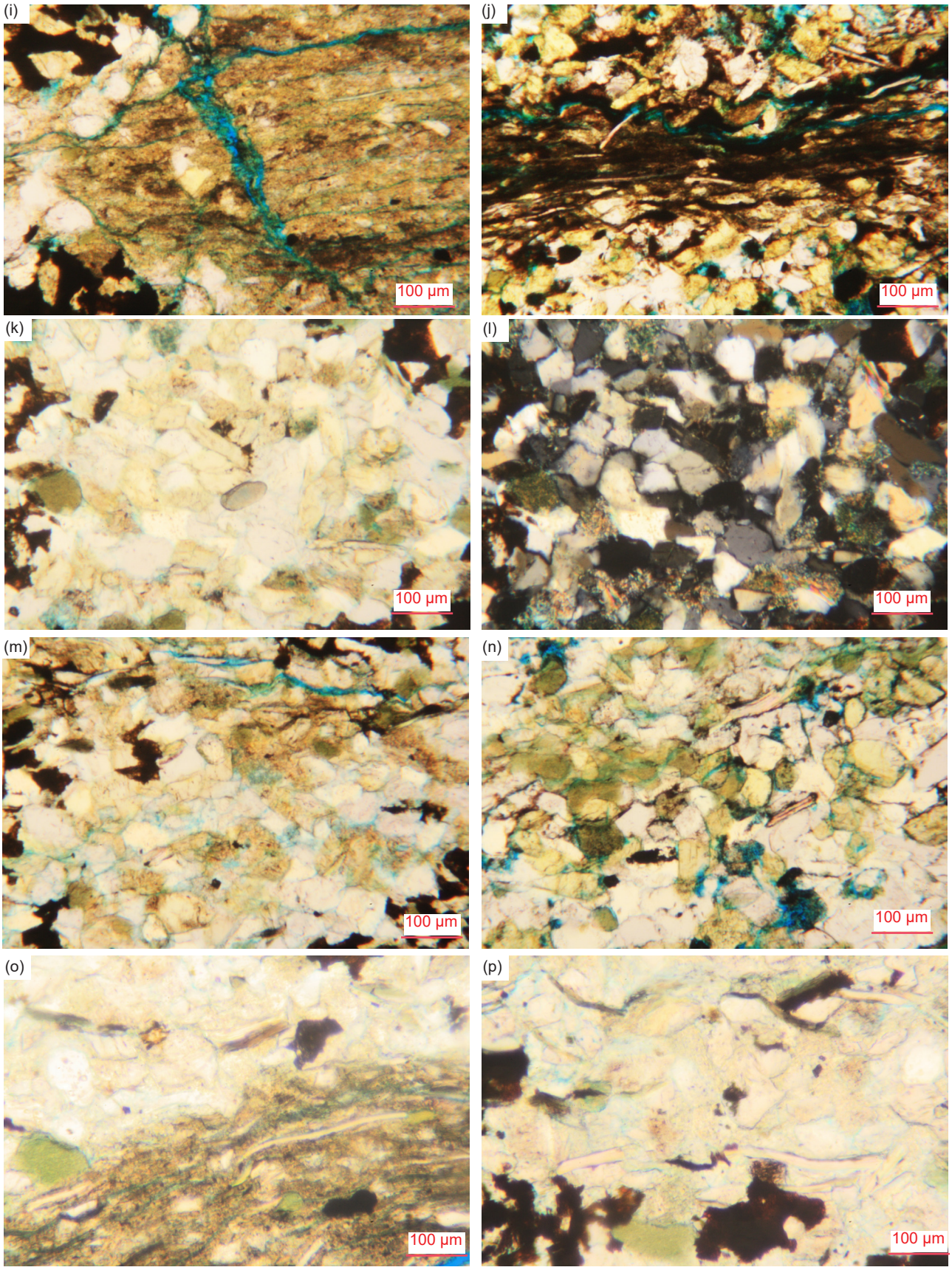
(i)
100 µm
(j)
100 µm
(k)
100 µm
(l)
100 µm
(m)
100 µm
(n)
100 µm
(o)
100 µm
(p)
100 µm

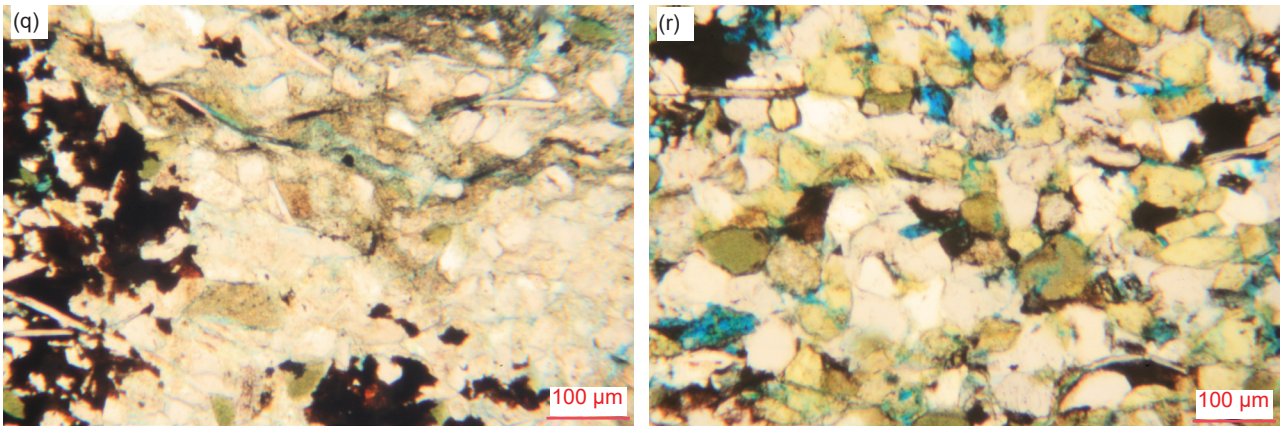

Fig. 34 (pages 135–137). Illite alteration of K-feldspar grains and laths and illite as cement in most of the Bright Angel Formation samples. (a) BAS-01, (b) BAS-02, (c), (d) HF-01, (e), (f) HF-02, (g), (h) HF-03, (i) HF-04, (j) HF-05, (k) HF-07, (l) HF-07 [(k) under crossed polars], (m) HF-07, (n) HF-08, (o), (p), (q) HF-09, and (r) HF-10.

the siderite may have resulted from replacement of dolomite (fig. 35o). Most of the mosaic in that sample is cemented with a combination of illite alteration and siderite (or dolomite partially covered with iron oxide), and found in patches consisting of a tightly-interlocking mosaic of tiny siderite grains between the quartz and K-feldspar grains.

Calcite and dolomite occur together between quartz, K-feldspar and glauconite grains and muscovite flakes in both distal samples (fig. 35a–d) but only in a single fold limb zone sample, a sandstone that also contains ankerite (fig. 35e–g) (table 2). Otherwise, the other fold samples contain dolomite (with siderite in one sample) between the mosaic grains regardless of whether in a siltstone or sandstone, or contain ankerite between the mosaic grains regardless of whether in a shale, siltstone, or sandstone (table 2). Furthermore, there appears to be no preferential occurrences of any of the carbonate minerals in the limb and hinge zone samples of the fold. Thus, these carbonate minerals do not seem to be products of the deformation. Some grains might even be detrital, but most of the carbonate minerals appear to be due to secondary alteration that post-dates lithification of these lithologies within the Bright Angel Formation.

If deformation in the fold had been brittle, that is, after cementation and lithification, then some localized fracturing of grains and the rock fabrics including the cement might be evident at the microscopic scale in samples from the fold, especially in the hinge zones. So, not surprisingly, there are a few *localized fracture zones* evident in all but one of the Bright Angel Formation samples in the fold (fig. 36). Such localized fracture zones might be expected in samples from the hinge zone of the fold in contrast to samples from the limbs. However, they occur in both hinge and limb zone samples. Where there is extensive illite alteration between the mosaic grains, it would appear that it has facilitated some fracturing and possible shearing of some mosaic grains along linear zones (fig. 36b–e, o, p, s), again irrespective of location in the limb or hinge zones. Otherwise, in the sandstone and siltstone samples from both the limb and hinge zones, fractures cross-cut the mosaics of quartz and K-feldspar grains, sometimes fracturing or even crushing some of those grains (fig. 36f, h–m, q, r). In some instances, the abundant presence of aligned muscovite flakes facilitated the fracturing along planes parallel to their alignment (fig. 36a, e, g, n–p, s). It is also worth noting that in many of these instances illite alteration has also been fractured, but no obvious shearing or fracturing of mosaic grains is evident so no movement has occurred. Perhaps significantly, in contrast, neither of the distal samples contain any localized fracture zones. This by no means makes it certain that the fracturing occurred during the deformation of the sandstone, siltstone, and shale beds in this fold, because these localized fracture zones occur in both the hinge and limb zone samples. Instead, some of this fracturing could have thus occurred after the folding deformation as a result of minor earth movements after lithification, ongoing even to the present (to be discussed below).

The Silica Cement

The primary cement binding the detrital grains together in all these samples of the Bright Angel Formation, whether sandstone, siltstone, or shale, is silica as quartz overgrowths (figs. 24 and 37). It is evident that in most instances this silica filled most of the initial pore spaces between the deposited sand and silt grains during and subsequent to compaction and during dewatering, leaving only very few, very small pore spaces in the resultant lithologies. The cement appears to be in pristine condition, that is, still in its original condition from precipitation during lithification. A close look at the rock fabric and

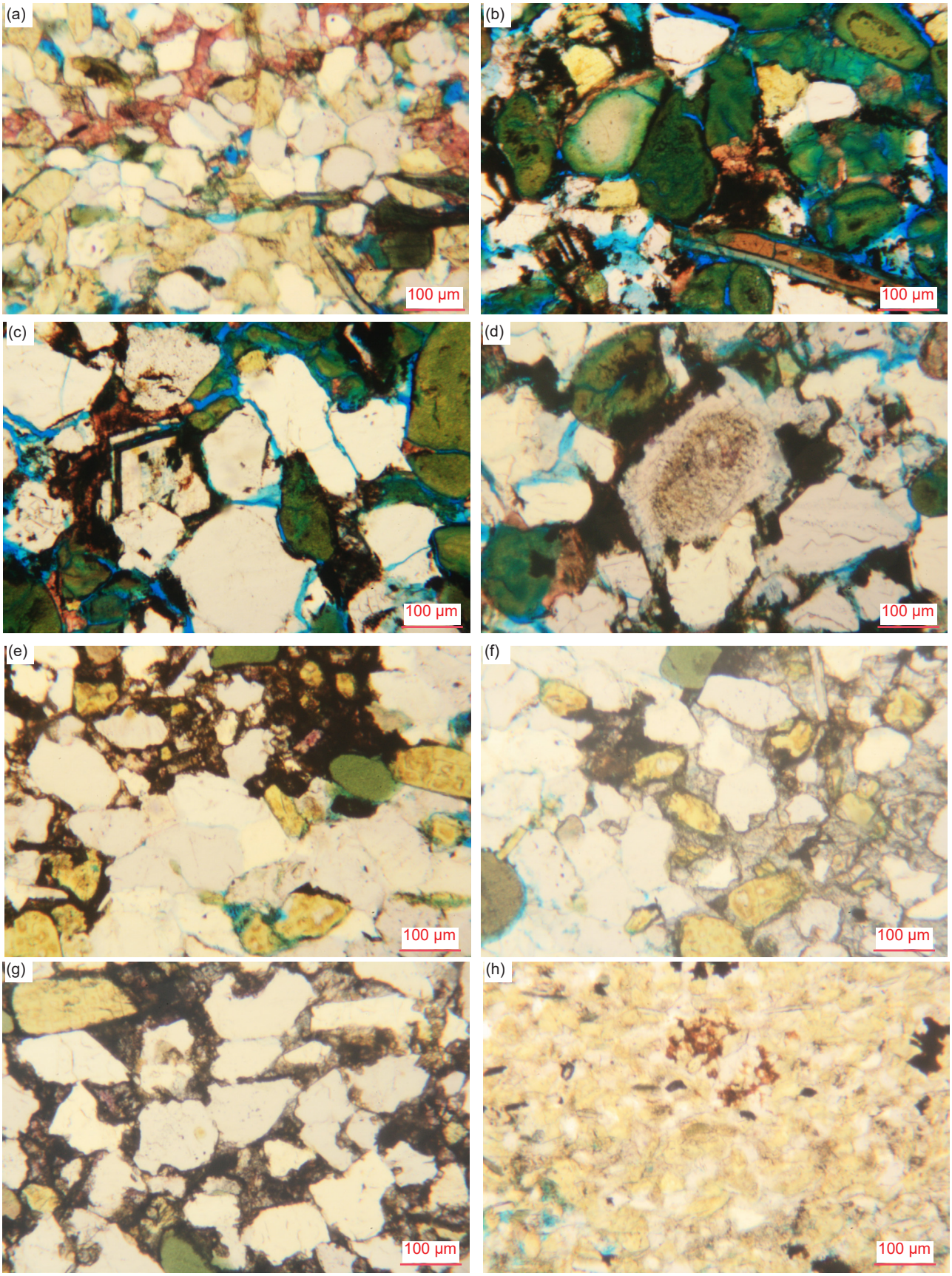
(a)
100 µm
(b)
100 µm
(c)
100 µm
(d)
100 µm
(e)
100 µm
(f)
100 µm
(g)
100 µm
(h)
100 µm

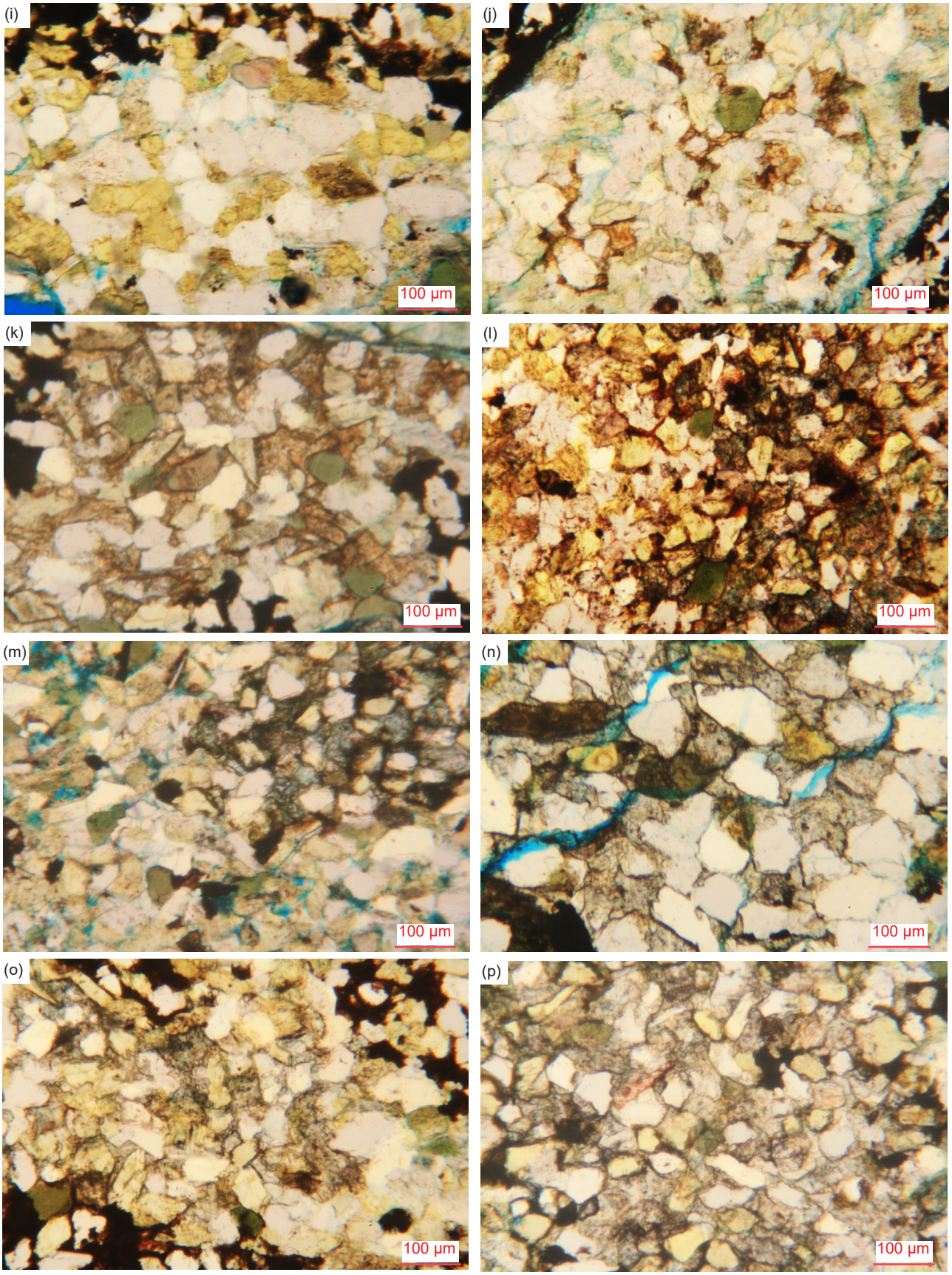
(i)
100 µm
(j)
100 µm
(k)
100 µm
(l)
100 µm
(m)
100 µm
(n)
100 µm
(o)
100 µm
(p)
100 µm

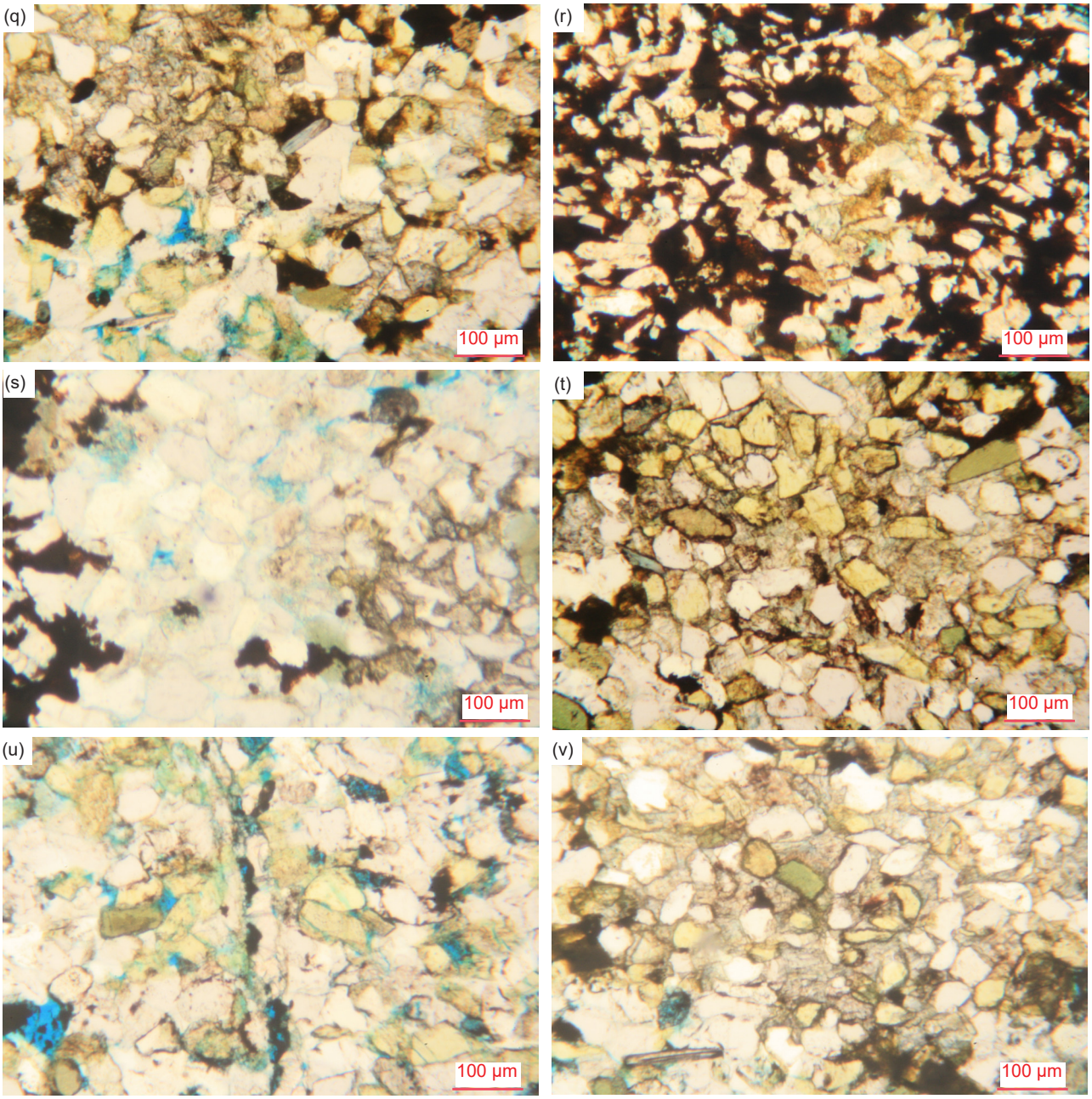

Fig. 35 (pages 138–140). The secondary carbonates, calcite (dark pink, sometimes accompanied by iron oxides) and dolomite (white and skeletal rhombs, sometimes also accompanied by iron oxides), as well as ankerite and siderite, as grains/crystals between the detrital quartz and K-feldspar grains, and as veinlets, in most of the Bright Angel Formation samples. (a) calcite BAS-01, (b), (c), (d) calcite and dolomite BAS-02, (e) ankerite HF-01, (f) dolomite HF-01, (g) ankerite HF-01, (h), (i) ankerite HF-02 (j), (k) ankerite HF-04, (l), (m) ankerite HF-05, (n) dolomite HF-06 (o) dolomite and siderite HF-07, (p), (q) dolomite HF-08, (r), (s) dolomite HF-09, and (t), (u), (v) dolomite HF-10.

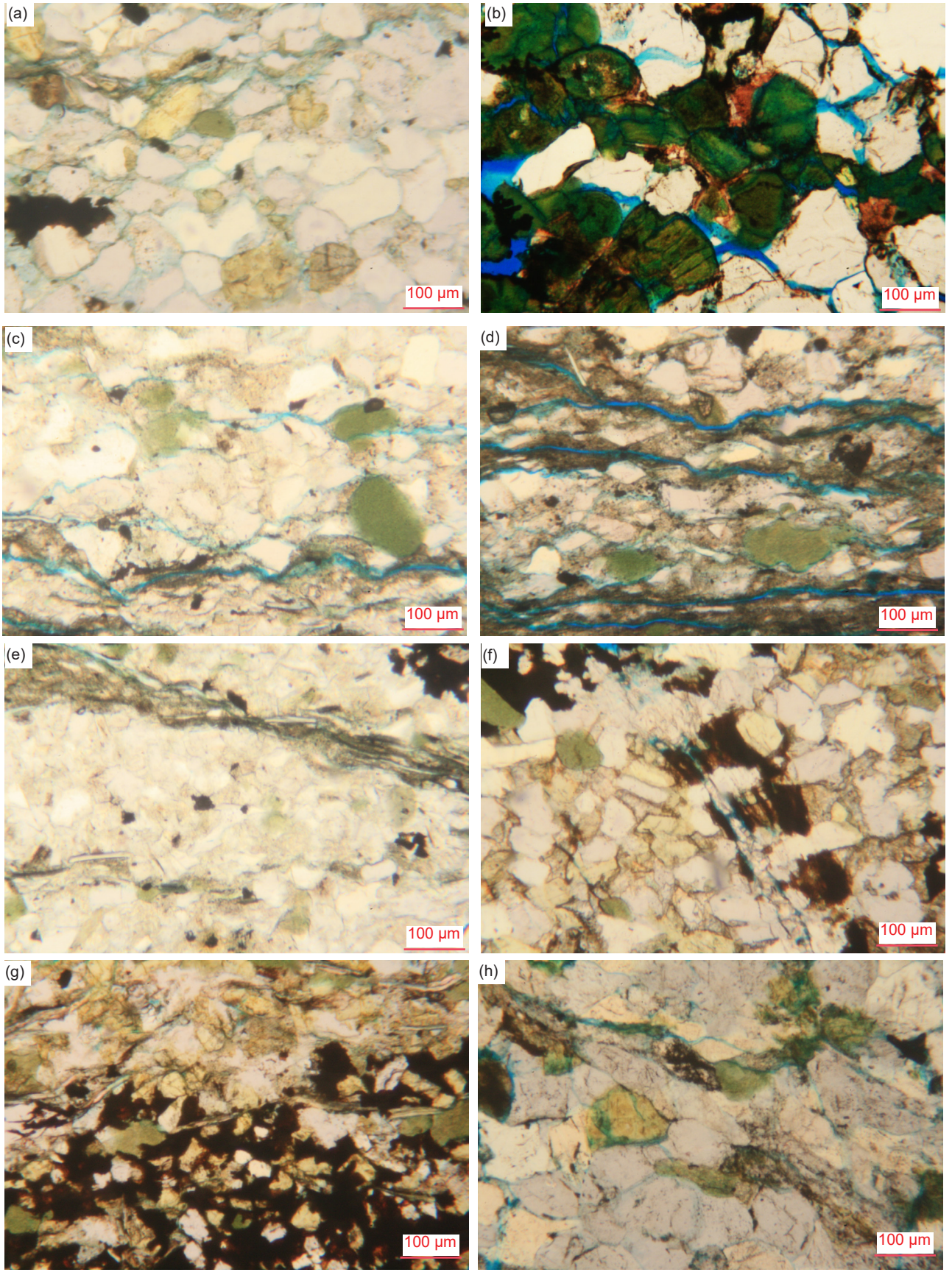
(a)
100 µm
(b)
100 µm
(c)
100 µm
(d)
100 µm
(e)
100 µm
(f)
100 µm
(g)
100 µm
(h)
100 µm

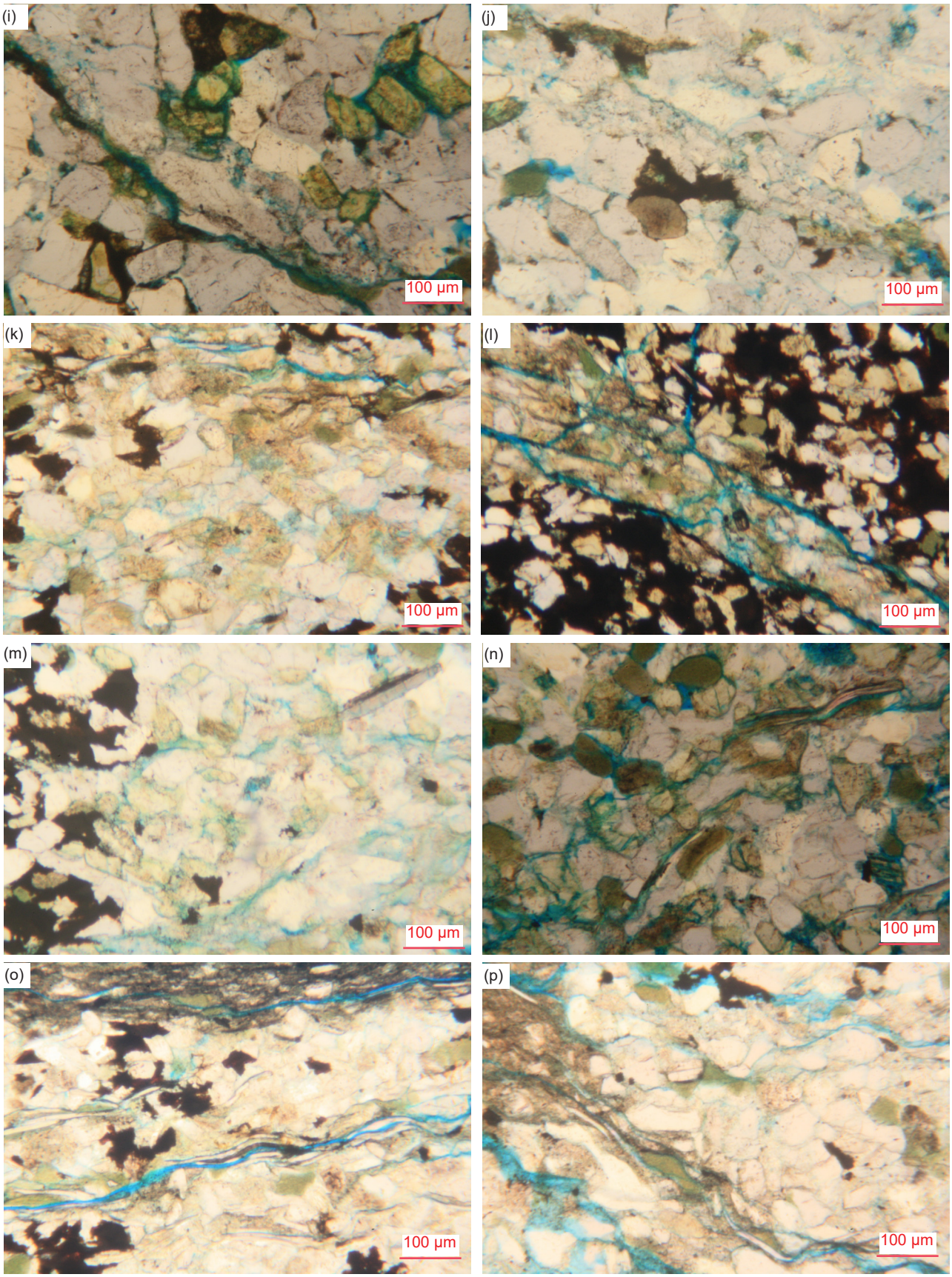
(i)
100 µm
(j)
100 µm
(k)
100 µm
(l)
100 µm
(m)
100 µm
(n)
100 µm
(o)
100 µm
(p)
100 µm

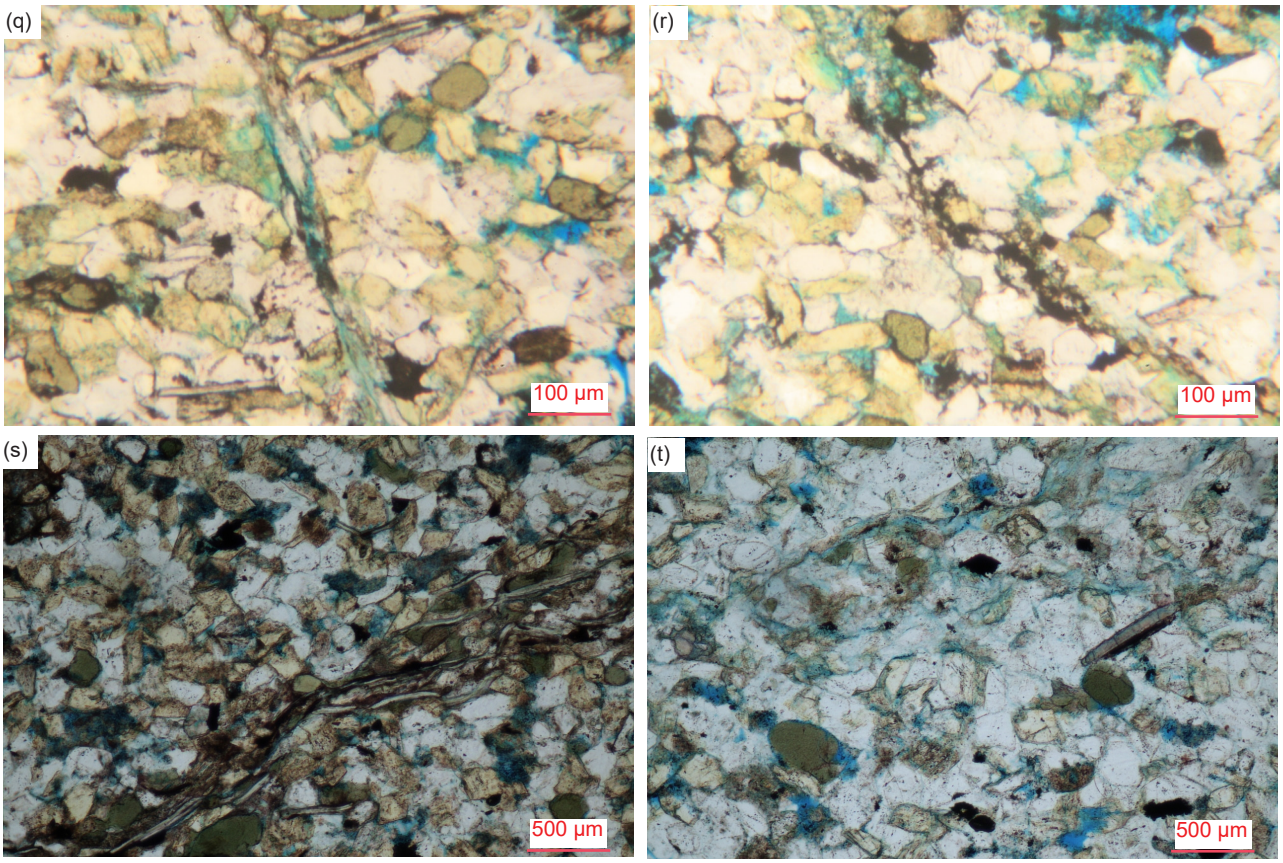

Fig. 36. Possible local fracture zones within the microscopic fabric of some samples of the Bright Angel Formation within the Whitmore Helipad fold. (a), (b) HF-02, (c), (d), (e) HF-03, (f) HF-04, (g) HF-05, (h), (i), (j) HF-06, (k), (l) HF-07, (m), (n) HF-08, (o), (p) HF-09, (q), (r) HF-10, (s) HF-05, and (t) HF-08.

the silica cement under the petrographic microscope, supplemented by scanning electron microscope (SEM) imaging, thus supports the observation that lithification occurred after the deformation. However, if lithification occurred before the deformation of these sandstone, siltstone, and shale beds in the fold, then the silica cement might show evidence of being fractured by the deformation but then being healed.

Petrographic Microscope Observations

The critical petrographic microscope observation is that the silica cement and the quartz overgrowths are in the same condition in the two distal samples (figs. 24a–c and 37a–d) as in the samples from the fold (figs. 24d–n and 37e–f'). Furthermore, there is no difference in the silica cement condition between the samples from the limb zones (fig. 37e–k, p–r, y–a', d', f') and the hinge zones (fig. 37l–o, s–x, b', c', e') in the fold, compared with the distal samples (fig. 37a–d). Thus, the effects and outcome of the lithification of the deposited sand and silt layers under the overburden pressure of the overlying strata and the slightly elevated temperature were uniform throughout the entire Bright Angel Formation.

As described already, the quartz and K-feldspar grains that dominate the rock fabric are still preserved in their original detrital condition, as evident in the many sub-rounded quartz grains that are outlined by dust and iron oxides with quartz overgrowths in optical continuity with them in many of the samples (figs. 24 and 37). And the observation that those quartz overgrowths meet at triple points, as do many of the overgrown quartz grains in which their original detrital shapes are not swell outlined (figs. 25 and 37), is consistent with that configuration being the most ergonomic as precipitation of the silica occurred around the detrital grains and grew out into the pore spaces between the compacted sand grains. Furthermore, the prevalence of overgrown quartz grains with no internal outlining of the original detrital grains would suggest that much of the silica that precipitated as quartz cement during dewatering of the sediment was derived from being dissolved in the pore waters from the edges of those original detrital quartz grains aided by pressure solution at grain-to-grain contacts as the quartz grains were compacted. Indeed, in some places this quartz cementation infilling between the quartz grains in optical continuity is so complete with the original grain boundaries and so indistinct that the fabric looks like a solid mass of quartz. The quartz cementation clearly had to have occurred early as

in some places the quartz grains are dominantly euhedral and angular due to the overgrowths being in optical continuity and not always discernible, while in other places there are quartz grains that are molded around other grains so the quartz cement must have overgrown the detrital grains in optical continuity.

It is also readily apparent that there was secondary alteration subsequent to the formation of the silica cement during dewatering and lithification of the sand and silt sediment layers to produce these sandstone, siltstone, and shale beds. As already noted, many of the K-feldspar grains and some of the muscovite flakes have been altered to illite, so that particularly in the shale beds and selvages the intensity of the illite alteration of the abundant tiny K-feldspar grains has resulted in the illite adding to the cement (fig. 34). Similarly, either concurrently or likely subsequently, in scattered areas carbonate alteration became the localized cement (fig. 35).

If deformation of these sandstone, siltstone, and shale beds in this fold occurred after lithification, then the cement would have fractured and then healed. However, there is no evidence of that, since the condition of the silica cement is the same in the samples from the hinge zones of the fold as in the samples from the limb zones and the distal samples. Any silica-carrying fluids permeating the sandstone, siltstone, and shale to heal the fractured silica cement would surely have also healed the fractures within the quartz grains (fig. 28), and perhaps even some of the more prominently-outlined sub-grains within the original detrital quartz grains that have them (fig. 26). However, the fractures and sub-grains in the quartz grains that have them have not been healed. To heal them and the cement would have required an adequate supply of silica in whatever connate water remained in the few very small pore spaces still within the compacted and lithified sandstone, siltstone, and shale beds. Furthermore, even though there are localized fracture zones evident in the rock fabric of all the samples from the fold's hinge zones (fig. 36f, g, k–p, s, t), there are also similar localized fracture zones in most of samples from the limb zones (fig. 36a–e, h–j, q, r). These localized fractures seem unlikely to be sufficient as pathways for externally derived silica-carrying fluids to permeate these lithologies to deposit the silica and heal fractures within quartz grains and sub-grains. Indeed, the only evidence of post-lithification alteration deposits around quartz and K-feldspar grains, infilling small residual pore spaces, and in a few places replacing the silica cement, or along fractures, are carbonate minerals (fig. 35).

The absence of localized fractures in the two distal samples, coupled with the lack of healing of the localized fractures within the fold samples, indicates that the fracturing in the fold is due to earth movements localized to the fold area that occurred after the deformation that produced the fold (discussed below). This is confirmed by the condition of the silica cement being the same in all samples, as well as the unhealed fractures and sub-grains within quartz grains in all samples.

SEM Observations

Whereas petrographic microscope observations produce two-dimensional images, the scanning electron microscope (SEM) produces three-dimensional images. This enabled closer examination of both the detrital quartz grains and the silica cement. Figs. 38–45 provide the SEM images at various recorded magnifications for selected samples—the two distal samples (BAS-01 and BAS-02), three samples from the two hinge zones in the fold (HF-05, HF-08, and HF-09), and three samples from the limbs of the fold (HF-02, HF-03, and HF-06) (see fig. 21).

It should be noted that the surfaces of the samples that were imaged were made by breaking the rocks open vertically, perpendicular to the bedding, identically to how the thin sections were cut. That could have resulted in broken grains and/or cement, which should be evident in the resultant images. Nevertheless, the features evident in these SEM images were found to be the same regardless of the location of the sample, whether distal to the fold or from the hinge and limb zones of the fold. That observation is critical because it reinforces the conclusion from the petrographic microscope examination that the conditions within the Bright Angel Formation since deposition of its constituent sand and silt grains, principally quartz grains with secondary K-feldspar grains and former laths, and muscovite flakes, have been uniform throughout the extent of this rock unit within Grand Canyon. That is, conditions in the history of the interlayered sandstone, siltstone, and shale beds have not been different during their deformation in this fold compared to the same beds distant from this fold. Detailed observations of each sample justify this conclusion.

Sample BAS-01 is from a fine-grained sandstone layer distal to the Whitmore Helipad fold (fig. 1). The progressive magnification of images (a)–(e) in fig. 38 reveal the very tight but still slightly open porosity in the broken surface of the clean quartz-cement-covered detrital quartz grains in sample BAS-01. To the right of center in fig. 38a can be seen a rounded detrital quartz grain which is magnified near the right-hand edge of fig. 38b. It has a clean rounded surface with a fracture across its top right-hand quadrant, all of which appears to be preservation

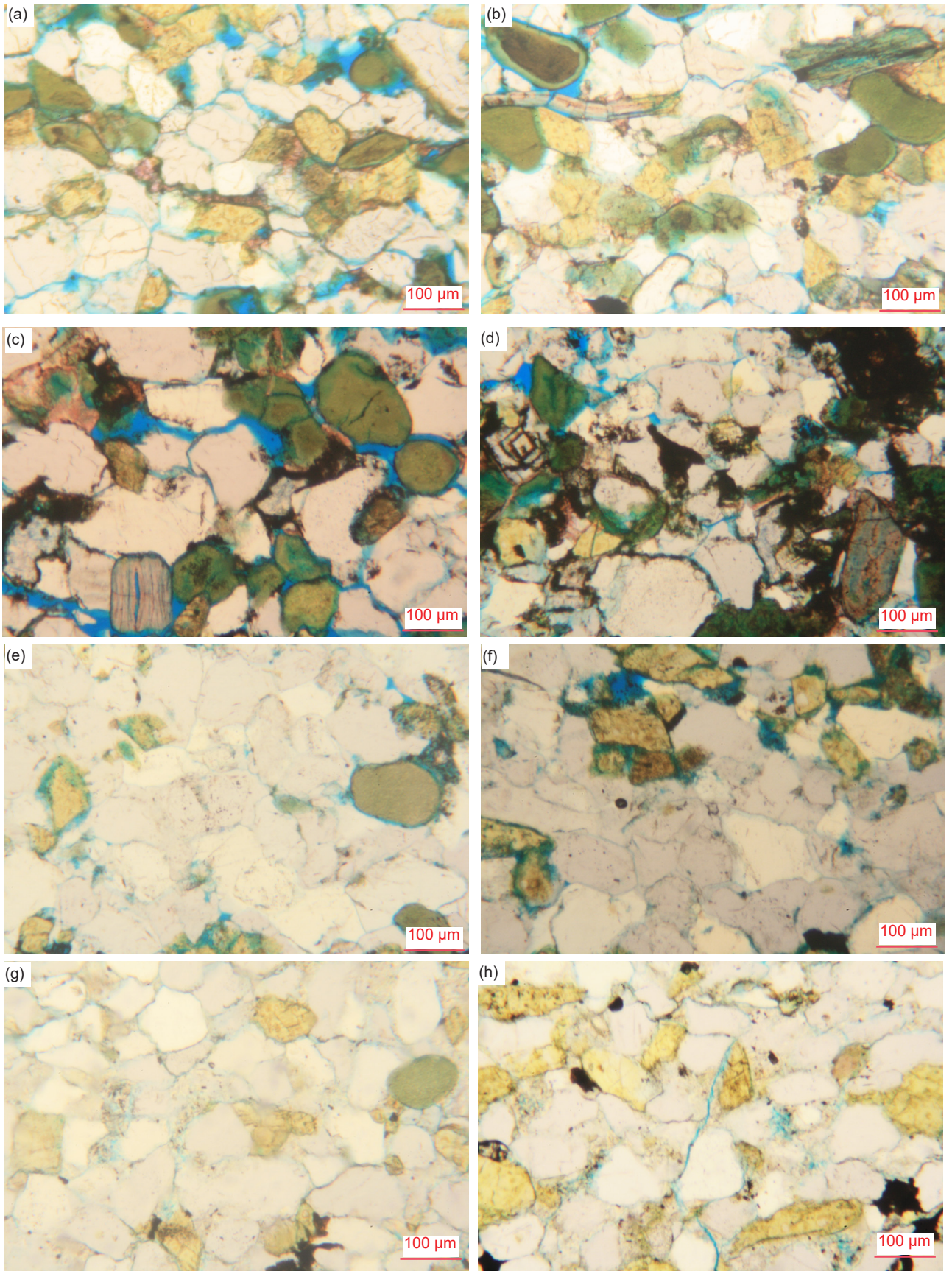
(a)
100 µm
(b)
100 µm
(c)
100 µm
(d)
100 µm
(e)
100 µm
(f)
100 µm
(g)
100 µm
(h)
100 µm

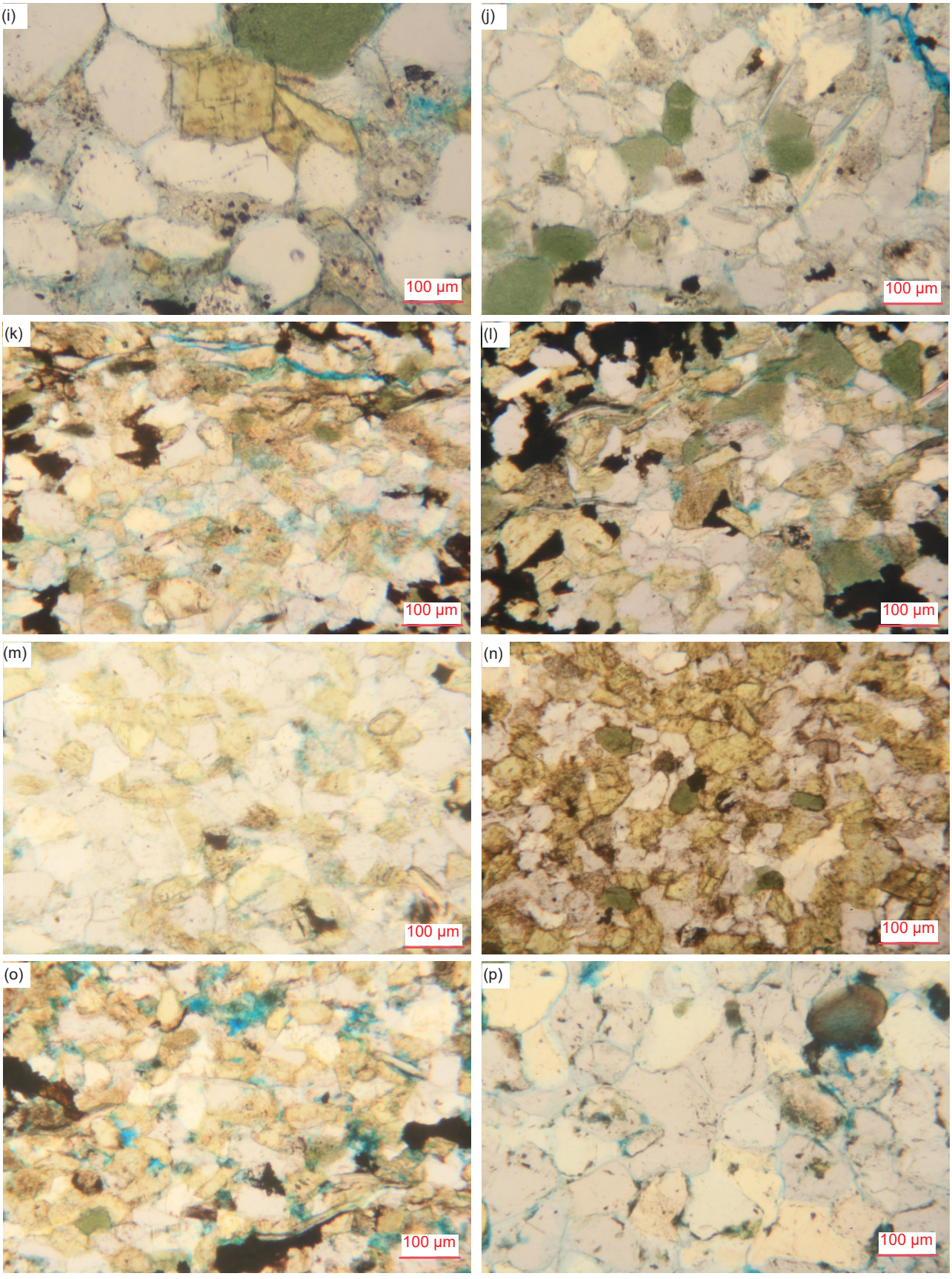
(i)
100 µm
(j)
100 µm
(k)
100 µm
(l)
100 µm
(m)
100 µm
(n)
100 µm
(o)
100 µm
(p)
100 µm

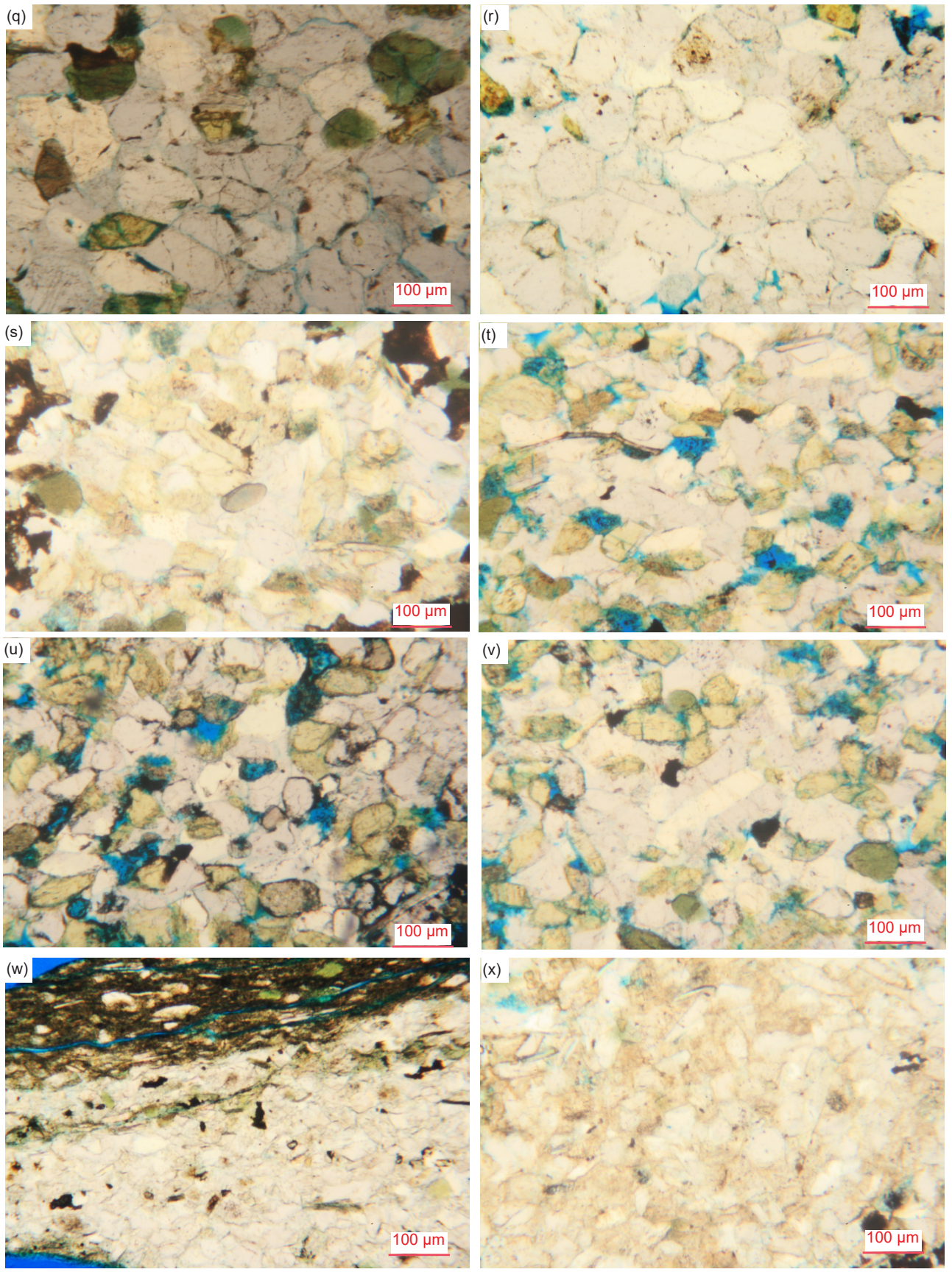
(q)
100 µm
(r)
100 µm
(s)
100 µm
(t)
100 µm
(u)
100 µm
(v)
100 µm
(w)
100 µm
(x)
100 µm

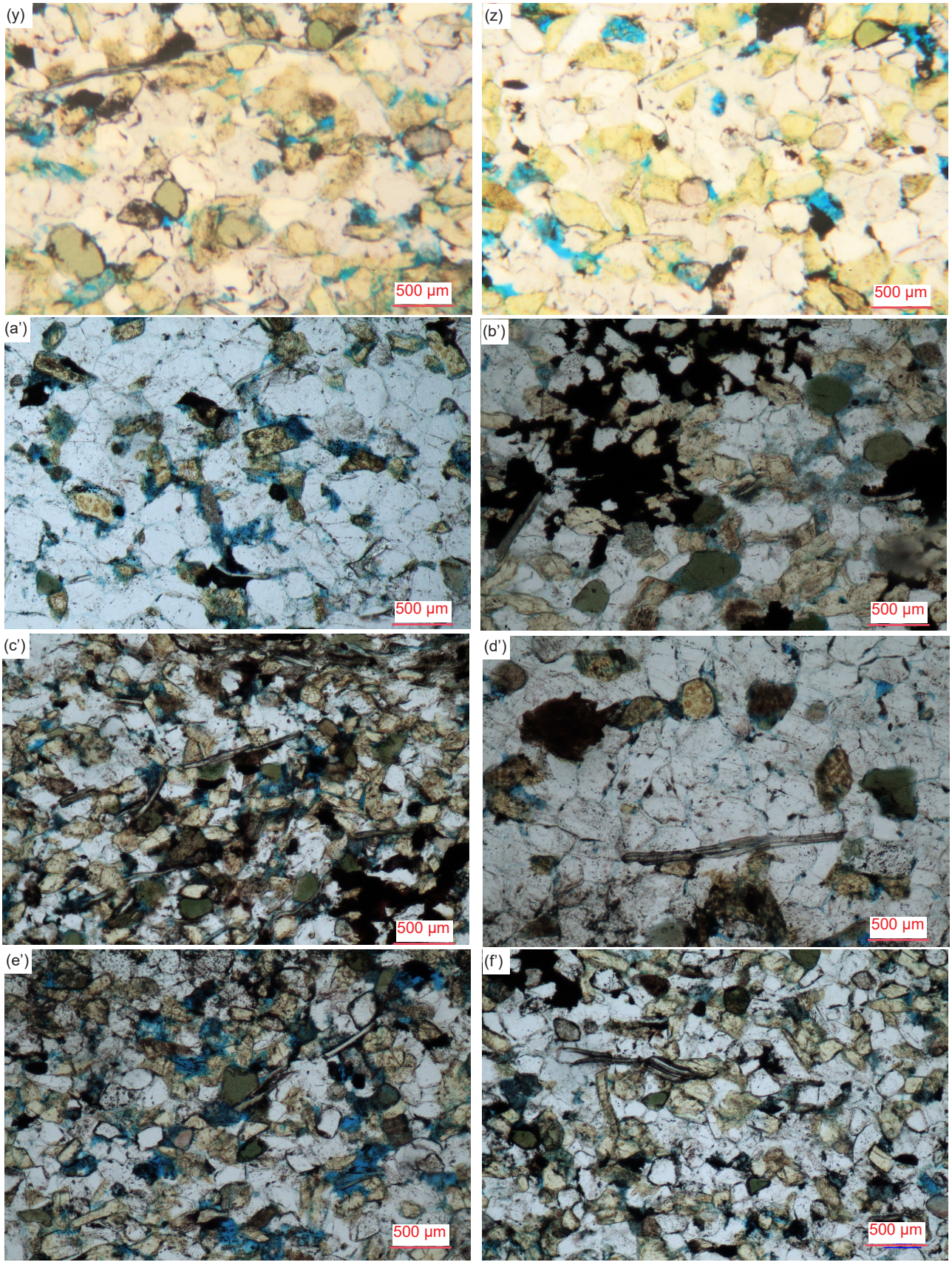

Fig. 37 (pages 145–148). The quartz cement between detrital grains within the Bright Angel Formation samples. (a), (b) BAS-01, (c), (d) BAS-02, (e), (f) HF-01, (g), (h), (i) HF-02, (j), (k) HF-03, (l), (m) HF-04, (n), (o) HF-05, (p), (q), (r) HF-06, (s) HF-07, (t), (u), (v) HF-08, (w), (x) HF-09, (y), (z) HF-10, (a') HF-01, (b') HF-04, (c') HF-05, (d') HF-06, (e') HF-08, and (f') HF-10.

of its original detrital state. While several other similarly rounded detrital quartz grains can be seen in fig. 38b, most of the detrital quartz grains are covered with quartz cement, which in magnified figs. 38c and 38d can be seen to consist of pristine crystal terminations and edges, indicating the cement grew over the detrital grains to infill pore spaces and has not been disturbed since crystallization. Indeed, in fig. 38d, the quartz cement covering the detrital grains in the bottom left-hand quadrant has evidence of growth zones, indicative of progressive growth of the cement, likely due to deposition from the pore fluids over some protracted time after the sediment deposition. Evident in figs. 38d and 38e is some minor illite growth on a few surfaces which is likely due to K-feldspar dissolution. This is best seen in fig. 38e in the top left-hand quadrant where there is the embayed surface of the top edge of a larger K-feldspar grain due to dissolution, and the illite has grown adjacent to it. That same larger K-feldspar grain in fig. 38e has some fracturing along its vertical axis plus a pocket of dissolution in its side that has exploited the internal exposure of the grain induced by the fracturing. Otherwise, the fractures are tight and show no evidence of any displacement, which means they are likely due to compactional loading after detrital grain deposition. Fig. 38f is an enlargement of the center right section of fig. 38b and includes the left-hand edge of the previously-highlighted rounded detrital quartz grain. It reveals the dissolution of the quartz cement surfaces around pore spaces and the growth of illite. Fig. 38g is a magnification of the area left of center in fig. 38f and shows again the dissolution of quartz cement crystal surfaces, as well as fracturing of some of the quartz cement around its crystal edges that likely is due to compactional loading, as there is no evidence of any displacement or disruption pertaining to the fractures. Finally, in fig. 38g the dissolution of some quartz cement surfaces and the growth of illite on them can be seen, as well as the growth zones in the pristine quartz cement crystals.

Sample BAS-02 is from another fine-grained sandstone layer distal to the Whitmore Helipad fold (fig. 1). As can be seen in the progressively magnified images (a)–(f) in fig. 39 of the broken-apart sample surface, it also consists of clean quartz-cement-covered detrital quartz grains. No original detrital quartz grain surfaces appear to be evident due to the prolific quartz cementation covering them throughout the sample. The porosity is very tight with some pore spaces still present, for example, below left of center in fig. 39b and magnified bottom center in fig. 38c. Some pristine quartz cement crystal terminations, faces, and edges are evident in figs. 39c–f, and even some growth zones, as well as pockets of dissolution on a few surfaces. Some minor illite growth can be seen associated with the areas of quartz cement dissolution. Otherwise, the broken-apart surfaces of the quartz cement are clean and there is no evidence of any post-deposition or post-cementation disruption of this sandstone apart from when the sample was broken apart for SEM examination. Fig. 39g is a magnification of the previously-noted pore space in the bottom center of fig. 39c and of the area below it and to its left, while fig. 39h is a magnification of the area to the right of center in fig. 39g.These two images show the same features as in the previous images—occasional residual pore spaces, clean broken-apart surfaces of the quartz-cement-covered detrital quartz grains, and some pristine quartz cement crystal faces, edges, and terminations, with a few trivial patches of dissolution and even more trivial illite growth. Of particular interest is what appears to be a thin muscovite flake spread over, molded across, and affixed to the broken-apart quartz cement surfaces of detrital quartz grains, which is best seen just below left of center in fig. 39h. This muscovite flake shows no evidence of any post-depositional disruption or distortion and is clearly a detrital flake that has survived intact in its detrital condition.

The SEM images in fig. 40 are of sample HF-02 from a shale bed within the Whitmore Helipad fold's lower limb, close to the lower hinge zone. Its location is marked in fig. 21. Figs. 40a–e show the progressive magnification of the broken-apart sample surface perpendicular to the thin horizontal laminations, which consist (in decreasing order) of K-feldspar and quartz grains, as well as illite (table 2). It is unclear how much of the quartz represents detrital grains, but it is evident in images (c)–(e) that the original detrital grains, whether K-feldspar or quartz, are covered in quartz cement. Fig. 40c is a magnification of the central area of fig. 40b, then fig. 40d magnifies the central area of fig. 40c, and fig. 40e magnifies the central area of fig. 40d, as can be recognized from the elongated cavity between the laminations in figs. 40b and c (likely induced by fracturing during the sample collection process—see fig. 22d), and from the relatively prominent and larger cleanly-broken-apart quartz cement surfaces. Between those relatively prominent and larger broken-part quartz cement surfaces in figs. 40d and e can be seen very thin crenulated (wavy) laminations that likely consist mostly of illite, which often has a micaceous (flat-lying sheet) habit, though some mud-sized K-feldspar and quartz grains may be also present. The illite likely grew from dissolution of detrital mud-sized K-feldspar and quartz grains after their deposition, rather than it being due to its own primary detrital deposition. The crenulations probably occurred due to post-

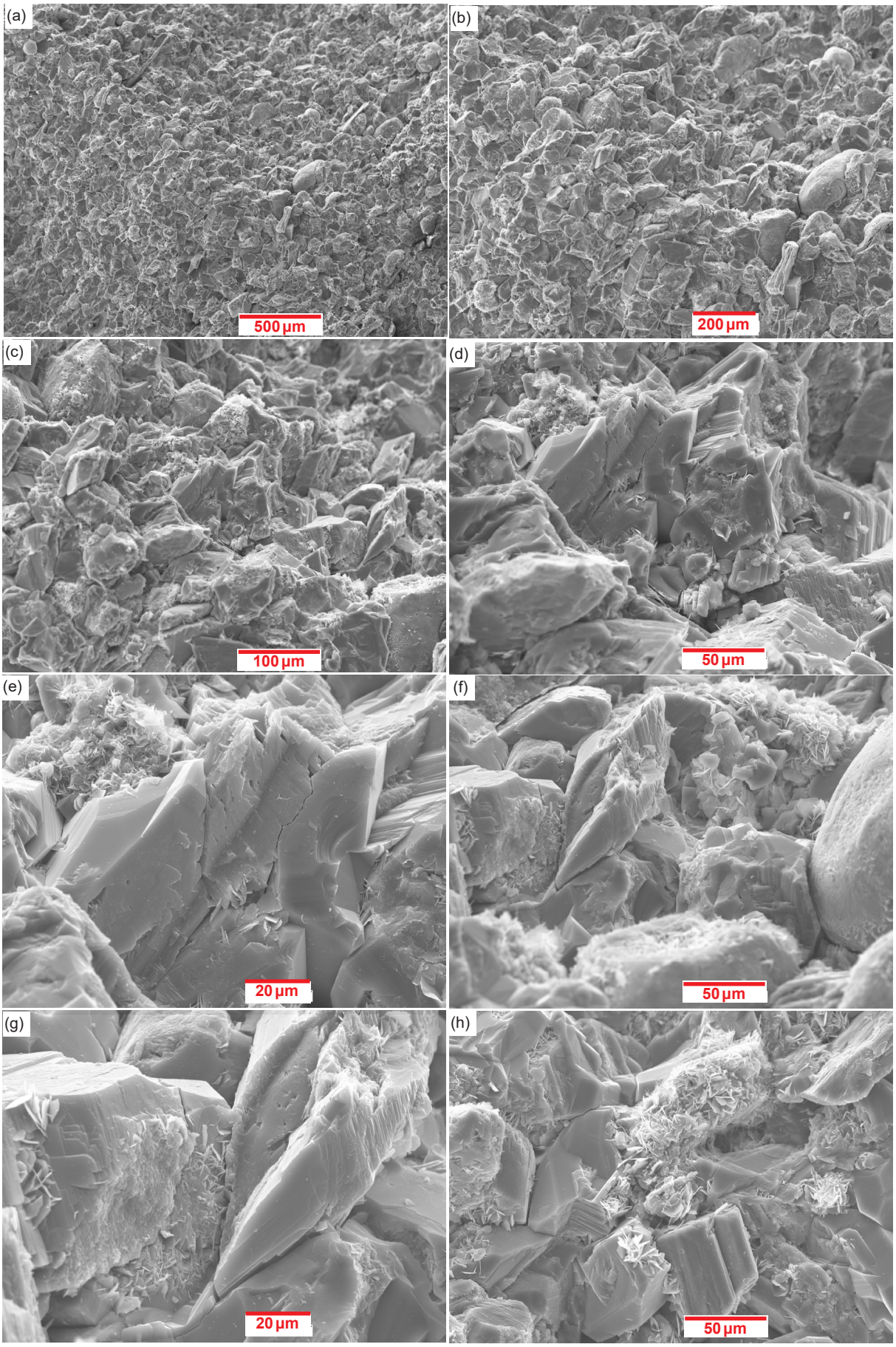
(a)
500 µm
(b)
200 µm
(c)
100 µm
(d)
50 µm
(e)
20 µm
(f)
50 µm
(g)
20 µm
(h)
50 µm

Fig. 38 (page 150). Scanning electron microscope (SEM) images of distal sample BAS-01 (see fig. 1 for its location). (a) 50X, (b) 100X, (c) 200X, (d) 500X, (e) 1000X, (f) 500X, (g) 1000X, and (h) 500X.

depositional compactional loading, and there is no evidence of any disruption or shearing of them. This is consistent only with folding after deposition but before cementation, because otherwise these crenulated laminations would have been disrupted and sheared. Fig. 40f is of the broken-apart surface of one of the fine-grained siltstone lenses or laminations within the shale (fig. 22d), that is not in any of the previous images of this sample. Fig. 40g is then the magnification of the central area in fig. 40f, and fig. 40h is then the magnification of the central area in fig. 40g. As also seen in the distal fine-grained sandstone samples BAS-01 and BAS-02 (figs. 38 and 39 described above), this fine-grained siltstone is well cemented with quartz cement covering the detrital grains (primarily quartz—fig. 23g), with almost no pore spaces, and with the broken-apart cement surfaces being clean. Some minor patchy dissolution of the quartz cement is evident in figs. 40g and h. There is also an open fracture which cuts sub-horizontally across the fabric of the quartz cement, but there is no displacement. Thus, there is no evidence of any disruption in this fold limb sample from the folding process which would be expected if cementation occurred before the folding, which implies the cementation occurred after the folding.

Sample HF-03 is similarly from a shale bed, its location being marked in fig. 21. It is also from the lower limb zone of the Whitmore Helipad fold. The images in figs. 41a–e show the progressive magnification of the very-finely-laminated sample's broken-apart surface, which is dominated by clean surfaces of quartz-cement-covered detrital quartz and K-feldspar grains, though illite is also a major component of the sample (table 2). It is very difficult to see, but the illite because of its micaceous habit may be wedged as ultra-thin laminations between the harder very thin quartz-cemented laminations that protrude out of the broken-apart sample surface. As in sample HF-02 described above, the illite could be due to post-depositional dissolution of originally-deposited mud-sized K-feldspar grains that were separated into those ultra-thin laminations, as K-feldspar is a major component of this sample also (table 2). There is a hint of this in fig. 41e, which also shows evidence of some dissolution of the quartz cement. Overall, the thin laminations are regularly spaced as would be expected for the depositional processes involved, and show no evidence of disruption after growth of the quartz cement. Furthermore, if there had been movements between the hard quartz-cemented laminations, that is, if they had slid against and past one another during bending of the layers in the fold after cementation, then there should be slickensides on the protruding exposed surfaces between the laminations. However, there is not even a hint of that in figs. 41d and e, which instead show the protruding exposed surfaces between the laminations are clean and smooth. This is consistent with the folding having occurred prior to cementation. Fig. 41f is the broken-apart very-finely-laminated surface of another portion of the sample, and imaged at a different inclination (angle). Fig. 41g is the magnified central area of fig. 41f, while fig. 41h is the magnified central area of fig. 41g. All the same observations are evident in figs. 41f–h as in figs. 41a–e. Additionally, in fig. 41h can be seen in the top left quadrant a crystal or piece of quartz cement affixed at a different angle to the broken-apart protruding end of the hard quartz-cemented laminations. Its significance is unclear.

Whitmore Helipad fold sample HF-05 is from a siltstone bed within the fold's lower hinge zone (see fig. 21 for its location). The SEM images of its broken-apart surface in fig. 42 show the clean quartz cement that has overgrown the detrital quartz and K-feldspar grains. Figs. 42b–e show the progressive magnification of the central area of fig. 42a, while fig. 42f magnifies an area in fig. 42a in the middle of the upper left quadrant, fig. 42g magnifies the area toward the right central edge of fig. 42f, and fig. 42h magnifies the area to the right of center in fig. 42g. This siltstone is so well cemented that there are hardly any pore spaces left, though some tiny pore spaces are evident in these images, especially at the higher magnifications in figs. 42c–e. The broken-apart quartz cement surfaces are clean and not disrupted in any way, or where protruding, do not show any slickensides that would indicate movements, shearing or grain-boundary sliding. There is, however, some evidence of minor dissolution of the quartz cement in figs. 42c–e, as well as the growth of illite adjacent to the dissolution. While K-feldspar and quartz are the major components in this siltstone (in that order of abundance), illite is still there in significant quantities (table 2), likely scattered across some of the exposed surfaces, as can be seen in figs. 42a–d. In fig. 42a to the left of center is a bright streaky crystal that is enlarged in fig. 42b above its central left edge, and is a flat-lying muscovite flake. This identification is confirmed in figs. 42f–h, in which other muscovite flakes are magnified. In those images the muscovite flakes are flat-lying, and protrude outwards because they are wedged between the quartz-cement-overgrown

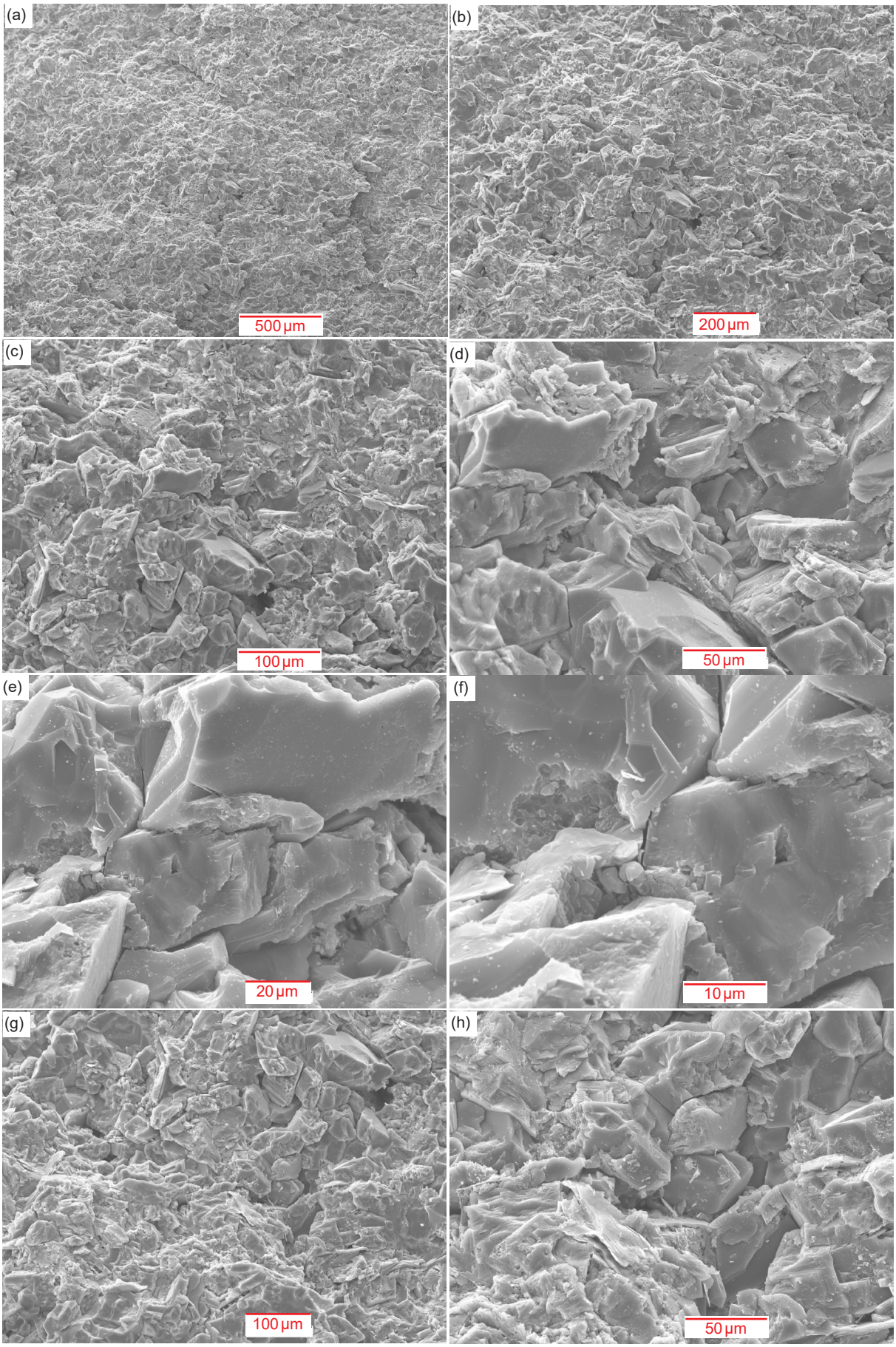
(a)
500 µm
(b)
200 µm
(c)
100 µm
(d)
50 µm
(e)
20 µm
(f)
10 µm
(g)
100 µm
(h)
50 µm

Fig. 39 (page 152). Scanning electron microscope (SEM) images of distal sample BAS-02 (see fig. 1 for its location). (a) 100X, (b) 200X, (c) 500X, (d) 1000X, (e) 1000X, (f) 2000X, (g) 200X, and (h) 500X.

detrital quartz and K-feldspar grains. Furthermore, the muscovite flakes are molded and bent around the quartz-cement-covered detrital grains without breaking. Indeed, the muscovite flakes are in this same condition in the thin sections (fig. 31). There is also no evidence either of any shearing between or displacement of the sheets within the flakes as seen in cross-section in both the thin sections and here in these SEM images. Displacement between sheets within the flakes and shearing of the flakes would be expected if the bending in the fold had occurred after cementation. This is because the cementation would have "locked" into position the muscovite flakes, so that if the folding then occurred the soft muscovite flakes would become the weak planes between the much harder quartz-cemented detrital grains and would have sheared and/or the internal sheets would have become displaced by sliding across one another. However, what is observed in both the thin-sections and the SEM images is that the muscovite flakes are still in their detrital condition Their bending would be due to compactional loading after deposition while still not cemented, and the folding of the layers would thus have to have been while the sediments were still soft, before the cementation, and because the quartz cement is still in pristine condition.

Whitmore Helipad fold sample MF-06 is from a fine-grained sandstone bed within the fold's middle limb zone (fig. 21 shows its location). The SEM image in fig. 43b is the magnified upper right quadrant of fig. 43a, while figs. 43c-e are the progressively magnified images of the central area of fig. 43b. These images show the rock fabric is well cemented by quartz that has overgrown the detrital grains which are overwhelmingly quartz with minor K-feldspar (table 2). The broken-apart quartz cement surface is clean. Indeed, figs. 43d and e show some excellent quartz cement crystal faces, edges and terminations that confirm the quartz cement is in pristine condition. However, some dissolution of the quartz cement can be seen in many scattered patches in figs. 43c–e, but there appears to be no growth of illite, which the XRD analysis confirms (table 2). This implies that the dissolution was at a late stage, probably due to the residual fluids in the remaining pore spaces after cementation and lithification. Furthermore, there also appears to be secondary quartz deposition in those quartz dissolution areas, as evidenced by the few scattered tiny quartz crystallites. Fig. 43f is a magnified image of a different portion of the broken-apart sandstone sample surface, while figs. 43g and h are progressively magnified images of the central area in fig. 43f. Fig. 43f shows the same features as in the previous images, especially the clean broken-apart surfaces of the quartz cement, and the areas of dissolution of the quartz cement. In fig. 43g and h a few scattered tiny quartz crystallites can be seen near areas of quartz cement dissolution, likely a result of precipitation from pore fluids that had dissolved some of the quartz cement. Also evident is the conchoidal fracturing of the quartz cement when the sample was broken apart for imaging.

Fig. 44 displays the SEM images of fine-grained sandstone sample HF-08, which is from a bed in the Whitmore Helipad fold's lower hinge zone (see fig. 21 for its location). Figs. 44b–d are the progressively magnified images of the central area of fig. 44a. They all show at different magnifications the scattered residual pore spaces within an otherwise well-cemented rock fabric consisting of quartz cement that has overgrown the detrital quartz and K-feldspar grains which make up the sandstone in roughly equal amounts (table 2). These pore spaces appear to be primarily due to dissolution of the quartz cement, and likely also some dissolution of the K-feldspar detrital grains, as evidenced by occasional scattered illite growth. Otherwise, the broken-apart surfaces of the quartz cement are clean, indicating the quartz cement is pristine without any evidence of prior disruption and subsequent healing, which would be expected if the folding occurred after cementation. Fig. 44e is the magnified image of the right-hand end of the top edge of fig. 44d and shows an oblique fracture through the quartz cement. The fracture does not appear to be due to the preparation of the sample for SEM imaging because it is confined to a limited area, extends from a pore space likely produced by dissolution of the quartz cement, and has tiny illite crystallites grown within it, especially in proximity to the pore space. There is also no displacement along the fracture. This all suggests the fracture was due to compactional loading. If the fracture was due to the folding event, then it would be more extensive rather than confined, and some displacement along its length would be expected. Fig. 44f is a magnified image of a small area in the bottom left portion of the left upper quadrant of fig. 44b, while figs. 44g and h are progressively magnified images of the prominent, fractured, rounded, quartz-cement-covered detrital grain to the left of center in fig. 44f. Again, this fracture is confined to just this rounded, quartz-cement-covered detrital grain, and there is no apparent displacement along its length. It is difficult to identify the detrital grain, but the presence of hairy illite grown on the rounded quartz

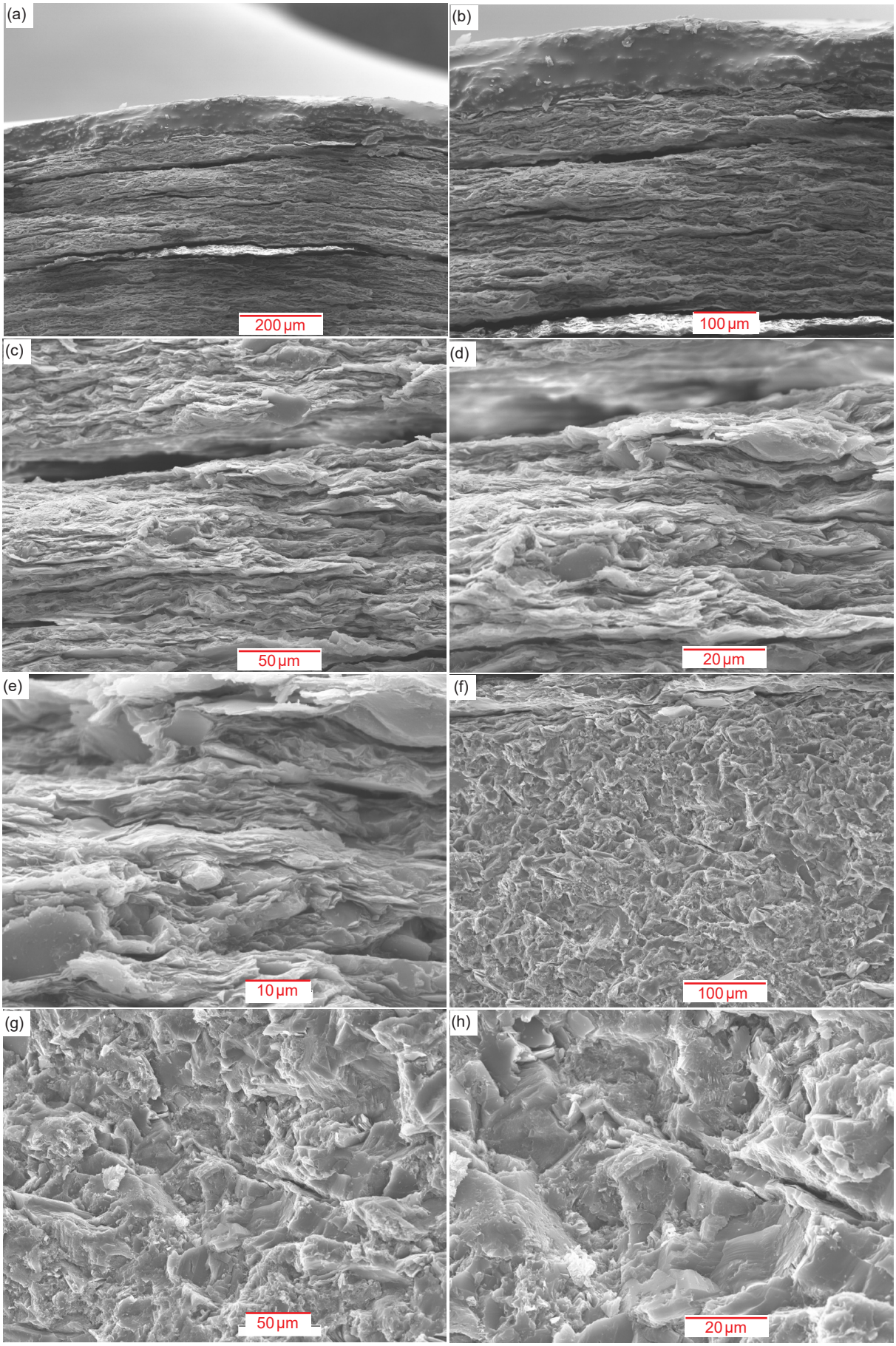
(a)
200 µm
(b)
100 µm
(c)
50 µm
(d)
20 µm
(e)
10 µm
(f)
100 µm
(g)
50 µm
(h)
20 µm

Fig. 40 (page 154). Scanning electron microscope (SEM) images of sample HF-02 from the Whitmore Helipad fold's lower limb zone, close to the lower hinge zone (see fig. 21 for its location). (a) 50X, (b) 100X, (c) 200X, (d) 500X, (e) 2000X, (f) 200X, (g) 500x, and (h) 1000X.

cement surface suggests the detrital grain beneath the quartz cement covering it is K-feldspar, which likely suffered dissolution within the fracture. The illite, which is a very minor component of this sandstone (table 2), is thus a late stage-growth from pore fluids after both cementation and compactional loading.

Sample HF-09 is a siltstone sample from the upper hinge zone of the Whitmore Helipad fold (see fig. 21 for its location), and its SEM images are in fig. 45. Figs. 45b–e are progressively magnified images of the central area of fig. 45a. They all show the broken-apart surface of the rock fabric, that is dominated by the quartz cement which has overgrown the detrital grains. There appear to be no dislocations within the quartz cement or of the rock fabric. However, there is also a lot of "dirtiness" on the broken-apart surface of the quartz cement due to the growth of illite in the many areas across the sample surface of dissolution of the quartz cement. The illite growth is a major component of this siltstone and is presumably due primarily to dissolution of the detrital K-feldspar grains which are mostly covered by the quartz cement, but which is predominant in the sample (table 2). Dissolution and illite growth is very evident in figs. 45c–e. Also prominent in figs.45d and 45e are the fracture pattern in the quartz cement, which looks "step-like". Fig. 45f is a magnification of the central portion of the upper-right quadrant of fig. 45b, and of the upper portion of the upper-right quadrant of fig. 45c. Figs. 45g and 45h are then progressive magnifications of the central area in fig. 45f. Apart from the same observations as in figs. 45a–e, the prominent feature in figs. 45f–h is the muscovite flake which can be seen edge-on right in the center of fig. 45f, and is progressively magnified in figs. 45g and 45h. It is wedged at a steep oblique angle within the quartz cement between detrital grains and its internal sheet structure is evident. Its ends are bent around the detrital grains and its upper end is slightly broken in the area of flexure. Both ends display minor fraying and splitting apart of the flake's internal sheets. The same features are also visible in the thin section of this sample (figs. 31s–v). They are consistent with this muscovite flake being preserved in its detrital condition. In contrast, there is no evidence either of any metamorphism of this flake, or of any shearing between or displacement of the sheets within this flake as seen in cross-section in these SEM images. Such displacement between sheets within the flake and shearing of the flake would be expected in this hinge zone if the bending in the fold had occurred after cementation. This is because the cementation would have "locked" into position the muscovite flake, so that if the folding then occurred the soft muscovite flake would become the weak plane between the much harder quartz-cemented detrital grains and would have sheared and/or the internal sheets would have become displaced by sliding past one another. The flake's bending could be due to compactional loading after deposition while still not cemented, and the folding of the layers would thus have to have been while the sediments were still soft, before the cementation. Also, cementation likely happened after the folding because the quartz cement is still in pristine condition, apart from the subsequent dissolution and illite growth, which can be also seen to the left of the muscovite flake in figs. 45g and 45h.

Overall, the key observation is that the fractures found in these samples, whether from the fold or distant locations, are simply not dissimilar to anything routinely found in unfolded rocks anywhere else, where the cause of the fractures is always due to compactional stresses. What is evident is that regardless of confining pressure, there is really no evidence of post-cementation active displacement of grains or even fractures that might be present. Many times, fractures in rocks elsewhere it is obvious that they are post-cementation. Those are generally linear, cross-cutting features that displace significantly cemented sedimentary laminations, including in shales. Such fractures are not observed in these Bright Angel Formation samples, especially the lengthy linear fractures one would expect, even though they would be expected. Yet here will always be weakened planes in sedimentary rocks.

Discussion

It is clearly crucial to first determine the likely temperature and pressure conditions the Bright Angel Formation was subjected to at the depth to which it was buried after its deposition, and before it was then uplifted with the Kaibab Plateau and simultaneously folded during the Laramide orogeny. Those determined temperature and pressure conditions will automatically rule out any expectation of certain macroscopic and microscopic features in the Bright Angel Formation within the Whitmore Helipad fold due to the deformation. Indeed, the observation of further macroscopic and microscopic features will confirm the deduced temperature and pressure conditions and enable a conclusive case to be made for ductile or brittle deformation, or for soft-sediment deformation, to have been involved in the folding mechanism, and it will also determine the

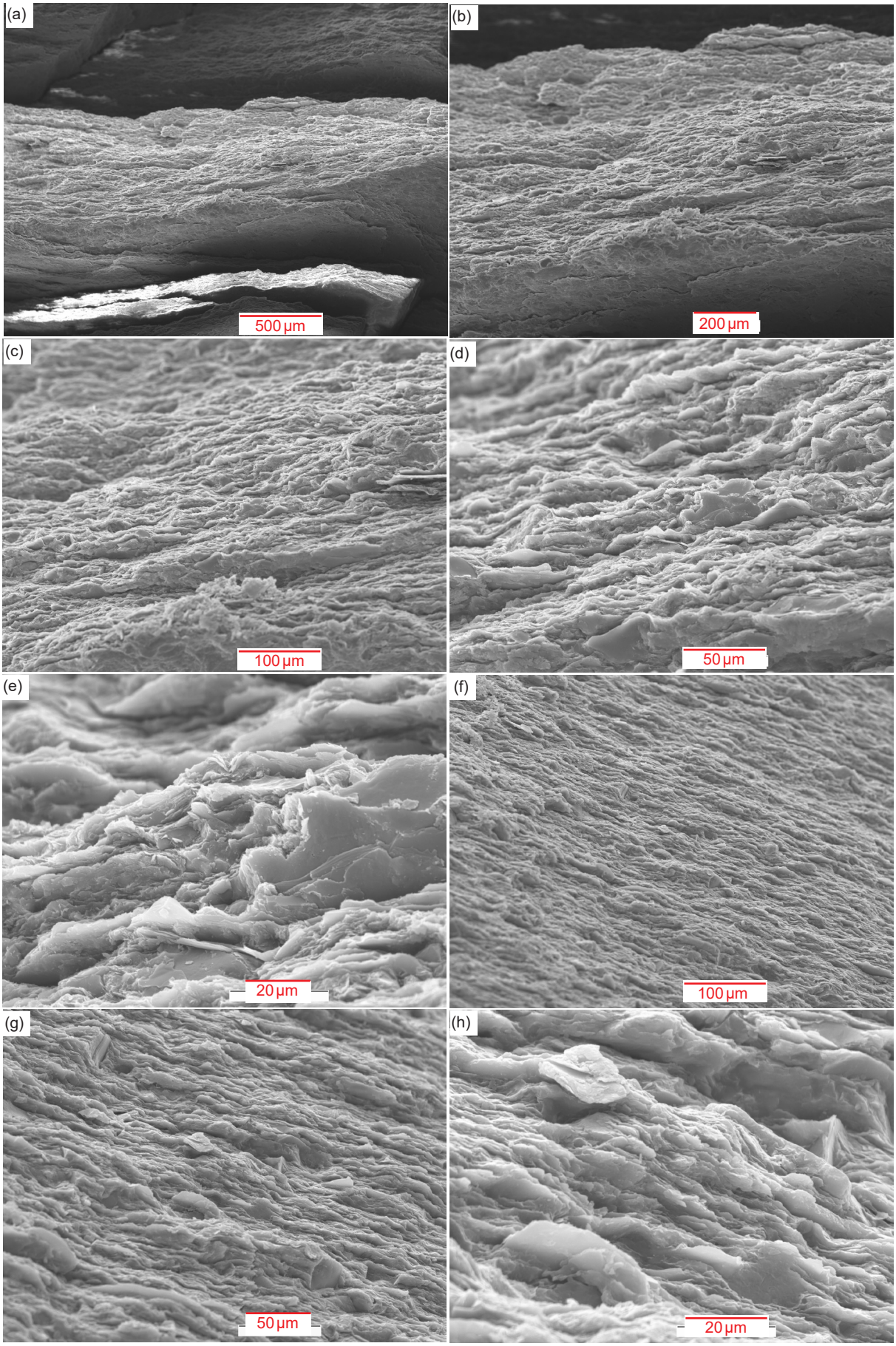
(a)
500 µm
(b)
200 µm
(c)
100 µm
(d)
50 µm
(e)
20 µm
(f)
100 µm
(g)
50 µm
(h)
20 µm

Fig. 41 (page 156). Scanning electron microscope (SEM) images of sample HF-03 from the Whitmore Helipad fold's lower limb zone (see fig. 21 for its location). (a) 50X, (b) 100X, (c) 200X, (d) 500X, (e) 1500X, (f) 200X, (g) 500X, and (h) 1500X.

timing of lithification with respect to the folding.

Temperature and Pressure Conditions at the Burial Depth

There are several methods for estimating the temperatures and pressures to which the Bright Angel Formation was subjected. First, it is easy to calculate the depth of burial because the thickness of the overlying strata has been measured. According to Blakey and Middleton (2012) the Paleozoic stratigraphic section in Grand Canyon comprises >1,000 m of strata, but their scaled stratigraphic column suggests a more detailed estimate of ~1,350 m (~4,430 ft). Then based on the diagrammatic cross-section in Morales (2003), the Grand Staircase of Mesozoic and Cenozoic strata total a thickness of ~1,220 m (~4,000 ft), although Karlstrom, Timmons, and Crossey (2012) suggest a thickness of ~2,000 m (~6,560 ft). Thus, the total conservatively estimated thickness of Phanerozoic strata in the Grand Canyon-Grand Staircase region would be ~3,350 m (~10,990 ft). However, that is a lower estimate than that of Dumitru, Duddy, and Green (1994), who estimated that the Cambrian strata of the Tonto Group, which includes the Bright Angel Formation, would have been, prior to the erosion of the Mesozoic section from off the top of the Grand Canyon's Paleozoic sequence, at a depth of burial of between 4.5 km (~14,750 ft) and 6 km (~19,500 ft). However, that estimate was based on apatite fission-track data. In any case, it is highly doubtful the entire thickness of the Grand Staircase was covering the Grand Canyon region, as it likely thinned dramatically, like the Grand Canyon Paleozoic sequence does to the north and northeast. Therefore, we can conclude that the Bright Angel Formation was possibly buried under ~3,300–4,500 m (~10,825–14,750 ft) of overlying strata which had progressively accumulated during the Phanerozoic.

Since the Tapeats Sandstone, which immediately underlies the Bright Angel Formation, sits unconformably on the Precambrian basement granites and schists in the Upper Granite Gorge of Grand Canyon, those granites and schists would have been buried under a similar thickness of Phanerozoic strata deposited directly on the granites and schists after erosion of the Great Unconformity. It is significant, therefore, that the biotite flakes within the Vishnu and Rama Schists of the Granite Gorge Metamorphic Suite contain very abundant ^{238}U and ^{210}Po radiohalos, while biotite flakes in several of the granite plutons of the Upper Granite Gorge contain somewhat fewer numbers of ^{238}U and ^{210}Po radiohalos (Snelling 2005a) (fig. 46). These radiohalos would have been readily annealed if the temperature at their burial depth under the overlying Phanerozoic strata had reached 150°C (Laney and Laughlin 1981). Thus, we can conclude that the burial temperature beneath the Phanerozoic strata did not reach 150°C, so the Bright Angel Formation was not likely buried as deeply as some claim.

A similar paleotemperature indicator is the presence of fission tracks in numerous minerals in the immediately underlying Tapeats Sandstone and immediately overlying Muav Formation. Snelling (2005b) reported fission tracks in zircon grains from tuff beds within the Tapeats Sandstone and the Muav Formation in the western Grand Canyon (fig. 47), while Snelling (2023a) reported fission tracks found in quartz grains in a sample from the Carbon Canyon fold (fig. 48). Fission tracks in both zircon and quartz have been experimentally determined to be annealed at elevated temperatures above 300°C (Sandhu et al. 1990). Naeser et al. (1989, 2001) and Dumitru, Duddy, and Green (1994) found that the apatite fission-tracks in the Proterozoic rocks below the partial annealing zone (below the base of the Redwall Limestone) yielded ages of 61–66 Ma, and the shortened fission-track lengths suggested that those rocks at the bottom of Grand Canyon cooled to temperatures of 60–65°C during uplift and erosion associated with the Laramide deformation, after the Proterozoic basement rocks had been at a burial temperature of ≥110°C during the late Cretaceous prior to the Laramide event. In contrast, Naeser et al. (1989) found that the fission-track ages of ~1,000 Ma obtained from zircons from Proterozoic basement rocks now exposed at river level indicated that those rocks had been at temperatures of ≤200°C for the last 1,000 million years.

Subsequently, Kelley, Chapin, and Karlstrom (2001) used apatite fission-track ages and track length data collected at river level in eastern Grand Canyon to calculate that the Proterozoic basement rocks had cooled during the Laramide deformation to 55–65°C. They also found, as did Naeser et al. (1989), that the apatite fission-track ages obtained from the Proterozoic rocks along the Colorado River generally increased toward the west, perhaps reflecting the differences in the uplift elevations and depositional thicknesses. Kelley and Karlstrom (2012) reported additional new apatite fission-track ages in eastern Grand Canyon and Marble Canyon. They also found that the apatite fission-track ages are progressively younger toward the east and northeast. For example, in the Supai Group the apatite fission-track ages

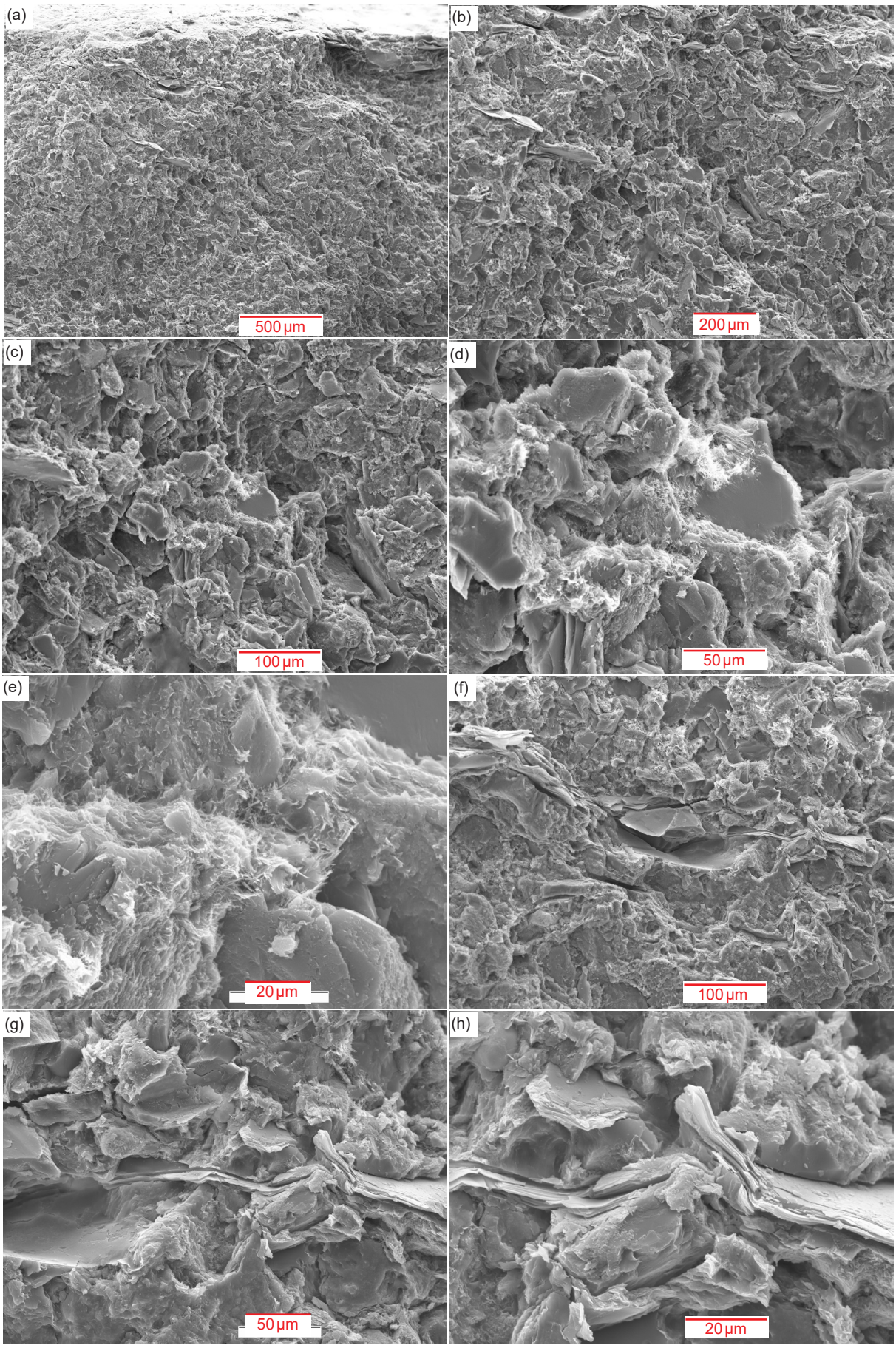
(a)
500 µm
(b)
200 µm
(c)
100 µm
(d)
50 µm
(e)
20 µm
(f)
100 µm
(g)
50 µm
(h)
20 µm

Fig. 42 (page 158). Scanning electron microscope (SEM) images of sample HF-05 from the Whitmore Helipad fold's lower hinge zone (see fig. 21 for its location). (a) 50X, (b) 100X, (c) 200X, (d) 500X, (e) 1500X, (f) 200X, (g) 500X, and (h) 1000X.

decreased from 127±13Ma near Grand Canyon village to 33±6Ma at river mile 12. Additionally, the apparent apatite fission-track cooling ages on the upthrown blocks on the major monoclines in the eastern Grand Canyon were higher at 80–90Ma than the 55–65Ma on the downwarped side of the East Kaibab Monocline. This suggested to them that the Supai Group in the downwarped side of the East Kaibab Monocline to the northeast in Marble Canyon had cooled through 110°C much later than in the East Kaibab uplift and was indicative of the erosional retreat of the Grand Staircase escarpment that exposes ~2km (~6,560ft) of Mesozoic strata which may have been stripped away from the Grand Canyon region.

Flowers et al. (2007) and Flowers, Wernicke, and Farley (2008) used apatite (U-Th)/He thermochronology data to constrain the cooling history of eastern Grand Canyon to <70°C. Eight samples from the Upper Granite Gorge yielded apatite (U-Th)/He dates of 23±3Ma to 55±7Ma, but their modeling suggested complete resetting had occurred during peak temperatures near the end of Cretaceous sedimentation, followed by cooling during the Laramide deformation event. In contrast, samples from Permian and Triassic sedimentary units in Marble Canyon to the northeast of Grand Canyon yielded a broad span of apatite (U-Th)/He dates of 5–104Ma, but they similarly explained the thermal history of those ages based on a large range of accumulated radiation damage due to the wide range of uranium contents of the detrital apatite grains.

Flowers and Farley (2012) added apatite $^{4}He/^{3}He$ thermochronology data to the discussion of the cooling history of Grand Canyon's basement rocks. They found that the $^{4}He/^{3}He$ spectra of single apatite grains from basement rocks in eastern Grand Canyon with differing (U-Th)/He dates, radiation damage and U-Th zonation yield a self-consistent cooling history that substantially validated the He diffusion kinetic model they applied. In their modeling, assuming a 20–25°C/km geothermal gradient, thermal histories were fitted through 110° to 120°C peak temperatures at 80 to 85Ma, as suggested by complete annealing of apatite fission-tracks at this time (Dumitru, Duddy, and Green, 1994), and cooling to the 20° to 25°C surface temperature by present-day. Statistically acceptable paths imposed tight constraints on the ~90° to 30°C thermal history experienced by eastern Grand Canyon, which are consistent with, but more restrictive than, the history inferred from the apatite (U-Th)/He dates alone (Flowers et al. 2009) and apatite fission-track data from the same area.

Finally, Peak et al. (2021) and Thurston et al. (2022) used zircon (U-Th)/He thermochronology data obtained from the Precambrian crystalline basement rocks in eastern Grand Canyon to constrain the thermal history of the unroofing of the Great Unconformity. They found that their data and models were also highly sensitive to late-stage reheating due to burial beneath ~3–4km (~9,840–13,120ft) of Phanerozoic strata prior to ca.60Ma. Their models that best matched observed date-equivalent uranium trends showed maximum burial temperatures of 140–160°C, which are in agreement with the available apatite (U-Th)/He and apatite fission-track data.

In contrast, as the basis for a totally different method to determine burial temperatures, experimental studies of the conversion of smectite to illite have demonstrated its potential use as a geothermometer (Essene and Peacor 1995; Huang, Longo, and Pevear 1993), which has been confirmed by field studies (Hillier et al. 1995; Pollastro 1993; Pytte and Reynolds 1989; Renac and Meunier 1995; Smart and Clayton 1985; Velde and Espitalié 1989; Velde and Lanson 1993). Similarly, many studies have demonstrated the value of using illite crystallinity as an indicator to distinguish between diagenesis, very low-grade metamorphism, and low-grade metamorphism (Barrenechea, Rodas, and Mas 1995; Blenkinsop 1988; Frey and Robinson 1999; Kisch 1983, 1987; Kubler 1964, 1967, 1968; Kubler and Goy-Eggenberger 2001).

However, the smectite/illite ratio relationship to temperature appears to be neither simple nor unequivocal, because of various factors such as the ion content and concentrations in interstitial waters and the geothermal gradient, not just at the present time but also during the history of the sediment pile. Nevertheless, Hower (1981) found clear relationships between depth, temperature, and the percent illite in illite interstratified with smectite in the sediments intersected by oil wells in the coast region of the Gulf of Mexico (fig. 49) (Pollastro 1993), one of which is directly comparable to the sedimentary sequence in the Grand Canyon-Colorado Plateau region. There Dumitru, Duddy, and Green (1994) estimated that the Cambrian strata of the Tonto Group, which includes the Bright Angel Formation, would have been, prior to the erosion of the Mesozoic section from the top of the Grand Canyon sequence, at a depth of burial of between 4.5km (~14,500ft) and 6km (~19,500ft), with their apatite fission-track data suggesting temperatures of between 110°

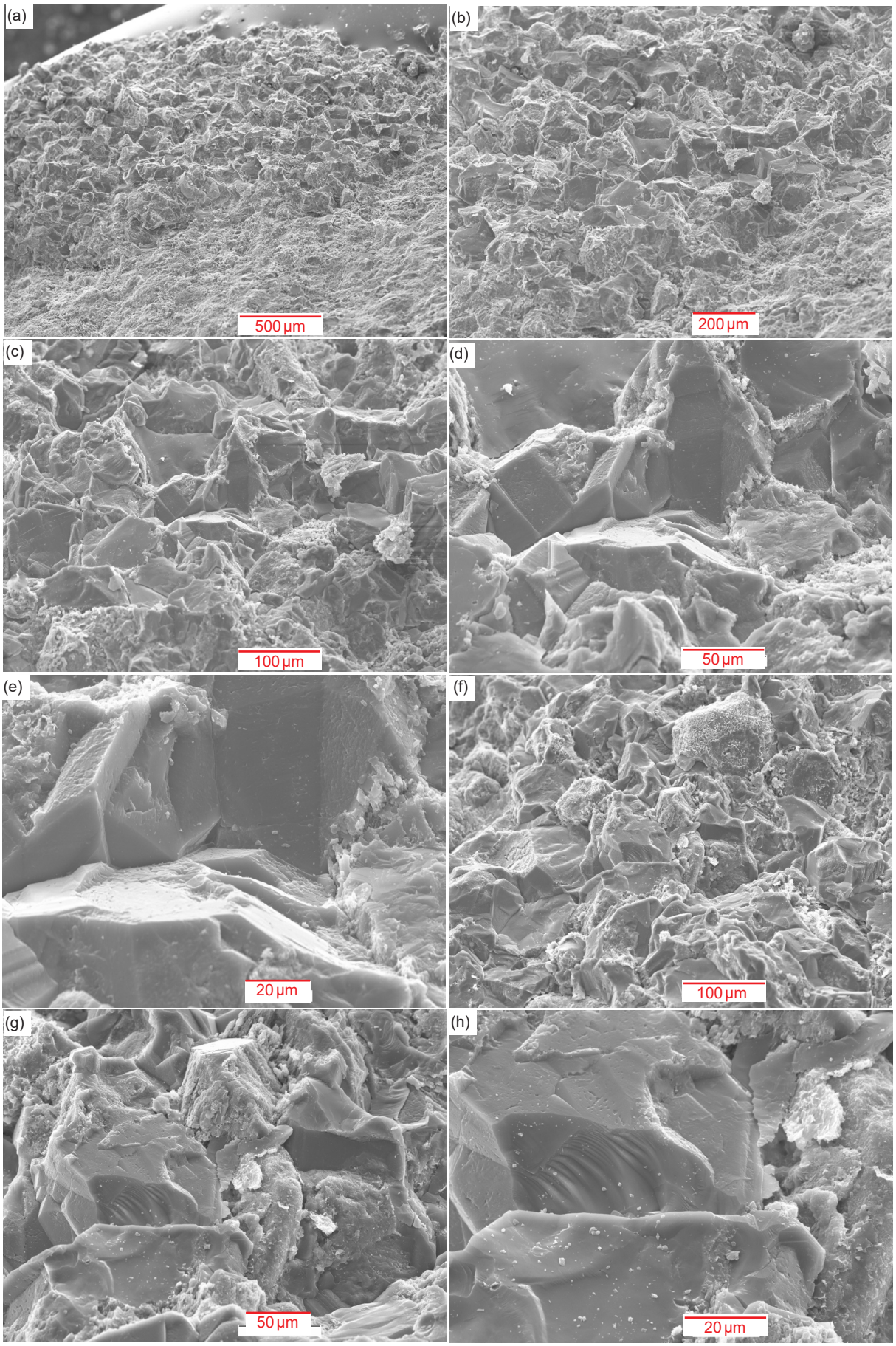
(a)
500 µm
(b)
200 µm
(c)
100 µm
(d)
50 µm
(e)
20 µm
(f)
100 µm
(g)
50 µm
(h)
20 µm

Fig. 43 (page 160). Scanning electron microscope (SEM) images of sample HF-06 from the Whitmore Helipad fold's middle limb zone (see fig. 21 for its location). (a) 50X, (b) 100X, (c) 200X, (d) 500X, (e) 1000X, (f) 200X, (g) 500X, and (h) 1000X.

and 130°C, as determined by subsequent studies discussed above. In fig. 49 the percent illite in the illite interstratified with smectite in two samples from thin tuff beds within the Muav Formation and Tapeats Sandstone (Tonto Group) in Grand Canyon, as reported by Snelling (2005b, 265, table 3), were plotted on the geothermal curve obtained for oil well (B), and projected onto the depth and temperature axes. This suggests that with that same geothermal gradient, where these tuff beds would have been, prior to the erosion of the Mesozoic strata above, at depths of 4,800–5,600 m (~15,700–18,400 ft) and subjected to temperatures of between 110° and 130°C. These values are consistent with the estimates by Dumitru, Duddy, and Green (1994) and subsequent studies discussed above.

Dumitru, Duddy, and Green (1994) based their estimation on a pre-Cretaceous geothermal gradient of 20–30°C/km, and the geothermal gradient in oil well (B) that penetrates Miocene strata (fig. 49) is of the order of 20°C/km. Such a geothermal gradient is not unreasonable in the time frame of the Genesis Flood cataclysm, given the catastrophic deposition of the thick Paleozoic and Mesozoic strata sequence (Austin 1994) and the elevated temperatures of the waters depositing those sediments (Austin et al. 1994). Thus, the estimates of depth and temperature based on the percent illite in the illite interstratified with smectite for these two tuff samples, though very approximate due to the likely large errors in the XRD determinations, are not unreasonable. Therefore, because of the consistency of these estimates with the apatite fission-track data of Naeser et al. (1989), Dumitru, Duddy, and Green (1994) and the subsequent studies discussed above, it seems reasonable to conclude that these two tuff units have since their burial only been subjected to maximum temperatures of 110–130°C, well below the 200±40°C temperature for total annealing of fission tracks in zircon (Harrison et al. 1979; Hurford 1985; Zeitler 1985) and the 150°C temperature for the total annealing of radiohalos (Laney and Laughlin 1981).

The significance of the Kubler Index values for illite crystallinity calculated from the XRD clay mineral analyses of the two samples from the two tuff units (Snelling 2005b, 265, table 3) are harder to interpret from the available literature, which primarily focuses on low-grade metamorphism of sedimentary strata sequences. Estimating the temperatures to which these two tuff units were subjected based on these approximate Kubler Index values depends on the value of the Kubler Index used to define the boundary between diagenesis and the lowest grade metamorphism, which is otherwise defined by mineralogical changes in the clay minerals (Kisch 1987; Kubler 1967). As indicated by Blenkinsop (1988), early studies using the Kubler Index for illite crystallinity all adopted different values of the index to define this crucial boundary, so standardization was warranted. Using the standardized definition of Kisch (1991) and Brime (1999) with a Kubler Index of 0.42 for the boundary between diagenesis and the lowest grade metamorphism, as successfully applied by Brime, Talent, and Mawson (2003), the estimated Kubler Index values for the Muav and Tapeats tuffs (Snelling 2005b, 265, table 3) indicate that they are on the lower temperature side of this boundary, so they only suffered diagenesis. Temperature estimates for that boundary place it at 150±50°C (Bucher and Frey 2002; Frey and Kisch 1987; Robinson and Merriman 1999). Thus, the Kubler Index values for these two tuff units are consistent with the estimate of 110–130°C for the temperatures to which these tuff units, and their host Tapeats Sandstone and Muav Formation, have been subjected from both the apatite fission-track data of Naeser et al. (1989), Dumitru, Duddy, and Green (1994) and the subsequent studies discussed above, and their smectite/illite ratios.

In conclusion, the consensus from all estimation methods is that the Bright Angel Formation (which is sandwiched between the Tapeats Sandstone and Muav Formation), prior to the Laramide deformation responsible for the Whitmore Helipad fold, would have been subjected to a burial temperature of 110–130°C. Then, during the Kaibab uplift, erosion caused the temperatures within the Bright Angel Formation to decrease to <70°C. However, estimates of the burial depth vary, but based on measured strata thickness it was concluded above that the Bright Angel Formation was possibly buried under ~3,300–4,500 m (~10,825–14,750 ft) of overlying strata which had progressively accumulated during the Phanerozoic. However, this is probably an overestimate of the thickness as the Phanerozoic strata which likely thinned to the south as previously discussed, and these strata (such as the Tapeats Sandstone and the Redwall Limestone) even vary in thickness within the walls of Grand Canyon. Thus, using a general overburden pressure gradient (Khan and Islam 2008), at those depths the overburden (confining) pressure on the Bright Angel Formation would have been ~0.3–0.4 kbar (~4,300–5,900 psi). According to Bucher and Frey (2002, 5, fig. 1.1) these pressure-temperature conditions are well within the pressure-temperature field of sedimentary diagenesis. Thus, it is consistent that the mineralogy

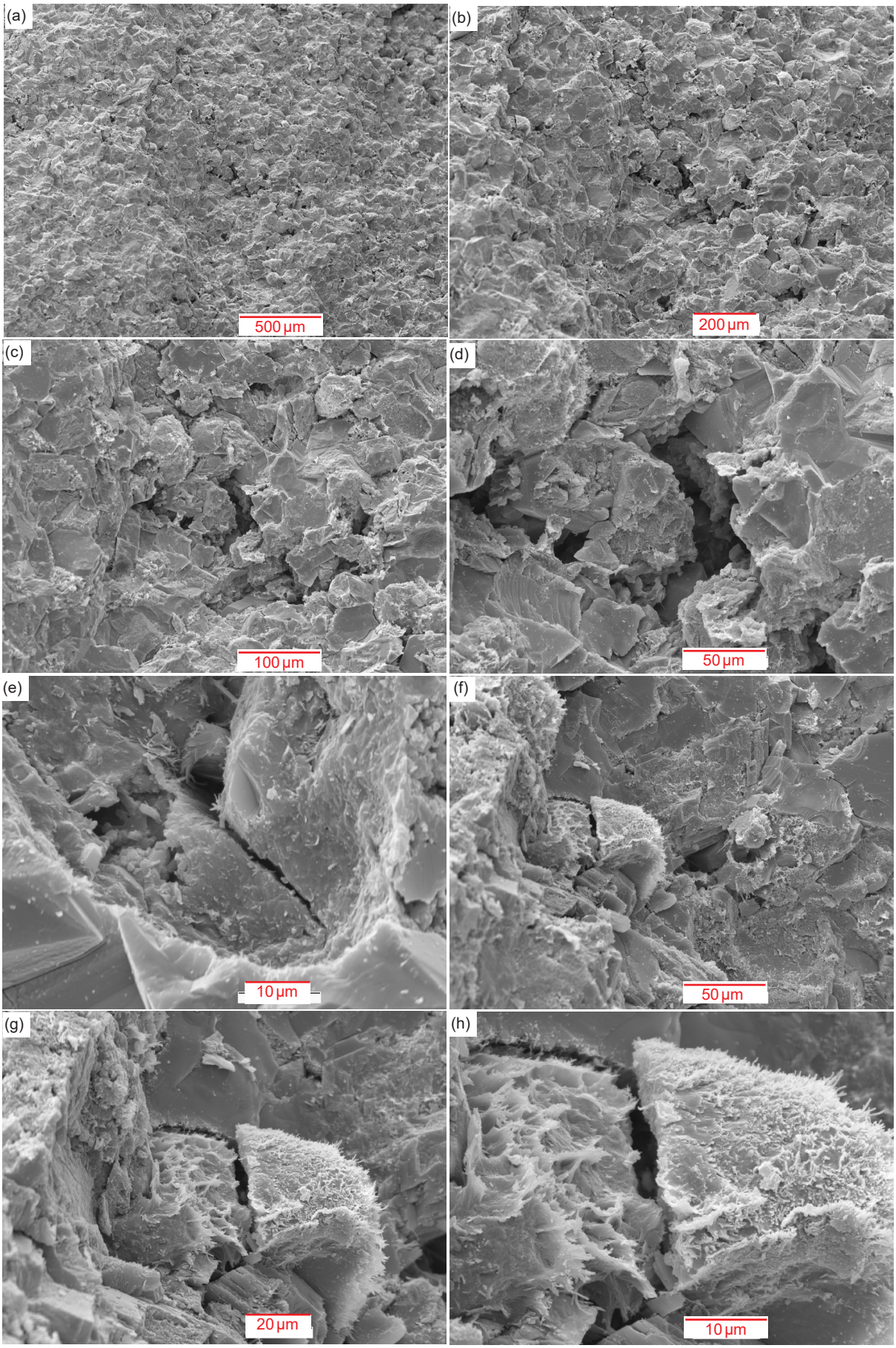
(a)
500 µm
(b)
200 µm
(c)
100 µm
(d)
50 µm
(e)
10 µm
(f)
50 µm
(g)
20 µm
(h)
10 µm

Fig. 44 (page 162). Scanning electron microscope (SEM) images of sample HF-08 from the Whitmore Helipad fold's lower hinge zone (see fig. 21 for its location). (a) 50X, (b) 100X, (c) 200X, (d) 500X, (e) 2500X, (f) 500X, (g) 1000X, and (h) 2000X.

and textures (macroscopic or microscopic) of the sandstones, siltstones, and shales within the Bright Angel Formation do not indicate any signs of any metamorphic changes to the detrital grains (Snelling 2021b), as confirmed by the petrographic and SEM observations reported in this study.

The Macroscopic Features

The next question to answer is whether the macroscopic features in the outcropping Bright Angel Formation within the Whitmore Helipad fold are consistent with ductile or brittle deformation of the sandstone, siltstone, and shale beds several hundred million years after their lithification, or with soft-sediment deformation of those beds very soon after their deposition and before lithification. As already noted, though, the Bright Angel Formation was most likely not buried deep enough to experience ductile deformation as it is well above the brittle-ductile transition zone, which occurs at a depth of 15–20 km (~49,000–65,600 ft) at temperatures of 250–400°C (Condie 2005; Zhamaletdinov 2019). On the other hand, under some near surface conditions, rock layers may remain coherent because the grains and/or beds within them can facilitate folding due to brittle deformation. Thus, most near surface rock layers undergo brittle fracturing and faulting, leaving the rock's grains fractured. Some coherent beds may slide past one another as the rock layers are folded via bedding plane slip or flexural slip, which should leave telltale features in outcrop, such as slickensides on the lithified bedding plane surfaces.

So, what do we observe in the Bright Angel Formation beds bent in the Whitmore Helipad fold (fig. 50)?

The distant view in fig. 50a shows the context of the fold (center) within the gently-dipping (to the left or ~east) thin layers of the Bright Angel Formation. In general, the buff-colored beds are sandstone, while the thin green and reddish-brown beds are siltstone and shale. The hinge zones and distances are open without shattering of the rock fabric, best seen in the nose of the lower hinge zone (fig. 50b). Also, it does not appear that there has been any thickening or thinning of the beds in either the limbs or the hinge zones, except for the bulging in the upper part of the lower hinge zone (fig. 50a–d). This monoclinal fold would be best classified according to Ramsay (1967) as a Class 1B parallel-concentric fold (fig. 14), and corresponds to a Donath and Parker (1964) flexural-slip fold (fig. 13). These features are contrary to what might be expected according to the claims of Huntoon (2003) and Hill and Moshier (2009) regarding the very similar Carbon Canyon fold (Snelling 2023a). Indeed, the thicknesses of the individual thin sandstone, siltstone, and shale beds are very consistent along their lengths when traced from one limb through the hinge zones and out into the opposite limb (fig. 50a, b), contrary to the claims by Hill and Moshier (2009) and Tapp and Wolgemuth (2016) that the bedding thickness changes along the similar Carbon Canyon fold (figs. 6 and 11). Certainly, the sandstone, siltstone, and shale beds have been pushed up by the upthrown block on the left (~eastern) side of the fold as they were upturned through the ~80° monoclinal fold hinges (figs. 10, 50a–c). There is a branch fault of the Hurricane Fault which underlies the Whitmore Helipad fold (fig. 8). The vertical movement along that branch fault would have produced the Whitmore Helipad fold. Furthermore, there is no change in the direction of the fold hinges between the two sets of sandstone beds on either side of the monoclinal flexure (figs. 10 and 50b). This is not the same as the claim of Tapp and Wolgemuth (2016) for the Carbon Canyon fold (fig. 11) in which their annotated red arrows exaggerate the trivial change of direction. And contrary to the claim about the Carbon Canyon fold by Tapp and Wolgemuth (2016) that hinge zones have been filled with weathered material or weaker deformed rock (figs. 11 and 12), there is no evidence whatsoever of that in the monoclinal hinge zones of the Whitmore Helipad fold. This further indicates that any bedding plane or flexural slippage was minimal between the sandstone, siltstone, and shale beds in the Whitmore Helipad fold.

There are no clusters of fractures in the two monoclinal hinge zones of the Whitmore Helipad fold, as would be expected if lithified rock had suffered from brittle deformation (fig. 50b, c). Fossen (2016, 157) has an illustration of fractures or joints that would have opened in a cluster around the stretched edge of the hinge zone of a folded bed as a result of strain during folding, yet such clusters are absent from the sandstone, siltstone, and shale beds in the hinge zones of the Whitmore Helipad fold (fig. 50b, c). However, two parallel fault planes can be seen obliquely cross-cutting the fold through the upper hinge zone and just above the nose of the lower hinge zone, but only trivial and minimal displacement has occurred, respectively (fig. 50b, c). Furthermore, along the extended downstream (~western) limb zone the interlayered thin sandstone, siltstone, and shale beds have been displaced only by ~1 m (~3 ft) along a very shallow-angled fault plane that is not parallel to the fault planes cross-cutting the two hinge zones (fig. 50d). The beds on the upthrust side of this fault

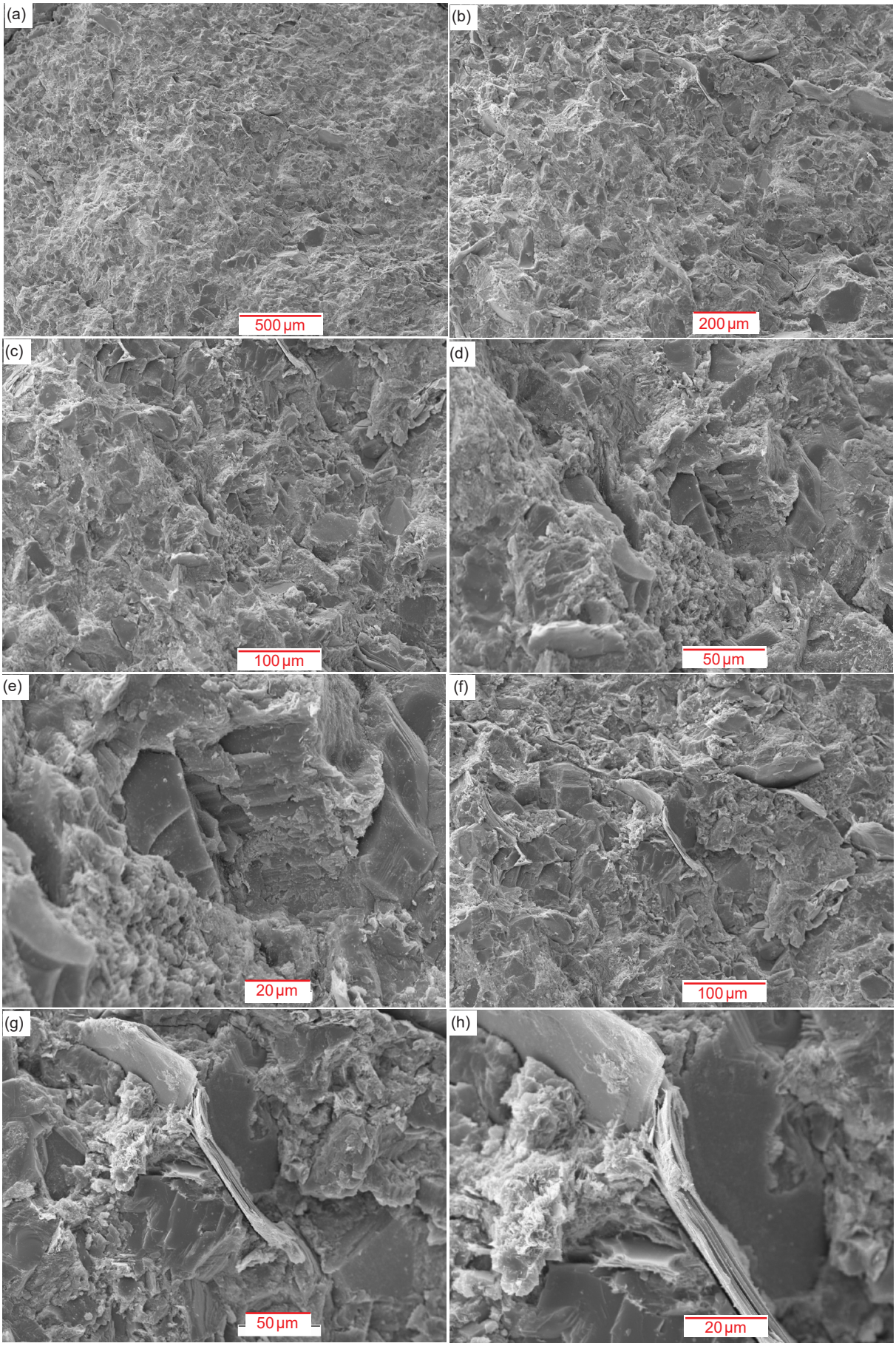
(a)
500 µm
(b)
200 µm
(c)
100 µm
(d)
50 µm
(e)
20 µm
(f)
100 µm
(g)
50 µm
(h)
20 µm

Fig. 45 (page 164). Scanning electron microscope (SEM) images of sample HF-09 from the Whitmore Helipad fold's upper hinge zone (see fig. 21 for its location). (a) 50X, (b) 100X, (c) 200X, (d) 500X, (e) 1000X, (f) 200X, (g) 500X, and (h) 1000X.

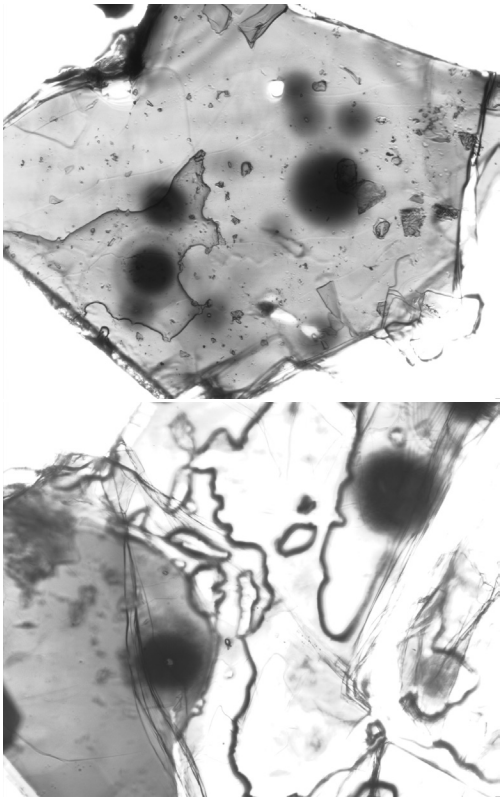

Fig. 46. ^{238}U and ^{210}Po radiohalos in biotite flakes from two samples of the Vishnu Schist of the Granite Gorge Metamorphic Suite in Grand Canyon. The larger diameter of the multi-ringed ^{238}U radiohalos is ~70 µm, and that of the smaller single-ringed ^{210}Po radiohalos is ~39 µm. (a) Sample VS-3. (b) Sample VS-6.

have also been slightly bent or flexed near the fault plane. This is not entirely what would be expected from brittle deformation if the sandstone, siltstone, and shale beds had already lithified, as they would have been abruptly displaced as they ruptured, rather than bent. On the other hand, this observation is exactly what would be expected during soft-sediment deformation as the unlithified sandstone, siltstone, and shale beds would have been pliable and thus "flow" or flexure smoothly into the faults as displacement occurred.

Fig. 50e provides a very close view of the lower part of the lower hinge zone in the vicinity of sample HF-4 (see fig. 21 for its location). The crumpled alternating thin sandstone (buff) and siltstone and shale (green) laminae are truncated in the cross-cutting fault plane. The same fault plane can also be seen in fig. 50f, which is a closer view of the upper portion of the lower hinge zone, the thicker buff sandstone bed to the right of the scale marker being the location of sample HF-08 (see fig. 21). The displacement along this obliquely cross-cutting fault plane is evident, as is the bulging of the upper interlayered buff sandstone and reddish-brown siltstone laminae in the hinge zone, visible also in fig. 50b. Such crumpling and bulging of these interlayered beds in the lower hinge zone is strongly indicative of flow of these lithologies while plastic. The differences in competency between the more brittle lithified hard sandstone beds and the comparatively less brittle lithified shale beds, due to the latter's constituents being of finer grain size and including softer illite (clay), has resulted in some pinching and boudinaging of the sandstone beds in part of the crumpling seen in fig. 50e (to the left of the scale marker). In contrast, if this crumpling was due to ductile deformation, then in fig. 50f there should be evidence of differential bulging of these interlayered beds due to these differences in competency. Instead, they have flowed identically in the bulging. So, overall, this plastic flow in these interlayered different lithologies evident in this lower hinge zone is strong evidence for soft-sediment deformation, the folding and faulting having occurred while these sediments were still water-saturated and not lithified. Such features have been replicated in simulated soft-sediment deformation experiments (discussed below).

Otherwise, there are no obvious fractures in the interlayered sandstone, siltstone, and shale beds in the Whitmore Helipad fold (fig. 50a–d), unlike the many fractures in the Carbon Canyon fold as on the annotated overlay provided by Tapp and Wolgemuth (2016) (fig. 11). This is not what would be expected from ductile deformation. Instead, there should be fractures in the hinge zones that should be open where the sandstone beds in particular were stretched on the outer curves of the folded beds and compressed tightly shut on the inside curves, such as in the curved buff sandstone layers above the reddish-brown interlayered beds of the lower hinge zone, to the left of the bulging layers area in fig. 50b. So, rather than fractures due to ductile deformation as Tapp and Wolgemuth (2016) imply, there are hairline-thick joints likely produced by contraction of the rock fabric during dewatering and lithification, and then especially during unloading of the confining overburden pressure as the overlying strata were eroded away during erosion of Grand Canyon and its side canyons. Joints are fractures or cracks with minute openings, with little to no displacement along their sharp walls (Fossen 2016; Schultz 2019). Indeed, one of the principal causes of the development of joints is the release of the vertical stress and thus the horizontal stress as well (to a lesser extent) during exhumation of the overburden (Fossen 2016), and in

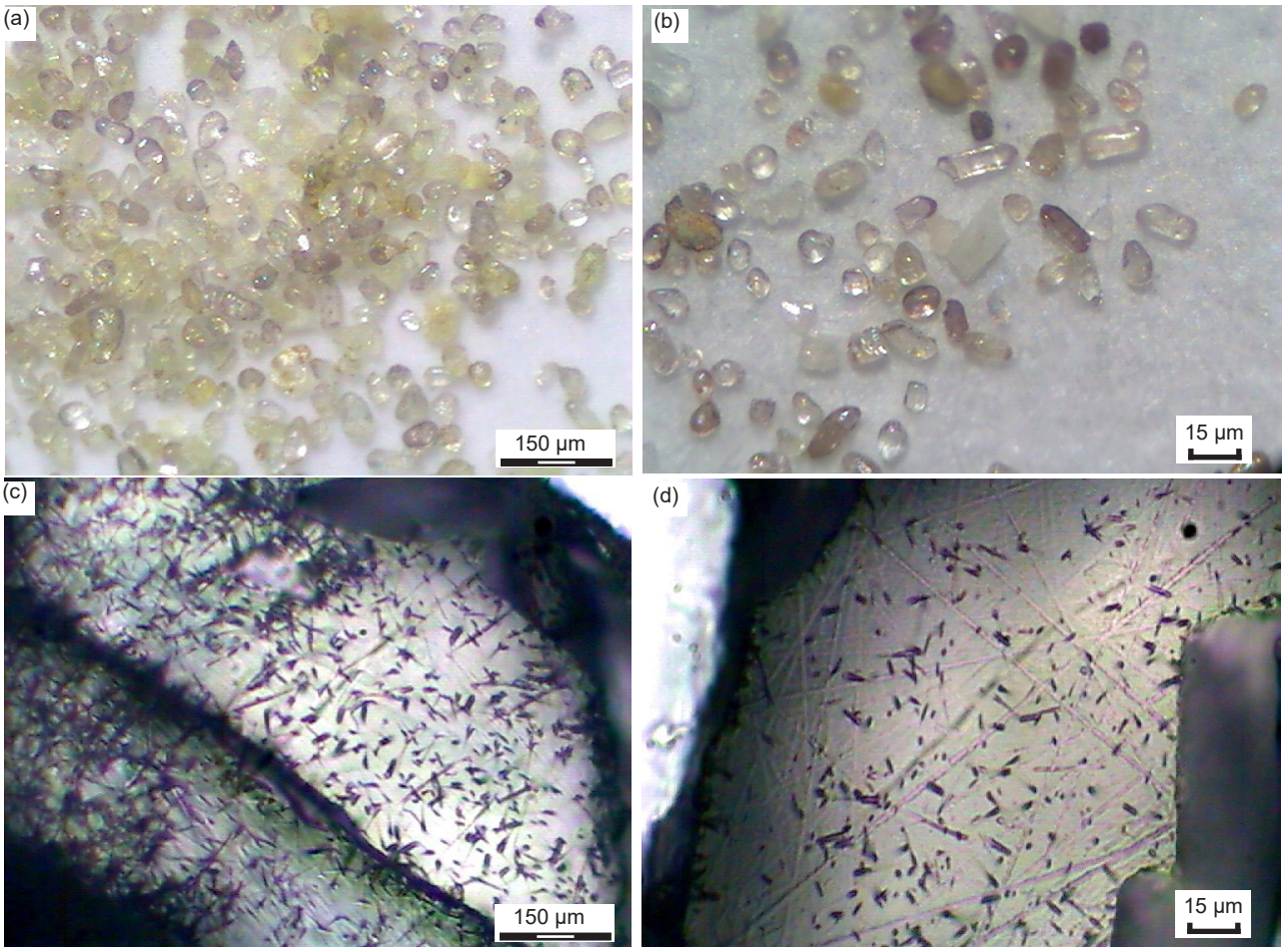

Fig. 47. Zircon grains as seen under a binocular microscope extracted from samples of the thin green tuff beds (a) in the upper Tapeats Sandstone at river mile 205.7 (sample TT-1), and (b) in the Muav Formation at river mile 180 (sample MT-3) (from Snelling 2005b, 234, fig. 9). The spontaneous fission tracks in the polished and etched surface of one mounted zircon grain under high magnification from each tuff bed (c) Tapeats sample TT-1, and (d) Muav sample MT-2 (from Snelling 2005b, 236, fig. 10).

this case, the erosion of Grand Canyon through the fold. And for the most part, joints come in populations defined by local stress fields, and are often regularly spaced according to the strength of the rock fabric (Groshong 1988; Fossen 2016; Schultz 2019), as can be seen in the annotated overlay of the Carbon Canyon fold provided by Tapp and Wolgemuth (2016) (fig. 11). Furthermore, joint spacing also depends

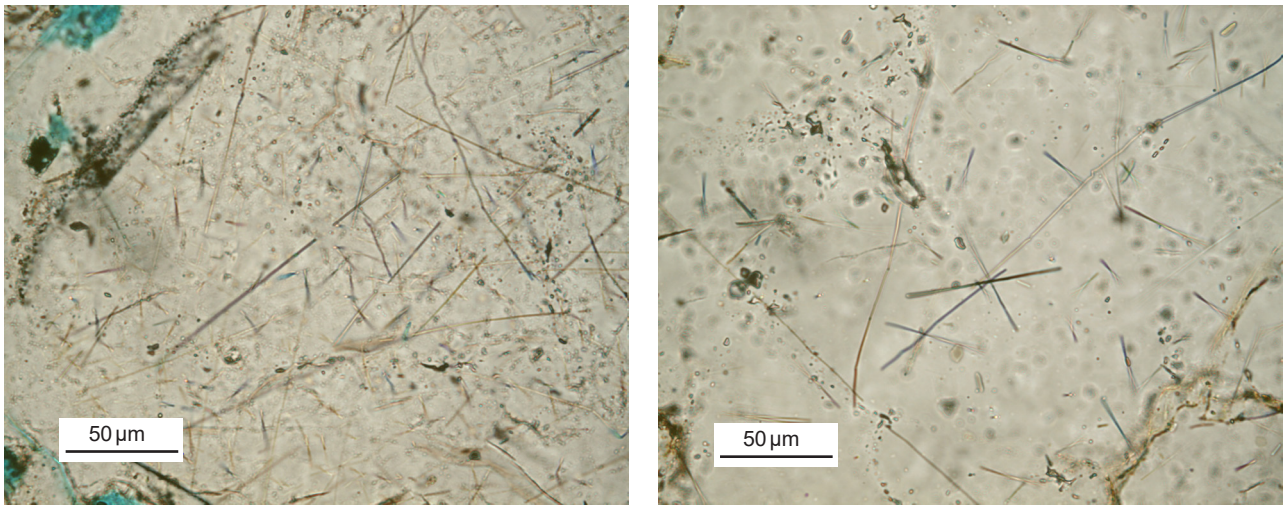

Fig. 48. Fission tracks in quartz grains within sample CCF-11 from one bed within the Carbon Canyon fold, from the limb close to the hinge zone (Snelling 2023a).

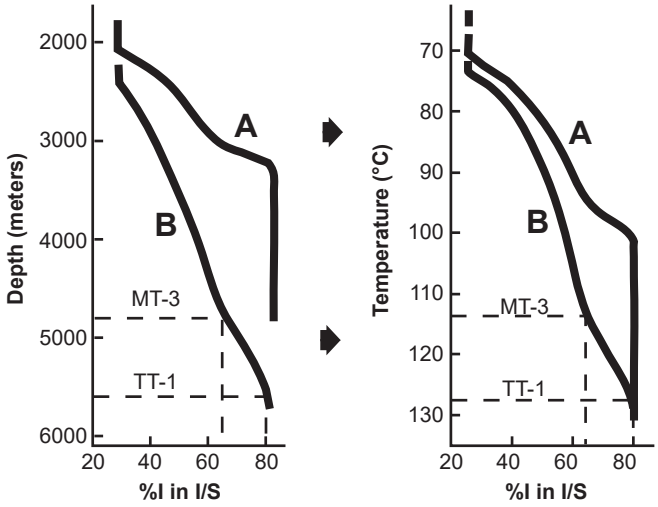

Fig. 49. Proportion of illite (I) layers in mixed-layer illite/smectite (I/S) versus depth (left) and temperature (right) for samples from (A) an oil well in Oligocene strata, and (B) an oil well in Miocene strata, in the Gulf of Mexico region (modified from Hower 1981). The %I in I/S data for the Muav tuff MT-3 and Tapeats tuff TT-1 samples are plotted on curve B and the interpreted depths and temperatures are projected from that curve (from Snelling 2005b).

on layer thickness, such that field observations and experimental work has demonstrated the very simple relationship that the joint spacing is more or less equal to the layer thickness, independent of scale (Fossen 2016; Narr and Suppe 1991; Silliphant, Engelder, and Gross 2002). This relationship is also somewhat evident in the Tapeats Sandstone beds bent in the Carbon Canyon fold (figs. 6 and 11), but difficult to see in the Whitmore Helipad fold (fig. 50). There is one other relevant field observation. If bedding plane slip or flexural slip has occurred, then the bedding planes between the sandstone, siltstone, and shale beds in the fold should have acted like fault plane surfaces and thus slickensides might be found on them. However, from field observations of the outcrop of the interlayered thin sandstone, siltstone, and shale beds in the Whitmore Helipad fold, no potential slickensides were found on any of the exposed bedding plane surfaces examined, which is consistent with the lack of other evidence of any bedding plane or flexural slip having occurred to accommodate their folding. Indeed, fig. 50g is a closer view of the overhanging underside of the buff sandstone beds above to the right of the intervening (middle) limb zone near the upper hinge zone, to the right of sample HF-10 (see fig. 21 for its location). On its horizontal bedding plane surface are well-preserved fossilized trails, probably of *Teichichnus* (annelids), with no hint of any slickensides. Both these preserved, undisturbed trace fossils and the lack of slickensides indicate no bedding plane slippage has occurred during folding. Thus, the major argument used by Tapp and Wolgemuth (2016) to insist this folding during the Laramide orogeny was due to ductile deformation has no macroscopic field evidence to support it.

So, do any of these field observations preclude the Whitmore Helipad fold being due to soft-sediment deformation before lithification of the Bright Angel Formation, rather than due to ductile and/or brittle deformation after its lithification? The short answer is definitely not, as demonstrated by experiments replicating soft-sediment deformation. Nabavi and Fossen (2021) have reviewed the history of such experiments, primarily undertaken in squeeze boxes with layers of dampened sand and/or clay, glass sides to the box and a crank handle for moving one end inwards towards the other fixed end so that the compressional folding of the dampened sediment layers can be simulated. Some excellent relevant examples are the simulation experiments of Rettger (1935), Handin et al. (1976), Friedman et al. (1976), Weinberg (1979), and Friedman, Hugman and Handin (1980). These and other experiments involved confining pressures, and yet the dampened sand and/or clay layers when compressionally folded would appear to have faithfully simulated soft-sediment deformation to produce folds similar and identical to those observed and classified as folding due to soft-sediment deformation in exposed outcrops of now lithified sedimentary layers elsewhere (for example, Waldron and Gagnon 2011, and Alsop et al. 2019). Even the folding of these interlayered sandstone, siltstone, and shale beds of the Bright Angel Formation have been simulated in these soft-sediment deformation experiments (fig. 9), along with accompanying minor faulting, fractures, and joints, identical to those observed in the Whitmore Helipad fold.

Waldron and Gagnon (2011) defined soft-sediment deformation, following Maltman (1984), as any deformation, other than vertical compaction, of a

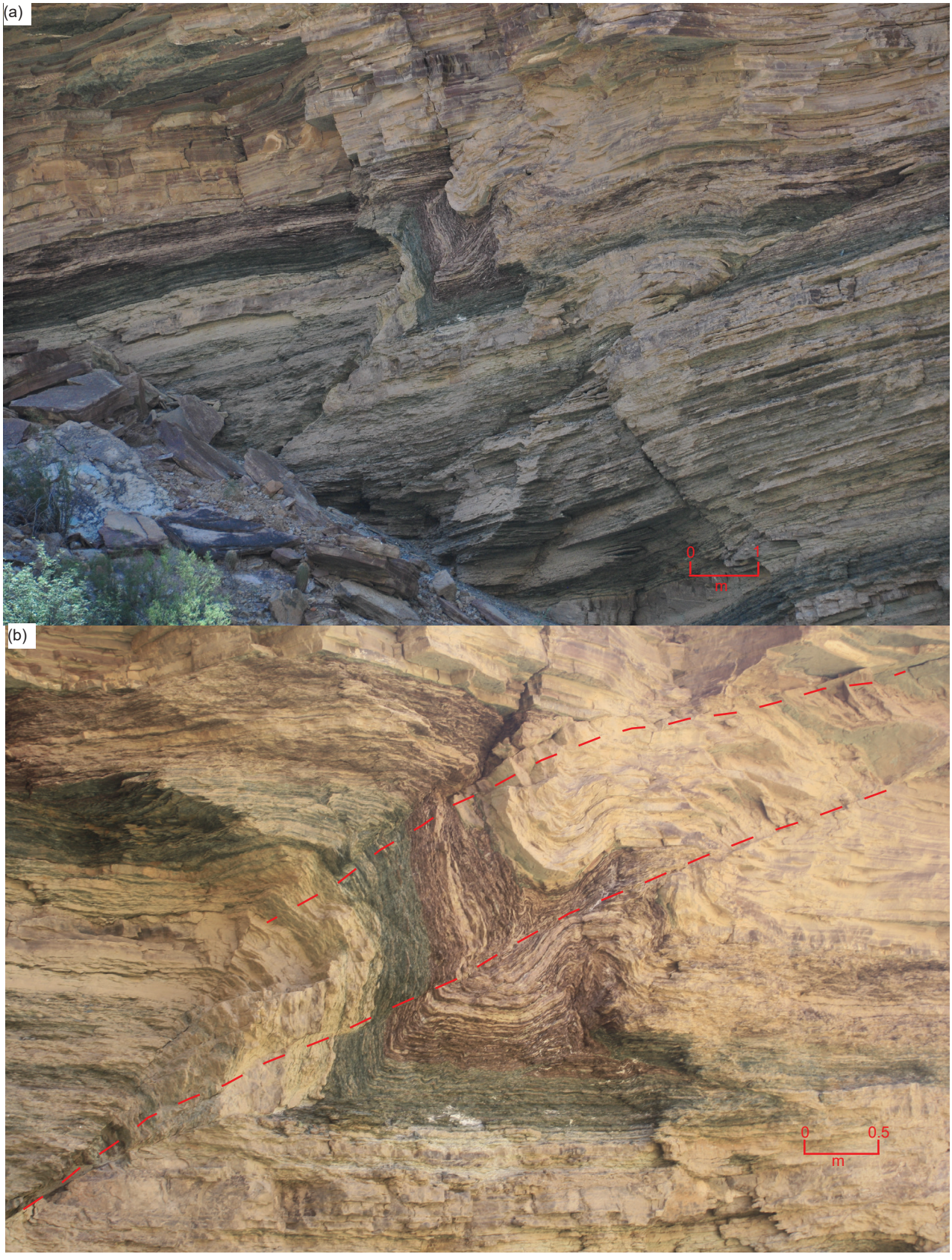
(a)
0
1
m
(b)
0
0.5
m

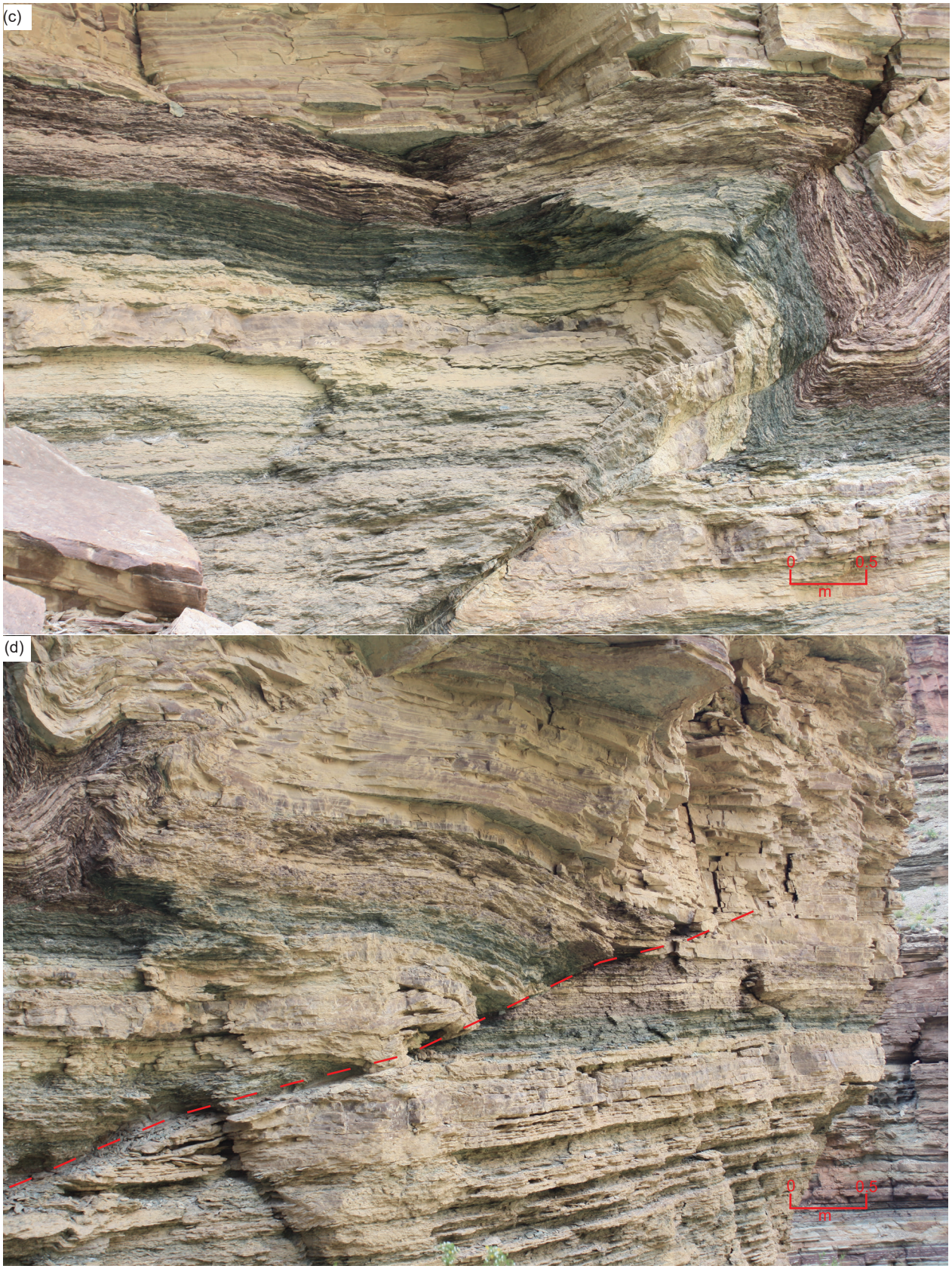
(c)
0
0.5
m
(d)
0
0.5
m

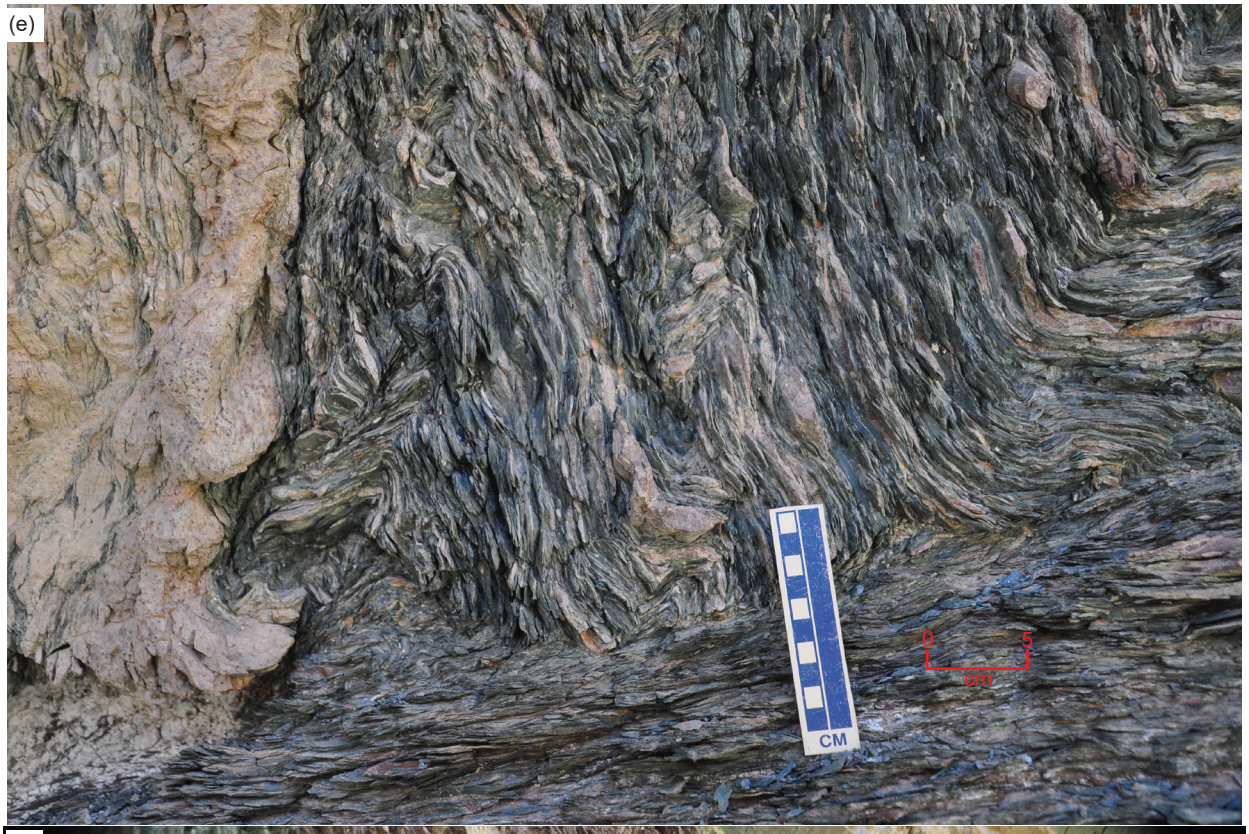
(e)
CM
0
5
cm


(f)
0
10
cm

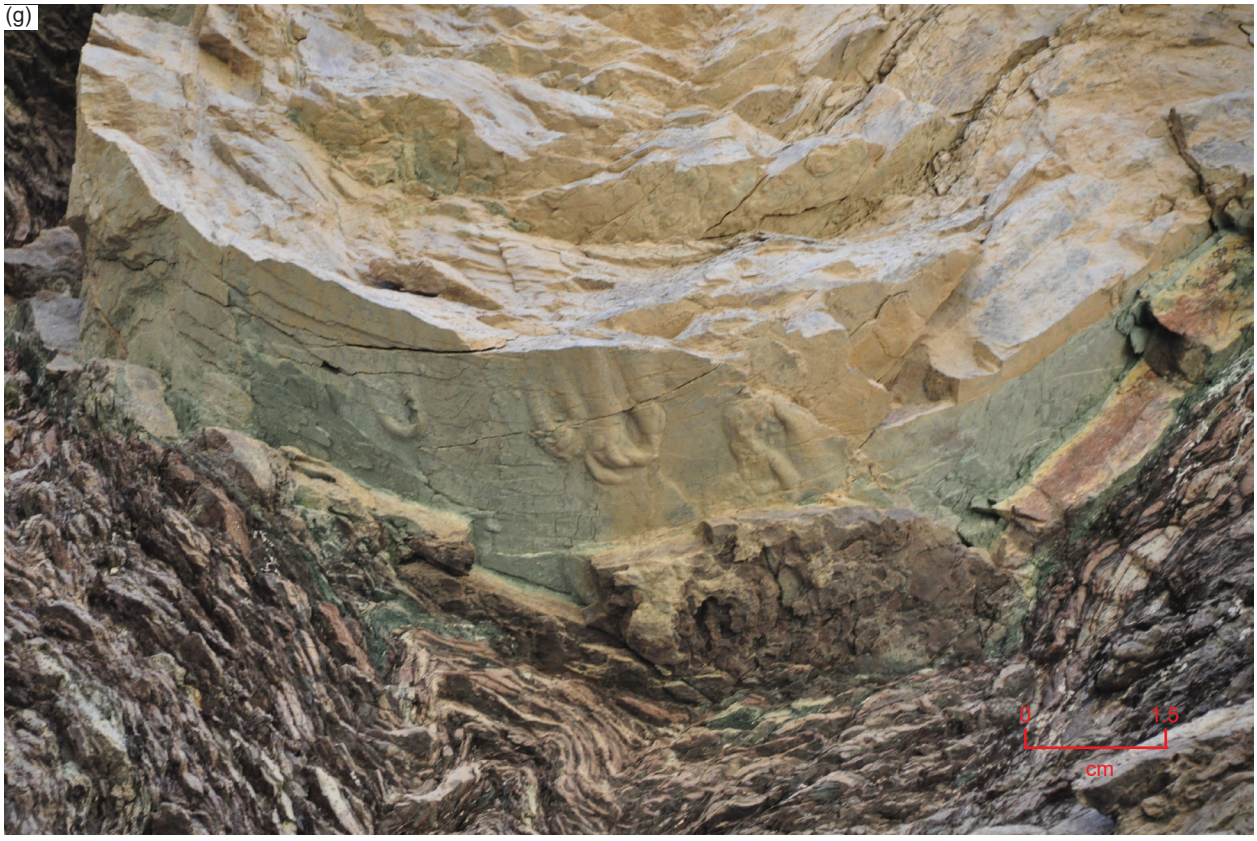

Fig. 50 (pages 168–171). The Whitmore Helipad fold, at river mile 187.4, river left, in the cliff face showing its macroscopic features, with scales as indicated. (a) A distant view of the context of the fold (center) within the gently-dipping (to the left or ~east) thin layers of the Bright Angel Formation. In general, the buff-colored beds are sandstone, while the thin green and reddish-brown beds are siltstone and shale. (b) A closer view of the fold, which has two hinge zones, and intervening and flanking limb zones. Two sub-parallel fault planes as marked can be seen obliquely cross-cutting the fold through the upper hinge zone and just above the nose of the lower hinge zone, but only trivial and minimal displacement has occurred, respectively. (c) A closer view of the extended upstream (~eastern) limb zone showing the interlayered thin sandstone, siltstone, and shale beds that have not thinned in the upper hinge zone. (d) A closer view of the extended downstream (~western) limb zone showing that the interlayered thin sandstone, siltstone, and shale beds have been displaced along a very shallow-angled fault plane (marked) that is not parallel to the fault planes cross-cutting the two hinge zones. (e) A very close view of the lower part of the lower hinge zone in the vicinity of sample HF-4 (see fig. 21 for its location). The crumpled alternating thin sandstone (buff) and siltstone and shale (green) laminae are truncated in the cross-cutting fault plane. (f) A closer view of the upper portion of the lower hinge zone, the thicker buff sandstone bed to the right of the scale marker being the location of sample HF-08 (see fig. 21). The displacement along the obliquely cross-cutting fault plane is evident, as is the bulging of the upper interlayered buff sandstone and reddish-brown siltstone laminae in the hinge zone, visible also in (b). (g) A closer view of the overhanging underside of the buff sandstone beds above to the right of the intervening limb zone near the upper hinge zone, to the right of sample HF-10 (compare with fig. 21 for its location). Well-preserved fossilized horizontal trails, probably of Teichichnus (annelids), can be seen with no hint of any slickensides, both of which indicate no bedding plane slippage has occurred during folding.

sediment or sedimentary rock that is achieved by rearrangement of the original sedimentary particles, without internal deformation of those particles or of any interstitial cement. They added that such soft-sediment deformation occurs primarily by the mechanism of grain-boundary sliding. In contrast, Borg et al. (1960) conducted a quantitative study of experimental deformation of sand grains washed from the St. Peter Sandstone of Illinois by applying a uniform confining pressure to simulate overburden pressure and differential load to simulate tectonic pressures. They found that purely cataclastic brittle deformation occurred resulting in fracturing of the sand grains was the most conspicuous feature. The fracture pattern was random under uniform deformation pressure, whereas the fracture-orientation patterns reflected the symmetry of the deformation under differential loading conditions. And most importantly, the apparent elongation and optic-axis orientations in the deformed samples were much the same as those in the undeformed sands. There was also no evidence that the experimental deformation had produced any deformation lamellae or that the overall occurrence of grains with undulose extinction had been changed. They found uniform loading did not reorient the fabric of the sands, whereas the differential loading (simulating tectonic deformation) resulted in preferred orientation of fractures, the optic axis, and apparent grain elongations, all of which reflected the orientations of the principal applied stresses.

In conclusion, all the features observed in the outcropping Bright Angel Formation beds deformed in the Whitmore Helipad fold, and described above (fig. 50), are identical to those recognized and classified as due to soft-sediment deformation, both in the simulation experiments and in outcrops in other geological settings. The minor faulting, and trivial fracturing and jointing within the interlayered sandstone, siltstone, and shale beds, and the "plastic" bulging of the thin layers above the lower hinge zone, of the Whitmore Helipad fold have all been replicated in soft-sediment deformation experiments and observed in other outcrops elsewhere. Thus, these observed features do not necessarily support the claims of Huntoon (2003), Hill and Moshier (2009) and Tapp and Wolgemuth (2016) that the Carbon Canyon fold, and by extension to the other folds produced during the Laramide orogeny, including this Whitmore Helipad fold, were produced by ductile deformation ~450 million years after deposition, lithification, and progressive deep burial of these Bright Angel Formation beds. Rather, the field evidence is still compatible with the Whitmore Helipad fold having been produced by soft-sediment deformation of these Bright Angel Formation beds very soon after deposition and deep burial, and all before final lithification. However, since grain-boundary sliding is regarded as the essential process in soft-sediment deformation and the results of that process and features such as undulose extinction and deformation lamellae in quartz grains regarded as due to ductile deformation are only observed under the microscope, the microscopic evidence is thus crucial to definitively determining the timing of, and the conditions under which, the Bright Angel Formation beds were deformed to produce the Whitmore Helipad fold.

The Microscopic Evidence

As reported above, the critical petrographic microscope observations are that the silica cement and the quartz overgrowths around original detrital quartz grains outlined by dust and iron-oxides are in the same condition (the quartz overgrowths being in optical continuity with the detrital quartz grains) in all the samples from the fold as in the distal samples (figs. 24 and 37). Furthermore, there is no difference in the silica cement condition between the sandstone, siltstone, and shale samples from the hinge and limb zones in the fold. The original rock fabrics are still evident, with the detrital quartz grains still angular to sub-rounded, varying in size from medium sand to fine silt in generally well-sorted textures. And while the distal samples mostly have a greater porosity than the fold samples, there is only a slight difference in the porosities of these lithologies between limb and hinge zone samples in the fold (table 2, last column). Additionally, the original detrital muscovite flakes are still wedged between and bent around the detrital quartz and K-feldspar grains, showing no evidence of any metamorphic changes or any shearing between or disruption of their internal sheets. Even some original detrital glauconite pellets are present still in their detrital condition. These petrographic microscope observations are also emphatically substantiated by the SEM observations. Thus, the effects and outcome of the lithification of the deposited sand and silt layers under the overlying overburden pressure and slightly elevated burial temperature are uniform throughout the resultant Bright Angel Formation. In other words, the folding must have occurred before lithification of the sandstone, siltstone, and shale beds and thus the Whitmore Helipad fold must have been produced by soft-sediment deformation.

There are no deformation lamellae or deformation kink bands in the quartz grains as examined under the petrological microscope (figs. 24–27). Those would have been evidence for ductile deformation as demonstrated in experiments (Borg et al. 1960; Carter, Christie, and Griggs 1964; Christie, Griggs, and Carter 1964; Groshong 1988; Vernon 2018),

so their complete absence is significant in ruling out ductile deformation. However, even though the quartz grains display uniform extinction and generally show no signs of undulose extinction under crossed polars, there are a few quartz grains where there is an appearance of slightly undulose extinction (fig. 27). These observations are also contrary to the outcomes of experiments on ductile deformation of quartz grains and microscope observations of quartz grains in ductile deformed rocks (Carter, Christie, and Griggs 1964; Groshong 1988; Vernon 2018; Wojtal, Blenkinsop, and Tikoff 2022). Those few quartz grains in the Bright Angel Formation samples in this study, from the limb zones of the Whitmore Helipad fold, with observed slightly undulose extinction (fig. 27g, h) can be easily explained. Either they could be an artifact of the original detrital quartz grains retaining unchanged the slight undulose extinction they had in their source rocks, or more likely, they acquired the slight undulose extinction during compaction. Borg and Maxwell (1956) and Borg et al. (1960) found that quartz grains in deformed sands and the undeformed St. Peter Sandstone, respectively, which had only experienced previous compaction exhibited a preponderance of grains with no undulatory extinction and only a few displaying various intensities of undulose extinction. On the other hand, Maxwell (1960) who did compaction experiments on sand and sandstone samples did not report any resulting undulose extinction. However, grain-to-grain compaction is known to cause undulose extinction due to grain rotation and contact point pressures during compaction (Adams, McKenzie and Guildford 1984; Scholle 1979; Ulmer-Scholle et al. 2015), these processes being reported in experiments by Chester et al. (2004, 2007), Chuhan et al. (2002), de Boer, Nagtegaal, and Duyvis (1977), Elias and Hajash (1992), Maxwell (1960), Miyakawa and Kawabe (2014) and Wolf and Chilingarian (1975), and are noted by Ulmer-Scholle et al. (2015). The pressure solution of a few quartz grains from compaction is also evident in some of the SEM images in this study in figs. 38–45.

Fractures within quartz grains are usually subtle and only more pronounced in a few grains with no preferred orientations and no dislocations along any of them (fig. 28). The pronounced fractures are in quartz grains in both distal and fold samples. In some samples there are occasional broken quartz grains (fig. 29). Although the breakage is sometimes pronounced, there is rarely any displacement of the pieces. And again, these occurrences are just as prevalent in samples distal to the fold as in samples from the fold. The SEM images (figs. 38–45), as described above, indicate that this fracturing of quartz grains is likely due to compaction produced by the overburden pressures of the overlying strata. Indeed, it was concluded from the SEM study that the fractures found in these samples, whether from the fold or distant locations, are simply not dissimilar to anything routinely found in unfolded rocks anywhere else, where the cause of the fractures is always due to compactional stresses. This is further confirmed by the detrital muscovite flakes in many of the samples in this study that are observed to have been bent around the detrital quartz (and K-feldspar) grains, including those detrital grains that have been fractured and broken. While a few muscovite flakes are also broken (fig. 31), bent and broken muscovite flakes are present as often in the distal samples as in the samples from the Whitmore Helipad fold, and they are just as prevalent in the hinge zones compared to in the limbs of the fold. Those detrital muscovite flakes would have been initially deposited flat between the quartz and K-feldspar grains parallel and sub-parallel to the bedding because of their sheet structure, but were then bent subsequently during compaction, which at the same time fractured some quartz grains and broke both a few quartz grains and even some of the muscovite flakes.

Sediment compaction producing fracturing of quartz grains has been thoroughly demonstrated in many experiments (Borg et al. 1960; Borg and Maxwell 1956; Carter, Christie, and Griggs 1964; Christie, Griggs, and Carter 1964; Chester et al. 2004, 2007; Chuhan et al. 2002; Elias and Hajash 1992; Gallagher et al. 1974; Groshong 1988; Karner et al. 2003; Maxwell 1960). In fact, the experiments demonstrate that a large overburden load that produced high confining pressures should, over a sustained period of hundreds of millions of years, have produced a lot of obvious fracturing and breakage of quartz grains, vastly more than the few subtle fractures and broken quartz grains observed in the Bright Angel Formation samples in this study, regardless of whether they are samples from the fold or distal to the fold. This latter observation is clearly at odds with that experimental outcome. It is thus possible to conclude that the overburden load overlying the Bright Angel Formation was not sustained for hundreds of millions of years because the overlying strata sequence was deposited in so short a time period that the overburden pressures could not be sustained long enough to compact the quartz grains, causing them to fracture and/or break. Alternatively, the overlying strata sequence may never have been thick to cause significant breakage.

However, could it be that the reason there are so few quartz grains with just subtle fractures and a few quartz grains with fractures, or are broken, is because of recrystallization and recovery? In those processes, any crystal lattice dislocations produced

by ductile deformation are freed and migrate to form sub-grain boundaries (Spry 1969; Hobbs, Means and Williams 1976). Thus, another claimed evidence for ductile deformation is the development of sub-grains within quartz grains (Groshong 1988; Vernon 2018; Wojtal, Blenkinsop and Tikoff 2022). Yet such sub-grains are supposed to be relatively evenly spaced and show small optically misorientation angles, and such dispersion of dislocations in bending the grains should produce undulose extinction grading into the slightly misoriented sub-grain boundaries. However, as already noted, there are only a few quartz grains where there is any appearance of slightly undulose extinction (fig. 27). Also, only a few quartz grains in every sample in this study contain sub-grains, regardless of the location of the sample in the fold or distal to the fold (fig. 26). And there are no uniform shapes or sizes of those sub-grains, most being irregularly-shaped and often vastly different in sizes within the same quartz grains. They are not significantly misoriented optically and the sharpness of the sub-grain boundaries varies between quartz grains. In many instances the sub-grains appear to have been features in the original quartz clasts because the dust and iron-oxides outlines of the quartz grains containing the sub-grains preserve their original detrital shapes (figs. 24 and 26), which suggests those quartz grains were eroded and transported from metamorphic source rocks. Overall, sub-grains within the few quartz grains in which they occur are trivial features, which suggests they are not related to the deformation of the sandstone, siltstone, and shale beds, especially as they occur in all samples, whether in the Whitmore Helipad fold or distant from it.

The SEM images overwhelmingly confirm that there has been no stress on the fabric of the sandstone, siltstone, and shale layers after their compaction and lithification to disrupt them, apart from perhaps some slight further compaction due to the confining pressure of the overlying strata sequence. That has resulted in trivial fracturing with no displacements in a few samples, as seen in some SEM images (figs. 38–45), and in some petrographic photomicrographs (figs. 28, 29, and 33). Nevertheless, the original detrital quartz and K-feldspar grains and muscovite flakes would have been initially compacted by the overburden pressure during the progressive deposition of the overlying strata, which would have reduced the sizes of the initial pore spaces as well as bending some muscovite flakes around the quartz and K-feldspar grains, fracturing some grains and flakes, and breaking some flakes. During subsequent dewatering and lithification, the silica in the pore water crystallized as quartz overgrowths to infill many residual pore spaces and cement the detrital grains together, with the overgrowths often meeting at triple points (fig. 25). Once cemented, the rock fabric has not been subsequently disturbed, as the SEM images (figs. 38–45) emphatically show. This again implies that the deformation responsible for the Whitmore Helipad fold must have occurred soon after deposition before cementation and lithification of the sandstone, siltstone, and shale beds, so the deformation that produced the fold had to be soft-sediment deformation rather than ductile deformation hundreds of millions of years after lithification. The SEM images (figs. 38–45) clearly show the localized dissolution of quartz and K-feldspar and growth of some illite that occurred during diagenesis due to that alteration breakdown of K-feldspar grains, while some petrographic images of some samples show the later secondary growth of minor carbonates infilling some residual pores spaces and cracks (fig. 35).

It has already been determined above that the pressure-temperature conditions of ~0.3–0.4 kbar (~4300–5900 psi) and 110–130°C to which these Bright Angel Formation beds were subjected were only in the diagenesis P-T field, well below even low-grade regional metamorphism and the necessary conditions for most ductile deformation. However, even during soft-sediment deformation it is postulated that both grain-boundary sliding and rotation of the detrital grains occurs (fig. 15a), yet there is no obvious definitive evidence of that process having occurred in these layers that is visible under either the petrographic or the scanning electron microscopes. Nevertheless, there is no preferred crystallographic orientation of the quartz grains since their extinction occurs at different angles (fig. 27), which would be expected from the random settling of quartz grains during deposition. Furthermore, there does not appear to be any overall direction of elongation of the quartz grains parallel to the bedding (figs. 23–25), which might be expected as evidence of grain-boundary sliding and rotation of the grains during compaction and subsequent soft-sediment deformation before cementation and lithification. Only locally, in one or two samples under magnification, might there appear to be a hint of some elongation of very occasional quartz grains parallel to the bedding, but that is normal for random settling during deposition, and at the macroscopic scale there is no evidence of grain elongation (fig. 23). Of course, the muscovite flakes are generally parallel and sub-parallel to the bedding, but that is a depositional feature due to the flatness of the flakes having caused such settling during deposition.

Thus, there is no definitive microscopic evidence of ductile deformation of the Bright Angel Formation beds within the Whitmore Helipad fold, either under

the petrological microscope or the scanning electron microscope. However, the conventional published accounts of the Laramide orogeny and monocline folding (DeCelles, Lawton, and Mitra 1995; DeCelles and Coogan 2006; Huntoon 1993, 2003; Ismat and Mitra 2005; Karlstrom and Timmons 2012; Matthews 1978; Reches 1978a; Sanz et al. 2008; Tindall and Davis 1999) insist that the folding was due to ductile deformation, yet all the features they describe as the macroscopic evidence for ductile deformation to fold the strata have all been replicated in simulation experiments involving the compressional folding of *dampened soft sediment layers* (Friedman et al. 1976; Friedman, Hugman, and Handin 1980; Handin et al. 1976; Nabavi and Fossen 2021; Rettger 1935; Weinberg 1979). Instead, all these simulation experiments using dampened *soft sediment* layers have demonstrated are the macroscopic features produced by soft-sediment deformation (and not by ductile deformation as often claimed). And these are the very same features observed in the Bright Angel Formation beds within the Whitmore Helipad fold. Thus, it is to be expected that the microscopic evidence is consistent with the folding being due to soft-sediment deformation having occurred soon after deposition of the sandstone, siltstone, and shale beds and before subsequent cementation and lithification.

The Dating of Bright Angel Formation Deposition and the Laramide Orogeny

So how can these macroscopic and microscopic observations be reconciled with the conventional published accounts of the Laramide orogeny and monocline folding (DeCelles and Coogan 2006; DeCelles, Lawton, and Mitra 1995; Huntoon 1993, 2003; Ismat and Mitra 2005; Karlstrom and Timmins 2012; Matthews 1978; Reches 1978a; Sanz et al. 2008; Tindall and Davis 1999)? Put simply, it is not a question of the tectonic processes involving the subduction and underplating of the Farallon plate being responsible for the uplift of the Colorado Plateau, which are not in dispute (Austin et al. 1994; Dickinson and Snyder 1978; Huntoon 2003; Karlstrom and Timmins 2012), but rather a huge disagreement with respect to timing. The macroscopic and microscopic evidence discussed above indicates that the monoclinal folding during plateau uplift was accompanied by soft-sediment deformation of the Bright Angel Formation beds in the Whitmore Helipad monoclinal fold along a branch fault to the Hurricane Fault and its associated Hurricane Monocline (fig. 8), and not by the ductile deformation claimed by Huntoon (2003), Hill and Moshier (2009) and Tapp and Wolgemuth (2016). This implies that the uplift and folding must have occurred very soon after deposition of the whole regional strata sequence before cementation and lithification of those strata. Yet the conventional view is that there were ~450 million years between deposition of the Bright Angel Formation at ~502–507 Ma (Karlstrom et al. 2018, 2020) and the Laramide orogeny at ~35–70 Ma (Huntoon 2003; Karlstrom and Timmins 2012).

Thus, this huge discrepancy between the claimed vast ages for the deposition of the Bright Angel Formation and the subsequent Laramide folding, and the macroscopic and microscopic evidence of rapid deposition of the whole strata sequence followed by soft-sediment deformation during the folding event, all prior to cementation and lithification of the Bright Angel Formation beds, needs to be reconciled. Snelling (2021b) has already resolved this issue with respect to the dating of the Bright Angel Formation at ~502–507 Ma, which depended on U-Pb dating of detrital zircons in the underlying Tapeats Sandstone (Snelling 2021a). The same resolution applies to the dating of the Laramide orogeny. Vardiman, Snelling, and Chaffin (2005) reported the technical details of six lines of evidence, including experimental confirmation, that during a past global catastrophe nuclear decay rates were likely grossly accelerated by potentially six orders of magnitude, such that ~600 or more million years' worth of nuclear decay at the decay rates measured today occurred within about a year, which they identified as the year-long biblical Flood cataclysm recorded in Genesis 6-9. On that basis, the deposition of the Bright Angel Formation dates to only the first few weeks of the Flood year, only ~4,350 years ago. Critics have pointed to the enormous quantities of heat that apparently would be released by such accelerated nuclear decay (Wiens 2016), yet Vardiman, Snelling, and Chaffin (2005) had already anticipated this criticism and provided plausible possible explanations, including the experimental fact that the radiohalos (which only form below 150°C) would have been annealed if such an enormous heat release had occurred (Laney and Laughlin 1981; Snelling 2005a).

However, Snelling (2021a, b) went further to demonstrate the problems with the U-Pb radioisotope dating of the Tapeats Sandstone and thus also the Bright Angel Formation, respectively, and of that dating method itself. Specifically, Karlstrom et al. (2018) obtained U-Pb ages for detrital zircons within the Tapeats Sandstone as "young" as only 407.2 million years old, and then did not explain how the supposedly 507–508 million years old Tapeats Sandstone can have included within it so many detrital zircons with U-Pb ages less than its supposed depositional age. Nor did they explain from where these "younger" detrital zircons within the Tapeats Sandstone originated. Indeed, how could even the 507–508 Ma detrital

zircons be incorporated in the Tapeats Sandstone if the underlying rocks that were eroded to provide the sand grains, including the zircon grains, are older than 507–508Ma? This question alone raises serious doubts as to the applicability and reliability of this technique for supposedly quantifying the apparent depositional ages of sedimentary rock units. Yet, not only is their methodology questionable, so must be the U-Pb dating method they used if it produced such illogical results. Snelling (2000, 2009, 2022b) has already provided details of numerous problems with the U-Pb dating method that are well-documented in the scientific literature. Furthermore, Snelling (2017a) reviewed all the determinations of the U-Pb decay rates (half-lives) and demonstrated that these crucial parameters are not yet precisely known, while Snelling (2017b, 2018, 2019) highlighted in detail the problems of common Pb, U, and Pb mobility, and mass fractionation respectively that plague all efforts to obtain accurate U-Pb age determinations.

Thus, once the subjectively interpreted U-Pb dates for the deposition of the Bright Angel Formation are demonstrated to be invalid, there is no valid scientific objection to assigning the deposition of the Bright Angel Formation to the first few weeks of the Flood year, only ~4,350 years ago. Similarly, the dating of the Laramide orogeny and the accompanying monocline folding at ~40–70Ma relies on the same and various other related radioisotope dating methods that are plagued by identical problems (Snelling 2000, 2009, 2022b). However, debate continues as to when the Laramide orogeny and monocline folding is envisaged to have occurred in the timing of the Genesis Flood cataclysm. Whitmore and Garner (2008) maintain it would have been at the end of the Flood year and continued into the early post-Flood years as the catastrophic plate tectonics of the Flood year reached isostatic equilibrium, causing mountains to rise all over the globe rapidly. Thus, the sinking of the new ocean floors (Austin et al. 1994; Baumgardner 2003; Snelling 2009, 2022b) and the uplift and exposure of these mountains (potentially described in Psalm 104:8; Barrick 2018) would have resulted in the draining of the last marine waters off the North American continent, as happened at the end of the Cretaceous. Others, like Clarey (2020) disagree, and place the Laramide orogeny within the year of the Flood, with the Cretaceous representing the Flood's last high-water stage, and the Laramide orogeny and the draining of the waters off the North American continent occurring in the latter half of the Flood year. But regardless, the Laramide orogeny occurred relatively recently, about 4,350 years ago.

The Timing of the Folding—Flood Deposition and Tectonics

Austin (1994) provided a detailed comprehensive description and account of the geological development of Grand Canyon strata in the context of the global Genesis Flood cataclysm and the canyon's erosion in the Flood's aftermath. In particular, he described the Bright Angel Formation as being deposited by the Flood waters advancing eastwards onto the western edge of the North American portion of the pre-Flood supercontinent after the initiation of the Flood event with the breaking up of the fountains of the great deep (Genesis 7:11) and the triggering of catastrophic plate tectonics (Austin et al. 1994; Baumgardner 2003). However, before the Bright Angel Formation was deposited there may have been a period (days or more) in which there was a significant amount of continental-scale erosion to bevel the Precambrian (pre-Flood) land surface to produce the Great Unconformity. In the Grand Canyon region this involved intensive catastrophic erosion to remove several thousand meters of Grand Canyon Supergroup strata (which appear to only have survived in several down-faulted blocks) and then to bevel the underlying metamorphic schists and granite plutons. Then after this period of destructive erosion, and subsequent to the localized deposition of the Sixtymile Formation, the Tapeats Sandstone along with the Bright Angel Formation as a fining upwards sequence represents the widespread (continental-scale) deposit of the Tonto Group. Snelling (2021b) provides more details of, and evidence for, the rapid deposition of the Bright Angel Formation in the first few weeks of the global Flood cataclysm.

Austin (1994) also diagrammatically envisaged a fining upwards model for the time transgressive rapid deposition of the Tonto Group strata as the powerful westward back underflow of the advancing Flood waters at a water flow speed of >2m/sec intensely scoured and catastrophically eroded all pre-Flood rocks to produce the Great Unconformity before sequentially depositing their load of sediments as horizontally segregated facies in the vertically stacked Tonto Group strata during the first weeks of the Flood year. Then followed the progressive rapid deposition of the overlying sedimentary strata sequence in the subsequent months as the Flood waters rose violently to sweep and deposit sediments rapidly in these layers, many of which can also be traced across the North American continent (Clarey 2020; Sloss 1963).

Baumgardner (2013, 2018a, b) has made considerable progress with numerical simulations of the catastrophic erosion of bedrock via cavitation to produce these sediments that were rapidly deposited on the continental plates as shallow waters moved rapidly around the surface of the rotating globe. His modeling posits that the dominant means for

sediment transport during the Flood was by rapidly flowing turbulent water, and that water motion was driven by large-amplitude tsunamis that were generated along subduction zone segments as the subducting plate and overriding plate, in a cyclic manner, locked and then suddenly released and slipped rapidly past one another. His calculations show that with plausible parameter choices average erosion and sedimentation rates on the order of 9 m/day (0.38 m/hr) occurred with tsunami-driven pulses of turbulent water that transported the generated sediments vast distances across the continental plate surfaces, sufficient to deposit the Bright Angel Formation within 3–10 days and most of the Paleozoic-Mesozoic strata during the initial 150-day rising and prevailing waters phase of the Flood (Genesis 7:18–24), thus accounting for nearly 70% of the Phanerozoic sediment layers that blanket the earth's continental surfaces today (Clarey and Werner 2023).

In the catastrophic plate tectonics model for the cataclysmic Flood event (Austin et al. 1994; Baumgardner 2003; Snelling 2009, 2022b), the plates moved the same as in conventional plate tectonics, but at rapid rates. In the case of the Farallon plate, as its subduction under the western edge of the North American flattened, possibly because it included subduction of a divergent boundary (Clarey 2020), it thickened the continental crust of western North America. Consequently, rapid isostatic equilibration began, resulting in the Laramide orogeny and the rise of the Colorado Plateau and the monocline folding in the Grand Canyon region and elsewhere in the Colorado Plateau.

The Bright Angel Formation beds were deposited rapidly in the first few weeks of the year of the biblical global Flood cataclysm only ~4,350 years ago (Snelling 2021b). In the subsequent months the overlying sedimentary strata were progressively deposited rapidly, their accumulating overburden pressures of ~0.3–0.4 kbar (~4,300–5,900 psi) compacting and dewatering the Bright Angel Formation beds at a possible maximum burial depth of ~3,300–4,500 m (~10,825–14,750 ft) where the temperatures rose to ~110–130°C. Then later in the Flood year, or as the Flood year ended, the Laramide uplift of the Colorado Plateau occurred, helping to drain off the Flood waters from the North American continent, eroding away almost all the Mesozoic strata off the plateau in the Grand Canyon region. Thus, in the Grand Canyon region the Laramide uplift caused bending of the whole Paleozoic strata sequence in the East Kaibab, Hurricane, and other monoclines as the reactivated Precambrian faults moved the underlying Precambrian basement, producing the Carbon Canyon and Monument folds in the Tapeats Sandstone (Snelling 2023a, b) and the Whitmore Helipad fold in the Bright Angel Formation. The Bright Angel Formation beds had for much of the Flood year remained relatively water-saturated and soft, even as they were increasingly compacted by the rapidly accumulating overlying strata. But because the compaction was so rapid very few microscopic effects of it are observed in the sandstone, siltstone, and shale beds. Then when the Laramide folding occurred, the Bright Angel Formation beds were bent in the Whitmore Helipad fold by soft-sediment deformation, consistent with both the observed macroscopic and microscopic features in the interlayered sandstone, siltstone, and shale beds. Only subsequently did the sand and silt in the Bright Angel Formation beds become cemented and lithified (without drying and exposure being necessary), again consistent with both the observed macroscopic and microscopic features in the sandstone, siltstone, and shale.

Post-Flood to Recent Tectonics

Finally, the three faults with little to no displacements within the Whitmore Helipad fold (figs. 21 and 50) as described above are consistent with minor faulting that can be replicated in soft-sediment deformation experiments, but could there have still been later earth movements after cementation and lithification of the interlayered sandstone, siltstone, and shale beds that may have added to this minor faulting produced earlier soft-sediment deformation? Any more recent slight movements along these faults in the Bright Angel Formation in the fold might have produced further occasional fracturing of the observed rock fabric and detrital quartz grains at the microscopic level (figs. 28 and 36). Snelling (2023a) did not report as much evidence of similar macroscopic faulting and microscopic fracturing in the Carbon Canyon fold, but did find similar evidence in the Monument fold (Snelling 2023b), both in the underlying Tapeats Sandstone. So, is there any evidence of later earth movements in this area that might have trivially affected the rocks in this fold?

Karlstrom and Timmons (2012, fig. 2F) documented ongoing micro-earthquakes still occurring in the Grand Canyon region, recorded over the last tens of years. Based on the offset of Quaternary (that is, post-Flood) basalts, they concluded it is clear that extensional deformation is ongoing today. The epicenters of these micro-earthquakes of different magnitudes have been concentrated in swarms in several zones coinciding with major fault zones which must thus be seismically active. These include a major swarm concentrated around and between the Hurricane and Toroweap Faults in the vicinity of the Whitmore Helipad fold (fig. 3). Karlstrom and Timmins (2012) suggest that because most of these

earthquakes are modest in terms of energy released (<5 on the Richter scale), these earthquakes probably represent relatively minor fault slips of several centimeters (<2 in) on existing faults. Noteworthy is the observation that no similar micro-earthquakes are occurring along the Butte Fault responsible for the East Kaibab Monocline and the Carbon Canyon fold, indicating it is not similarly seismically active.

Of all the faults in the region, the Hurricane Fault has been the most active in recent history. Billingsley and Wellmeyer (2003) mapped a 6–8 m (~20–26 ft) displacement of the Quaternary (post-Flood) basalts on the Uinkaret Plateau not far to the north of the Whitmore Helipad fold (fig. 8). The 1992 St. George earthquake (Richter magnitude 5.8) was attributed to the Hurricane Fault, caused significant damage, and triggered a massive landslide (Stewart et al. 1997). Amoroso, Pearthree, and Arrowsmith (2004) reported measured movements along the Hurricane Fault of 0.15 to 0.25 mm/yr. Thus, this evidence may be consistent with trivial movements along faults and fractures in the Whitmore Helipad fold after cementation and lithification of the Bright Angel Formation layers that were deformed in the fold when the sediments were still soft, which would be consistent with the recent (that is, post-Flood) history of earthquakes due to earth movements along the Hurricane Fault.

Another indication of activity along these fault zones in the Grand Canyon region is the distribution of travertines and, especially, the travertine-depositing springs where helium isotopes from the mantle have been detected (Karlstrom and Timmons 2012, fig. 2F). Crossey et al. (2009) and Crossey and Karlstrom (2012) determined that these springs represent the upward transfer of deep-seated fluids along faults, which is a highly sensitive gauge of ongoing tectonism, perhaps even more sensitive than the distribution of earthquakes. Springs in Grand Canyon that carry mantle-derived helium include some associated with the Hurricane and Toroweap Faults near the Whitmore Helipad fold (Karlstrom and Timmons 2012, fig. 2F). These are indicative of deposition from travertine springs recently, that is, post-Flood since the Grand Canyon was carved. Even Karlstrom and Timmins (2012) thus admit that these springs and travertines may be the youngest tectonic features of Grand Canyon and may represent ongoing small extensional slip along these reactivated faults.

Therefore, imperceptible earth movements have happened since the Laramide uplift of the Colorado Plateau that produced the Whitmore Helipad fold and since the carving of the Grand Canyon, including along the Hurricane Fault in proximity to the Whitmore Helipad fold, and are ongoing today. Those may have been capable of inducing trivial movements along the minor faults and fractures that are evident in the Bright Angel Formation beds within the Whitmore Helipad fold. Furthermore, the spring waters that carried calcium carbonate up the Hurricane Fault zone and deposited it as travertine on nearby cliff walls might also explain the later secondary calcite deposition within residual pore spaces and cracks within some of the Bright Angel Formation beds.

Summary and Conclusions

The interlayered sandstone, siltstone, and shale beds of the Cambrian Bright Angel Formation are bent in the Whitmore Helipad fold where they have been monoclinally folded along a branch of the Hurricane Fault exposed in the Colorado River corridor of western Grand Canyon. This occurred during the Laramide orogeny at ~40–70 Ma when the Colorado Plateau including in the Grand Canyon region was uplifted. However, the Bright Angel Formation had been deposited at 502–507 Ma, so after ~450 million years it should have been fully cemented and lithified. Thus, when its sandstone, siltstone, and shale beds were bent in the Whitmore Helipad fold, they should have suffered ductile deformation via bedding plane or flexural slip and grain-boundary sliding. And in the hinge zones particularly the lithified sandstone, siltstone, and shale should have fractured. However, even during a superficial inspection of this fold it is evident that there is no significant or more intense fracturing of the lithologies in the hinge zones, compared to along the limbs of the fold. Thus, the sandstone, siltstone, and shale beds look as though they were bent smoothly, perhaps while they were still unlithified and soft. Yet such a conclusion is preposterous if there were ~450 million years between deposition and lithification of the Bright Angel Formation, and its subsequent deformation to form the Whitmore Helipad fold.

To date there had not been a detailed investigation of the Whitmore Helipad fold to examine the bent sandstone, siltstone, and shale beds, especially their microscopic features, to determine if their folding was due to ductile deformation (as conventionally claimed) or due to soft-sediment deformation. Thus ten samples of the Bright Angel Formation were collected from the Whitmore Helipad fold, from hinge zones and from along the limb zones, as well as two samples from approximately the same stratigraphic position in the Bright Angel Formation at a considerable distance of miles from the fold. This strategy was adopted so that the samples from the fold could be compared with the distal samples acting as a "control" to ascertain any differences between the folded and unfolded ("background") sandstone, siltstone and shale beds.

An initial study detailed all previous investigations of the Bright Angel Formation. From petrographic

examination of 12 Bright Angel Formation samples it was concluded that the fine-grained sandstones and the siltstone layers consist of well-sorted, angular to sub-rounded quartz and K-feldspar grains, some even sub-euhedral, muscovite flakes, and even glauconite grains and occasional brachiopod shell fragments, that are all still in their detrital condition with no indications of the silica cement having been disturbed since lithification of the sandstones and siltstones, or of any metamorphic changes to these constituents or the rock fabric. The shales consist of alternating thin laminae of siltstone with quartz and K-feldspar grains, and selvages of softer iron-oxide-stained, very-fine-grained illite, along with muscovite flakes mostly aligned with the bedding. These observations, as well as the sedimentary structures and the body fossils and fossil traces preserved in the Bright Angel Formation were deemed consistent with its rapid deposition.

For this study the macroscopic and microscopic features that should or could be present if the Bright Angel Formation beds in the Whitmore Helipad fold had been bent via ductile deformation were described in detail. For example, at the macroscopic scale, bedding plane slip or flexural slip should have produced slickensides on bedding plane surfaces, and there should be thickening of hinge zones in the fold and thinning of limb zones, as well as more fracturing in the hinge zones compared to the limbs. Field observations were obtained to test these expectations. At the microscopic scale there should minimally be evidence of grain-boundary sliding, rotation of grains, and fracturing of grains, and within many quartz grains there should be sub-grains, undulose extinction, deformation lamellae and even deformation kink bands. Both petrographic observations were made and scanning electron microscope (SEM) images obtained to ascertain whether these microscopic features are present in the sandstone, siltstone, and shale beds, especially also comparing the samples from the hinge and limb zones in the fold with the distal samples.

The field observations of the sandstone, siltstone, and shale beds in the fold are inconsistent with ductile deformation. While bedding plane or flexural slip might have occurred, no slickensides were found on any exposed bedding plane surfaces, which instead preserved undisturbed trace fossils. There is no thickening of the sandstone, siltstone, and shale beds in the hinge zones, except for bulging of these layers laterally above the lower hinge zone. And the fractures present are confined to within the beds in both the limb and hinge zones and do not display evidence of being due to brittle fracturing. Instead, they are consistent with just being the result of joint development due to lateral shrinkage of the sediments during dewatering. All these and other features, such as the bulging of the siltstone and shale beds laterally above the lower hinge zone of the fold, have been replicated using damp soft sediment layers in experiments simulating compressional folding, which equates to soft-sediment deformation. On the other hand, none of the microscopic features expected from ductile deformation were present in any of the samples, and the samples from the hinge and limb zones of the fold were essentially identical to the distal samples. There are no deformation lamellae or deformation kink bands in the quartz grains which rarely displayed even trivial undulose extinction, and there is no obvious evidence of any rotation of grains or grain-boundary sliding. The few quartz grains containing sub-grains are instead likely derived from the metamorphic source rocks rather than being a product of ductile deformation, and the occasional subtle fractures in some quartz grains and broken quartz grains are consistent with that trivial fracturing being due to compaction of those sand and silt grains under the confining overburden pressures. Furthermore, the SEM images clearly demonstrate that the silica (quartz) cement binding the sand grains has not been disrupted since lithification, with many quartz cement crystals still being pristine with terminal faces intact. Thus, both the macroscopic and microscopic evidence are conclusively consistent only with soft-sediment deformation before cementation and lithification.

Therefore, since the bending of the Bright Angel Formation beds in the Whitmore Helipad fold must be due to soft-sediment deformation, the claimed ~450 million years between deposition of the sandstone, siltstone and shale beds and the Laramide uplift responsible for the folding must be in error and are thus eliminated. Instead, the Bright Angel Formation had to be folded while still relatively water-saturated and soft, soon after deposition, and before complete cementation and lithification. The problems with the radioisotope dating methods and the U-Pb dates obtained for the underlying Tapeats Sandstone rule out the vast claimed ages. This scenario can all be easily reconciled with rapid deposition of the Bright Angel Formation during the first few days to weeks of the biblical global Flood cataclysm only ~4,350 years ago, and rapid deposition of up to ~3,300–4,500 m (~10,825–14,750 ft) of overlying sedimentary layers during the catastrophic plate tectonics of the Flood year. Then, near or at the end of Flood year, the Farallon plate underplated the western North American plate, causing isostatic reequilibration which resulted in the Laramide uplift of the Colorado Plateau and monocline folding in the Grand Canyon region now exposed in the Whitmore Helipad fold. Because the Bright Angel Formation beds were still relatively wet and soft after less than a year of rapid

burial, they easily responded to the soft-sediment deformation to form the smooth bending (without brittle fracturing) in the Whitmore Helipad fold before the beds were cemented and lithified to sandstone, siltstone, and shale (without drying and exposure being necessary). Altogether, nearly 500 million years of claimed geologic history are eliminated. And since the Flood, continued isostatic reequilibration in western Grand Canyon has resulted in further isolated movements on the Hurricane Fault that have caused minor faulting in the Whitmore Helipad fold and fracturing within the lithified Bright Angel Formation beds.

Acknowledgements

All samples were collected under the authority of National Park Service Scientific Research and Sampling Permit # GRCA-2017-SCI-0052 dated June 23, 2017, issued by the Grand Canyon National Park's Research Office, and Permit #032767 issued by the Hualapai Department of Natural Resources dated July 27, 2017. The Alliance Defending Freedom (ADF) team led by then Senior Counsel Gary McCaleb is especially thanked for their legal work that led to a successful lawsuit against viewpoint discrimination in the permit application and granting process. Tom Vail, founder of Canyon Ministries who encouraged this research from its start, is also thanked for organizing with Terry Vallely, and assisted by their wives Paula and Kathy, respectively, the August 6–12, 2017, research raft trip down the Colorado River through Grand Canyon to collect the samples, facilitated by Grand Canyon National Park Special Use Permit #GRCA-3701 issued June 26, 2017. Special thanks go to Tom Vail and Dr. John H. Whitmore, Senior Professor of Geology at Cedarville University, Ohio for their invaluable field assistance, without which the samples would not have been collected, especially after I was injured early in the trip. Ray Strom of Calgary Rock and Materials Services, Inc. is thanked for the thin sections he prepared, and for the XRD and SEM analyses, as well as for the use of his research microscope for photography. Cedarville University is also thanked for the use of their geologic research microscope and Dr. John H. Whitmore for his advice, support, and encouragement. The helpful comments and edits from three kind reviewers were much appreciated. This research was fully funded by many generous donors to Answers in Genesis and has had the full support of the Answers in Genesis leadership team under Ken Ham. Our production assistant Laurel Hemmings is also thanked for her work in preparing this paper for publication. Nevertheless, I take full responsibility for the content of this paper.

References

Adams, A.E., W.S. MacKenzie, and C. Guildford. 1984. *Atlas of Sedimentary Rocks Under the Microscope*. Harlow, Essex, England: Longman Group Limited.

Allison, I., R.L. Barnett, and R. Kerrich. 1979. "Superplastic Flow and Changes in Crystal Chemistry of Feldspars." *Tectonophysics* 53, nos. 1–2 (1 March): T41–46.

Alsop, G.I., Roberta Weinberger, S. Marco, and T. Levi. 2019. "Identifying Soft-Sediment Deformation in Rocks." *Journal of Structural Geology* 125 (August): 248–255.

Altenberger, U., and S. Wilhelm. 2000. "Ductile Deformation of K-Feldspar in Dry Eclogite Facies Shear Zones in the Bergen Arcs, Norway." *Tectonophysics* 320, no. 2 (15 May): 107–121.

Amoroso, Lee, Philip A. Pearthree, and J. Ramón Arrowsmith. 2004. "Paleoseismology and Neotectonics of the Shivwits Section of the Hurricane Fault, Northwestern Arizona". *Bulletin of the Seismological Society of America* 94, no. 5 (October 1): 1919–1942.

Anderson, John J., Peter D. Rowley, Robert J. Fleck, and A.E.M. Nairn. 1975. *Cenozoic Geology of Southwestern High Plateaus of Utah*. Boulder, Colorado: Geological Society of America. *Special Paper 160*.

Ashby, M.F., and R.A. Verall. 1973. "Diffusion-Accommodated Flow and Superplasticity." *Acta Metallurgica* 21, no. 2 (February): 149–163.

Austin, Steven A. ed. 1994. *Grand Canyon: Monument to Catastrophe*. Santee, California: Institute for Creation Research.

Austin, Steven A., John R. Baumgardner, D. Russell Humphreys, Andrew A. Snelling, Larry Vardiman, and Kurt P. Wise. 1994. "Catastrophic Plate Tectonics: A Global Flood Model of Earth History." In *Proceedings of the Third International Conference on Creationism*. Edited by Robert E. Walsh, 609–621. Pittsburgh, Pennsylvania: Creation Science Fellowship.

Aydin, Atilla, and Arvid M. Johnson. 1983. "Analysis of Faulting in Porous Sandstones." *Journal of Structural Geology* 5, no. 1: 19–31.

Bailey, S.W., R.A. Bell, and C.J. Peng. 1958. "Plastic Deformation of Quartz in Nature." *Geological Society of America Bulletin* 69, no. 11 (November 1): 1443–1466.

Baldwin, Christopher T., Paul K. Strother, John H. Beck, and Eben Rose. 2004. "Palaeoecology of the Bright Angel Shale in the Eastern Grand Canyon, Arizona, USA, Incorporating Sedimentological, Ichnological and Palynological Data." In *The Application of Ichnology to Paleoenvironmental and Stratigraphic Analysis*. Edited by D. McIlroy, 213–236. London, United Kingdom: The Geological Society of London. *Special Publication 228*.

Barber, D.J. 1985. "Dislocations and Microstructures." In *Preferred Orientation in Deformed Metals and Rocks: An Introduction to Modern Texture Analysis*. Edited by Hans-Rudolf Wenk, 149–182. London, United Kingdom: Academic Press.

Barber, David J., and Philip G. Meredith, eds. 1990. *Deformation Processes in Minerals, Ceramics and Rocks*. Boston, Massachusetts: Unwin Hyman.

Barrenechea, J.F., M. Rodas, and J.R. Mas. 1995. "Clay Mineral Variations Associated with Diagenesis and Low-Grade Metamorphism of Early Cretaceous Sediments in

the Cameros Basin, Spain." *Clay Minerals* 30, no. 2 (June): 119–133.

Barrick, William D. 2018. "Exegetical Analysis of Psalm 104:8 and Its Possible Implications for Interpreting the Geological Record." In *Proceedings of the Eighth International Conference on Creationism*. Edited by John H. Whitmore, 95–102. Pittsburgh, Pennsylvania: Creation Science Fellowship.

Baumgardner, John R. 2003. "Catastrophic Plate Tectonics: The Physics Behind the Genesis Flood." In *Proceedings of the Fifth International Conference on Creationism*. Edited by Robert L. Ivey, Jr., 113–126. Pittsburgh, Pennsylvania: Creation Science Fellowship.

Baumgardner, John. 2013. "Explaining the Continental Fossil-Bearing Sediment Record in Terms of the Genesis Flood: Insights from Numerical Modeling of Erosion, Sediment Transport and Deposition Processes on a Global Scale." In *Proceedings of the Seventh International Conference on Creationism*. Edited by Mark Horstemeyer, article 3. Pittsburgh, Pennsylvania: Creation Science Fellowship.

Baumgardner, John. 2018a. "Numerical Modeling of the Large-Scale Erosion, Sediment Transport, and Deposition Processes of the Genesis Flood." *Answers Research Journal* 11 (June 27): 149–170. https://answersresearchjournal.org/numerical-modeling-genesis-flood-2/.

Baumgardner, John. 2018b. "Understanding How the Flood Sediment Record was Formed: The Role of Large Tsunamis." In *Proceedings of the Eighth International Conference on Creationism*. Edited by John H. Whitmore, 287–305. Pittsburgh, Pennsylvania: Creation Science Fellowship.

Becker, Alexander. 1994. "Bedding-Plane Slip Over a Pre-Existing Fault, An Example: The Ramon Fault, Israel." *Tectonophysics* 230, nos. 1–2 (15 February): 91–104.

Becker, Alexander. 1995. "Quartz Pressure Solution: Influence of Crystallographic Orientation." *Journal of Structural Geology* 17, no. 10 (October): 1395–1405.

Behrmann, Jan H. 1983. "Microstructure and Fabric Transitions in Calcite Tectonics from the Sierra Alhamilla (Spain)." *Geologische Rundschau* 72, no. 2 (June): 605–618.

Behrmann, Jan H. 1985. "Crystal Plasticity and Superplasticity in Quartzite: A Natural Example." *Tectonophysics* 115, nos. 1–2 (10 May): 101–129.

Behrmann, Jan H., and D. Mainprice. 1987. "Deformation Mechanisms in a High-Temperature Quartz-Feldspar Mylonite: Evidence for Superplastic Flow in the Lower Continental Crust." *Tectonophysics* 140, nos. 2–4 (1 September): 297–305.

Behzadi, H., and A.K. Dubey. 1980. "Variation of Interlayer Slip in Space and Time During Flexural Folding." *Journal of Structural Geology* 2, no. 4: 453–457.

Bell, Tim H. 1978. "Syntectonic Nucleation of New Grains in Deformed Mica." *Tectonophysics* 51, nos. 3–4 (20 December): T31–T37.

Bell, Tim H., and Scott E. Johnson. 1989. "The Role of Deformation Partitioning in the Deformation and Recrystallization of Plagioclase and K-Feldspar in the Woodroffe Thrust Mylonite Zone, Central Australia." *Journal of Metamorphic Geology* 7, no. 2 (March): 151–168.

Benesh, N.P., A. Plesch, J.H. Shaw, and E.K. Frost. 2007. "Investigation of Growth Fault Bend Folding Using Discrete Element Modeling: Implications for Signatures of Active Folding Above Blind Thrust Faults." *Journal of Geophysical Research* 112, no. B3: B03S04. doi:10.1029/2006JB004466.

Bestmann, Michel, and David J. Prior. 2003. "Intragranular Dynamic Recrystallization in Naturally Deformed Calcite Marble: Diffusion Accommodated Grain Boundary Sliding as a Result of Subgrain Rotation Recrystallization." *Journal of Structural Geology* 25, no. 10: 1597–1613.

Billia, Marco A., Nicholas E. Timms, Virginia G. Toy, Rob D. Hart, and David J. Prior. 2013. "Grain Boundary Dissolution Porosity in Quartzofeldspathic Ultramylonites: Implications for Permeability Enhancement and Weakening of Mid-Crustal Shear Zones." *Journal of Structural Geology* 53 (August): 2–14.

Billingsley, George H., and Jessica L. Wellmeyer. 2003. *Geologic Map of the Mount Trumbull 30′ × 60′ Quadrangle, Mohave and Coconino Counties, Northwestern Arizona*. Washington DC: U.S. Geological Survey, *Geologic Investigations Series* I–2766.

Blakey, Ronald C., and Larry T. Middleton. 2012. "Geologic History and Paleogeography of Paleozoic and Early Mesozoic Sedimentary Rocks, Eastern Grand Canyon, Arizona." In *Grand Canyon Geology: Two Billion Years of Earth's History*. Edited by J. Michael Timmons and Karl E. Karlstrom, 81–92. Boulder, Colorado: Geological Society of America. *Special Paper 489*.

Blenkinsop, Tom G. 1988. "Definition of Low-Grade Metamorphic Zones Using Illite Crystallinity." *Journal of Metamorphic Geology* 6, no. 5 (September): 623–636.

Blenkinsop, Tom G., and M.R. Drury. 1988. "Stress Estimates and Fault History from Quartz Microstructures." *Journal of Structural Geology* 10, no. 7: 673–684.

Boggs, Sam, Jr. 1995. *Principles of Sedimentology and Stratigraphy*. 2nd ed., 79–107. Upper Saddle River, New Jersey: Prentice-Hall.

Bons, Paul D., and Bas den Brok. 2000. "Crystallographic Preferred Orientation Development by Dissolution-Precipitation Creep." *Journal of Structural Geology* 22, nos. 11–12 (November): 1713–1722.

Borg, Iris Y., and John Crawford Maxwell. 1956. "Interpretation of Fabrics of Experimentally Deformed Sands." *American Journal of Science* 254, no. 2 (February 1): 71–81.

Borg, Iris Y., Melvin Friedman, John Handin, and Donald V. Higgs. 1960. "Experimental Deformation of St. Peter Sand: A Study of Cataclastic Flow." In *Rock Deformation (A Symposium)*. Edited by David Griggs and John Handin, 133–191. Boulder, Colorado: Geological Society of America. *Memoir 79*.

Borg, Iris Y., and Hugh C. Heard. 1970. "Experimental Deformation of Plagioclases." In *Experimental and Natural Rock Deformation*. Edited by P. Paulitsch, 375–403. Berlin, Germany: Springer-Verlag.

Borja, Ronaldo I., Kossi M. Sama, and Pablo F. Sanz. 2003. "On the Numerical Integration of Three-Invariant Elastoplastic Constitutive Models." *Computer Methods in Applied Mechanics and Engineering* 192, nos. 9–10 (28 February): 1227–1258.

Borja, Ronaldo I. 2006. "Conditions for Instabilities in Collapsible Solids Including Volume Implosion and Compaction Banding." *Acta Geotechnica* 1 (22 August): 107–122.

Boullier, Anne-Marie, and Y. Guegen. 1975. "SP-Mylonites: Origin of Some Mylonites by Superplastic Flow."

Contributions to Mineralogy and Petrology 50, no. 2 (June): 93–104.

Brime, C. 1999. "Metamorfismo de Bajo Grado: Diferencias en Escala o Diferencias en Grado Metamórfico?" *Trabajos de Geologia* 21, no. 21: 61–66.

Brime, C., John A. Talent, and Ruth Mawson. 2003. "Low-Grade Metamorphism in the Palaeozoic Sequence of the Townsville Hinterland, Northeastern Australia." *Australian Journal of Earth Sciences* 50, no. 5 (October): 751–767.

Bucher, Kurt, and Martin Frey. 2002. *Petrogenesis of Metamorphic Rocks*. 7th ed. Berlin, Germany: Springer-Verlag.

Burkhard, Martin. 1993. "Calcite Twins, Their Geometry, Appearance and Significance as Stress-Strain Markers and Indicators of Tectonic Regime: A Review." *Journal of Structural Geology* 15, nos. 3–5 (March–May): 351–368.

Busch, Jay P., and Ben A. van der Pluijm. 1995. "Calcite Textures, Microstructures and Rheological Properties of Marble Mylonites in the Bancroft Shear Zone, Ontario, Canada." *Journal of Structural Geology* 17, no. 5 (May): 677–688.

Carter, Neville L. 1971. "Static Deformation of Silica and Silicates." *Journal of Geophysical Research* 76, no. 23 (10 August): 5514–5540.

Carter, Neville L., John M. Christie, and David T. Griggs. 1964. "Experimental Deformation and Recrystallization of Quartz." *The Journal of Geology* 72, no. 6 (November): 687–733.

Chapin, Charles E., and Steven M. Cather. 1983. "Eocene Tectonics and Sedimentation in the Colorado Plateau-Rocky Mountain Area." In *Rocky Mountain Foreland Basins and Uplifts*. Edited by J. D. Lowell, 33–56. Denver, Colorado: Rocky Mountain Association of Geologists.

Chapple, William M., and John H. Spang. 1974. "Significance of Layer-Parallel Slip During Folding of Layered Sedimentary Rocks." *Geological Society of America Bulletin* 85, no. 1 (October 1): 1523–1534.

Chester, Frederick M., Judith S. Chester, Andreas K. Kronenberg, and Andrew Hajash. 2007. "Subcritical Creep Compaction of Quartz Sand at Diagenetic Conditions: Effects of Water and Grain Size." *Journal of Geophysical Research* 112, no. B6 (June): B06203. doi:10.1029/2006JB004317.

Chester, Judith S., S. C. Lenz, Frederick M. Chester, and R. A. Lang. 2004. "Mechanisms of Compaction of Quartz Sand at Diagenetic Conditions." *Earth and Planetary Science Letters* 220, nos. 3–4: 435–451.

Christie, John M., David T. Griggs, and Neville L. Carter. 1964. "Experimental Evidence of Basal Slip in Quartz." *The Journal of Geology* 72, no. 6 (November): 734–756.

Christie, John M., and A. J. Ardell. 1974. "Substructures of Deformation Lamellae in Quartz." *Geology* 2, no. 8 (August): 405–408.

Chuhan, Fawad A., Arild Kjeldstad, Knut Bjørlykke, and Kaare Høeg. 2002. "Porosity Loss in Sand by Grain Crushing—Experimental Evidence and Relevance to Reservoir Quality." *Marine and Petroleum Geology* 19, no. 1 (January): 39–53.

Clarey, Timothy. 2020. *Carved in Stone: Geological Evidence of the Worldwide Flood*. Dallas, Texas: Institute for Creation Research.

Clarey, Timothy L., and Davis J. Werner. 2023. "A Progressive Global Flood Model Confirmed by Rock Data Across Five Continents." In *Proceedings of the Ninth International Conference on Creationism*. Edited by John H. Whitmore, 412–445. Cedarville, Ohio: Cedarville University International Conference on Creationism.

Condie, Kent C. 2005. "The Crust." In *Earth as an Evolving Planetary System*. Edited by Kent C. Condie, 13–58. Burlington, New Jersey: Academic Press.

Cooke, Michelle L., and D. D. Pollard. 1997. "Bedding-Plane Slip in Initial Stages of Fault-Related Folding." *Journal of Structural Geology* 19, nos. 3–4 (March): 567–581.

Cooke, Michelle L., and Chad A. Underwood. 2001. "Fracture Termination and Step-over at Bedding Interfaces Due to Frictional Slip and Interface Opening." *Journal of Structural Geology* 23, nos. 2–3 (3 February): 223–238.

Cooke, Michelle L., P. Mollema, D. D. Pollard, and A. Aydin. 2000. "Interlayer Slip and Joint Localization in the East Kaibab Monocline, Utah: Field Evidence and Results from Numerical Modeling." In *Forced Folds and Fractures*. Edited by John W. Cosgrove and Mohammed S. Ameen, 23–49. London: The Geological Society. *Special Publication 169*.

Couples, G. D., and H. Lewis. 1999. "Effects of Interlayer Slip in Model Forced Folds." In *Forced Folds and Fractures*. Edited by John W. Cosgrove and Mohammed S. Ameen, 129–144. London: The Geological Society. *Special Publication 169*.

Cox, Stephen F., and Michael A. Etheridge. 1982. "Fiber Development in Deformed Hydrothermally Altered Acid Volcanic Rock." In *Atlas of Deformational and Metamorphic Rock Fabrics*. Edited by Graham J. Borradaile, M. Brian Bayly, and Chris McA. Powell, 304–305. New York, New York: Springer.

Crook, A. J. L., D. R. J. Owen, S. M. Wilson, and J. G. Yu. 2006. "Benchmarks for the Evolution of Shear Localisation with Large Relative Sliding in Frictional Materials." *Computer Methods in Applied Mechanics and Engineering* 195, nos. 37–40: 4991–5010.

Crossey, Laura J., Karl E. Karlstrom, Abraham E. Springer, Dennis Newell, David R. Hilton, and Tobias Fischer. 2009. "Degassing of Mantle-Derived CO_2 and He from Springs in the Southern Colorado Plateau Region—Neotectonic Connections and Implications for Groundwater Systems." *Geological Society of America Bulletin* 121, nos. 7–8: 1035–1053.

Crossey, Laura J., and Karl E. Karlstrom. 2012. "Travertines and Travertine Springs in Eastern Grand Canyon: What They Tell Us About Groundwater, Paleoclimate, and Incision of Grand Canyon." In *Grand Canyon Geology: Two Billion Years of Earth's History*. Edited by J. Michael Timmons, and Karl E. Karlstrom, 131–143. Boulder, Colorado: Geological Society of America. *Special Paper 489*.

Cundall, P. A., and O. D. L. Strack. 1979. "A Discrete Numerical Model for Granular Assemblies." *Geotechnique* 29, no. 1 (March): 47–65.

Davis, George H. 1978. "Monocline Fold Pattern of the Colorado Plateau." In *Laramide Folding Associated with Basement Block Faulting in the Western United States*. Edited by Vincent Matthews III, 215–233. Boulder, Colorado: Geological Society of America. *Memoir 151*.

Davis, George H., and S. E. Tindall. 1996. "Discovery of Major Right-Handed Laramide Strike-Slip Faulting Along the Eastern Margin of the Kaibab Uplift, Colorado Plateau,

Utah." *EOS, Transactions of the American Geophysical Union* 77, no. 46, F641–F642.

Davis, George H., and Stephen J. Reynolds. 1996. *Structural Geology of Rocks and Regions*. 2nd ed. New York, New York: John Wiley & Sons.

de Boer, R.B., P.J.C. Nagtegaal, and E.M. Duyvis. 1977. "Pressure Solution Experiments on Quartz Sand." *Geochimica et Cosmochimica Acta* 41, no. 2 (February): 257–264.

de Bresser, J.H.P., J.H. ter Heege, and C.J. Spiers. 2001. "Grain Size Reduction by Dynamic Recrystallization: Can it Result in Major Rheological Weakening?" *International Journal of Earth Sciences (Geologische Rundschau)* 90, no. 1 (May): 28–45.

DeCelles, Peter G., and James C. Coogan. 2006. "Regional Structure and Kinematic History of the Sevier Fold-and-Thrust Belt, Central Utah." *Geological Society of America Bulletin* 118, nos. 7–8 (July 1): 841–864.

DeCelles, Peter G., Timothy F. Lawton, and Gautam Mitra. 1995. "Thrust Timing, Growth of Structural Culminations, and Synorogenic Sedimentation in the Type Sevier Orogenic Belt, Western United States." *Geology* 23, no. 8 (August 1): 699–702.

den Brok, Bas. 1996. "The Effect of Crystallographic Orientation on Pressure Solution in Quartzite." *Journal of Structural Geology* 18, no. 6 (June): 859–860.

den Brok, S.W.J. 1998. "Effect of Microcracking on Pressure-Solution Strain Rate: The Gratz Grain-Boundary Model." *Geology* 26, no. 10 (October 1): 915–918.

den Brok, S.W.J., and C.J. Spiers. 1991. "Experimental Evidence for Water Weakening of Quartzite by Microcracking Plus Solution-Precipitation Creep." *Journal of the Geological Society of London* 148, no. 3 (May): 541–548.

Dickinson, William R. 1981. "Plate Tectonic Evolution of the Southern Cordillera." In *Relations of Tectonics to Ore Deposits in the Southern Cordillera.* Edited by William R. Dickinson and William D. Payne, 113–135. Tucson, Arizona: Arizona Geological Society, *Digest 14*.

Dickinson, William R., and Walter S. Snyder. 1978. "Plate Tectonics of the Laramide Orogeny." In *Laramide Folding Associated with Basement Block Faulting in the Western United States*. Edited by Vincent Matthews III, 355–366. Boulder, Colorado: Geological Society of America. *Memoir 151*.

Dickinson, William R., Margaret A. Klute, Michael J. Hayes, Susanne U. Janecke, Erik A. Lundin, Mary A. McKittrick and Mark D. Olivares. 1987. "Laramide Tectonics and Paleogeography Inferred from the Sedimentary Record in Laramide Basins of Central Rocky Mountain Region." *Geological Society of America Abstracts with Programs* 20, no. 5: 271.

Donath, Fred A., and Ronald B. Parker. 1964. "Folds and Folding." *Geological Society of America Bulletin* 75, no. 1 (January 1): 45–62.

Dornbusch, H.-J., K. Weber, and W. Skrotzki. 1994. "Development of Microstructure and Texture in High-Temperature Mylonites from the Ivrea Zone." In *Textures of Geological Materials*. Edited by H.J. Bunge, S. Siegesmund, W. Skrotzki, and K. Weber, 187–201. Oberursel, Germany: DGM Informationsgesellschaft-Verlag.

Dott, Robert H. 1964. "Wacke, Graywacke and Matrix—What Approach to Immature Sandstone Classification?" *Journal of Sedimentary Petrology* 34, no. 3 (September 1): 625–632.

Drury, Martyn R. 1993. "Deformation Lamellae in Metals and Minerals." In *Defects and Processes in the Solid State: Geoscience Applications: The McLaren Volume*. Edited by J.N. Boland, and J.D. Fitz Gerald, 195–212. Amsterdam, The Netherlands: Elsevier.

Drury, Martyn R., F.J. Humphreys, and S.H. White. 1985. "Large Strain Deformation Studies Using Polycrystalline Magnesium as a Rock Analogue. Part II: Dynamic Recrystallization Mechanisms at High Temperatures." *Physics of the Earth and Planetary Interiors* 40, no. 3 (1 November): 208–222.

Drury, Martyn R., and Janos L. Urai. 1990. "Deformation-Related Recrystallization Processes." *Tectonophysics* 172, nos. 3–4 (1 February): 235–253.

Dumitru, Trevor A., Ian R. Duddy, and Paul F. Green. 1994. "Mesozoic-Cenozoic Burial, Uplift, and Erosion History of the West-Central Colorado Plateau." *Geology* 22, no. 6 (June 1): 499–502.

Dumitru, Trevor A., Phillip B. Gans, David A. Foster, and Elizabeth L. Miller. 1991. "Refrigeration of the Western Cordilleran Lithosphere during Laramide Shallow-Angle Subduction." *Geology* 19, no. 11 (November 1): 1145–1148.

Durney, D.W. 1972. "Solution-Transfer, an Important Geological Deformation Mechanism." *Nature* 235, no. 5337 (11 February): 315–317.

Edington, J.W., K.N. Melton, and C.P. Cutler. 1976. "Superplasticity." *Progress in Materials Science* 21, nos. 1–2: 61–170.

Elias, Brian P., and Andrew Hajash, Jr. 1992. "Changes in Quartz Solubility and Porosity Due to Effective Stress: An Experimental Investigation of Pressure Solution." *Geology* 20, no. 5 (May 1): 451–454.

Elston, Donald P. 1989. "Correlations and Facies Changes in Lower and Middle Cambrian Tonto Group, Grand Canyon, Arizona." In *Geology of Grand Canyon, Northern Arizona (with Colorado River Guides)*. Edited by Donald P. Elston, George H. Billingsley, and Richard A. Young, 131–136. Washington, DC: American Geophysical Union.

Epard, J.-L., and Richard H. Groshong Jr. 1995. "Kinematic Model of Detachment Folding Including Limb Rotation, Fixed Hinges and Layer-Parallel Strain." *Tectonophysics* 247, nos. 1–4 (July): 85–103.

Erickson, S. Gregg, and William R. Jamison. 1995. "Viscous-Plastic Finite-Element Models of Fault-Bend Folds." *Journal of Structural Geology* 17, no. 4 (April): 561–573.

Essene, E.J., and D.R. Peacor. 1995. "Clay Mineral Thermometry—A Critical Perspective." *Clays and Clay Minerals* 43 (1 October): 540–553.

Etchecopar, A., and G. Vasseur. 1987. "A 3-D Kinematic Model of Fabric Development in Polycrystalline Aggregates: Comparisons with Experimental and Natural Examples." *Journal of Structural Geology* 9, nos. 5–6: 705–717.

Etheridge, Michael A., Bruce E. Hobbs, and Mervyn S. Paterson. 1973. "Experimental Deformation of Single Crystals of Biotite." *Contributions to Mineralogy and Petrology* 38, no. 1 (March): 21–36.

Etheridge, Michael A., and Bruce E. Hobbs. 1974. "Chemical and Deformational Controls on Recrystallization of Mica." *Contributions to Mineralogy and Petrology* 43, no. 2 (June): 111–124.

Etheridge, Michael A., and J.C. Wilkie. 1979. "Grainsize

Reduction, Grain Boundary Sliding and the Flow Strength of Mylonites." *Tectonophysics* 58, nos. 1–2 (10 September): 159–178.

Etheridge, Michael A., and Ron H. Vernon. 1981. "A Deformed Polymictic Conglomerate—The Influence of Grain Size and Composition on the Mechanism and Rate of Deformation." *Tectonophysics* 79, nos. 3–4 (10 November): 237–254.

Fairbairn, Harold W. 1939. "Correlation of Quartz Deformation with its Crystal Structure." *American Mineralogist* 24, no. 6 (June 1): 351–368.

Fitz Gerald, J.D., Michael A. Etheridge, and Ron H. Vernon. 1983. "Dynamic Recrystallization in a Naturally Deformed Albite." *Textures and Microstructures* 5: 219–237.

Flowers, Rebecca M., David L. Shuster, B.P. Wernicke, and Ken A. Farley. 2007. "Radiation Damage Control on Apatite (U-Th)/He Dates from the Grand Canyon Region, Colorado Plateau." *Geology* 35, no. 5 (May 1): 447–450.

Flowers, Rebecca M., B.P. Wernicke, and Ken A. Farley. 2008. "Unroofing, Incision and Uplift History of the Southwestern Colorado Plateau from Apatite (U-Th)/He Thermochronometry." *Geological Society of America Bulletin* 120, nos. 5–6 (May 1): 571–587.

Flowers, Rebecca M., and Ken A. Farley. 2012. "Apatite ^{4}He/^{3}He and (U-Th)/He Evidence for an Ancient Grand Canyon." *Science* 338, no. 6114 (29 November): 1616–1619.

Flowers, Rebecca M., Richard A. Ketcham, David L. Shuster, and Ken A. Farley. 2009. "Apatite (U–Th)/He Thermochronometry Using a Radiation Damage Accumulation and Annealing Model." *Geochimica et Cosmochimica Acta* 73, no. 8 (15 April): 2347–2365.

Folk, Robert Louis. 1955. "Student Operator Error in Determination of Roundness, Sphericity, and Grain Size." *Journal of Sedimentary Petrology* 25, no. 4 (1 December): 297–301.

Folk, Robert L. 1966. "A Review of Grain-Size Parameters." *Sedimentology* 6, no. 2 (March): 73–93.

Folk, Robert L. 1980. *Petrology of Sedimentary Rocks*. Austin, Texas: Hemphill Publishing Co.

Fossen, Haakon. 2016. *Structural Geology*. 2nd ed. Cambridge, United Kingdom: Cambridge University Press.

Foster, John R. 2011. "Trilobites and Other Fauna from Two Quarries in the Bright Angel Shale (Middle Cambrian, Series 3, Delamaran), Grand Canyon National Park, Arizona." In *Cambrian Stratigraphy and Paleontology of Northern Arizona and Southern Nevada, The 16th Field Conference of the Cambrian Stage Subdivision Working Group, International Subcommission on Cambrian Stratigraphy, Flagstaff, Arizona, and Southern Nevada, United States.* Edited by J. Stewart Hollingsworth, Frederick A. Sundberg, and John R. Foster, 99–120. Flagstaff, Arizona: Museum of Northern Arizona. *Bulletin 67*.

Frey, Martin, and Hanan J. Kisch. 1987. "Scope of Subject." In *Low Temperature Metamorphism*. Edited by Martin Frey, 1–8. Glasgow, United Kingdom: Blackie.

Frey, Martin, and D. Robinson. eds. 1999. *Low-Grade Metamorphism*. London, United Kingdom: Blackwell Science.

Friedman, Melvin. 1963. "Petrofabric Analysis of Experimentally Deformed Calcite-Cemented Sandstones." *The Journal of Geology* 71, no. 1 (January): 12–37.

Friedman, Melvin, John Handin, John M. Logan, Kyung D. Min, and D.W. Stearns. 1976. "Experimental Folding of Rocks Under Confining Pressure: Part III. Faulted Drape Folds in Multilithologic Layered Specimens." *Geological Society of America Bulletin* 87, no. 7 (July 1): 1049–1066.

Friedman, Melvin, R.H.H. Hugman III, and John Handin. 1980. "Experimental Folding of Rocks Under Confining Pressure, Part VIII—Forced Folding of Unconsolidated Sand and of Lubricated Layers of Limestone and Sandstone." *Geological Society of America Bulletin* 91, no. 5 (May 1): 307–312.

Gallagher, J.J. Jr., Melvin Friedman, John Handin, and G.M. Sowers. 1974. "Experimental Studies Relating to Microfracture in Sandstone." *Tectonophysics* 21, no. 3 (February): 203–247.

Gangi, Anthony F., Kyung D. Min, and John M. Logan. 1977. "Experimental Folding of Rocks Under Confining Pressure: Part IV—Theoretical Analysis of Faulted Drape-Folds." *Tectonophysics* 42, nos. 2–4 (20 October): 227–260.

Gapais, Denis. 1989. "Shear Structures Within Deformed Granites: Mechanical and Thermal Indicators." *Geology* 17, no. 12 (December 1): 1144–1147.

Gehrels, George E., Ronald C. Blakey, Karl E. Karlstrom, J. Michael Timmons, William Dickinson, and Mark Pecha. 2011. "Detrital Zircon U-Pb Geochronology of Paleozoic Strata in the Grand Canyon, Arizona." *Lithosphere* 3, no. 3 (June 1): 183–200.

Ghosh, Subir Kumar. 1968. "Experiments of Buckling of Multilayers which Permit Interlayer Gliding." *Tectonophysics* 6, no. 3 (September): 207–249.

Gilotti, Jane A., and Joseph M. Hull. 1990. "Phenomenological Superplasticity in Rocks." In *Deformation Mechanisms, Rheology and Tectonics*. Edited by Robert J. Knipe, and Ernest H. Rutter, 229–240. London, United Kingdom: Geological Society of London. *Special Paper 54*.

Goodwin, Laurel B., and Basil Tikoff. 2002. "Competency Contrast, Kinematics, and the Development of Foliations and Lineations in the Crust." *Journal of Structural Geology* 24, nos. 6–7 (June–July): 1065–1085.

Gottstein, G., and H. Mecking. 1985. "Recrystallization." In *Preferred Orientation in Deformed Metals and Rocks: An Introduction to Modern Texture Analysis*. Edited by Hans-Rudolf Wenk, 183–218. London, United Kingdom: Academic Press.

Gratier, J.-P., J. Richard, F. Renard, S. Mittempergher, M.-L. Doan, G. Di Toro, J. Hadizadeh, and A.-M. Boullier. 2011. "Aseismic Sliding of Active Faults by Pressure Solution Creep: Evidence from the San Andreas Fault Observatory at Depth." *Geology* 39, no. 12 (December 1): 1131–1134.

Green, Harry W. 1992. "Analysis of Deformation in Geological Materials." In *Minerals and Reactions at the Atomic Scale: Transmission Electron Microscopy*. Edited by Peter R. Buseck, 425–454. Washington, DC: Mineralogical Society of America. *Reviews in Mineralogy*, vol. 27.

Green, H.W., and S.V. Radcliffe. 1972. "The Nature of Deformation Lamellae in Silicates." *Bulletin of the Geological Society of America* 83, no. 3 (March): 847–852.

Green, H.W., David T. Griggs, and John M. Christie. 1970. "Syntectonic and Annealing Recrystallization of Fine-Grained Quartz Aggregates." In *Experimental and Natural Rock Deformation*. Edited by Peter Paulitsch, 272–335. Berlin, Germany: Springer-Verlag.

Griggs, David T. 1936. "Deformation of Rocks Under High Confining Pressures: I. Experiments at Room Temperature." *The Journal of Geology* 44, no. 5 (July–August): 541–577.

Griggs, David T. 1939. "Creep of Rocks." *The Journal of Geology* 47, no. 3 (April–May): 225–251.

Griggs, David T. 1974. "A Model of Hydrolytic Weakening in Quartz." *Journal of Geophysical Research* 79, no. 11 (10 April): 1653–1661.

Griggs, David T., M.S. Paterson, H.C. Heard, and Fred J. Turner. 1960. "Annealing Recrystallization in Calcite Crystals and Aggregates." Boulder, Colorado: Geological Society of America. *Memoir* 79, 21–37.

Groshong, Richard H. Jr. 1988. "Low-Temperature Deformation Mechanisms and Their Interpretation." *Geological Society of America Bulletin* 100, no. 9 (September 1): 1329–1360.

Groves, G.W., and A. Kelly. 1963. "Independent Slip Systems in Crystals." *Philosophical Magazine* 8, no. 89 (20 August): 877–887.

Guiton, Martin L.E., Yves M. Leroy, and William Sassi. 2003. "Activation of Diffuse Discontinuities and Folding of Sedimentary Layers." *Journal of Geophysical Research* 108, no. B4 (April): 2183. doi:10.1029/2002JB001770.

Hafner, W. 1951. "Stress Distributions and Faulting." *Geological Society of America Bulletin* 62, no. 4 (April 1): 373–398.

Handin, John, Melvin Friedman, Kyung D. Min, and L.J. Pattison. 1976. "Experimental Folding of Rocks Under Confining Pressure: Part II. Buckling of Multi-Layered Rock Beams." *Geological Society of America Bulletin* 87, no. 7 (July): 1035–1048.

Hansen, Edward C., and Iris Y. Borg. 1962. "The Dynamic Significance of Deformation Lamellae in Quartz of a Calcite-Cemented Sandstone." *American Journal of Science* 260, no. 5 (1 May): 321–336.

Hansen, Edward C., Iris Y. Borg, and John C. Maxwell. 1959. "Dynamic Significance of Quartz Lamellae." *Journal of Geophysical Research* 64, no. 8 (August): 1104–1105.

Hansen, L.N., Mark E. Zimmerman, and D.L. Kohlstedt. 2011. "Grain Boundary Sliding in San Carlos Olivine: Flow Law Parameters and Crystallographic-Preferred Orientation." *Journal of Geophysical Research* 116, no. B8: B08201. doi:10.1029/2011JB008220.

Harrison, Tim Mark, Richard Lee Armstrong, C.W. Naeser, and J.E. Harakal. 1979. "Geochronology and Thermal History of the Coast Plutonic Complex, near Prince Rupert, British Columbia." *Canadian Journal of Earth Sciences* 16, no. 3 (March): 400–410.

Hatcher, Robert D. Jr., and Christopher M. Bailey. 2020. *Structural Geology*. 3rd ed. New York, New York: Oxford University Press.

Hennig-Michae, Christa. 1977. "Microscopic Structure Studies of Experimentally and Naturally Deformed Hematite Ores." *Tectonophysics* 39, nos. 1–3 (20 April): 255–271.

Hill, Carol A., and Steve O. Moshier. 2009. "Flood Geology and the Grand Canyon: A Critique." *Perspectives on Science and Christian Faith* 61, no. 2 (June): 99–115.

Hillier, S., J. Mátyás, A. Matter, and G. Vasseur. 1995. "Illite/Smectite Diagenesis and Its Variable Correlation with Vitrinite Reflectants in the Pannonian Basin." *Clays and Clay Minerals* 43 (1 April): 174–183.

Hippertt, J.F. 1994. "Microstructures and *C*-Axis Fabrics Indicative of Quartz Dissolution in Sheared Quartzites and Phyllonites." *Tectonophysics* 229, nos. 3–4 (30 January): 141–163.

Hiraga, Takehiko, Tomonori Miyazaki, Hidehiro Yoshida, and Mark E. Zimmerman. 2013. "Comparison of Microstructures in Superplastically Deformed Synthetic Materials and Natural Mylonites: Mineral Aggregation via Grain Boundary Sliding." *Geology* 41, no. 9 (September): 959–962.

Hirth, Greg, and Jan Tullis. 1992. "Dislocation Creep Regimes in Quartz Aggregates." *Journal of Structural Geology* 14, no. 2 (February): 145–159.

Hobbs, Bruce E. 1968. "Recrystallization of Single Crystals of Quartz." *Tectonophysics* 6, no. 5 (November): 353–401.

Hobbs, Bruce. E., A.C. McLaren, and M.S. Patterson. 1972. "Plasticity of Single Crystals of Synthetic Quartz." In *Flow and Fracture of Rocks*. Edited by Hugh C. Heard, Iris Y. Borg, Neville L. Carter, and C.B. Raleigh, 29–53. Washington DC: American Geophysical Union. *Geophysical Monograph Series*, vol. 16.

Hobbs, Bruce E., Winthrop D. Means, and Paul F. Williams. 1976. *An Outline of Structural Geology*. New York, New York: Wiley.

Horne, Richard, and Nicholas Culshaw. 2001. "Flexural-Slip Folding in the Meguma Group, Nova Scotia, Canada." *Journal of Structural Geology* 23, no. 10 (October): 1631–1652.

Hower, J. 1981. "Shale Diagenesis." In *Clays and the Resource Geologist*. Edited by Fred J. Longstaffe, 60–80. Quebec City, Canada: Mineralogical Association of Canada. *Short Course Handbook 7*.

Huang, Wuu-Liang, John M. Longo, and David R. Pevear. 1993. "An Experimentally Derived Kinetic Model for Smectite-to-Illite Conversion and Its Use as a Geothermometer." *Clays and Clay Minerals* 41, no. 2 (1 April): 162–177.

Hubbert, M. King. 1951. "Mechanical Basis for Certain Familiar Geologic Structures." *Geological Society of America Bulletin* 62, no. 4 (April 1): 355–372.

Hughes, Amanda N., and John H. Shaw. 2015. "Insights into the Mechanics of Fault-Propagation Folding Style." *Geological Society of America Bulletin* 127, nos. 11–12 (November 1): 1752–1765.

Huntoon, Peter W. 1993. "Influence of Inherited Precambrian Basement Structure on the Localization and Form of Laramide Monoclines, Grand Canyon, Arizona." In *Laramide Basement Deformation in the Rocky Mountain Foreland of the Western United States*. Edited by Christopher J. Schmidt, Ronald B. Chase, and Eric A. Erslev, 243–256. Boulder, Colorado: Geological Society of America. *Special Paper 280*.

Huntoon, Peter W. 2003. "Post-Precambrian Tectonism in the Grand Canyon Region." In *Grand Canyon Geology*. 2nd ed. Edited by Stanley S. Beus, and Michael Morales, 222–259. New York, New York: Oxford University Press.

Hurford, Anthony J. 1985. "On the Closure Temperature for Fission Tracks in Zircon." *Nuclear Tracks and Radiation Measurements* 10, no. 3 (January): 415.

Ilg, Bradley R., Karl E. Karlstrom, David P. Hawkins, and Michael L. Williams. 1996. "Tectonic Evolution of Paleoproterozoic Rocks in the Grand Canyon: Insights into Middle-Crustal Processes." *Geological Society of America Bulletin* 108, no. 9 (September 1): 1149–1166.

Ingerson, Earl, and Joseph L. Ramisch. 1942. "Origin of Shapes of Quartz Sand Grains." *American Mineralogist* 27, no. 9 (1 September): 595–606.

Ismat, Zeshan, and Gautam Mitra. 2005. "Fold-Thrust Belt Evolution Expressed in an Internal Thrust Sheet, Sevier Orogen: The Role of Cataclastic Flow." *Geological Society of America Bulletin* 117, nos. 5–6 (May 1): 764–782.

Jackson, Ian, Ulrich H. Faul, and Richard Skelton. 2014. "Elastically Accommodated Grain-Boundary Sliding: New Insights from Experiment and Modeling." *Physics of the Earth and Planetary Interiors* 228 (March): 203–210.

Jessell, M.W. 1988a. "Simulation of Fabric Development in Recrystallizing Aggregates—I. Description of the Model." *Journal of Structural Geology* 10, no. 8: 771–778.

Jessell, M.W. 1988b. "Simulation of Fabric Development in Recrystallizing Aggregates—II. Example Model Runs." *Journal of Structural Geology* 10, no. 8: 779–793.

Johnson, Scott E., Ron H. Vernon, and Phaedra Upton. 2004. "Foliation Development and Progressive Strain-Rate Partitioning in the Crystallizing Carapace of a Tonalite Pluton: Microstructural Evidence and Numerical Modeling." *Journal of Structural Geology* 26, no. 10: 1845–1865.

Jones, Craig H., G. Lang Farmer, Brad Sageman, and Shijie Zhong. 2011. "Hydrodynamic Mechanism for the Laramide Orogeny." *Geosphere* 7, no. 1 (February 1): 183–201.

Kamb, W. Barclay. 1959. "Theory of Preferred Crystal Orientation Developed by Crystallization Under Stress." *The Journal of Geology* 67, no. 2 (March): 153–170.

Karlstrom, Karl E., and J. Michael Timmons. 2012. "Faulting and Uplift in the Grand Canyon Region." In *Grand Canyon Geology: Two Billion Years of Earth's History*. Edited by J. Michael Timmons, and Karl E. Karlstrom, 93–107. Boulder, Colorado: Geological Society of America. *Special Paper 489*.

Karlstrom, Karl E., Bradley R. Ilg, Michael L. Williams, David P. Hawkins, Samuel A. Bowring, and S.J. Seaman. 2003. "Paleoproterozoic Rocks of the Granite Gorges." In *Grand Canyon Geology*. 2nd ed. Edited by Stanley S. Beus, and Michael Morales, 9–38. New York, New York: Oxford University Press.

Karlstrom, Karl E., J. Michael Timmons, and Laura J. Crossey. 2012. "Introduction to Grand Canyon Geology." In *Grand Canyon Geology: Two Billion Years of Earth's History*. Edited by J. Michael Timmons, and Karl E. Karlstrom, 1–6. Boulder, Colorado: Geological Society of America. *Special Paper 489*.

Karlstrom, Karl E., James W. Hagadorn, George E. Gehrels, William Matthews, Mark D. Schmitz, Lauren Madronich, Jacob Mulder, Mark Pecha, Dominique Giesler, and Laura J. Crossey. 2018. "Cambrian Sauk Transgression in the Grand Canyon Region Redefined by Detrital Zircons." *Nature Geoscience* 11, no. 6 (28 May): 438–443.

Karlstrom, Karl E., M.T. Mohr, Mark D. Schmitz, Frederick A. Sundberg, S.M. Rowland, Ronald C. Blakey, John R. Foster, Laura J. Crossey, Carol M. Dehler and James W. Hagadorn. 2020. "Redefining the Tonto Group of Grand Canyon and Recalibrating the Cambrian Time Scale." *Geology* 48, no. 5: 425–430.

Karner, Stephen L., Frederick M. Chester, Andreas K. Kronenberg, and Judith S. Chester. 2003. "Subcritical Compaction and Yielding of Granular Quartz Sand." *Tectonophysics* 377, nos. 3–4 (31 December): 357–381.

Kelley, Shari A., Charles E. Chapin, and Karl E. Karlstrom. 2001. "Laramide Cooling Histories of the Grand Canyon, Arizona, and the Front Range, Colorado, Determined from Apatite Fission-Track Thermochronology." In *Colorado River: Origin and Evolution*. Edited by Richard A. Young and Earle E. Spamer, 37–42. Grand Canyon, Arizona: Grand Canyon Association. *Monograph 12*.

Kelley, Shari A., and Karl E. Karlstrom. 2012. "The Laramide and Post-Laramide Uplift and Erosional History of the Eastern Grand Canyon: Evidence from Apatite Fission-Track Thermochronology." In *Grand Canyon Geology: Two Billion Years of Earth's History*. Edited by J. Michael Timmons and Karl E. Karlstrom, 109–117. Boulder, Colorado: Geological Society of America. *Special Paper 489*.

Kelly, Anthony, and G.W. Groves. 1970. *Crystallography and Crystal Defects*. London, United Kingdom: Longman.

Kenkmann, Thomas., and Georg Dresen. 2002. "Dislocation Microstructure and Phase Distribution in a Lower Crustal Shear Zone—An Example from the Ivrea-Zone, Italy." *International Journal of Earth Sciences (Geologische Rundschau)* 91, no. 3 (8 December): 445–458.

Kennedy, L.A., and J.C. White. 2001. "Low-Temperature Recrystallization in Calcite: Mechanisms and Consequences." *Geology* 29, no. 11 (November 1): 1027–1030.

Khan, M. Ibrahim, and M. Rafiqul Islam. 2008. "Reservoir Engineering and Secondary Recovery." In *The Petroleum Engineering Handbook: Sustainable Operations*. Edited by M. Ibrahim Khan, and M.R. Islam, 189–241. Amsterdam, The Netherlands: Elsevier, Gulf Publishing Company Imprint.

Kisch, H.J. 1983. "Mineralogy and Petrology of Burial Diagenesis (Burial Metamorphism) and Incipient Metamorphism in Clastic Rocks." In *Diagenesis in Sediments and Sedimentary Rocks*. Vol. 2. Edited by Gunnar Larsen, and George V. Chilingar, 289–493. Amsterdam, The Netherlands: Elsevier.

Kisch, H.J. 1987. "Correlation Between Indicators of Very Low-Grade Metamorphism." In *Low Temperature Metamorphism*. Edited by Martin Frey, 227–304. New York, New York: Chapman and Hall.

Kisch, H.J. 1991. "Illite Crystallinity: Recommendations on Sample Preparation, X-Ray Diffraction Settings, and Interlaboratory Samples." *Journal of Metamorphic Geology* 9, no. 6 (November): 665–670.

Knipe, Robert J. 1989. "Deformation Mechanisms—Recognition from Natural Tectonites." *Journal of Structural Geology* 11, nos. 1–2: 127–146.

Kruhl, Jörn H. 2001. "Crystallographic Control on the Development of Foam Textures in Quartz, Plagioclase and Analogue Material." *International Journal of Earth Sciences (Geologische Rundschau)* 90, no. 1 (22 March): 104–117.

Kruhl, Jörn H., and Mark Peternell. 2002. "The Equilibration of High-Angle Grain Boundaries in Dynamically Recrystallized Quartz: The Effect of Crystallography and Temperature." *Journal of Structural Geology* 24, nos. 6–7 (June–July): 1125–1137.

Kübler, B. 1964. "Les Argiles, Indicateurs de Métamorphisme." *Revue de L'Institut Française de Pétrole* 19: 1093–1112.

Kübler, B. 1967. "La Cristallinité d'Illite et les Zones Tout à Fait Supérieures du Métamorphisme." In *Etages Tectoniques, Colloque de Neûchatel*, 105–122. Neûchatel, Switzerland: Institute de Géologie, Université de Neûchatel.

Kübler, B. 1968. "Evaluation Quantitative de Métamorphisme par la Cristallinité de l'Illite." *Centre de Recherches de Pau Société Nationale de Pétroles d'Aquitaine Bulletin* 2: 385–397.

Kübler, B., and D. Goy-Eggenberger. 2001. "La Cristallinité de l'Illite Revisitée: un-Bilan des Connaissances Acquises ces Trente Dernières Années." *Clay Minerals* 36, no. 2 (June): 143–157.

Kuenen, P.H. and L.U. de Sitter. 1938. "Experimental Investigation into the Mechanism of Folding." *Leidshe Geologische Mededeelingen* 10: 217–240.

Lafrance, B., Barbara E. John, and James S. Scoates. 1996. "Syn-Emplacement Recrystallization and Deformation Microstructures in the Poe Mountain Anorthosite, Wyoming." *Contributions to Mineralogy and Petrology* 122, no. 4 (January): 431–440.

Laney, Randy, and A. William Laughlin. 1981. "Natural Annealing of Pleochroic Haloes in Biotite Samples from Deep Drill Holes, Fenton Hill, New Mexico." *Geophysical Research Letters* 8, no. 5 (May): 501–504.

Langdon, Terence G. 1970. "Grain Boundary Sliding as a Deformation Mechanism During Creep." *The Philosophical Magazine* 22, no. 178: 689–700.

Law, Richard D. 1990. "Crystallographic Fabrics: A Selective Review of Their Applications to Research in Structural Geology." In *Deformation Mechanisms, Rheology and Tectonics*. Edited by Robert J. Knipe, and Ernest H. Rutter, 335–352. London, United Kingdom: Geological Society of London. *Special Paper 54*.

Law, Richard D. 2014. "Deformation Thermometry Based on Quartz *c*-Axis Fabrics and Recrystallization Microstructures: A Review." *Journal of Structural Geology* 66 (September): 129–161.

Lee, L.C., and S.J. Morris. 2010. "Anelasticity and Grain Boundary Sliding." *Proceedings of the Royal Society A* 466, no. 2121 (24 March): 2651–2671.

Lee, L.C., S.J.S. Morris, and J. Wilkening. 2011. "Stress Concentrations, Diffusionally Accommodated Grain Boundary Sliding and the Viscoelasticity of Polycrystals." *Proceedings of the Royal Society A* 467, no. 2130 (22 December): 1624–1644.

Lister, Gordon S., Mervyn S. Paterson, and Bruce E. Hobbs. 1978. "The Simulation of Fabric Development in Plastic Deformation and its Application to Quartzite: The Model." *Tectonophysics* 45, nos. 2–3 (February): 107–158.

Lister, Gordon S., and Bruce E. Hobbs. 1980. "The Simulation of Fabric Development During Plastic Deformation and its Application to Quartzite: The Influence of Deformation History." *Journal of Structural Geology* 2, no. 3: 355–370.

Liu, Lijun, Michael Gurnis, Maria Seton, Jason Saleeby, R. Dietmar Müller, and Jennifer M. Jackson. 2010. "The Role of Oceanic Plateau Subduction in the Laramide Orogeny." *Nature Geoscience* 3, no. 5 (28 March): 353–357.

Lloyd, Geoffrey E., and Brett Freeman. 1994. "Dynamic Recrystallization of Quartz Under Greenschist Conditions." *Journal of Structural Geology* 16, no. 6 (June): 867–881.

Lonergan, Lidia, Claudio Borlandelli, Ashley Taylor, Mark Quine, and Kevin Flanagan. 2007. "The Three-Dimensional Geometry of Sandstone Injection Complexes in the Gryphon Field, United Kingdom, North Sea." In *Sand Injectites: Implications for Hydrocarbon Exploration and Production*. Edited by A. Hurst, and J. Cartwright, 103–112. Tulsa, Oklahoma: The American Association of Petroleum Geologists. *Memoir 87*.

Maltman, Alex. 1984. "On the Term 'Soft-Sediment Deformation.'" *Journal of Structural Geology* 6, no. 5: 589-592.

Mancktelow, Neil S., and Giorgio Pennacchioni. 2004. "The Influence of Grain Boundary Fluids on the Microstructure of Quartz-Feldspar Mylonites." *Journal of Structural Geology* 26, no. 1 (January): 47–69.

Mares, V.M., and A.K. Kronenberg. 1993. "Experimental Deformation of Muscovite." *Journal of Structural Geology* 15, nos. 9–10 (September–October): 1061–1075.

Martin, Daryl L. 1985. "Depositional Systems and Ichnology of the Bright Angel Shale (Cambrian), Eastern Grand Canyon, Arizona." Master's thesis (unpublished manuscript). Flagstaff, Arizona: Northern Arizona University.

Masberg, H.P., E. Hoffer, and S. Hoernes. 1992. "Microfabrics Indicating Granulite-Facies Metamorphism in the Low-Pressure Central Damara Orogen, Namibia." *Precambrian Research* 55, nos. 1–4 (March): 243–257.

Massey, Matthew A., David J. Prior, and David P. Moecher. 2011. "Microstructure and Crystallographic Preferred Orientation of Polycrystalline Microgarnet Aggregates Developed During Progressive Creep, Recovery, and Grain Boundary Sliding." *Journal of Structural Geology* 33, no. 4 (April): 713–730.

Matsuoka, Hajime, and Teruo Nakai. 1974. "Stress-Deformation and Strength Characteristics of Soil under Three Different Principal Stresses." *Proceedings of Japan Society of Civil Engineers* 232 (December): 59–70.

Matthews, Vincent, III, ed. 1978. *Laramide Folding Associated with Basement Block Faulting in the Western United States*. Boulder, Colorado: Geological Society of America. *Memoir 151*.

Matthews, William, Bernard Guest, and Lauren Madronich. 2018. "Latest Neoproterozoic to Cambrian Detrital Zircon Facies of Western Laurentia." *Geosphere* 14, no. 1 (February): 243–264.

Maxwell, John C. 1960. "Experiments on Compaction and Cementation of Sand." In *Rock Deformation (A Symposium)*. Edited by David Griggs and John Handin, 105–132. Boulder, Colorado: Geological Society of America. *Memoir 79*.

McBride, Earle F. 1963. "A Classification of Common Sandstones." *Journal of Sedimentary Petrology* 33, no. 3 (1 September): 664–669.

McClay, K.R. 1977. "Pressure Solution and Coble Creep in Rocks and Minerals: A Review." *Journal of the Geological Society of London* 134, no. 1 (October): 57–70.

McKee, Edwin D. 1932. "Some Fucoids from the Grand Canyon." *Grand Canyon Study Notes* 7, no. 8 (October): 58-161.

McKee, Edwin D. 1945. "Stratigraphy and Ecology of the Grand Canyon Cambrian: Part 1. Cambrian History of the Grand Canyon Region." *Carnegie Institute of Washington Publication* 563, 1–168. Washington, D.C.: Carnegie Institute of Washington.

McLaren, A.C., and J.A. Retchford. 1969. "Transmission Electron Microscope Study of the Dislocations in Plastically Deformed Synthetic Quartz." *Physica Status Solidi* 33, no. 2: 657–668.

McRae, Stuart G. 1972. "Glauconite." *Earth-Science Reviews* 8, no. 4 (December): 397–440.

Means, W.D., and Z.G. Xia. 1981. "Deformation of Crystalline Materials in Thin Section." *Geology* 9, no. 11 (November 1): 538–543.

Means, W.D. 1989. "Synkinematic Microscopy of Transparent Polycrystals." *Journal of Structural Geology* 11, no. 1–2:163–174.

Means, W.D. 1990. "Kinematics, Stress, Deformation and Material Behavior." *Journal of Structural Geology* 12, no. 8: 953–971.

Menegon, Luca, Florian Fusseis, Holger Stünitz, and Xianghui Xiao. 2015. "Creep Cavitation Bands Control Porosity and Fluid Flow in Lower Crustal Shear Zones." *Geology* 43, no. 3 (March): 227–230.

Middleton, Larry T., and David K. Elliott. 2003. "Tonto Group." In *Grand Canyon Geology*. 2nd ed. Edited by Stanley S. Beus and Michael Morales, 90–106. New York, New York: Oxford University Press.

Mitra, Shankar, and Jan Tullis. 1979. "A Comparison of Intracrystalline Deformation in Naturally and Experimentally Deformed Quartzites." *Tectonophysics* 53, nos. 1–2 (1 March): T21–T27.

Miyakawa, Kazuya, and Iwao Kawabe. 2014. "Pressure Solution of Quartz Aggregates Under Low Effective Stress (0.42–0.61MPa) at 25–45°C." *Applied Geochemistry* 40 (January): 61–69.

Morales, Michael. 2003. "Mesozoic and Cenozoic Strata of the Colorado Plateau near the Grand Canyon." In *Grand Canyon Geology*. 2nd edition. Edited by Stanley S. Beus, and Michael Morales, 212–221. New York, New York: Oxford University Press.

Morris, S.J.S., and Ian Jackson. 2009. "Diffusionally Assisted Grain-Boundary Sliding and Viscoelasticity of Polycrystals." *Journal of Mechanics and Physics of Solids* 57, no. 4 (April): 744–761.

Mühlhaus, H.-B., F. Dufour, L. Moresi, and Bruce E. Hobbs. 2002. "A Director Theory for Visco-Elastic Folding Instabilities in Multilayered Rock." *International Journal of Solids and Structures* 39, nos. 13–14 (June–July): 3675–3691.

Mukai, Hiroki, Håkon Austrheim, Christine V. Putnis, and Andrew Putnis. 2014. "Textural Evolution of Plagioclase Feldspar Across a Shear Zone: Implications for Deformation Mechanism and Rock Strength." *Journal of Petrology* 55, no. 8 (August): 1457–1477.

Murrell, Stanley A.F. 1990. "Brittle-to-Ductile Transitions in Polycrystalline Non-Metallic Materials." In *Deformation Processes in Minerals, Ceramics and Rocks*. Edited by D.J. Barber, and P.G. Meredith, 109–137. Boston, Massachusetts: Unwin Hyman.

Nabavi, Seyed Tohid, and Haakon Fossen. 2021. "Fold Geometry and Folding—A Review." *Earth-Science Reviews* 222 (November): 103812

Naeser, Chris W., Ian R. Duddy, Donald P. Elston, Terry A. Dumitru, and Paul F. Green. 1989. "Fission-Track Dating: Ages for Cambrian Strata and Laramide and Post-Middle Eocene Cooling Events from the Grand Canyon, Arizona." In *Geology of Grand Canyon, Northern Arizona (with Colorado River Guides): Lees Ferry to Pierce Ferry, Arizona*. Edited by Donald P. Elston, George H. Billingsley, and Richard A. Young, 139–144. Washington, DC: American Geophysical Union.

Naeser, Chris W., Ian R. Duddy, Donald P. Elston, Terry A. Dumitru and Paul F. Green. 2001. "Fission-Track Analysis of Apatite and Zircon from the Grand Canyon, Arizona." In *Colorado River: Origin and Evolution*. Edited by Richard A. Young and Earle E. Spamer, 31–36. Grand Canyon, Arizona: Grand Canyon Association. *Monograph 12*.

Narr, W., and John Suppe. 1991. "Joint Spacing in Sedimentary Rocks." *Journal of Structural Geology* 13, no. 9: 1037–1048.

Nicolas, A., and Jean-Paul Poirier. 1976. *Crystalline Plasticity and Solid State Flow in Metamorphic Rocks*. New York, New York: Wiley Interscience.

Niño, Fernando, Hervé Philip, and Jean Chéry. 1998. "The Role of Bed-Parallel Slip in the Formation of Blind Thrust Faults." *Journal of Structural Geology* 20, no. 5 (14 May): 503–516.

Noble, Levi F. 1914. "The Shinumo Quadrangle, Grand Canyon District, Arizona." *U.S. Geological Survey Bulletin* 549.

Noble, Levi F. 1922. "A Section of the Paleozoic Formations of the Grand Canyon at the Bass Trail." *U.S. Geological Survey Professional Paper* 131-B: 23–73.

Owen, G. 1987. "Deformation Processes in Unconsolidated Sands." In *Deformation of Sediments and Sedimentary Rocks*. Edited by M.E. Jones, and R.M.F. Preston, 11–24. Oxford, United Kingdom: Blackwell Scientific Publications. *Geological Society Special Publication 29*.

Passchier, Cees W., and Rudolph A.J. Trouw. 1996. *Microtectonics*. Berlin, Germany: Springer-Verlag.

Paterson, Mervyn S., and Francis J. Turner. 1970. "Experimental Deformation of Constrained Crystals of Calcite in Extension." In *Experimental and Natural Rock Deformation*. Edited by P. Paulitsch, 109–141. Berlin, Germany: Springer-Verlag.

Paterson, Mervyn S. 1978. *Experimental Rock Deformation—The Brittle Field*. Berlin, Germany: Springer-Verlag.

Paterson, Mervyn S. 2001. "A Granular Flow Theory for the Deformation of Partially Molten Rock." *Tectonophysics* 335, nos. 1–2 (25 June): 51–61.

Peak, B.A., Rebecca M. Flowers, F.A. Macdonald, and J.M. Cottle. 2021. "Zircon (U-Th)/He Thermochronology Reveals Pre-Great Unconformity Paleotopography in the Grand Canyon Region, USA." *Geology* 49, no. 12 (August 12): 1462–1466.

Peters, Shanan E., and Robert R. Gaines. 2012. "Formation of the 'Great Unconformity' as a Trigger for the Cambrian Explosion." *Nature* 484, no. 7394 (April 18): 363–366.

Pettijohn, Francis J. 1954. "Classification of Sandstones." *The Journal of Geology* 62, no. 4 (July): 360–365.

Pettijohn, Francis J. 1957. *Sedimentary Rocks*. New York, New York: Harper.

Pettijohn, Francis J., Paul E. Potter, and Raymond Siever. 1973. *Sand and Sandstone*. Berlin, Germany: Springer-Verlag.

Poirier, Jean-Paul., and Michel Guillopé. 1979. "Deformation Induced Recrystallization of Minerals." *Bulletin de Minéralogie* 102, nos. 2–3: 67–74.

Poirier, Jean-Paul. 1985. *Creep of Crystals. High-Temperature Deformation Processes in Metals, Ceramics and Minerals*. New York, New York: Cambridge University Press.

Pollastro, Richard M. 1993. "Considerations and Applications of the Illite/Smectite Geothermometer in Hydrocarbon-Bearing Rocks of Miocene to Mississippian Age." *Clays and Clay Minerals* 41, no. 2 (1 April): 119–133.

Powell, Chris McA. 1982. "Overgrowths and Mica Beards on

Rounded Quartz Grains Enclosed by Cleavage Folia." In *Atlas of Deformational and Metamorphic Rock Fabrics*. Edited by Graham J. Borradaile, M. Brian Bayly, and Chris McA. Powell, 300–301. New York, New York: Springer-Verlag.

Powers, Maurice Cary. 1953. "A New Roundness Scale for Sedimentary Particles." *Journal of Sedimentary Petrology* 23, no. 2: 117–119.

Pytte, A.M., and R.C. Reynolds. 1989. "The Thermal Transformation of Smectite to Illite." In *Thermal History of Sedimentary Basins*. Edited by Nancy D. Naeser, and Thane H. McCulloh, 133–140. Berlin, Germany: Springer-Verlag.

Ramsay, John G. 1967. *Folding and Fracturing of Rocks*. New York, New York: McGraw-Hill.

Ramsay, John G. 1974. "Development of Chevron Folds." *Geological Society of America Bulletin* 85, no. 11 (November 1): 1741–1754.

Reches, Ze'ev. 1978a. "Development of Monoclines: Part I. Structure of the Palisades Creek Branch of the East Kaibab Monocline, Grand Canyon, Arizona." In *Laramide Folding Associated with Basement Block Faulting in the Western United States*. Edited by Vincent Matthews III, 235–271. Boulder, Colorado: Geological Society of America. *Memoir 151*.

Reches, Ze'ev. 1978b. "Analysis of Faulting in Three-Dimensional Strain Field." *Tectonophysics* 47, nos. 1–2 (19 May): 109–129.

Reches, Ze'ev, and Arvid M. Johnson. 1978. "Development of Monoclines: Part II. Theoretical Analysis of Monoclines." In *Laramide Folding Associated with Basement Block Faulting in the Western United States*. Edited by Vincent Matthews III, 273–311. Boulder, Colorado: Geological Society of America. *Memoir 151*.

Reches, Ze'ev, and James H. Dieterich. 1983. "Faulting of Rocks in Three-Dimensional Strain Fields. I. Failure of Rocks in Polyaxial, Servo-Control Experiments." *Tectonophysics* 95, nos. 1–2 (20 May): 111–132.

Reches, Ze'ev. 1983. "Faulting of Rocks in Three-Dimensional Strain Fields. II. Theoretical Analysis." *Tectonophysics* 95, nos. 1–2 (20 May): 133–156.

Ree, J.-H. 1994. "Grain Boundary Sliding and Development of Grain Boundary Openings in Experimentally Deformed Octachloropropane." *Journal of Structural Geology* 16, no. 3 (March): 403–418.

Renac, C., and A. Meunier. 1995. "Reconstruction of Palaeothermal Conditions in the Passive Margin Using Illite-Smectite Mixed-Layer Series (BA1 Scientific Deep Drill-Hole, Ardeche, France)." *Clay Minerals* 30, no. 2 (June): 107–118.

Resser, Charles E., 1945. "Cambrian Fossils of the Grand Canyon: Part II. Cambrian History of the Grand Canyon Region." *Carnegie Institute of Washington Publication* 563, pp. 168–232. Washington, DC: Carnegie Institute of Washington.

Rettger, R.E. 1935. "Experiments on Soft-Rock Deformation." *Bulletin of the American Association of Petroleum Geologists* 19, no. 2 (February): 271–292.

Robinson, D., and R.J. Merriman. 1999. "Low-Temperature Metamorphism: An Overview." In *Low-Grade Metamorphism*. Edited by Martin Frey, and Doug Robinson, 1–9. Oxford, England: Blackwell.

Rose, Eben C. 2003. "Depositional Environment and History of the Cambrian Tonto Group, Grand Canyon, Arizona." Master's thesis (unpublished manuscript). Flagstaff, Arizona: Northern Arizona University.

Rose, Eben C. 2006. "Nonmarine Aspects of the Cambrian Tonto Group of the Grand Canyon, USA, and Broader Implications." *Palaeoworld* 15, nos. 3–4 (August–November): 223–241.

Rose, Eben C. 2011. "Proposed Modification of the Nomenclature and a Revised Depositional Model for the Cambrian Tonto Group of the Grand Canyon, Arizona." In *Cambrian Stratigraphy and Paleontology of Northern Arizona and Southern Nevada, The 16th Field Conference of the Cambrian Stage Subdivision Working Group, International Subcommission on Cambrian Stratigraphy, Flagstaff, Arizona, and Southern Nevada, United States.* Edited by J. Stewart Hollingsworth, Frederick A. Sundberg, and John R. Foster, 77–98. Flagstaff, Arizona: Museum of Northern Arizona. *Bulletin 67*.

Roth, Wolfgang H., Joel Sweet, and Richard E. Goodman. 1982. "Numerical and Physical Modeling of Flexure Slip Phenomena and Potential for Fault Movement." *Rock Mechanics Supplement* 12: 27–46.

Rowland, Richard A. 1946. "Grain-Shape Fabrics of Clastic Quartz." *Geological Society of America Bulletin* 57, no. 6 (June 1): 547–564.

Rutter, Ernest H. 1974. "The Influence of Temperature, Strain Rate and Interstitial Water in the Experimental Deformation of Calcite Rocks." *Tectonophysics* 22, nos. 3–4 (June): 311–334.

Rutter, Ernest H. 1976. "The Kinetics of Rock Deformation by Pressure Solution." *Philosophical Transactions of the Royal Society of London* A283, no. 1312 (October 12): 203–219.

Sandhu, A.S., Lakhwant Singh, R.C. Ramola, Surinder Singh, and H.S. Virk. 1990. "Fission Track Annealing in Minerals." *International Journal of Radiation Applications and Instrumentation. Part D. Nuclear Tracks and Radiation Measurements* 17, no. 3 (January): 267–269.

Sanz, Pablo F., Ronaldo I. Borja, and David D. Pollard. 2007. "Mechanical Aspects of Thrust Faulting Driven by Far-Field Compression and Their Implications for Fold Geometry." *Acts Geotechnica* 2, no. 1 (18 April): 17–31.

Sanz, Pablo F., David D. Pollard, Patricia F. Allwardt, and Ronaldo I. Borja. 2008. "Mechanical Models of Fracture Reactivation and Slip on Bedding Surfaces During Folding of the Asymmetric Anticline at Sheep Mountain, Wyoming." *Journal of Structural Geology* 30, no. 9 (September): 1177–1191.

Schmid, S.M., J.N. Boland, and Mervyn S. Paterson. 1977. "Superplastic Flow in Fine-Grained Limestone." *Tectonophysics* 43, nos. 3–4 (10 December): 257–292.

Schmid, Stefan M. 1982. "Microfabric Studies as Indicators of Deformation Mechanisms and Flow Laws Operative in Mountain Building." In *Mountain Building Processes*. Edited by K.J. Hsu, 95–110. London, United Kingdom: Academic Press.

Schmid, Stefan M., and M. Casey. 1986. "Complete Fabric Analysis of Some Commonly Observed Quartz c-Axis Patterns." In *Mineral and Rock Deformation: Laboratory Studies (The Paterson Volume)*. Edited by Bruce E. Hobbs, and H.C. Heard, 263–286. Washington, DC: American Geophysical Union. *Geophysical Monograph*, vol. 36.

Schmid, Stefan M., R. Panozzo, and S. Bauer. 1987. "Simple Shear Experiments on Calcite Rocks: Rheology and Microfabric." *Journal of Structural Geology* 9, nos. 5–6: 747–778.

Schmid, S.M., Mervyn S. Paterson and J.N. Boland. 1980. "High Temperature Flow and Dynamic Recrystallization in Carrara Marble." *Tectonophysics* 65, nos. 3–4 (1 June): 245–280.

Scholle, Peter A. 1979. *A Color Illustrated Guide to Constituents, Textures, Cements, and Porosities of Sandstones and Associated Rocks*. Tulsa, Oklahoma: The American Association of Petroleum Geologists. *Memoir 28*.

Schultz, Richard A. 2019. *Geologic Fracture Mechanics*. Cambridge, United Kingdom: Cambridge University Press.

Scott, Anthony, Mario Vigorito, and Andrew Hurst. 2009. "The Process of Sand Injection: Internal Structures and Relationships with Host Strata (Yellowbank Creek Injectite Complex, California, U.S.A.)." *Journal of Sedimentary Research* 79, no. 8 (August 1): 568–583.

Shea, William T. Jr., and Andreas K. Kronenberg. 1993. "Strength and Anisotropy of Foliated Rocks with Varied Mica Contents." *Journal of Structural Geology* 15, nos. 9–10 (September–October): 1097–1121.

Silliphant, Laura J., Terry Engelder, and Michael R. Gross. 2002. "The State of Stress in the Limb of the Split Mountain Anticline, Utah: Constraints Placed by Transected Joints." *Journal of Structural Geology* 24, no. 1 (January): 155–172.

Simo, J.C., and R.L. Taylor. 1985. "Consistent Tangent Operators for Rate-Independent Elastoplasticity." *Computer Methods in Applied Mechanics and Engineering* 48, no. 1 (February): 101–118.

Simpson, Carol. 1986. "Fabric Development in Brittle-to-Ductile Shear Zones." *Pure and Applied Geophysics* 124, nos. 1–2 (January): 269–288.

Sloss, Laurence L. 1963. "Sequences in the Cratonic Interior of North America." *Geological Society of America Bulletin* 42, no. 2 (February 1): 93–114.

Smart, G., and T. Clayton. 1985. "The Progressive Illitization of Interstratified Illite-Smectite from Carboniferous Sediments of Northern England and its Relationship to Organic Maturity Indicators." *Clay Minerals* 20, no. 4 (9 July): 455–466.

Snelling, Andrew A. 2000. "Geochemical Processes in the Mantle and Crust." In *Radioisotopes and the Age of the Earth: A Young-Earth Creationist Research Initiative*. Edited by Larry Vardiman, Andrew A. Snelling, and Eugene F. Chaffin, 123–304. El Cajon, California: Institute for Creation Research, and St. Joseph, Missouri: Creation Research Society.

Snelling, Andrew A. 2005a. "Radiohalos in Granites: Evidence for Accelerated Nuclear Decay." In *Radioisotopes and the Age of the Earth: Results of a Young-Earth Creationist Research Initiative*. Edited by Larry Vardiman, Andrew A. Snelling, and Eugene F. Chaffin, 101–207. El Cajon, California: Institute for Creation Research, and Chino Valley, Arizona: Creation Research Society.

Snelling, Andrew A. 2005b. "Fission Tracks in Zircons: Evidence for Abundant Nuclear Decay." In *Radioisotopes and the Age of the Earth: Results of a Young-Earth Creationist Research Initiative*. Edited by Larry Vardiman, Andrew A. Snelling, and Eugene F. Chaffin, 209–324. El Cajon, California: Institute for Creation Research, and Chino Valley, Arizona: Creation Research Society.

Snelling, Andrew A. 2009. *Earth's Catastrophic Past: Geology Creation and the Flood*. Dallas, Texas: Institute for Creation Research.

Snelling, Andrew A. 2017a. "Determination of the Decay Constants and Half-Lives of Uranium-238 (^{238}U) and Uranium-235 (^{235}U), and the Implications for U-Pb and Pb-Pb Radioisotope Dating Methodologies." *Answers Research Journal* 10 (January 18): 1–38. https://answersresearchjournal.org/radioisotope-decay-uranium/.

Snelling, Andrew A. 2017b. "Problems with the U-Pb Radioisotope Dating Methods—1. Common Pb." *Answers Research Journal* 10 (July 26): 121–167. https://answersresearchjournal.org/ problems-radioisotope-dating-u-pb-1/.

Snelling, Andrew A. 2018. "Problems with the U-Pb Radioisotope Dating Methods—2. U and Pb Mobility." *Answers Research Journal* 11 (June 13): 85–140. https://answersresearchjournal.org/problems-radioisotope-dating-u-pb-2/.

Snelling, Andrew A. 2019. "Problems with the U-Pb Radioisotope Dating Methods—3. Mass Fractionation." *Answers Research Journal* 12 (November 3): 355–392. https://answersresearchjournal.org/problems-radioisotope-dating-u-pb-3/.

Snelling, Andrew A. 2021a. "The Petrology of the Tapeats Sandstone, Tonto Group, Grand Canyon, Arizona." *Answers Research Journal* 14 (June 23): 159–254. https://answersresearchjournal.org/petrology-tapeats-sandstone-tonto-group/.

Snelling, Andrew A. 2021b. "The Petrology of the Bright Angel Formation, Tonto Group, Grand Canyon, Arizona." *Answers Research Journal* 14 (September 8): 303–414. https://answersresearchjournal.org/petrology-bright-angel-tonto-group/.

Snelling, Andrew A. 2022a. "The Petrology of the Muav Formation, Tonto Group, Grand Canyon, Arizona." *Answers Research Journal* 15 (August 10): 139–262. https://answersresearchjournal.org/geology/petrology-muav-formation-tonto-group/.

Snelling, Andrew A. 2022b. *The Genesis Flood Revisited*. Green Forest, Arkansas: Master Books; and Hebron, Kentucky: Answers in Genesis.

Snelling, Andrew A. 2023a. "The Carbon Canyon Fold, Eastern Grand Canyon, Arizona." *Answers Research Journal* 16 (February 22): 1–124. https://answersresearchjournal.org/geology/carbon-canyon-fold-arizona/.

Snelling, Andrew A. 2023b. "The Monument Fold, Central Grand Canyon, Arizona." *Answers Research Journal* 16 (August 9): 301–432. https://answersresearchjournal.org/geology/monument-fold-grand-canyon/.

Spry, Alan. 1969. *Metamorphic Textures*. Oxford, United Kingdom: Pergamon.

Stel, H. 1986. "The Effect of Cyclic Operation of Brittle and Ductile Deformation on the Metamorphic Assemblage in Cataclasites and Mylonites." *Pure and Applied Geophysics* 124, nos. 1–2 (January): 289–307.

Stewart, Meg E., Wanda J. Taylor, Philip A. Pearthree, Barry J. Solomon, and Hugh A. Hurlow. 1997. "Neotectonics, Fault Segmentation, and Seismic Hazards Along the Hurricane Fault in Utah and Arizona: An Overview of Environmental Factors." *Brigham Young University Geology Studies* 42

Part II: 235–278.

Strother, Paul K., and John H. Beck. 2000. "Spore-like Microfossils from Middle Cambrian Strata: Expanding the Meaning of the Term Cryptospore." In *Pollen and Spores: Morphology and Biology*. Edited by M.M. Harley, C.M. Morton, and S. Blackmore, 413–424. Kew, United Kingdom: Royal Botanic Gardens.

Strother, Paul K., Christopher T. Baldwin, John H. Beck, and Eben Rose. 2004. "An Integrated Sedimentological, Ichnological and Palynological Study of the Paeloecology of the Middle Cambrian, Bright Angel Shale, Grand Canyon, Arizona." *Palynology* 28, no. 1: 265.

Stünitz, Holger. 1998. "Syndeformational Recrystallization—Dynamic or Compositionally Induced?" *Contributions to Mineralogy and Petrology* 131, nos. 2–3 (April): 219–236.

Stünitz, Holger, and J.D. Fitz Gerald. 1993. "Deformation of Granitoids at Low Metamorphic Grade. II: Granular Flow in Albite-Rich Mylonites." *Tectonophysics* 221, nos. 3–4 (30 May): 299–324.

Sundberg, Marshall, and Reid F. Cooper. 2010. "A Composite Viscoelastic Model for Incorporating Grain Boundary Sliding and Transient Diffusion Creep: Correlating Creep and Attenuation Responses for Materials with a Fine Grain Size." *Philosophical Magazine* 90, no. 20 (28 May): 2817–2840.

Suppe, John. 1983. "Geometry and Kinematics of Fault-Bend Folding." *American Journal of Science* 283, no. 7 (September): 648–721.

Suppe, John., and Donald A. Medwedeff. 1990. "Geometry and Kinematics of Fault-Propagation Folding." *Ecologae Geologicae Helvetiae* 83, no. 3 (January): 409–454.

Tanner, P.W. Geoff. 1989. "The Flexural-Slip Mechanism." *Journal of Structural Geology* 11, no. 6: 635–655.

Tapp, Bryan, and Ken Wolgemuth. 2016. "Broken and Bent Rock: Fractures, Faults, and Folds." In *The Grand Canyon, Monument to an Ancient Earth; Can Noah's Flood Explain the Grand Canyon?* Edited by Carol Hill, Gregg Davidson, Tim Helble, and Wayne Ranney, 116–127. Grand Rapids, Michigan: Kregel Publications.

Taylor, Wilson A., and Paul K. Strother. 2008. "Ultrastructure of Some Cambrian Palynomorphs from the Bright Angel Shale, Arizona, USA." *Review of Palaeobotany and Palynology* 151 (July): 41–50.

Thompson, Graham R., and John Hower. 1975. "The Mineralogy of Glauconite." *Clays and Clay Minerals* 23 (1 August): 289–300.

Thurston, Olivia G., William R. Guenthner, Karl E. Karlstrom, Jason W. Ricketts, Matthew T. Heizler, and J. Michael Timmons. 2022. "Zircon (U-Th)/He Thermochronology of Grand Canyon Resolves 1250Ma Unroofing at the Great Unconformity and <20Ma Canyon Carving." *Geology* 50, no. 2 (November 2): 222–226.

Tindall, Sarah E., and George H. Davis. 1999. "Monocline Development by Oblique-Slip Fault-Propagation Folding: The East Kaibab Monocline, Colorado Plateau, Utah." *Journal of Structural Geology* 21, no. 10 (October): 1303–1320.

Tullis, Jan. 1983. "Deformation of Feldspars." In *Feldspar Mineralogy*. 2nd ed. Edited by Paul H. Ribbe, 297–323. Washington, DC: Mineralogical Society of America. *Reviews in Mineralogy*. Vol. 2.

Tullis, Jan, John M. Christie, and David T. Griggs. 1973. "Microstructures and Preferred Orientations of Experimentally Deformed Quartzites." *Geological Society of America Bulletin* 84, no. 1 (January 1): 297–314.

Tullis, Jan, and Richard A. Yund. 1987. "Transition from Cataclastic Flow to Dislocation Creep of Feldspar: Mechanisms and Microstructures." *Geology* 15, no. 7 (July 1): 606–609.

Tullis, Jan, and Richard A. Yund. 1991. "Diffusion Creep in Feldspar Aggregates: Experimental Evidence." *Journal of Structural Geology* 13, no. 9: 987–1000.

Tullis, Jan, Richard A. Yund, and J. Farver. 1996. "Deformation-Enhanced Fluid Distribution in Feldspar Aggregates and Implications for Ductile Shear Zones." *Geology* 24, no. 1 (January 1): 63–66.

Tullis, Jan, Holger Stünitz, C. Teyssier, and R. Heilbronner. 2000. "Deformation Microstructures in Quartzo-Feldspathic Rocks." In *Stress, Strain and Structure: A Volume in Honor of W D Means*. Edited by Mark W. Jessell and Janos L. Urai. *Journal of the Virtual Explorer*. Vol. 2.

Turner, Francis J. 1948. "Note on the Tectonic Significance of Deformation Lamellae in Quartz and Calcite." *Transactions of the American Geophysical Union* 29, no. 4 (August): 565–569.

Twiss, Robert J. 1974. "Structure and Significance of Planar Deformation Features in Synthetic Quartz." *Geology* 2, no. 7 (July 1): 329–332.

Twiss, Robert J. 1976. "Some Planar Deformation Features, Slip Systems, and Submicroscopic Structures in Synthetic Quartz." *The Journal of Geology* 84, no. 6 (November): 701–724.

Udden, Johan August. 1914. "Mechanical Composition of Clastic Sediments." *Bulletin of the Geological Society of America* 25, no. 1 (January 1): 655–744.

Ulmer-Scholle, Dana S., Peter A. Scholle, Juergen Schieber, and Robert J. Raine. 2015. *A Color Guide to the Petrography of Sandstones, Siltstones, Shales and Associated Rocks*. Tulsa, Oklahoma: The American Association of Petroleum Geologists. *Memoir 109*.

Urai, Janos L. 1983. "Water-Assisted Dynamic Recrystallization and Weakening in Polycrystalline Bischofite." *Tectonophysics* 96, nos. 1–2 (1 April): 125–157.

Urai, Janos L., W.D. Means, and Gordon S. Lister. 1986. "Dynamic Recrystallization of Minerals." In *Mineral and Rock Deformation: Laboratory Studies (The Paterson Volume)*. Edited by Bruce E. Hobbs, and H.C. Heard, 161–199. Washington, DC: American Geophysical Union, *Geophysical Monograph*. Vol. 36.

Vardiman, Larry, Andrew A. Snelling, and Eugene F. Chaffin. eds. 2005. *Radioisotopes and the Age of the Earth: Results of a Young-Earth Creationist Research Initiative*. El Cajon, California: Institute for Creation Research; and Chino Valley, Arizona: Creation Research Society.

Velde, B., and J. Espitalié. 1989. "Comparison of Kerogen Maturation and Illite/Smectite Composition in Diagenesis." *Journal of Petroleum Geology* 12, no. 1 (January): 103–110, 1989.

Velde, B., and B. Lanson. 1993. "Comparison of I/S Transformation and Maturity of Organic Matter at Elevated Temperatures." *Clays and Clay Minerals* 41 (1 April): 178–183.

Vernon, Ron H. 1965. "Plagioclase Twins in Some Mafic Gneisses from Broken Hill, Australia." *Mineralogical Magazine* 35, no. 271 (September): 488–507.

Vernon, Ron H. 1975. "Deformation and Recrystallization of a Plagioclase Grain." *American Mineralogist* 60, nos. 9–10 (October 1): 884–888.

Vernon, Ron H. 1976. *Metamorphic Processes: Reactions and Microstructure Development*. London, United Kingdom: Murby; and New York, New York: Wiley.

Vernon, Ron H. 1977a. "Relationships Between Microstructures and Metamorphic Assemblages." *Tectonophysics* 39, nos. 1–3 (20 April): 439–452.

Vernon, Ron H. 1977b. "Microfabric of Mica Aggregates in Partly Recrystallized Biotite." *Contributions to Mineralogy and Petrology* 61, no. 2 (January): 175–185.

Vernon, Ron H. 1981. "Optical Microstructure of Partly Recrystallized Calcite in Some Naturally Deformed Marbles." *Tectonophysics* 78, nos. 1–4 (1 October): 601–612.

Vernon, Ron H., V.A. Williams, and William F. D'Arcy. 1983. "Grain-size Reduction and Foliation Development in a Deformed Granitoid Batholith." *Tectonophysics* 92, nos. 1–3 (10 February): 123–145.

Vernon, Ron H. 2000. *Beneath Our Feet: The Rocks of Planet Earth*. Cambridge, United Kingdom: Cambridge University Press.

Vernon, Ron H., S.E. Johnson, and E.A. Melis. 2004. "Emplacement-Related Microstructures in the Margin of a Deformed Pluton: The San José Tonalite, Baja California, Mexico." *Journal of Structural Geology* 26, no. 10 (October): 1867–1884.

Vernon, Ron H. 2018. *A Practical Guide to Rock Microstructure*. 2nd ed. Cambridge, United Kingdom: Cambridge University Press.

Walcott, Charles D. 1890. "Study of a Line of Displacement in the Grand Canyon of the Colorado in Northern Arizona." *Geological Society of America Bulletin* 1: 49–64.

Waldron, John W.F., and Jean-François Gagnon. 2011. "Recognizing Soft-Sediment Structures in Deformed Rocks of Orogens." *Journal of Structural Geology* 33, no. 3 (March): 271–279.

Wanless, Harold R. Jr. 1973. "Cambrian of the Grand Canyon—A Reevaluation of the Depositional Environment." Ph.D. Thesis (unpublished manuscript). Baltimore, Maryland: Johns Hopkins University.

Watanabe, Hiroyuki, Kouhei Kurimoto, Tokuteru Uesugi, Yorinobu Takigawa, and Kenji Higashi. 2013. "Accommodation Mechanisms for Grain Boundary Sliding as Inferred from Texture Evolution During Superplastic Deformation." *Philosophical Magazine* 93, no. 22 (29 April): 2913–2931.

Weinberg, David M. 1979. "Experimental Folding of Rocks Under Confining Pressure: Part VII. Partially Scaled Models of Drape Folds." *Tectonophysics* 54, nos. 1–2 (10 April): 1–24.

Wentworth, Chester K. 1922. "A Scale of Grade and Class Terms for Clastic Sediments." *The Journal of Geology* 30, no. 5 (July–August): 377–392.

Wheeler, John. 1992. "Importance of Pressure Solution and Coble Creep in the Deformation of Polymineralic Rocks." *Journal of Geophysical Research* 97, no. B4 (10 April): 4679–4586.

Whisonant, Robert C. 1970. "Influence of Texture Upon the Response of Detrital Quartz to Deformation of Sandstones." *Journal of Sedimentary Petrology* 40, no. 3 (September 1): 1018–1025.

White, S. 1973a. "Syntectonic Recrystallization and Texture Development in Quartz." *Nature* 244, no. 5144 (3 August): 276–278.

White, S. 1973b. "Deformation Lamellae in Naturally Deformed Quartz." *Nature Physical Science* 245 (10 September): 26–28.

White, S.H. 1977. "Geological Significance of Recovery and Recrystallization Processes in Quartz." *Tectonophysics* 39, nos. 1–3 (20 April): 143–170.

Whitmore, John H., and Paul A. Garner. 2008. "Using Suites of Criteria to Recognize Pre-Flood, Flood, and Post-Flood Strata in the Rock Record with Application to Wyoming (USA)." In *Proceedings of the Sixth International Conference on Creationism*. Edited by Andrew A. Snelling, 425–448. Pittsburgh, Pennsylvania: Creation Science Fellowship; and Dallas, Texas: Institute for Creation Research.

Wiens, Roger. 2016. "So Just How Old is That Rock?" In *The Grand Canyon, Monument to an Ancient Earth: Can Noah's Flood Explain the Grand Canyon?* Edited by Carol A. Hill, Gregg Davidson, Tim Helble, and Wayne Ranney, 88–97. Grand Rapids, Michigan: Kregel Publications.

Wilson, Colin J.L., and Ian A. Bell. 1979. "Deformation of Biotite and Muscovite: Optical Microstructure." *Tectonophysics* 58, nos. 1–2 (10 September): 179–200.

Wintsch, R.P., and K. Yi. 2002. "Dissolution and Replacement Creep: A Significant Deformation Mechanism in Mid-Crustal Rocks." *Journal of Structural Geology* 24, nos. 6–7 (June–July): 1179–1193.

Wolf, Karl H., and George V. Chilingarian. 1975. "Diagenesis of Sandstones and Compaction." In *Compaction of Coarse-Grained Sediments. I.* Edited by George V. Chilingarian, and Karl H. Wolf, 69–444. Amsterdam, The Netherlands: Elsevier. *Developments in Sedimentology 18B*.

Wojtal, Steven, Tom Blenkinsop, and Basil Tikoff. 2022. *An Integrated Framework for Structural Geology: Kinematics, Dynamics, and Rheology of Deformed Rocks*. Hoboken, New Jersey: John Wiley and Sons.

Yardley, Bruce W.D., W.S. MacKenzie, and C. Guildford. 1990. *Atlas of Metamorphic Rocks and their Textures*. Harlow, United Kingdom: Longman.

Yund, Richard A., and Jan Tullis. 1991. "Compositional Changes of Minerals Associated with Dynamic Crystallization." *Contributions to Mineralogy and Petrology* 108, no. 3 (September): 346–355.

Zeitler, P. K. 1985. "Closure Temperature Implications of Concordant $^{40}Ar/^{39}Ar$ Potassium Feldspar and Zircon Fission-Track Ages from High-Grade Terranes." *Nuclear Tracks and Radiation Measurements* 10, no. 3: 441–442.

Zhamaletdinov, Abdullkhay A. 2019. "On the Nature of the Brittle-Ductile Transition Zone in the Earth's Crust (Review)." In *The Study of Continental Lithosphere Electrical Conductivity, Temperature and Rheology*. Edited by Abdullkhay A. Zhamaletdinov, and Yury L. Rebetsky, 13–21. *Springer Proceedings in Earth and Environmental Sciences*. Cham, Switzerland: Springer International Publishing.

Supplementary Material

Appendix—Location and Petrographic Descriptions of Bright Angel Formation Samples.